GEOCHEMISTRY OF THE SABIE RIVER BASALT FORMATION IN THE CENTRAL LEBOMBO, KAROO IGNEOUS PROVINCE

by

Russell James Sweeney

VOLUME I

Text and Diagrams

Thesis submitted in fulfilment of the requirements
for the degree of
Doctor of Philosophy

Department of Geochemistry
University of Cape Town

April, 1988

This thesis is dedicated to my wife
Beverly Ann
in deep appreciation for all her sacrifices
over the last ten years.
Without her it would not have been possible.

Plausible impossibilities should be preferred to unconvincing possibilites

Aristotle, 264-322 BC

ABSTRACT

The Sabie River Basalt Formation is a group of tholeiitic basaltic rocks erupted *ca* 190 Ma ago in the eastern zone of the Karoo Igneous Province of southern Africa. It is traceable over a distance of 700 km from Zululand, northwards along the Lebombo monocline into the Transvaal and south-east Zimbabwe. An abrupt compositional change in this formation occurs about halfway down its length in the vicinity of the Sabie and Komati Rivers: basalts to the north are known to be enriched in certain incompatible elements relative to basalts in the south, which are comparable in geochemistry to most basaltic rocks in the southern part of the Karoo Igneous Province.

New data obtained in this work include 134 major and trace element whole-rock analyses, some 400 analyses of constituent minerals, 38 $^{87}Sr/^{86}Sr$ ratio determinations, 19 $^{143}Nd/^{144}Nd$ ratio determinations, 16 common Pb determinations and 12 oxygen isotope analyses.

The "normal" (N) and "enriched" basaltic rocks are distinguished by differences in the concentrations of Ti, P, Zr, Nb, Y, La, Ce and Nd (high field strength elements). Broadly these differences are substantiated by K, Rb, Ba and Sr, but with much more overlap. The "enriched" group of basaltic rocks has been further subdivided into a low-Fe "enriched" (LFE) group and a high-Fe "enriched" group (HFE). The LFE-group basalts, which predominate at the base of the stratigraphic sections, are considered to be equivalent to basalts occurring in the N. Lebombo. In the central Lebombo N-group basalts predominate in the mid- and upper portions of the sections and HFE-group basalt occurs near the top of each section. Interbedding of all basalt groups occurs in the Sabie River section at the northern end of the study area, while the N- and HFE-group basalts are interbedded in the Crocodile and Komati River sections further to the south. The decrease in LFE-group basalt abundance southwards is accompanied by an increase in N-group basalt abundance. HFE-group basalts appear to be unique to the central Lebombo area of the Karoo Igneous Province and are volumetrically less significant than N- or LFE-group basalts.

Petrogenetic models involving closed-system fractional crystallization; coupled assimilation (of granitic crust) fractional crystallization; replenished, tapped and fractionated magma chambers and partial melting are

examined. Granitic crustal contamination appears to have been significant only in some samples of the N group where assimilation of granitic material has proceeded in a bulk fashion described by an AFC model. RTF models are dynamically more realistic than closed-system fractional crystallization models and explain increases in incompatible elements with decreasing MgO in the LFE and HFE groups. Variations in the N group, however, require varying degrees of partial melting of a N-type source to be explained fully. RTF models may explain the absence of any stratigraphic correlations of element abundances in the three groups. The HFE group may be related to an uncontaminated N-type parent composition by a combination of continued fractional crystallization from an N-group parent composition and varying degrees of partial melting of an N-type source. The only petrogenetic process by which the N and LFE groups may be related is different degrees of partial melting. However, this demands a source composition which has no resemblance on trace element and isotopic grounds, to observed mantle xenolith compositions. The preferred model is one in which the LFE group is derived from old sub-cratonic mantle similar to garnet-bearing "cold" peridotite xenoliths and the N group from a source similar in composition to estimates of primitive mantle.

The existence of two types of mantle derived continental flood basalt magmas occurs in other Mesozoic basalt provinces in "southern" Gondwanaland (e.g. Kirwanveggan of Antarctica, Etendeka of Namibia and the Parana Basin of South America). It is suggested that there is a geographical association of LFE-type basalts with Archaean crust (or Archaean crust re-worked in low temperature - high pressure events) and N-type basalts with post-Archaean crust (or Archaean crust re-worked in high temperature - low pressure events). This model suggests the derivation of the LFE group, from old sub-cratonic lithospheric mantle relatively enriched in incompatible elements and the N group being derived from more recently accreted and less enriched lithospheric mantle underlying younger crustal terraines.

VOLUME I : Table of Contents

VOLUME II : Table of Contents

Tables

Figures

1. INTRODUCTION

1.1 GEOLOGICAL SETTING

The fragmentation of the Gondwanaland supercontinent was preceded and accompanied by a period of increased igneous activity from the late Triassic to the Cretaceous. Major manifestations of this increased igneous activity are the volcanic sequences which are represented by the present day erosional remnants in southern Africa (Karoo: Jurassic to early Cretaceous), Antarctica (Ferrar and Kirkpatrick: Jurassic), Tasmania (Jurassic), South America (Parana: late Jurassic to early Cretaceous) and India (Deccan: late Cretaceous to early Tertiary).

In the southern African sub-continent the Jurassic to early Cretaceous extrusive and intrusive volcanic events (the Karoo Igneous Province) followed almost directly after the prolonged sedimentation of the Karoo Supergroup (Eales *et al.*, 1984). Karoo volcanic rocks cover an area of some 140000 km^2 and represent the eroded remnants of a volcanic province which must have covered most of southern Africa. These volcanics range in age from Cretaceous (*ca* 120-130 Ma, Siedner and Mitchell, 1976; Erlank *et al.*, 1984) in the Etendeka region in the west to the early Jurassic (200 Ma, Eales *et al.*, 1984) volcanics of the Nuanetsi region in the east (Fig. 1.1). Eales *et al.* (1984) have documented in detail the distribution and age of Karoo volcanics. Here the geological characteristics of the main outcrop areas of Karoo volcanics are briefly summarized, with special emphasis on Karoo basic rocks, while simplified stratigraphic sections are given in Fig. 1.2. For perspective it is appropriate to mention at the outset that this study is concerned with the basic rocks of the central Lebombo region.

1.1.1 Central Area (Lesotho and the north-east Cape Province)

The Karoo volcanics of the Central Area are described by Marsh and Eales (1984). These flat-lying volcanics attain a maximum thickness of 1400 m and are dominated by low-MgO tholeiitic basalts with only trivial volumes of silicic (andesitic-dacitic) volcanics (Marsh and Eales, 1984). The bulk of this basaltic sequence is dominated by the compositionally monotonous Lesotho

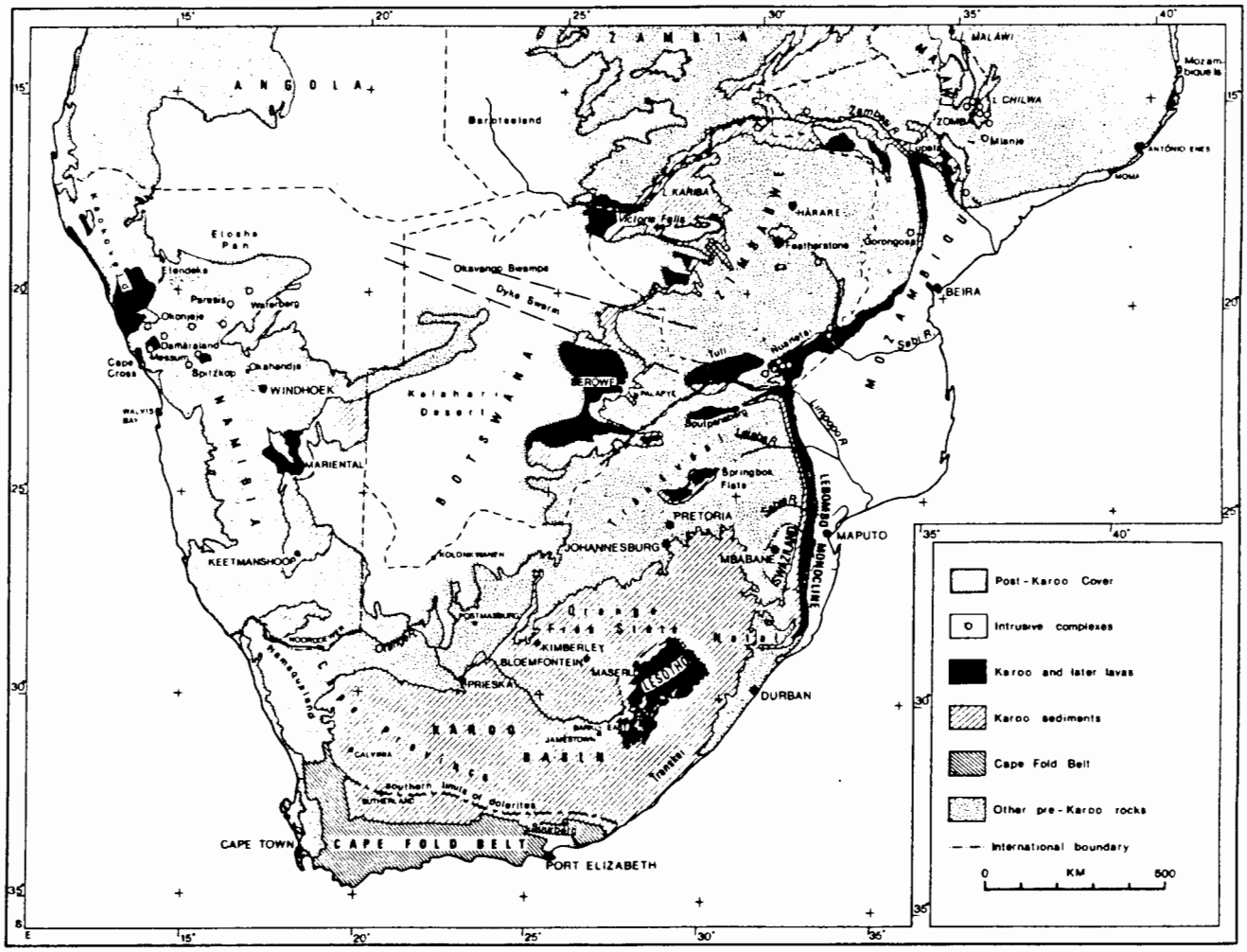

Figure 1.1. Simplified geological map showing the distribution of Karoo basalt outcrops in southern Africa (fig. 1, Eales *et al.*, 1984).

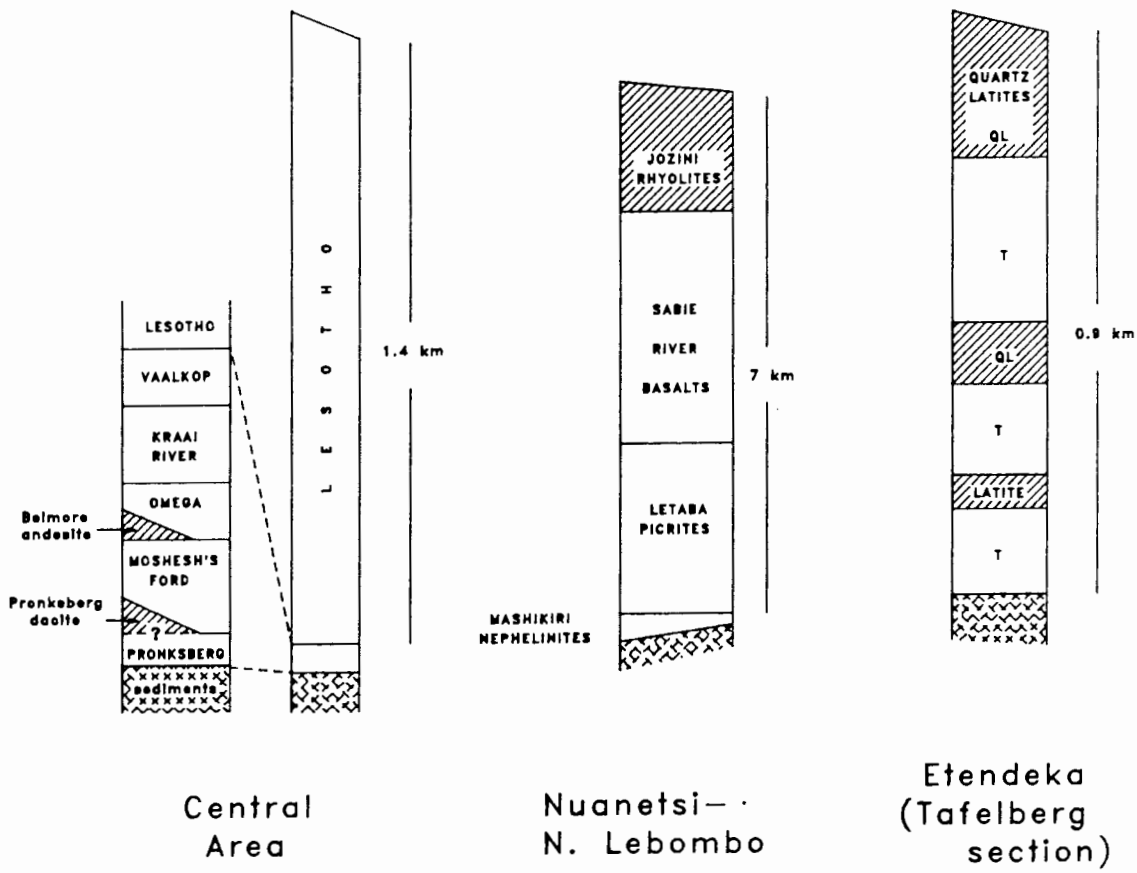

Figure 1.2. Simplified stratigraphy of principle areas of extrusive volcanics in the Karoo Igneous Province (after fig. 2, Hawkesworth *et al.*, 1984). Note that the quartz latite in the Tafelberg section is not laterally persistent and therefore does not reflect abundance of this rock-type in the Etendeka generally (S. C. Milner, pers. comm., 1988).

Formation. Considerable compositional diversity occurs in basalts below the Lesotho Formation at the base of the succession but they are minor in volume (Fig. 1.2; Marsh and Eales, 1984). On the other hand remnants of the Lesotho Formation occur near Mariental in Namibia and the Springbok Flats region of the N. Transvaal (Fig. 1.1), while dolerites with a Lesotho-like chemistry occur throughout the Karoo Province. This indicates that the Lesotho magma type is the most dominant in the Karoo Igneous Province.

1.1.2 North-west Namibia

The Karoo volcanics occurring in north-west Namibia (Fig. 1.1) have been described in detail by Erlank *et al.* (1984). These volcanics and associated intrusives were emplaced at the onset of the opening of the South Atlantic Rift between Africa and South America (Duncan *et al.*, 1984b; Erlank *et al.*, 1984). The most extensive outcrop is in the Etendeka region (>15000 km^2) where the sequence develops a maximum thickness of 900 m at Tafelberg (Fig. 1.2, Erlank *et al.*, 1984). The Tafelberg section, however, is not strictly representative of abundances of the different rock types in the Etendeka region which, generally, are estimated to be: 65% basic-intermediate basalt (MgO = 6.8-2.3%, SiO_2 = 51.8-57.8%); <1% latite (average SiO_2 = 59.23%) and 34% quartz-latite (average SiO_2 = 68.00%), which are all interbedded throughout the volcanic section (Erlank *et al.*, 1984; S. C. Milner, pers. comm.). Most basalts and dolerites in the Etendeka area form a distinct clan of basic magmas (Duncan *et al.*, 1984) but some early dolerites are compositionally similar to the rocks of the monotonous Lesotho Formation in the Central Area.

1.1.3 The Lebombo Monocline

The Lebombo monocline (Figs. 1.1, 1.3) is essentially a north-south flexure stretching *ca* 700 km from a position approximately 200 km north-east of Durban to the Limpopo River. The stratigraphy of the Lebombo Monocline has been established by Cleverly and Bristow (1979) and is generalized in Fig. 1.2. The geology of specific areas of the Lebombo Monocline has been comprehensively dealt with by many authors: S. Lebombo: Bristow (1976), Saggerson and Bristow (1983);

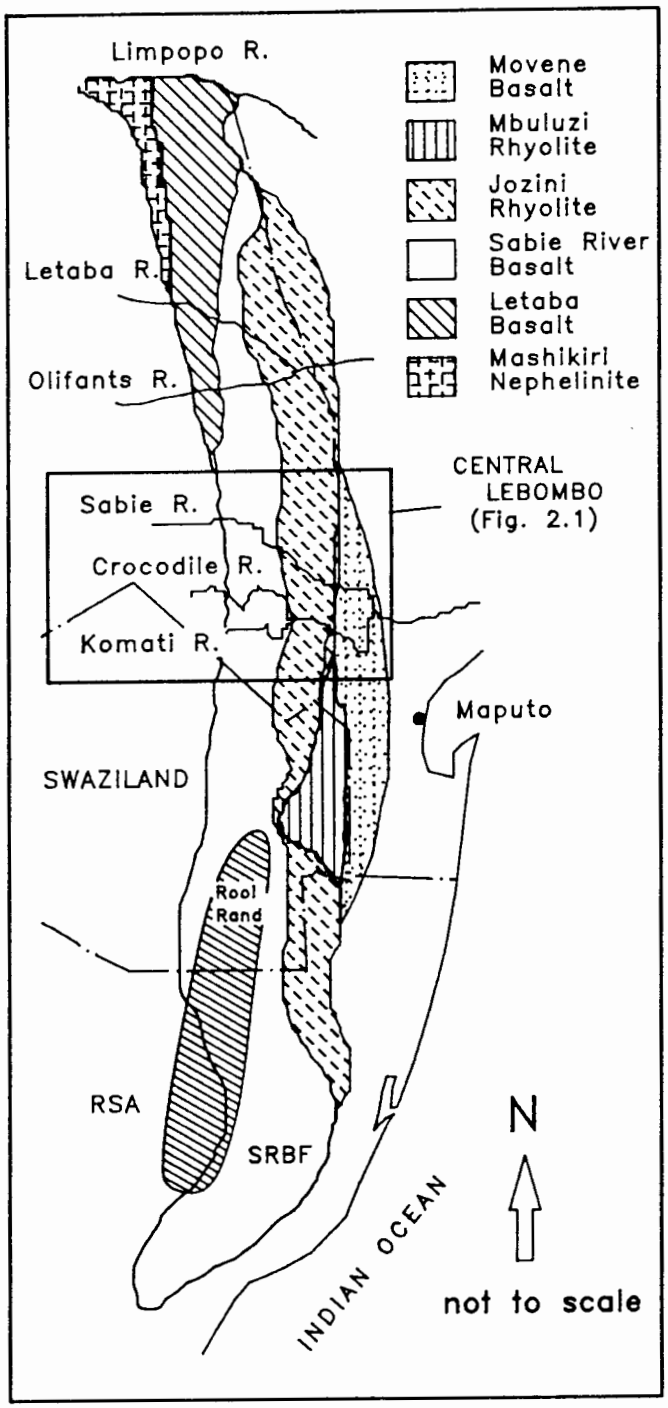

Figure 1.3. Sketch map of the Lebombo Monocline (after fig. 1, Cleverly *et al.*, 1984).

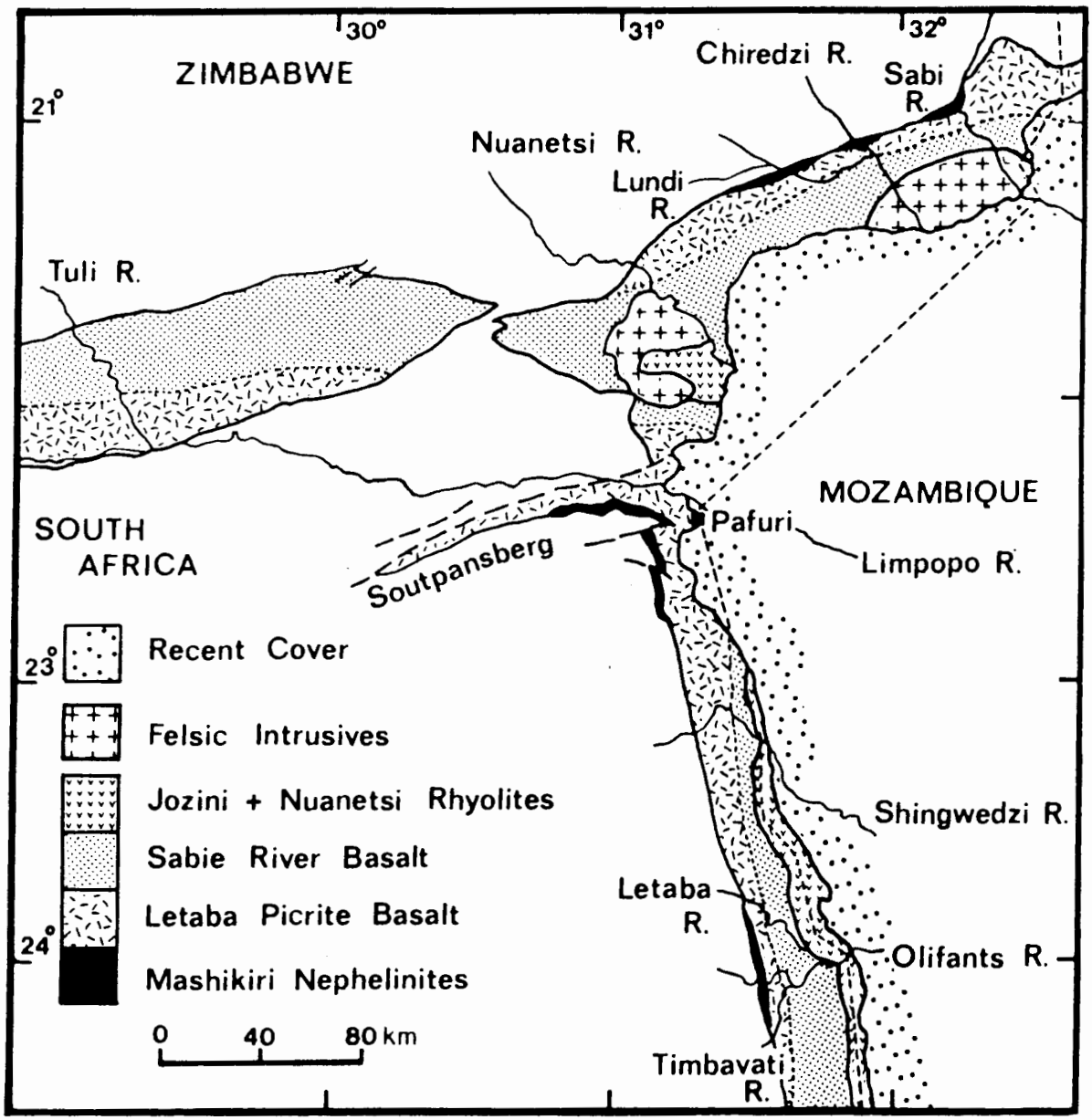

Figure 1.4. Geological map of the N. Lebombo and Nuanetsi-Sabi region of south-east Zimbabwe (fig.1 , Bristow, 1984b).

Rooi Rand - Saggerson *et al.* (1983), Armstrong *et al.* (1984); Swaziland - Cleverly (1977, 1979), Betton (1978); N. Lebombo picrites and nephelinites: Bristow (1980, 1984a, 1984b); low-MgO basalts of the Sabie River Basalt Formation (SRBF): Bristow (1980), Cox and Bristow (1984).

The Lebombo volcanics dip between 10-45° to the east. The axis of maximum monoclinal flexure (i.e. steepest dip) lies within the basalt succession in the southern Lebombo (Bristow, 1976) and at the base of the overlying rhyolites in northern Swaziland (Cleverly, 1977). In the central Lebombo dips in the basalt succession increase progressively eastward.

The Mashikiri Nephelinite Formation lies at the base of the Karoo volcanic sequence in the N. Lebombo (Figs. 1.2 and 1.4). These flows are characteristically nepheline-normative (Bristow, 1984b). Overlying these rocks and overstepping them southwards is the Letaba Basalt Formation consisting of picritic basalts with MgO in the range 9-25%. These picritic basalts attain their maximum stratigraphic thickness of 4000 m just south of Pafuri in the N. Lebombo and decrease in thickness southward (Fig. 1.4) until they pinch out south of the Olifants River (Bristow, 1984a). The Mashikiri Nephelinite Formation and the Letaba Basalt Formation are both absent in the central Lebombo, the field area of this study.

The picritic basalts of the Letaba Basalt Formation are overlain by the low-MgO (MgO <9%) basalts of the Sabie River Basalt Formation (SRBF) with some limited interbedding. A maximum age of 200 $\pm$5 Ma for the basalts of the SRBF was obtained by Allsopp and Roddick (1984) for a kimberlite pipe (Dokolwayo) in Swaziland which cross-cuts Karoo sediments underlying the mafic volcanics but not the volcanics themselves. A minimum age of 179 $\pm$4 Ma for the SRBF is provided by Rb-Sr dating of the overlying Jozini Rhyolites in the southern, central and northern Lebombo (Allsopp *et al.*, 1984). Thus, the basalts of the SRBF in the Lebombo were erupted 200 Ma to 180 Ma ago, which is consistent with some K-Ar ages around 193 Ma (Fitch and Miller, 1984).

The basalts of the SRBF are overlain, with some localized interbedding, by the rhyolites of the Jozini Formation, which in turn are overlain by the rhyolites of the Mbuluzi Formation (Cleverly, 1979). In some instances distinctive intercalations of rhyolite with the SRBF are observed. In the N. Lebombo the rhyolites of the Olifants Beds are found halfway up the SRBF

succession (Bristow, 1982). In Swaziland the Mkutshane Beds are found near the base of the SRBF and the Twin Ridge Beds near the top of the basalt succession (Cleverly and Bristow, 1979; Cleverly *et al.*, 1984). In the S. Lebombo the Coeyana Beds are found interbedded near the top of the SRBF (Saggerson and Bristow, 1983). The Olifants and Twin Ridge Beds have compositions similar to the Jozini Rhyolite, while the Mkutshane and Coeyana Beds are geochemically distinct (Cleverly *et al.*, 1984). However, unlike the silicic volcanics in the Etendeka region of north-west Namibia, the interbedded rhyolites of the Lebombo do not occupy significant portions of the basaltic section and individual units interbedded with the SRBF can rarely be traced laterally for distances greater than 10 km (Cleverly *et al.*, 1984).

The Movene Basalt Formation, occurring stratigraphically above the rhyolites, has been described by Assuncao *et al.* (1962) and Wachendorf (1971, 1973), but has not been investigated in this study.

1.1.4 Tuli-Nuanetsi-Sabi Area (south-east Zimbabwe)

At Nuanetsi in south-east Zimbabwe the north-south trending Lebombo monocline swings to the north-east and becomes a synclinal structure (Figs. 1.1, 1.4). To the west of the Nuanetsi syncline is the Tuli syncline and limited work on the Karoo volcanics in this region carried out by Vail *et al.* (1969) is summarized in Eales *et al.* (1984). The Karoo volcanics in the Nuanetsi-Sabi area have been described by Cox *et al.* (1965), Cox (1970), Cox and Bristow (1984) and Bristow (1984a). The volcanic stratigraphy in this area is essentially similar to that of the Lebombo (Figs. 1.2 and 1.4).

1.1.5 Intrusive Rocks

Intrusive sills and transgressive sheets of basaltic composition are usually located within Karoo sediments underlying the basalts, with dykes becoming more common towards the top of the Karoo sedimentary succession (Eales *et al.*, 1984). In some instances dolerite dykes are concentrated in prominent swarms of parallel dykes, e.g. the Rooi Rand dyke swarm in the southern Lebombo area (Fig. 1.3) which has been described by

Saggerson *et al.* (1983) and Armstrong *et al.* (1984). In most areas, however, the absence of any obvious volcanic centre or any major dyke swarm suggests that the major basaltic sequences were erupted from a more diffuse system of fissures having a wide range of orientations (e.g. in the Central Karoo Basin, Marsh and Eales, 1984).

Among the acid rocks intruding basaltic flows in the Karoo Igneous Province are several large granophyre bodies in the SRBF of the Lebombo monocline. These are intruded close to the SRBF-Jozini Rhyolite contact and may be sill-like in character (Eales *et al.*, 1984). Other predominantly felsic intrusive complexes are the Dembe-Divula Complex in the Nuanetsi area (Vail, 1962, 1966) and the Main Granophyre in the Sabi area of south-east Zimbabwe (Fig. 1.4).

1.1.6 Areas of unexposed Mesozoic volcanics in southern Africa

The area of unexposed Mesozoic volcanics appears to be greater than the sub-aerial exposure (Eales *et al.*, 1984). One example is the coastal plain of Mozambique where the flexuring of the Lebombo carries the Karoo volcanics beneath the Cretaceous-Tertiary sediments to the east (Fig. 1.1). There is good evidence from geophysical and borehole data that volcanic rocks extend as far as the present coast at Maputo (Darracott and Kleywegt, 1974). Furthermore, volcanics have been intersected in deep wells near the Mozambique coast north of Maputo more than 300 km east of the Lebombo outcrops (Eales *et al.*, 1984). The question remains, however, whether these volcanics are part of the Karoo Igneous event (Jurassic-early Cretaceous) and possibly related to the Movene Basalt Formation, or whether they are later effusions resulting directly from the opening of the south Indian Ocean as represented by the present continental margins.

Sub-outcrops of basalt in the central Kalahari (E. Botswana) have an estimated area of 150000 km^2, roughly six times the size of the Central Area remnant (Eales *et al.*, 1984). Likewise in W. Zambia, borehole data (Ridgway and Money, 1981) indicates the presence of Karoo basalts beneath the Kalahari sands and alluvium of that region.

1.2 SCOPE OF THIS STUDY

Cox *et al.* (1967) showed that differences existed between the chemistry of the low-MgO Karoo basalts of Nuanetsi (Zimbabwe) to the north and those of Swaziland and Basutoland (Lesotho) to the south. The basalts to the north (SRBF of Nuanetsi and the N. Lebombo) are relatively enriched in some incompatible elements (i.e. K, Ti, P, Ba, Sr and Zr) while the basalts to the south (SRBF in the S. Lebombo and the entire basalt section in the Central Area) are relatively depleted in these elements. Cox *et al.* (1967) introduced the terms 'northern high-K' province and 'southern low-K' province. Bristow (1980), Cox (1983) and Cox and Bristow (1984) established that the compositional change between these two basalt types takes place relatively rapidly between the Sabie and Komati River sections in the central Lebombo (Fig. 1.3). These authors, however, could not locate or define the nature of this change precisely due to the lack of detailed sampling.

The first phase of this study is to establish as exactly as possible the nature of the geochemical variations in time and space within the basaltic rocks of the central Lebombo and this constitutes the essentially descriptive portion of this thesis (Chapters 2 - 5). This has been achieved by detailed sampling and geochemical analysis of basaltic flows of the SRBF and of dolerites intrusive into the basalt section. Previous studies (Cox *et al.*, 1967; Bristow, 1980; Cox, 1983 and Cox and Bristow, 1984) defined the change in the basalts of the SRBF from north to south on geochemical grounds only and thus the different basaltic rock types are defined here solely on the basis of their geochemistry. The defined rock types are then examined for a comprehensive set of geochemical variables (e.g. major oxides, trace elements, Sr-, Nd-, Pb- and O-isotope ratios). Following geochemical characterization of the rock-types, they are examined to see whether petrographic distinctions and mineral chemistry can be correlated with geochemistry. The manner in which each rock type is distributed geographically and stratigraphically is also described.

The interpretive aspects of the thesis (Chapters 6 - 10) involve a detailed examination of various petrological models to try to account for the variations observed within and between each of the basaltic rock types. Possible petrological models are examined in an order which is most probably opposite to that in which the processes occurred. This has been carried out to remove the modifying effects which processes such as fractional

crystallization and assimilation of crust may have had on primary or parental magma compositions. This enables constraints to be placed on the nature and composition of the underlying mantle sources and the dynamic processes (e.g. the tectonic regime) which enabled the magmas to reach the surface. The variations in the compositions of the basalts in the central Lebombo are then viewed in a regional context and compared to similar variations in the Springbok Flats region (Marsh, 1984), the Etendeka Formation of north-west Namibia (Duncan, 1987) and the basalts of the Serra Geral Formation in the Parana basin of South America (Bellieni *et al.*, 1984a, 1984b, 1986; Mantovani *et al.*, 1985; Petrini *et al.*, 1987).

1.3 SAMPLING AND ANALYTICAL STRATEGY

The exposure of the SRBF in the central Lebombo is very poor away from sections along the Sabie, Crocodile and Komati Rivers. The exposure on the Komati River is relatively poor, thus most of the sampling was confined to the Sabie and Crocodile river sections. An attempt was made to obtain at least a sample suitable for semi-quantitative analysis (Appendix A) of every basalt and dolerite exposed in the section. Samples denoted with the prefix 'RSS' originate from the Sabie River area, 'RSC' and 'RSV' from the Crocodile River area, 'RSK' from the Komati River area and 'FV' from an area about halfway between the Sabie and Olifants Rivers (Sweni Stream). Samples prefixed 'CL' are from Bristow (1980), have been reported in Duncan *et al.* (1984) and were taken on the Sabie and Komati Rivers only. Sample locality information is given in Appendix D.

All reasonably homogeneous samples of basalts and dolerites (excluding very porphyritic samples) were analysed for critical elements such as Ti, K, Rb, Sr and Zr by the semi-quantitative slab analysis technique described in Appendix A. In the absence of any obvious differences in hand-specimen between rock types, this enabled the selection of samples for more accurate quantitative analysis and allowed comprehensive geochemical coverage to be obtained for the stratigraphic sections considered. Isotopic (radiogenic and stable) and REE determinations were subsequently carried out on selected samples. Mineral analyses were obtained for samples selected from each basalt type. Analytical techniques used in the generation of data reported in Appendix C are described in Appendix A.

2. GENERAL GEOLOGY AND VOLCANOLOGY OF THE SABIE RIVER BASALT FORMATION IN THE CENTRAL LEBOMBO

Picrite basalts and nephelinites are absent from the succession in the central Lebombo and the SRBF rests directly on aeolian sandstones of the Clarens Formation. In the Sabie River section, the Clarens Formation is successively underlain by red coloured sandstones (Elliot Formation?), feldspathic sandstones (Molteno Formation?) and an intercalated series of shale and sandstone units (Ecca or Beaufort Formations?). These Karoo sediments (SACS, 1980) are approximately 300 m thick in total and lie unconformably on Archaean granite gneisses. Interbedding of the basalts with the underlying sandstones and with the overlying rhyolites is infrequent in the central Lebombo, making the boundaries of the SRBF easily delineated. The interfluvial boundaries of the SRBF on Fig. 2.1 are recognized by obvious changes in both soil and vegetation type. The major rock types which constitute the SRBF are discussed below.

2.1 BASALTS

As noted previously (Chapter 1), the basalts of the SRBF in the central Lebombo were erupted about 190 Ma ago. Despite their Jurassic age, the basalts show many of the volcanological features typical of recent basaltic flows. Subaerial basaltic lava flows in general can be separated into three morphological types: pahoehoe, blocky and aa lavas. These distinctions were formulated from observations of Hawaiian lava flows made in the last century. Pahoehoe lava is characterized by a smooth undulating or hummocky surface in contrast to the rough jagged aa surface and the irregular blocky surface of block lava. The distinction is dependent upon the physical properties of a magma - the most important of which appears to be the relationship between viscosity and rate of shear strain or turbulence in a flow (MacDonald, 1967; Peterson and Tilling, 1980). The less turbulent, hotter and therefore less viscous a magma, the greater is the tendency for pahoehoe lava to develop. It is important to stress, however, that there is a complete gradation from pahoehoe to aa to block lava governed by an increase in viscosity and turbulence (Hulme, 1974; Peterson and Tilling, 1980).

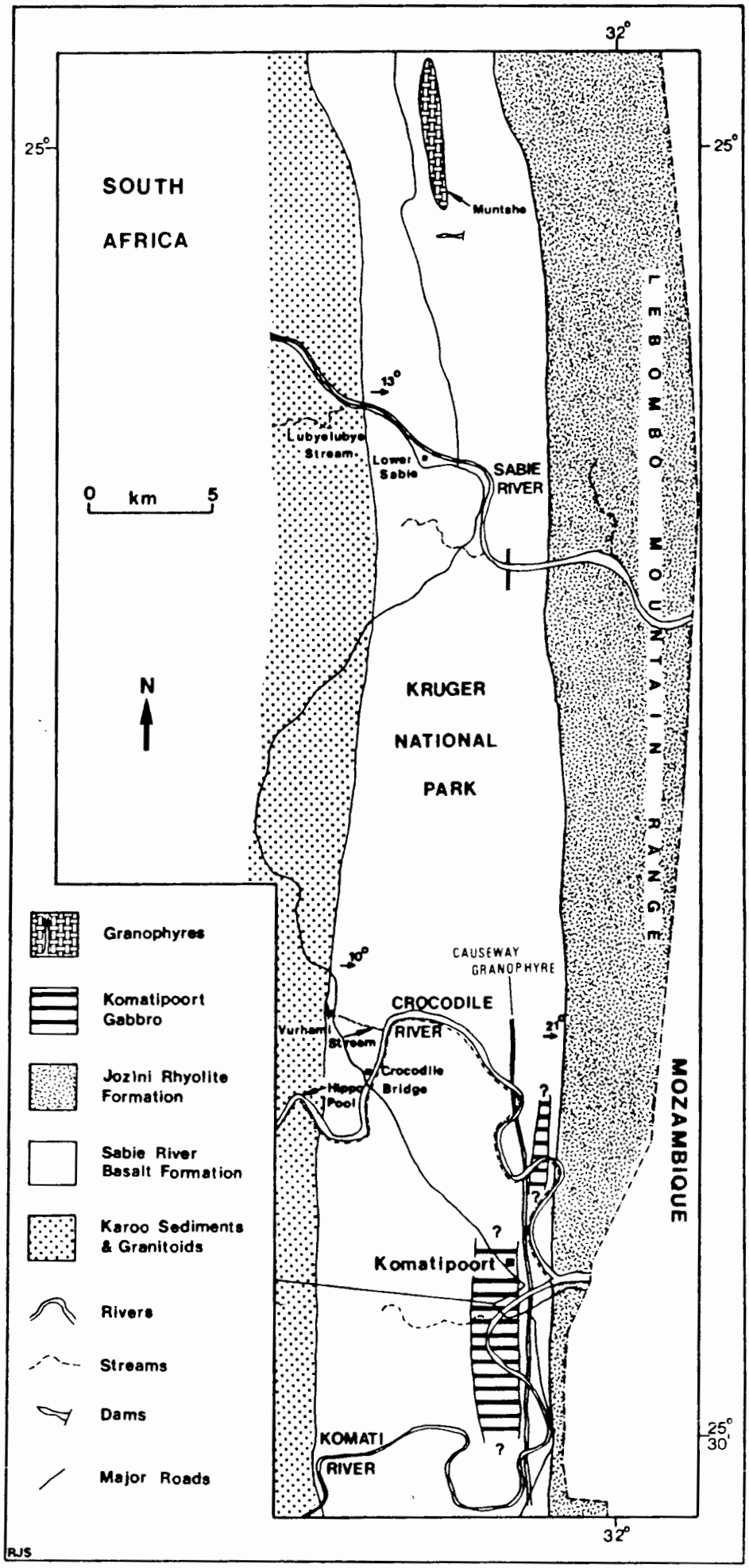

Figure 2.1. Geological map of the central Lebombo.

The characteristic angular and massive nature of block lava was found preserved in only one relatively thick flow (RSC6, *ca* 20 m) near the base of the Crocodile River stratigraphic section. The lack of amygdales suggests a low volatile content and possibly higher viscosity. The remainder of basaltic flows in the central Lebombo have characteristics of pahoehoe lava.

Basalts of the SRBF were extruded as a series of flows of highly variable thickness (2-20 m). Typically these flows have a massive lower portion grading upwards into an amygdaloidal flow top. The definition of flow boundaries is largely a problem of semantics. Where the time interval between two flows is large enough to permit the development of a sediment horizon this decision is straightforward. It is less obvious when a boundary is represented by oxidation of the underlying flow top and pipe amygdales in the base of the overlying flow. A series of apparently thin (1-3 m thick) basalt flows may just be lobes representing pulses of the same eruption.

A petrographic distinction between basaltic rock types may be made on the presence or absence of phenocrysts. The only phenocryst phase visible in hand specimen is feldspar, which rarely exceed 10% (by volume).

A number of the features discussed below may be illustrated by an idealised cross-section of a flow in Fig. 2.2.

2.1.1 Amygdales

Amygdales are mineral fillings in vesicles in a volcanic rock. Two possible origins for amygdales exist: they may form <u>during</u> the extrusion event by the migration of the volatile component in a lava or they may be deposited in vesicles due to the <u>later</u> circulation of water in the lava pile. It is likely that minerals such as calcite in vesicles are the product of circulating groundwaters, while crystalline epidote may be deposited in vesicles at the higher temperatures prevalent in a newly solidified flow.

Aside from the typical spherical shape of most amygdales, other morphologies exist:

(i) <u>Pipe amygdales</u>. Where present these amygdales are restricted to the lower 20 cm of a flow. Typically 2-6 cm in length, pipe amygdales are the result of nucleation at the flow base together with possible

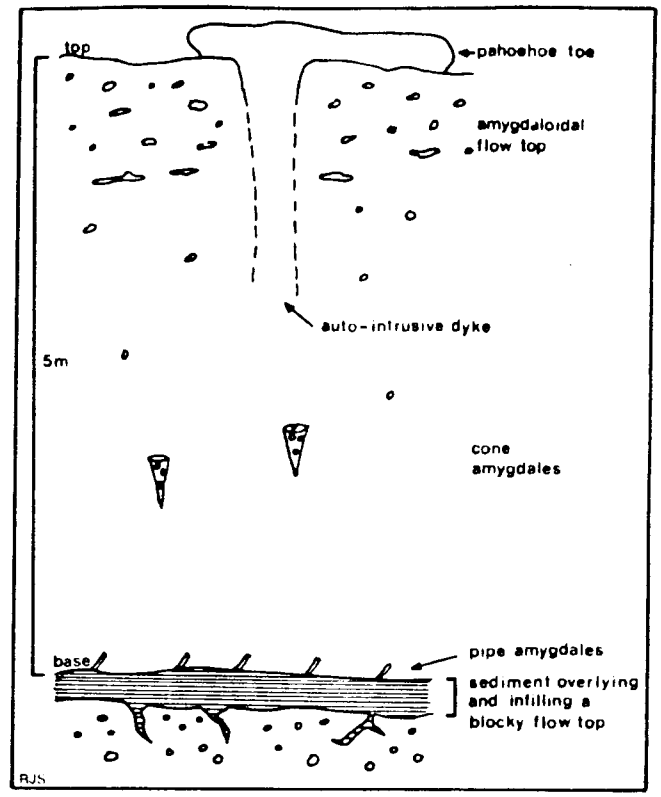

Figure 2.2. Idealised cross-section of a basaltic flow.

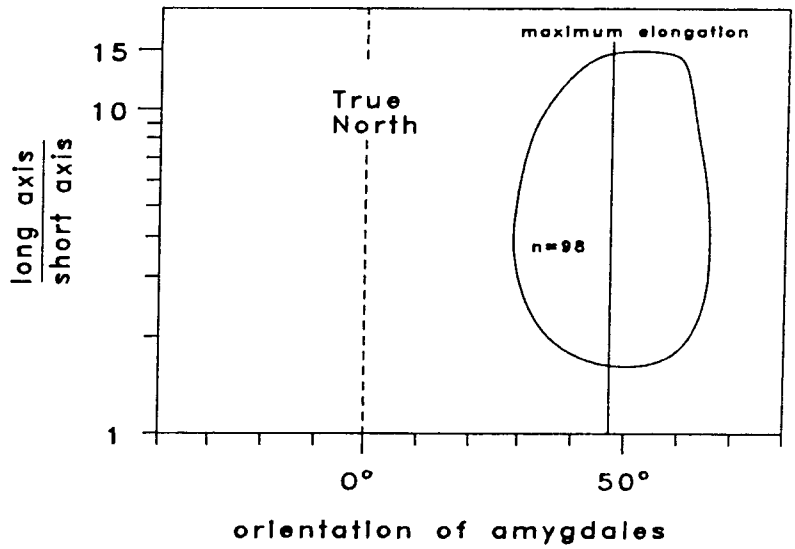

Figure 2.3. Strain analyses of deformed amygdales (incorporating 98 measurements) in a basalt (RSS145) flow-top in the Sabie section (M. K. Watkeys, pers. comm., 1987).

volatilization of moisture on the surface over which the lava flows. Differential lava flow rates at the base of flows causes these amygdales to assume an inclination, the azimuth of which indicates the direction of flow movement. In order to define accurately the direction(s) from which the basalts generally were derived from, it would be necessary to obtain a comprehensive set of measurements. Furthermore, even when observed these pipe amgdales may easily assume an orientation indicating local movements only (e.g. of flow lobes) and not the net flow direction. It is suggested that the accumulation of many measurements in a flow may give a less ambiguous result. Unfortunately poor outcrop prevented such a study. However, when many measurements (n=98) of deformed amygdales in a flow-top (RSS46, Appendix D) on the Sabie River were subjected to a strain analysis, the axis of maximum dimension was aligned on an azimuth of 45-50° east of true north (Fig. 2.3). This study was carried out by M. K. Watkeys of this department using software developed by M. von Veh of the Precambrian Research Unit (UCT). Thus, this flow may have been derived from the north-east or south-west of its present location. The rarity of dolerites intruding the basement to the west, however, suggests a north-east derivation. Obviously these results could not be extrapolated to the basalt succession in general.

(ii) Cone amygdales. Although not ubiquitous these amygdales typically occur towards the top of the more massive lower portion of a basalt flow (Fig. 2.2) where the association of a number of individual amygdales defines the cone. They are the result of a decrease in confining pressure upward from a nucleation point and therefore expansion and dispersion of a "bubble-stream" upwards.

2.1.2 Pillows

Pillows are pillow-shaped pods formed when basaltic lava is extruded underwater. Fingers of successive lava flows ooze upwards and over the crests of their predecessors. The similarity of pillow basalt structures to pahoehoe toes has often led to confusion. The most obvious morphological differences are the downward pointing apex of a pillow and the presence of interstitial material filling in spaces between pillows. The only definite example of a pillow basalt in the area was observed at the base of the

succession on the Vurhami Stream (Fig. 2.1). Their presence implies that the initial lava erupted into an aqueous environment at this locality. The total absence of pillow basalts higher in the succession and their infrequent occurrence at the base of the SRBF, suggests that water was present only in ephemeral pans or lakes on the underlying sediments, with the bulk of the basalt sequence being erupted sub-aerially.

2.1.3 Internal flow structures

Alternating amygdaloidal and amygdaloidal-free bands on a 5-10 cm scale are often observed and give the weathered surface of a basalt a 'ropy' appearance (Fig. 2.4). It is suggested that these are internal flow structures resulting from the differential small-scale movements of lava within a flow.

2.1.4 Pahoehoe toes.

These are lava 'toes' which project from the edge of an advancing flow and consequently are found predominantly at the base of flows, although successive toes may overide each other. The oxidised material which delineates the margins of these toes may be due either to palaeo-oxidation or to preferential oxidation of a chilled glassy skin by later circulating waters (Fig. 2.5).

2.1.5 Basaltic dykes.

Flow tops often have a preponderance of cross-cutting basaltic dykes (Fig. 2.6). These dykes are distinguished from true dolerite dykes by very irregular development and commonly amygdaloidal margins with no obvious chilling, thereby implying emplacement when the host lava was still hot. MacDonald (1967) has described auto-intrusive dykes in Hawaiian lavas where fluid lava from the central part of a flow is injected into fractures in the solidifying crust and bulges up through the cracks, sometimes spreading out on the former flow surface as pahoehoe toes. This is an attractive explanation for these cross-cutting basaltic features observed in the SRBF and explains their preponderance on and/or in the amygdaloidal upper reaches

(a)

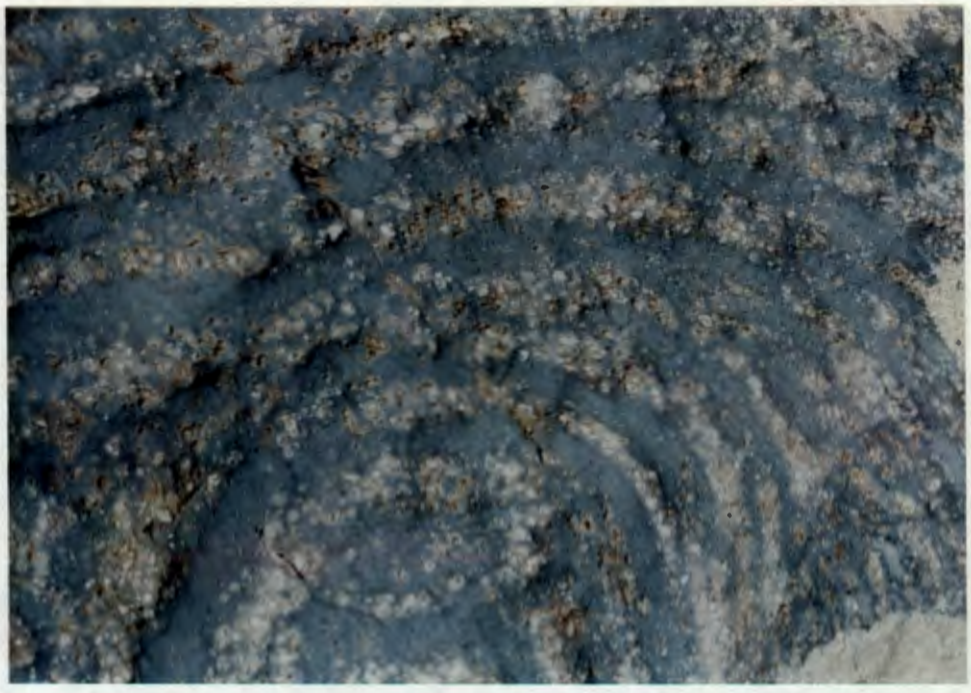

scale 2 cm

(b)

Figure 2.4. Alternating amgdaloidal and amygdale-free zones in some basaltic flows (a) result from small-scale differential movement within a flow and gives outcrops a 'ropy' appearence (b).

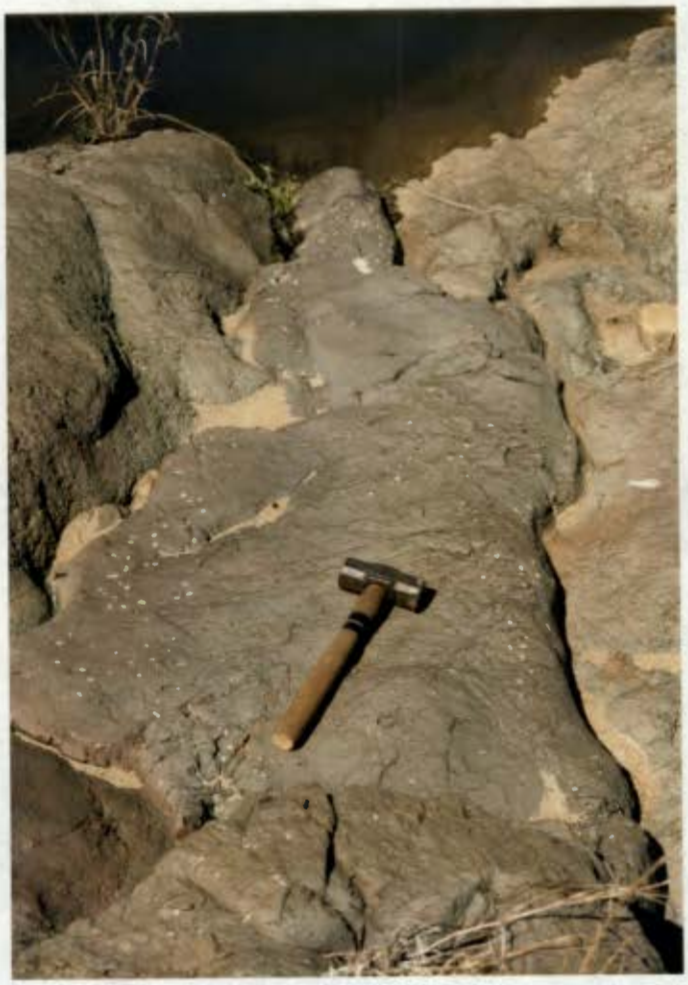

Figure 2.5. Pahoehoe toe on a flow top on the Vurhami Stream.

(a)

(b)

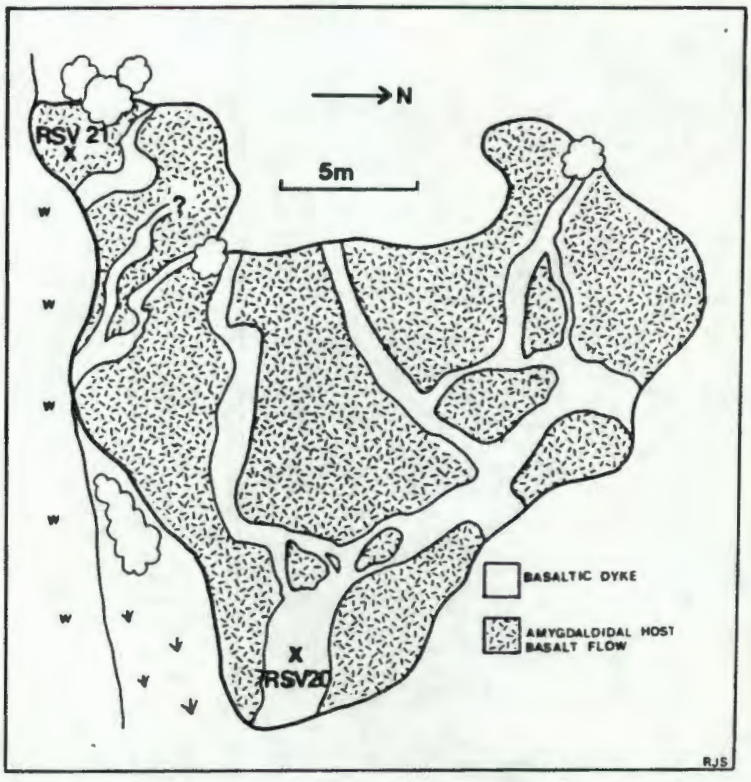

Figure 2.6. Photograph (a) and sketch (b) of a basalt flow on the Vurhami Stream from which samples of a basaltic dyke (RSV20) and the host flow (RSV21) were taken.

Table 2.1. Analyses of basaltic dyke and host-flow samples, samples taken across a flow and samples of a composite dyke and its contact rock. All Fe is reported as Fe_2O_3t.

	RSV18	RSV19	RSV20	RSV21	RSC38	RSC39	RSC40	RSS86	RSS87	RSS88	RSS102	Jozini Rhyolite
%												
SiO_2	51.54	50.73	50.84	53.19	49.72	47.88	49.81	70.07	59.54	48.92	69.58	69.50
TiO_2	2.89	2.84	2.96	2.72	3.71	3.65	3.49	.62	1.84	2.96	.78	.57
Al_2O_3	13.29	12.96	13.48	12.45	12.20	11.93	11.90	12.99	12.95	14.86	11.08	12.89
Fe_2O_3t	11.81	12.11	11.75	11.02	16.53	16.24	16.33	4.49	10.23	14.05	8.05	6.42
MnO	.15	.14	.16	.15	.20	.26	.23	.10	.16	.19	.14	.14
MgO	5.29	5.67	5.30	5.17	3.57	3.95	3.39	.36	2.24	3.03	.51	.55
CaO	9.63	7.20	9.55	7.07	7.21	7.52	7.37	1.65	4.61	7.73	4.15	1.98
Na_2O	1.78	2.75	1.59	2.48	3.03	2.51	2.60	3.32	2.80	2.99	3.49	3.19
K_2O	1.96	2.41	2.11	1.81	1.22	.93	1.54	4.72	3.36	1.66	1.98	4.59
P_2O_5	.47	.46	.48	.41	.84	.82	.91	.15	.55	1.10	.24	.16
H_2O-	.66	.64	.59	.93	.35	.53	.36	.38	.41	.57	-	-
LOI	.88	1.77	1.23	2.07	1.30	2.82	1.50	.74	1.00	1.84	-	-
TOTAL	100.36	99.68	100.04	99.48	99.87	99.05	99.49	99.61	99.68	99.91	100.00	100.00
ppm												
Nb	16.8	15.7	16.7	16.6	37	40	45	91	58	35	65	93
Zr	346	331	355	330	458	443	500	953	680	417	762	1155
Y	37	36	36	36	63	59	69	110	91	64	79	115
Sr	795	1040	741	738	521	219	523	170	315	535	361	184
Rb	32	54	41	37	40	20.0	40	141	92	45	56	133
Ba	653	879	640	858	695	289	738	1500	1055	567	1235	1320
Sc	24	22	24	20	27	31	29	8.9	22	24	9.9	11
La	40	38	40	35	50	49	55	110	78	47	68	-
Ce	84	83	91	80	116	109	126	226	164	109	150	-
Nd	58	61	65	54	80	78	89	131	102	80	98	-
Zn	119	121	126	114	169	164	171	95	122	146	155	124
Cu	50	51	45	50	367	325	443	12.0	90	256	38	13
Ni	121	119	115	93	33	33	16.2	<1.5	12.9	7.1	<1.7	0
Co	51	50	50	46	45	44	40	4.5	23	35	3.6	24
Cr	119	117	119	85	2.9	3.5	<2.4	<1.6	6.6	<2.4	<1.8	11
V	238	215	244	229	286	290	206	4.1	110	135	4.0	6.4

Sample descriptions:

RSV18	:	auto-intrusive dyke in RSV19
RSV19	:	massive basalt
RSV20	:	auto-intrusive dyke in RSV21
RSV21	:	amygdaloidal basalt
RSC38	:	ropy basalt |
RSC39	:	amygdaloidal basalt | flow cross-section
RSC40	:	ropy basalt |
RSS86	:	granophyric dyke - center
RSS87	:	granophyric dyke - margin
RSS88	:	mafic rock at dyke contact
RSS102	:	welded ash-fall tuff (normalized vol. free)
Jozini Rhyolite	:	average from Duncan *et al.* (1984b) for central Lebombo rhyolites (n=2, vol. free).

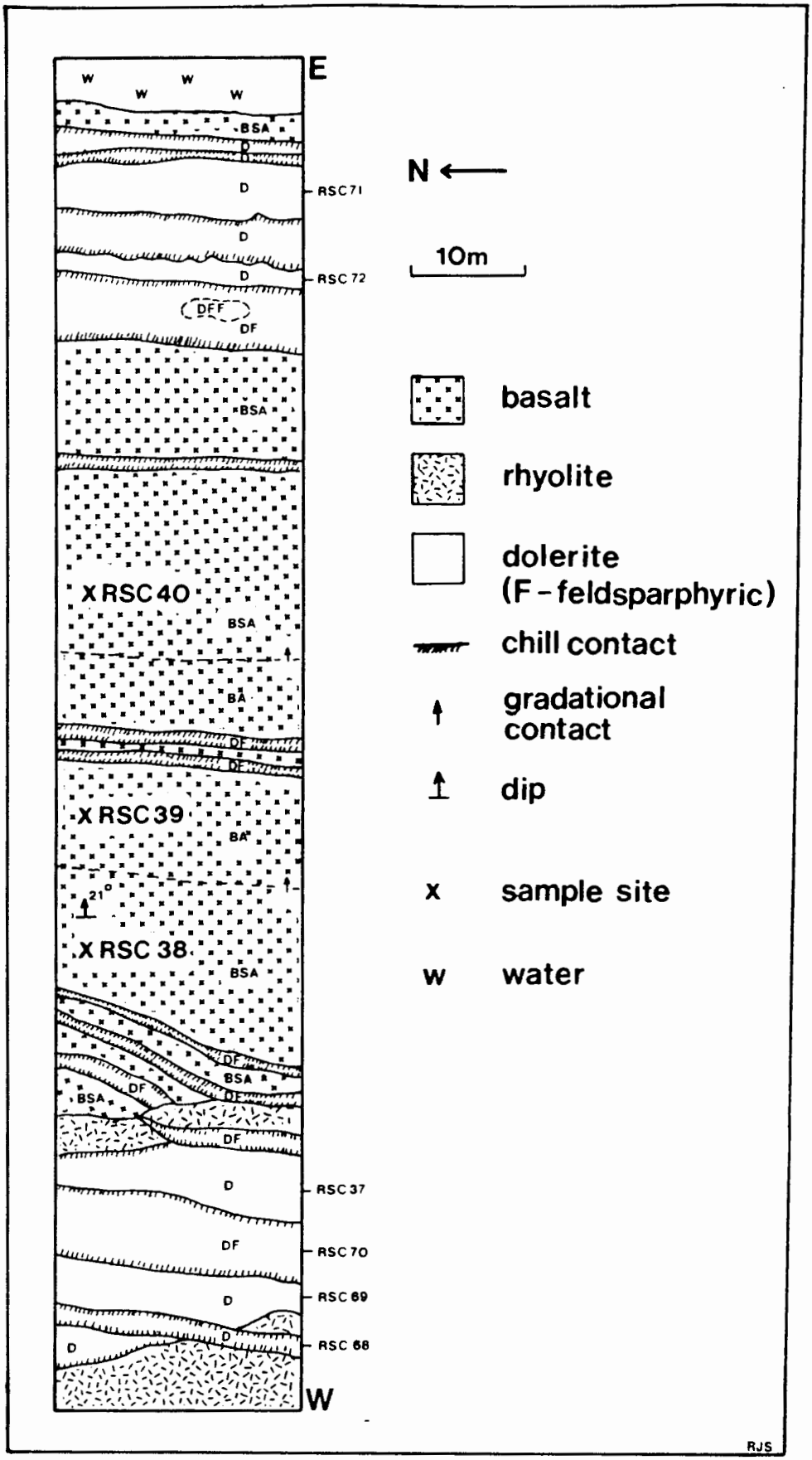

Figure 2.7. Sketch showing the location of samples RSC38, RSC39 and RSC40 taken through a *ca* 20 m thick flow in the Crocodile River section 1 km north-east of Komatipoort (Appendix D).

of a flow. Furthermore, the similarity in immobile element (e.g. Ti, P, Nb, Zr, Y, LREE, Ni and Cr) content between these auto-intrusions and their respective host-basalt supports this explanation (Table 2.1). The host-flows in both instances (RSV19 and RSV21) are more altered relative to the basaltic dykes and the more mobile elements (e.g. K, Rb and Ba) may have been affected by alteration.

2.1.6 "Within-flow" variation

Samples RSC38, RSC39 and RSC40 represent different portions of a single flow about 20 m thick (Fig. 2.7). Within this flow there appears to be a gradation from sparsely amygdaloidal basalt (RSC38) to amygdaloidal basalt (RSC39) and back to sparsely amygdaloidal basalt (RSC40) up-section. RSC38 and RSC40 (sparsely amygdaloidal) are geochemically very similar, whereas RSC39 has a lower K, Na, Ba, Rb and Sr content (Table 2.1). This may be a reflection of a greater degree of leaching of these relatively more mobile elements from the more permeable amygdaloidal part of the flow. To minimize this problem the massive portion of flows was sampled where possible and an attempt was made to exclude amygdaloidal material from the material processed for analysis.

2.2 INTRUSIVE ROCKS

2.2.1 Dolerites

Dolerite dykes are the most common intrusive rock type in the SRBF and are estimated to comprise 10-15% of the river sections considered. No unequivocal examples of dolerite sills were observed within the SRBF in the central Lebombo. The dolerite dykes dip at between 65-85° to the west, i.e. they are approximately perpendicular to the host basaltic strata. The implication is that their intrusion took place before monoclinal warping began. Eales *et al.* (1984) suggested that the Lebombo probably marks the sudden transition from normal continental crust to thinned crust. Further, it is suggested here that the monoclinal structure is tensional in tectonic origin (Wernicke and Burchfiel, 1982) and represents the western margin of a basin to the east, formed with the rifting of Gondwanaland and now filled

with Cretaceous-Tertiary sediments of the Mozambique Plateau. Thus, the generally north-south orientation of the dykes implies crustal extension in an east-west direction. It has been established by many authors (Du Toit, 1929; Cox 1978; Norton and Sclater, 1979; Scrutton *et al.*, 1979) that the breakup of Gondwanaland represents the large scale manifestation of such tensional stress in Jurassic-Cretaceous times in southern Africa. It has been suggested (Watkeys and Sweeney, in prep.) that initial rifting in the Lebombo involved east-west movement which was followed by north-south movement and the eventual separation of Antarctica from the African mainland.

The virtual absence of dolerite dykes in the overlying Jozini Rhyolite in the central Lebombo is the most convincing field evidence relating these dykes to the basalts. Cleverly (1979) notes the rarity of dolerite dykes intruding the rhyolite succession in Swaziland. No volcanic centre associated with the SRBF in the central Lebombo (and the Lebombo generally, Cox and Bristow, 1984) has been identified, which suggests eruption of the basalts from a diffuse series of fissures now represented in the hypabyssal zone by dolerite dykes.

2.2.2 Komatipoort Complex

The Komatipoort Complex is a conformable sheet-like gabbroic body approximately 600 m thick and about 7 km long (N-S dimension) which intrudes the SRBF near Komatipoort (Fig. 2.1) and has been examined in detail by Saggerson and Logan (1970) and Logan (1979). The gabbroic body to the north-east of the main intrusion is considered in this study to represent a separate intrusion and is not part of the main body of the Complex as mapped by Logan (1979). The intrusive nature of the Complex is confirmed by the metamorphism of the adjacent country-rock basalts.

The Complex is divided by Logan (1979) into 4 major roughly concordant units:

(1) olivine gabbro unit (base to *ca* 20 m),
(2) clinopyroxene-plagioclase cumulate gabbro (100-200 m thick),
(3) granophyric gabbro (100-200 m thick) and
(4) feldspathic gabbro (100-200 m thick).

The 150 m thick granophyre sill intrusive into the complex (Logan, 1979) was

not observed by the present author.

The Sr-isotope systematics of this complex were examined by Allsopp *et al.* (1984) and should provide a minimum age for the SRBF. Whether the different units defined by Logan (1979) are considered separately or jointly, only ages in excess of the inferred age of emplacement were obtained (Allsopp *et al.*, 1984). A mixing-line hypothesis, involving isotopically unequilibrated plagioclase xenocrysts and a melt as end-members, is suggested as an explanation by Allsopp *et al.* (1984). Aside from the analysis of two samples from the gabbroic units of the Complex (RSK1 and RSC45), it has not been further investigated in this study.

2.2.3 Felsic dykes

Acid rocks (SiO_2 >65%) intrusive into the SRBF are present as felsic dykes (10-40 m wide) or much larger granophyre bodies, i.e. the Muntshe granophyre intrusion (Fig. 2.1) which forms a prominent hill rising above the basalt plain north of the Sabie River. These larger acid bodies may represent the feeders to the overlying Jozini Rhyolites. Felsic dykes intrude the Sabie River section at least in two localities. One acid dyke in the Crocodile River area (the 'Causeway Granophyre', Fig. 2.1) is traceable along strike (N-S) for about 20 km. As in the case of the dolerites, these dykes dip steeply to the west and are approximately perpendicular to the enclosing strata. One example (RSS86), intrusive into the base of the Jozini Formation in the Sabie River section, is an exception and has an east-west strike and a near vertical dip. Towards the only exposed margin of this dyke mafic xenoliths are observed and grade into a homogeneous mafic zone (RSS87) with the margin represented by a rock of basaltic composition (RSS88, Table 2.1). Another more thoroughly mixed composite dyke was sampled on the Vurhami Stream (RSV8 and RSV8m). Unfortunately no comment can be made on the style of mixing as no mafic end-member was observed in the example on the Sabie River and a felsic end-member was absent in the example on the Vurhami Stream. However, to achieve the degree of mixing observed between silicic and mafic melts in both examples, the intrusion of each end-member must have been almost synchronous.

2.3 VOLCANICLASTIC ROCKS

The distinction between rocks of pyroclastic or sedimentary volcaniclastic origin found to occur within the SRBF in the central Lebombo is often equivocal.

Sediment (RSC7) in-filling the irregular blocky flow top near the base of the Crocodile River section (RSC6) is characterized (Appendix B) by alternating layers of
(1) predominantly feldspar with long acicular needles of an opaque oxide and an interstitial ferruginous cement; and
(2) feldspar and quartz in approximately equal proportions and interstitial ferruginous cement.
It is likely that the quartz-containing layers have a dominant sedimentary volcaniclastic origin. It is difficult, however, to envisage a sedimentary process capable of producing the intercalated bands (*ca* 1 cm thick) composed primarily of feldspar. It is suggested these bands may be reworked air-fall tephra.

A *ca* 4 m thick unit interbedded with the SRBF at the top of the Sabie River section (Appendix D) is interpreted as a high-temperature ash-fall tuff. Petrographically a sample (RSS102, Table 2.1) is composed of: abundant amygdales (mainly quartz-filled), phenocrysts (mainly plagioclase with some pyroxene and opaques) and occasional small (0.5-2 cm) mafic xenoliths in a welded holocrystalline groundmass (Appendix B). Geochemically the sample is acidic and similar to the Jozini Rhyolite in the central Lebombo (Table 2.1).

Despite the difficulty in estimating the proportion of the volcanic component in the sediments developed on flow-tops, it is concluded that volcaniclastic rocks are volumetrically insignificant within the basalt succession.

2.4 SUMMARY

Basaltic rocks are clearly the only volumetrically significant rock-type within the delineated margins of the SRBF (Fig. 2.1). These occur primarily as basalt flows (*ca* 85-90%) with dolerite comprising *ca* 10-15% of the observed exposure, intruding the section as dykes dipping steeply (60-85°)

to the west. Dykes were rarely observed intruding rocks west of the SRBF, infrequently the base of the Jozini Formation to the east and rarely observed further up in this formation. Other intrusive rocks include the gabbroic Komatipoort Complex, relatively thin granophyre dykes and larger acidic intrusions (e.g. the Muntshe Granophyre).

3. GEOCHEMICAL VARIATIONS

3.1 INTRODUCTION

The approach adopted in this section is to characterize geochemically the basaltic rock types of the Sabie River Formation in the central Lebombo. Initially the distinction between rock types is achieved using a set of elements unlikely to be significantly affected by alteration. The distribution of other elements is then considered with respect to the rock types defined. The effect of alteration, particularly on the distribution of the more mobile elements (e.g. K, Rb and Ba) is then considered. Finally isotopic (Sr-, Nd-, Pb- and O-systems) data is presented. All the data referred to in this chapter is given in Appendix C.

This geochemical approach is necessary as initial geochemical data on samples collected from the central Lebombo (Bristow, 1980) revealed no consistent correlation between geochemical composition and the petrography of samples. In addition the stratigraphic distribution of rock types cannot be detailed from this initial sampling and this is one of the questions this thesis will address.

3.2 GEOCHEMICAL DEFINITION OF BASALTIC ROCK TYPES

3.2.1 Rock Types

It is important to stress that all rock-types investigated in this study are tholeiitic, with either quartz or olivine in the CIPW norm. In this study the terms "normal" and "enriched" are used in place of the "southern" and "northern" province respectively, used by Cox *et al.* (1967). The term "normal" (N) is adopted in view of the similarity in incompatible element abundance in the Sabie River Formation basalts to those of the voluminous Lesotho Formation of the Central Area of the Karoo Igneous Province (Marsh and Eales, 1984) and continental flood basalts (CFB's) in general (i.e. Parana - Bellieni *et al.*, 1984a, 1984b; Columbia River - Carlson *et al.*, 1981, Prestvik and Goles, 1985; Deccan - Mahoney *et al.*, 1982, Cox and Hawkesworth, 1985; and a summary of continental volcanism in Dupuy

and Dostal, 1984).

Cox and Bristow (1984) recognized a low-K ("normal") lineage and an intermediate and high-K ("enriched") lineage in the SRBF and included K, Ti, P, Zr, Ba and Sr in their set of elements showing distinct differences in abundance between these lineages. In this study "enriched" rock types are identified by Zr contents >250 ppm and TiO_2 >2.5% with "normal"-types (N) containing Zr <270 ppm and TiO_2 <2.7% (Fig. 3.1a). Immediately apparent is the bimodality in the "enriched" group with respect to MgO and Fe_2O_3t (total Fe expressed as Fe_2O_3) contents (Fig. 3.1b). The one group is characterized by much higher Fe_2O_3t (>14.5%) and lower MgO (generally <5%) contents and is called the high-Fe "enriched" (HFE) group or type. The other is called the low-Fe "enriched" (LFE) group or type with Fe_2O_3t <13.5% and MgO generally >5% (Fig. 3.1c). All three groups have distinctively different Zr/Y ratios (Fig. 3.1d).

Thus the elements which most consistently discriminate between the three rock-types are Zr, Ti and Fe, all of which were determined by the semi-quantitative slab technique (Appendix A) on virtually every sample collected. Where a sample may be unambiguously classified with one of the geochemically defined groups, this classification is given in the sample descriptions for the slab data (on microfiche, Appendix C). All the samples analysed quantitatively are classified with one of the three rock types defined (Fig. 3.1).

Although some samples of the HFE-type were previously analysed (CL105 and CL115; Bristow, 1980) these were not recognized as a distinct rock type and were included (Cox and Bristow, 1984; Duncan *et al.* 1984b) in the "enriched" group as typified by N. Lebombo and Nuanetsi low-MgO samples (the LFE-group here). The HFE-type is not currently recognized in any other part of the Karoo Igneous Province and may be unique to the central Lebombo.

Based on experience, the set of elements offering the best distinction between the "normal" and "enriched" types comprises Ti, P, Zr, Nb, Y and LREE. The greater susceptibility of elements such as K, Ba and Rb to movement as a consequence of processes such as alteration prompts their exclusion from this set. The term 'high field strength elements' (HFSE) is used to collectively describe the set of discriminating elements above, rather than the term 'incompatible elements' which would include K, Rb and

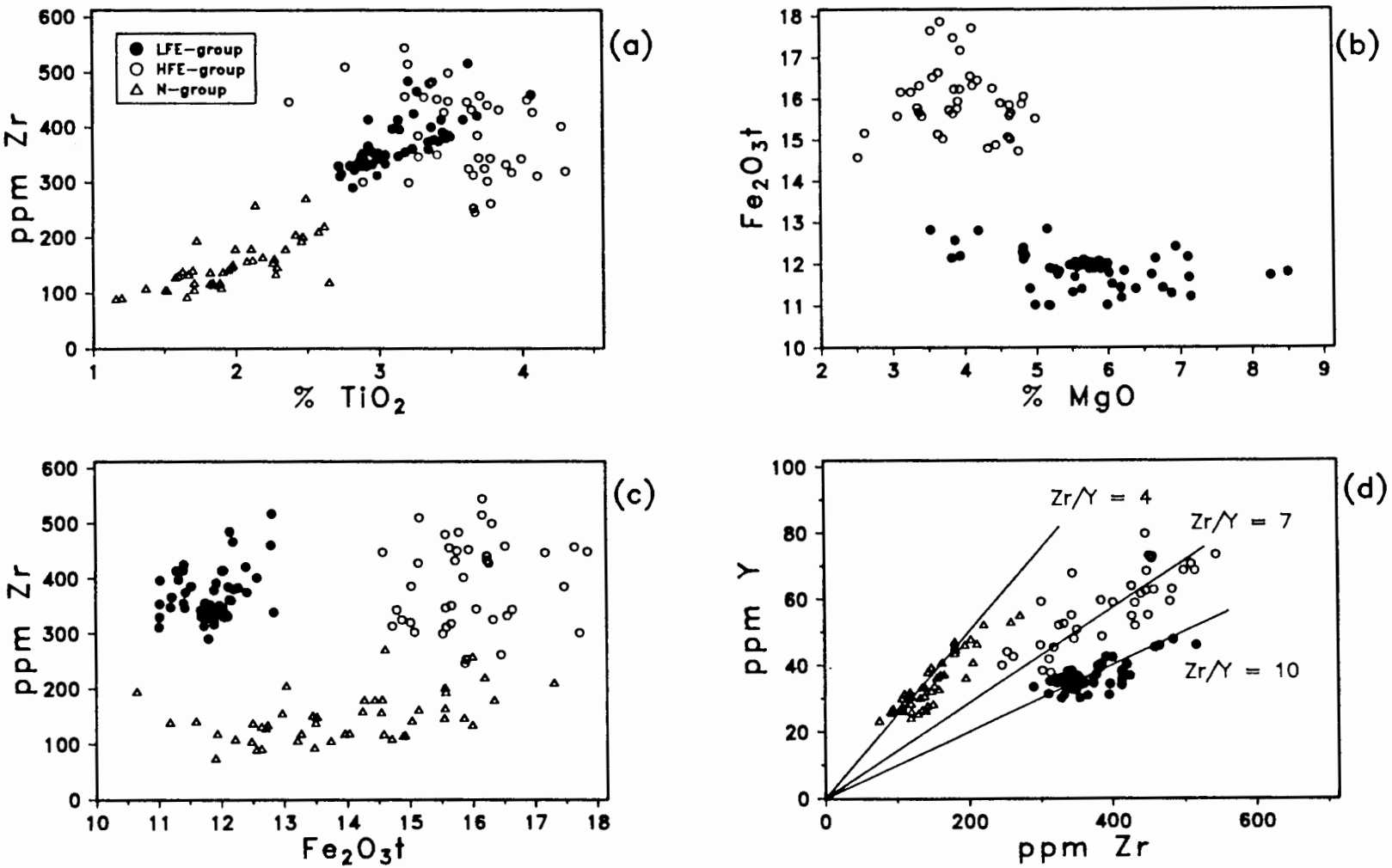

Figure 3.1. Geochemical discrimination between the "enriched" groups and the "normal" group (a); the low-Fe and high-Fe "enriched" groups (b) and all three groups (c and d). Basalt and dolerite (n=119) data are plotted. Data are unnormalized with Fe as Fe_2O_3.

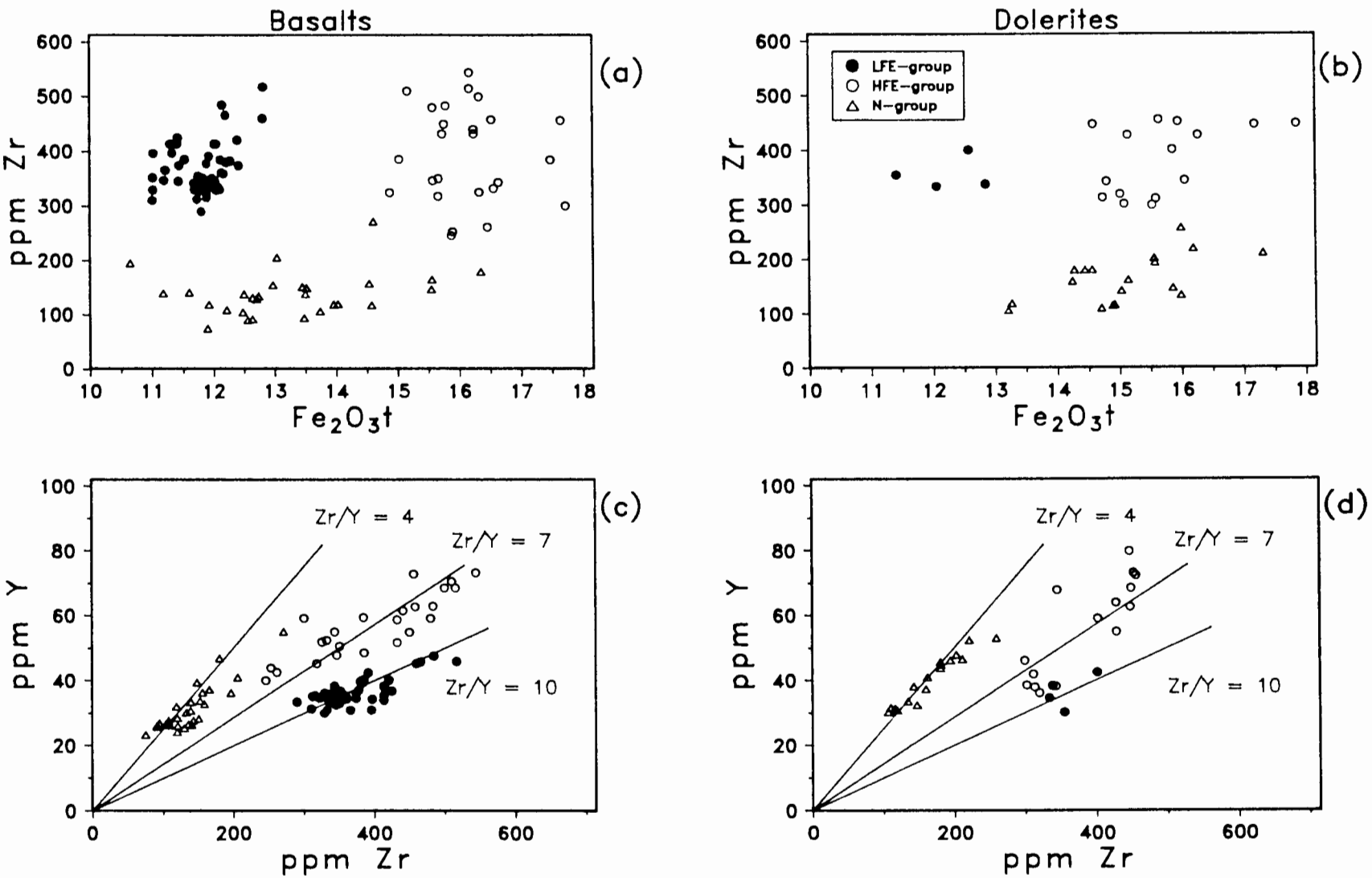

Figure 3.2. Basalt (a and c) and dolerite (b and d) data for the three groups are plotted separately on geochemical discrimination diagrams. Data are unnormalized with Fe as Fe_2O_3.

Ba. The field strength of an element is a measure of the ionic charge/ionic radius ratio of the most stable oxidation state. Therefore, elements such as V, Ni, Cr, Sc, Co, Zn, Cu, U and Th could also be described as HFSE. However, the term is used here in a selective fashion, to include only those minor and trace HFSE which show consistent differences in concentration between the "normal" and "enriched" types and are above XRF detection limits (Appendix A). Averages and ranges of compositions for the three rock types are given in Table 3.1.

3.2.2 Dolerite/basalt comparison

Dolerites and basalts have both been included on the discrimination diagrams shown in Fig. 3.1, but when considered separately, occupy fields similar to those on Fig. 3.1 for the three groups (Fig. 3.2). Thus each basalt group appears to be represented by dolerite dykes of similar geochemistry. The relative abundance of dolerite dykes in the basalt section (10-15% of the section) and the virtual absence of such dykes in the overlying Jozini Rhyolite in the central Lebombo (Chapter 2) imply that these dykes were feeders to the SRBF. These dykes are also somewhat different in composition to the Rooi Rand dolerite swarm further south (see Duncan *et al.*, 1984b, for a comparison of Rooi Rand and southern Lebombo or "normal" basaltic types).

3.2.3 Normative mineralogy

As stated previously all the basalt types in this study are typically tholeiitic with respect to their normative mineralogy. The calculation of CIPW norms enables a comparison between extrusive (sometimes glassy) basalts and intrusive (more coarse-grained) dolerites of the geochemically defined rock types. Most samples of the LFE and HFE groups have small amounts of quartz (<5%) in their norm (silica oversaturated) and only occasionally small amounts of olivine (<10%, silica saturated). Samples of the N group are evenly divided between quartz and olivine normative varieties.

3.3 MAJOR AND TRACE ELEMENT VARIATIONS

3.3.1 Variation diagrams

Data for basaltic rocks plotted in Fig. 3.3 are reported in Table C1 (Appendix C) and is the same data set used to compute the averages and ranges given in Table 3.1. All data is plotted *vs* MgO.

SiO_2 contents in the HFE and N groups increase with decreasing MgO. Al_2O_3 is negatively correlated with MgO for the LFE group and positively correlated with MgO for the HFE and N groups together (Fig. 3.3c). As well as the obvious differences in Fe_2O_3t content between HFE and LFE groups, the considerable range in Fe_2O_3t content of N group basaltic rocks should be noted. CaO decreases with decreasing MgO for all groups, although the LFE group has consistently lower and more diverse concentrations (Fig. 3.3e).

With the exception of Y, the HFSE (Ti, P, Zr, Nb, La, Ce, Nd) have greater concentrations in the LFE group relative to N group samples. The Y contents of "primitive" N-group samples are initially lower than concentrations in LFE-group samples of a similar MgO, content but in some samples increases more rapidly with decreasing MgO than the LFE group, finally reaching higher concentration levels (Fig. 3.3k). There is, however, a spread of Y abundances (30-50 ppm) in evolved N-group samples (Fig. 3.3k). The greater range of concentrations in the N group relative to the LFE group over a similar range in MgO content (7-5% MgO), is characteristic of the HFSE in general. The HFE group, however, is characterized by even greater HFSE concentration ranges for a 2% MgO range than either the LFE or N groups. The HFE group not only reaches greater levels of HFSE content than the LFE group, but the trend of the HFE group "straddles" that of the LFE group for some of the HFSE (Ti, Zr, La, Ce and Nd). This is important since it provides evidence against the HFE group being related to the LFE group by a continuous liquid-line-of-descent. In contrast, when the N and HFE groups are considered jointly, the HFSE (with the exception of Y) describe a continuous increasing trend with decreasing MgO. An exception to this are three N-group samples with MgO <4% which are distinguished from the remainder of the group by their highly plagioclase-phyric nature (>30 % plagioclase phenocrysts and 70-80% total plagioclase in the mode). Obviously the presence of a much greater modal abundance of plagioclase will affect whole-rock chemistry significantly. Furthermore, it is unlikely that such a proportion of plagioclase crystals grew in-situ; rather a cumulate origin is

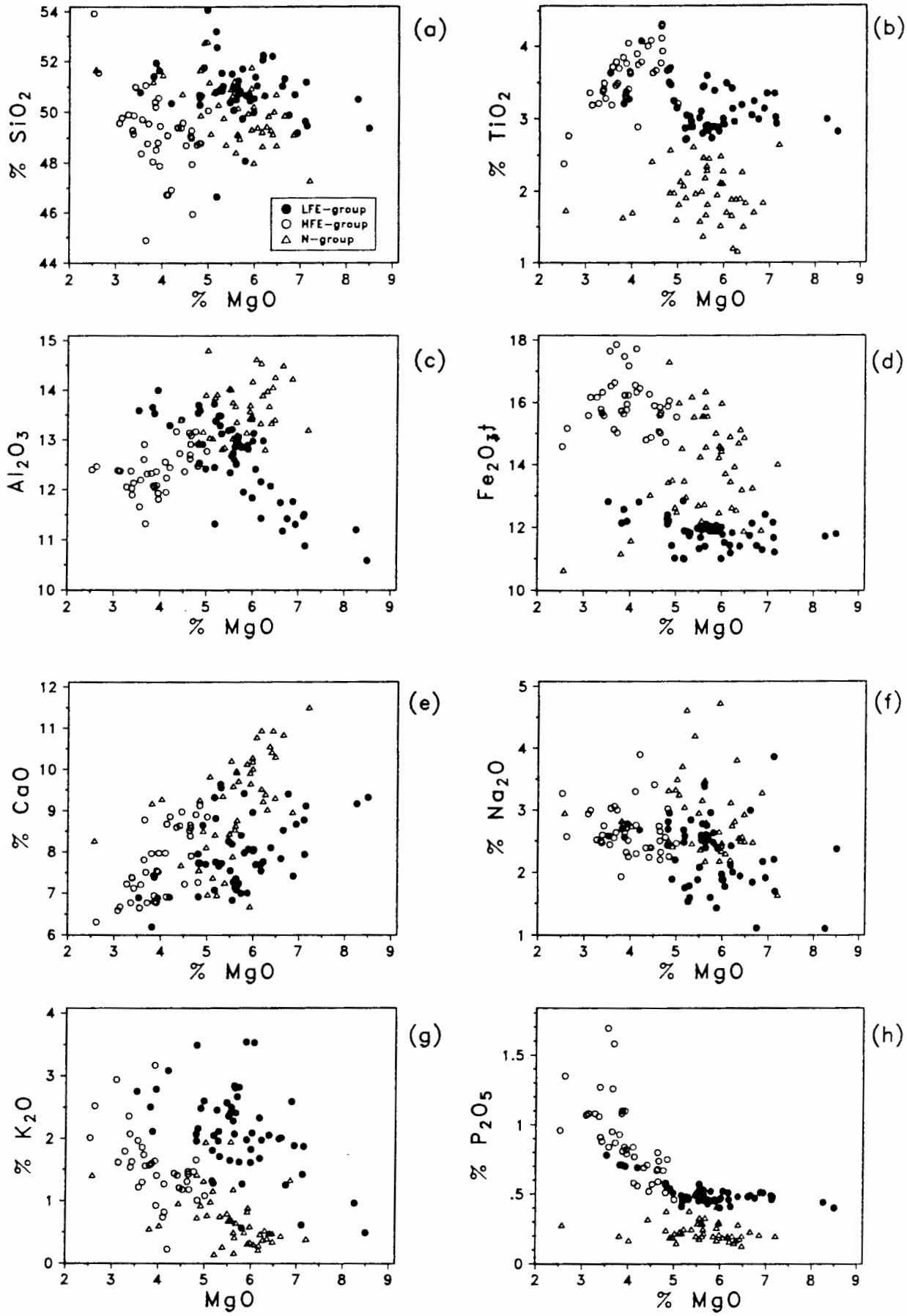

Figure 3.3. Variation diagrams: data (n=140) for selected elements are plotted *vs* MgO. REE data plotted are XRF data and Th and Pb data include only precise XRF determinations carried out on the sample set analysed for their Sr-isotope content. Data are unnormalized with Fe as Fe_2O_3.

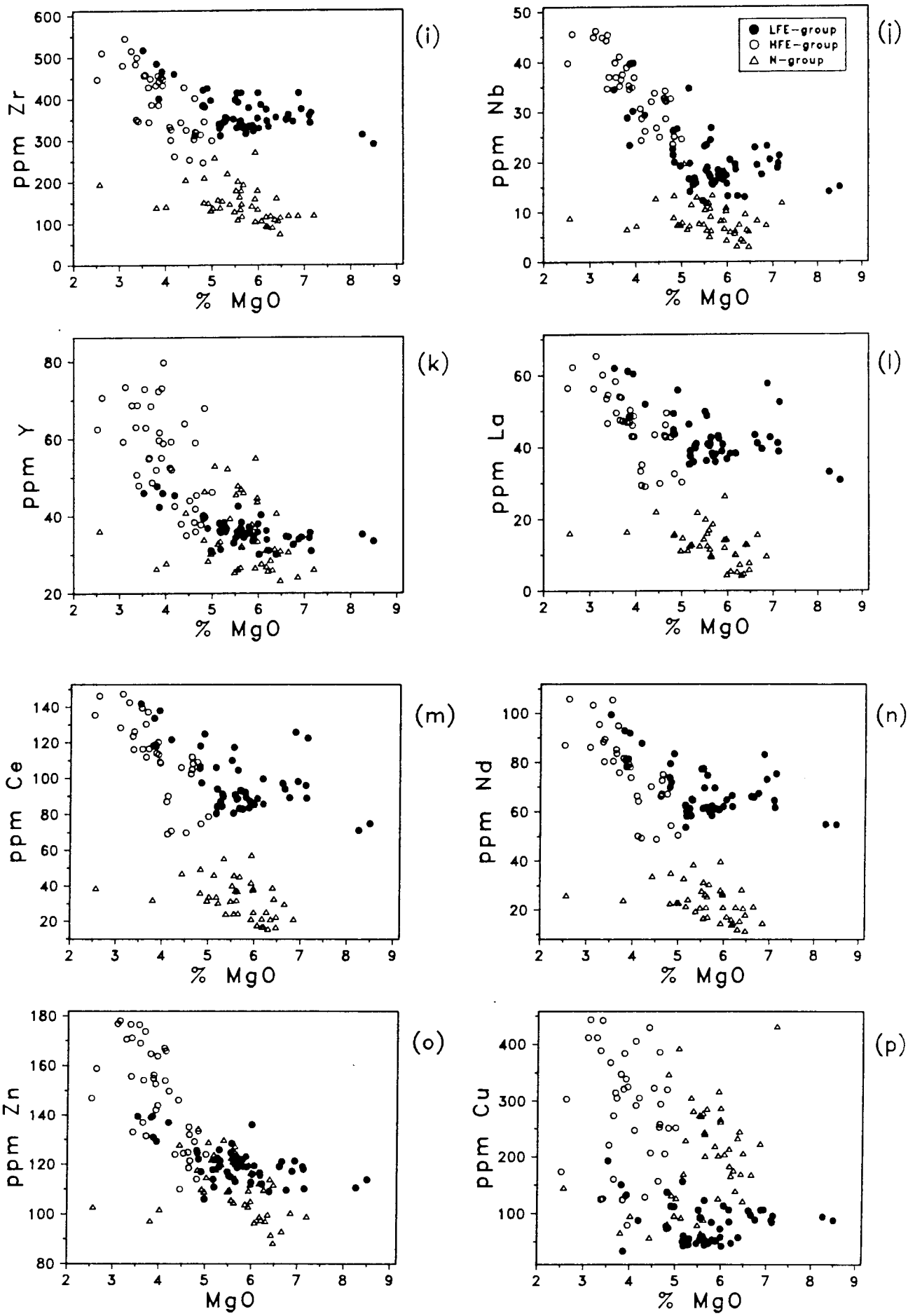
(i)
ppm Zr
% MgO
(j)
ppm Nb
% MgO
LFE-group
HFE-group
N-group
(k)
ppm Y
% MgO
(l)
ppm La
% MgO
(m)
ppm Ce
% MgO
(n)
ppm Nd
% MgO
(o)
ppm Zn
MgO
(p)
ppm Cu
% MgO

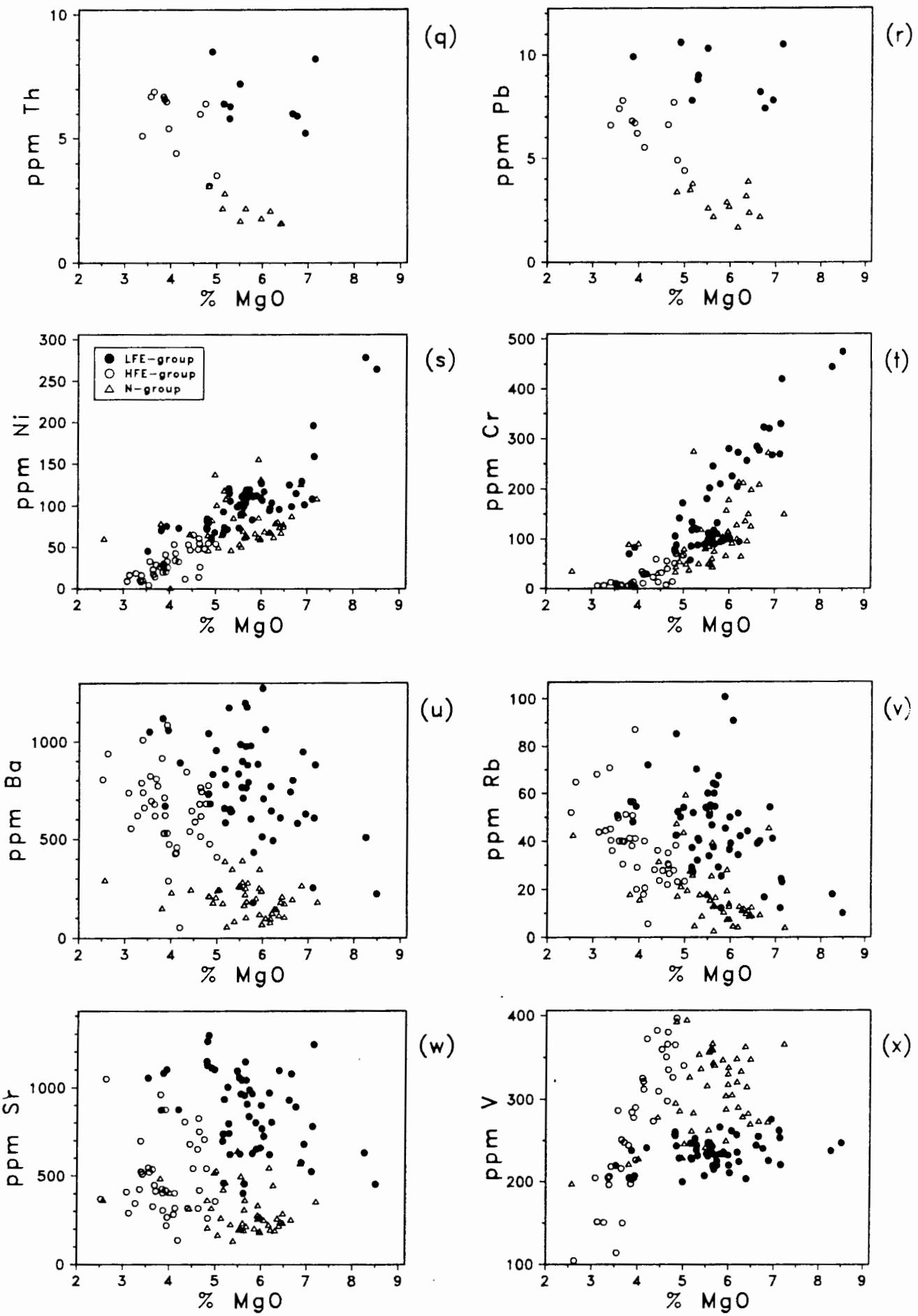
(q)
ppm Th
% MgO
(r)
ppm Pb
% MgO
(s)
LFE-group
HFE-group
N-group
ppm Ni
% MgO
(t)
ppm Cr
% MgO
(u)
ppm Ba
% MgO
(v)
ppm Rb
% MgO
(w)
ppm Sr
% MgO
(x)
ppm V
% MgO

Table 3.1. Ranges, means and standard deviations for data obtained by XRF for the three basaltic groups. Data is unnormalized with Fe reported as total Fe_2O_3 (given in Table C1, Appendix C).

LFE-group:

	basalts					dolerites					all				
	min.	max.	mean	sd	n	min.	max.	mean	sd	n	min.	max.	mean	sd	n
%															
SiO_2	46.65	54.06	50.77	1.15	50	50.77	52.19	51.43	.74	4	46.65	54.06	50.82	1.13	54
TiO_2	2.72	4.07	3.13	.30	50	2.87	3.37	3.08	.24	4	2.72	4.07	3.12	.29	54
Al_2O_3	10.59	14.00	12.58	.85	50	12.07	13.72	13.09	.74	4	10.59	14.00	12.61	.84	54
Fe_2O_3t	11.01	12.82	11.83	.42	50	11.41	12.85	12.23	.64	4	11.01	12.82	11.86	.44	54
MnO	.13	.17	.15	.01	50	.15	.18	.16	.02	4	.13	.17	.15	.01	54
MgO	3.53	8.50	5.74	.98	50	3.87	6.39	5.28	1.06	4	3.53	8.50	5.70	.98	54
CaO	6.19	9.63	7.91	.83	50	7.24	9.31	8.01	.94	4	6.19	9.63	7.91	.83	54
Na_2O	1.10	3.85	2.29	.55	50	1.94	2.68	2.43	.33	4	1.10	3.85	2.30	.54	54
K_2O	.49	3.54	2.10	.69	50	1.32	2.67	2.04	.55	4	.49	3.54	2.10	.68	54
P_2O_5	.40	.78	.50	.08	50	.45	.71	.53	.12	4	.40	.78	.50	.08	54
ppm															
Nb	12.3	34	19.7	4.8	50	13.0	35	22	9.8	4	12.3	35	19.8	5.2	54
Zr	290	517	368	47	50	334	401	357	31	4	290	517	367	46	54
Y	30	48	36	3.9	50	30	42	36	5.3	4	30	48	36	4.0	54
Sr	402	1290	862	230	50	697	1095	945	186	4	402	1290	868	227	54
Rb	10.0	101	46	19.1	50	29	63	46	14.1	4	10.0	101	46	18.7	54
Th	5.2	8.5	6.6	1.2	8	6.4	6.6	6.5	.1	2	5.2	8.5	6.6	1.1	10
Pb	7.4	10.6	9.1	1.3	8	7.8	9.9	8.9	1.5	2	7.4	10.6	9.0	1.2	10
Ba	179	2105	808	309	50	608	789	681	77	4	179	2105	798	299	54
Sc	16.9	30	23	2.6	50	18.9	24	22	2.5	4	16.9	30	23	2.6	54
La	31	62	43	7.5	44	37	49	44	5.9	3	31	62	43	7.3	47
Ce	71	142	98	17.2	44	93	118	106	12.4	3	71	142	98	17.0	47
Nd	54	99	68	10.8	44	60	78	67	9.9	3	54	99	68	10.6	47
Zn	106	139	120	7.2	50	109	131	119	9.0	4	106	139	120	7.3	54
Cu	42	193	81	33	50	33	156	74	56	4	33	193	80	34	54
Ni	45	278	107	42	50	26	110	75	37	4	27	278	105	42	54
Co	39	56	48	3.9	50	42	49	46	3.6	4	39	56	47	3.9	54
Cr	10	474	168	107	50	4.5	256	102	109	4	4.5	474	163	108	54
V	200	276	236	17	50	203	246	230	18.8	4	200	276	235	17	54

/Table 3.1

HFE-group:

	basalts					dolerites					all				
	min.	max.	mean	sd	n	min.	max.	mean	sd	n	min.	max.	mean	sd	n
%															
SiO_2	44.89	51.55	48.74	1.55	25	47.95	53.92	49.72	1.42	15	44.89	53.92	49.11	1.56	40
TiO_2	2.77	4.04	3.53	.32	25	2.38	4.31	3.65	.49	15	2.38	4.31	3.58	.39	40
Al_2O_3	11.66	13.41	12.33	.38	25	11.33	13.17	12.54	.52	15	11.33	13.41	12.41	.45	40
Fe_2O_3t	14.88	17.72	16.13	.73	25	14.58	17.86	15.69	.91	15	14.58	17.86	15.96	.82	40
MnO	.18	.26	.21	.02	25	.20	.27	.23	.02	15	.18	.27	.22	.02	40
MgO	2.62	4.81	3.78	.53	25	2.52	5.00	4.23	.65	15	2.52	5.00	3.95	.61	40
CaO	6.31	8.97	7.38	.77	25	5.86	9.12	8.16	.83	15	5.86	9.12	7.67	.87	40
Na_2O	1.93	3.89	2.74	.42	25	2.20	3.27	2.54	.28	15	1.93	3.89	2.67	.38	40
K_2O	.23	3.17	1.63	.68	25	1.01	2.01	1.49	.26	15	.23	3.17	1.58	.56	40
P_2O_5	.51	1.69	.92	.28	25	.46	1.58	.83	.27	15	.46	1.69	.89	.28	40
ppm															
Nb	24	46	36	7.3	25	25	41	33	4.7	15	24	46	35	6.5	40
Zr	246	545	395	88	25	300	456	383	64	15	246	545	391	80	40
Y	35	73	56	10.5	25	36	80	56	15.1	15	35	80	56	12.2	40
Sr	136	1050	486	224	25	261	824	497	200	15	136	1050	490	213	40
Rb	5.5	87	42	18.6	25	22	52	33	8.3	15	5.5	87	38	16.0	40
Th	4.4	6.7	5.7	1.1	4	3.1	6.9	5.4	1.5	7	3.1	6.9	5.5	1.3	11
Pb	5.5	7.4	6.6	.8	4	4.4	7.8	6.3	1.3	7	4.4	7.8	6.4	1.1	11
Ba	53	1085	667	224	25	408	845	623	140	15	53	1085	651	196	40
Sc	21	36	27	3.4	25	18.7	42	29	5.9	15	18.7	42	28	4.5	40
La	29	65	47	10.6	22	30	56	45	7.6	13	29	65	46	9.5	35
Ce	69	147	113	23	22	75	137	110	18.8	13	69	147	112	21	35
Nd	49	106	80	16.3	22	51	95	73	12.6	13	49	106	77	15.2	35
Zn	110	178	154	20	25	119	174	137	13.5	15	110	178	148	19.8	40
Cu	125	444	313	91	25	79	430	228	99	15	79	444	281	102	40
Ni	4.3	72	29	17.8	25	11.9	61	36	18.7	15	4.3	72	32	18.2	40
Co	34	52	43	4.8	25	31	50	42	5.2	15	30	52	43	4.9	40
Cr	2.9	51	16	14.1	25	3.0	71	35	27	15	2.9	71	23	21.8	40
V	104	372	253	77	25	96	397	280	94	15	96	397	263	83	40

/Table 3.1

N-group:

	basalts					dolerites					all				
	min.	max.	mean	sd	n	min.	max.	mean	sd	n	min.	max.	mean	sd	n
%															
SiO_2	47.30	52.78	50.35	1.33	28	48.00	50.95	49.67	.73	18	47.30	52.78	50.09	1.17	46
TiO_2	.99	2.65	1.83	.40	28	1.51	2.62	2.12	.30	18	.99	2.65	1.94	.39	46
Al_2O_3	12.60	17.26	13.99	1.21	28	12.53	14.49	13.43	.50	18	12.53	17.26	13.77	1.03	46
Fe_2O_3t	10.65	16.35	13.24	1.34	28	13.21	17.31	15.06	1.03	18	10.65	17.31	13.95	1.51	46
MnO	.12	.24	.17	.03	28	.19	.25	.22	.02	18	.12	.25	.19	.03	46
MgO	2.57	7.21	5.45	.96	28	4.84	6.66	5.88	.50	18	2.57	7.21	5.62	.83	46
CaO	6.68	11.50	8.63	1.14	28	9.26	10.94	10.13	.49	18	6.68	11.50	9.22	1.19	46
Na_2O	1.63	4.73	3.10	.71	28	2.20	3.25	2.51	.21	18	1.63	4.73	2.87	.64	46
K_2O	.15	1.95	.81	.50	28	.17	.83	.54	.19	18	.15	1.95	.70	.43	46
P_2O_5	.13	.41	.22	.06	28	.15	.38	.26	.07	18	.13	.41	.23	.06	46
ppm															
Nb	3.0	18.4	8.0	3.2	28	4.1	19.7	9.7	3.8	18	3.0	19.7	8.6	3.5	46
Zr	75	272	139	40	28	107	259	164	44	18	75	272	149	43	46
Y	23	55	32	7.4	28	30	53	40	7.9	18	23	55	35	8.5	46
Sr	133	642	370	134	28	167	309	230	39	18	133	642	315	127	46
Rb	4.0	59	23	16.2	28	2.7	19.7	12.5	5.1	18	2.7	59	19.1	14.0	46
Th	2.1	2.8	2.4	.4	3	1.6	3.1	2.0	.5	10	1.6	3.1	2.1	.5	13
Pb	1.7	3.8	3.0	1.1	3	1.7	3.9	2.7	.7	10	1.7	3.9	2.8	.7	13
Ba	57	393	203	86	28	70	350	202	79	18	57	393	202	82	46
Sc	18.4	45	29	7.6	28	28	43	38	3.9	18	18.4	45	33	7.7	46
La	4.3	26	12.5	5.1	24	4.5	22	13.3	5.2	16	4.3	26	12.8	5.1	40
Ce	15.6	57	30	10.8	24	21	55	36	10.4	16	15.6	57	32	11.0	40
Nd	11.4	40	21	7.1	24	15.4	39	26	6.6	16	11.4	40	23	7.2	40
Zn	88	130	110	11.0	28	92	134	113	12.1	18	88	134	111	11.4	40
Cu	58	432	165	88	28	169	393	255	58	18	58	432	200	89	40
Ni	<2.5	156	84	30	28	47	132	85	19.9	18	<2.5	156	78	27	40
Co	35	58	51	4.3	28	47	58	50	3.2	18	35	58	51	3.9	40
Cr	32	276	107	70	28	45	210	104	46.6	18	32	276	106	61	40
V	198	367	285	46	28	273	395	338	32.5	18	198	395	306	48	40

suggested in which instance these samples cannot represent a liquid-line-of-descent from the remainder of the N group.

More precise Th and Pb data were obtained using XRF techniques (Appendix A) for the sample set analysed for Sr- isotope compositions, and these data are plotted in Fig. 3.3q and r. Th and Pb also show consistent differences between the basaltic groups. Increasing concentration levels with decreasing MgO content are observed for the HFE and N groups together while concentrations in the LFE group are greater and more scattered than those in the N group.

Ni, Cr and Co (not shown) contents in all three groups decrease consistently with decreasing MgO (Fig. 3.3s, t). V in the HFE group decreases dramatically (400 to 100 ppm) within a relatively small MgO range (5-3% MgO). The LFE group, however, shows only a slight decrease in V content with decreasing MgO. The distribution of V with MgO within the N group is not systematic and concentration levels are generally greater than those of the LFE group.

The similar chemical characteristics of K, Rb and Ba are reflected by their similar distribution in the three groups (Fig. 3.3g, u, v). The large ionic radii (>1.3A) and a strong affinity for oxygen gives them the name 'large-ion-lithophile elements' (LILE). These elements have generally greater concentrations in the LFE and HFE groups relative to the N group, although the spread of data in all groups is considerable.

The LFE group has both a considerable range in Sr contents and an apparently random distribution of this element with MgO (Fig. 3.3w). The majority of N- and HFE-group samples have Sr contents in the range 200-700 ppm with means of 315 ppm and 490 ppm respectively (Table 3.1), which is higher than usual for continental flood basalts in general (e.g. Lesotho Formation has a mean Sr content of 192 ppm, Duncan *et al.* 1984b).

3.3.2 Rare earth elements

REE data for La, Ce and Nd was obtained on the entire sample set by XRF spectrometry. More complete REE analyses (by spark-source mass spectrography - SSMS) of a relatively "evolved" and an "unevolved" basalt from each group, are depicted in Fig. 3.4a. In Fig. 3.4b the fields for each group are

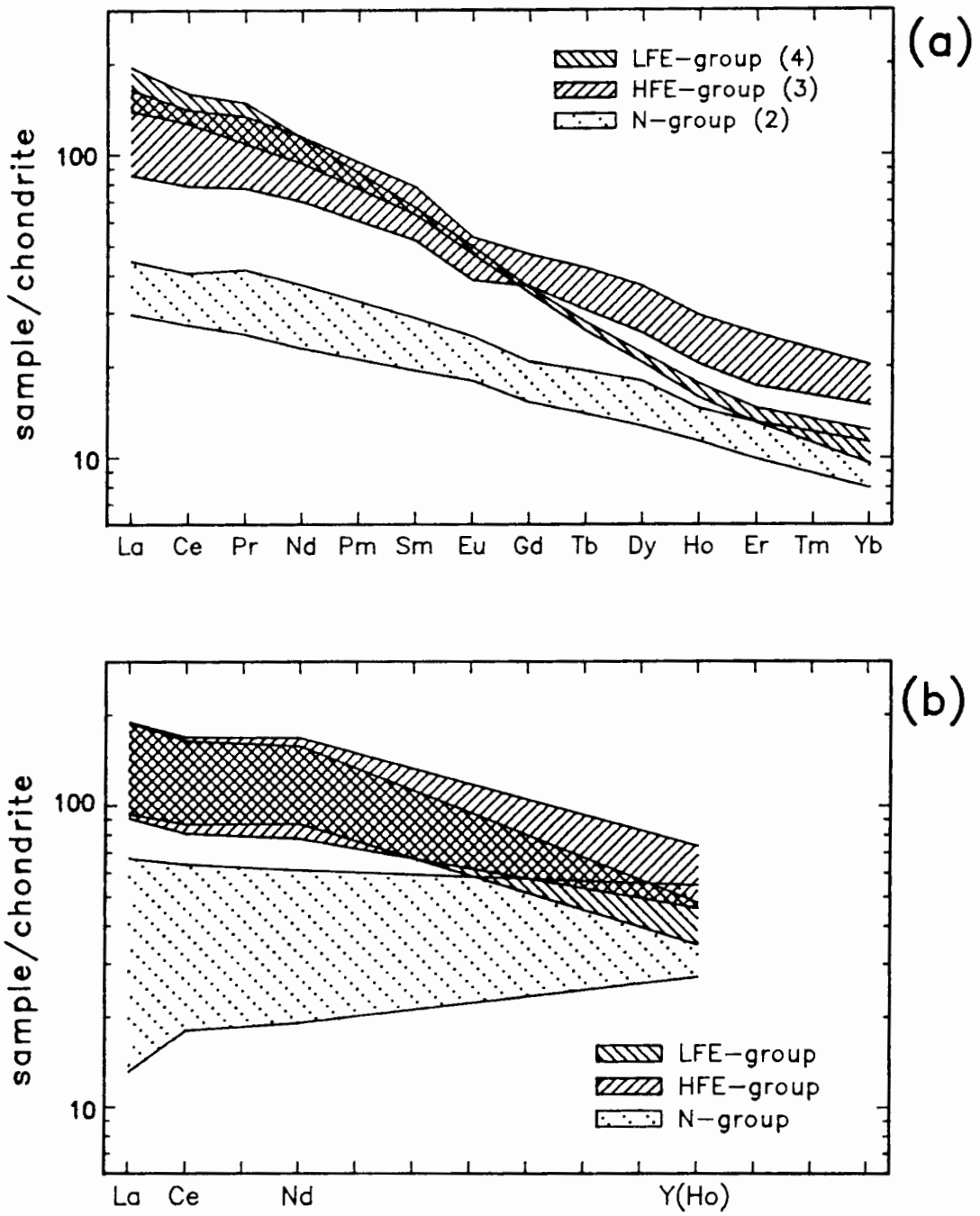

Figure 3.4. (a) REE spark source data (SSMS, number of determinations are given in brackets) includes samples (prefexed 'CL') reported in Duncan *et al.* (1984a);
(b) REE range for all sample data (determined by XRF). Chondrite normalizing values are: La .328, Ce .865, Pr .123, Nd .63, Sm .203, Eu .077, Gd .276, Tb .052, Dy .343, Ho .078, Er .225, Tm .034 and Yb .220 (Nakamura, 1978, and Frey *et al.* 1968). The chondrite normalizing value for Y is 1.96 (Haskin *et al.*, 1968).

defined by XRF data for La, Ce, Nd and Y (plotted in place of Ho on ionic radius criteria, Eby, 1975). The substitution of Y for Ho to approximate HREE behaviour does, however, indicate greater levels of HREE enrichment than is suggested by Fig. 3.4a. Despite this approximation the relative positions of each group in Fig. 3.4a are preserved. Generally, therefore, the N and LFE groups differ by their degree of LREE enrichment. The HFE group, however, has significantly flatter patterns relative to the LFE group and differs from both the LFE and N groups by greater HREE concentrations.

3.3.3 Post-extrusion (sub-solidus) alteration

The effects of alteration on whole-rock geochemistry is considered. Two approaches are used:
(1) an application of an index of alteration (Nesbitt and Young, 1982) attempts to evaluate the degree of alteration based on the major element content of a sample and
(2) a comparison of data from relatively unaltered samples, selected by observation of thin-sections, with the remainder of the data set.

Nesbitt and Young (1982) have proposed a chemical index of alteration (CIA) using molecular proportions:

$$CIA = [Al_2O_3/(Al_2O_3 + CaO^* + Na_2O + K_2O)] \times 100$$

where CaO^* is the amount of CaO incorporated in the silicate fraction of the rock. A correction is made for the apatite content but not the carbonate content as CO_2 has not been determined in these rocks. CIA values for unaltered plagioclase, augite and magnetite/ilmenite are approximately 50, 6 and 100 respectively. Consequently fresh basaltic rocks have values between 30-45 with alteration causing an increase in the CIA value. Fig. 3.5a shows that all the basaltic analyses obtained in this study fall in the range 34-45. Unfortunately in this instance, the CIA index is also a fractionation index, and increases with decreasing MgO. Thus it is not particularly useful for detecting subtle alteration effects. Furthermore, the broad positive correlation of Rb with CIA (Fig. 3.5b) is not expected if it is assumed that this mobile element is lost due to post-eruptive alteration. Values for the CIA index of about 60 have been obtained for soil developed on the basalts (LFE-group) about 80 km north of the Sabie River just east of Satara (Table

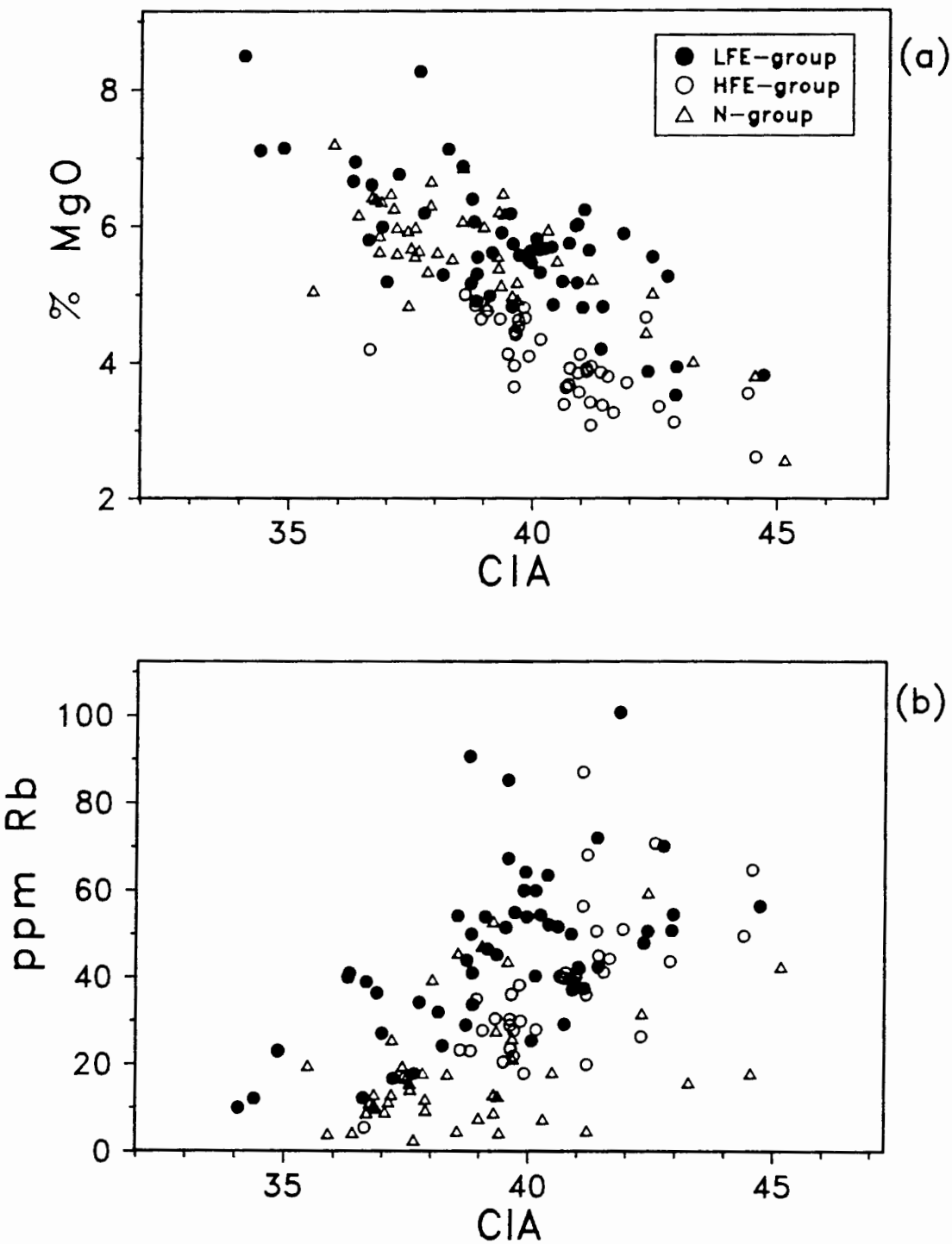

Figure 3.5. Calculated index of alteration (CIA, defined in the text) *vs* MgO (a) and Rb (b) for all basaltic samples (n=140). Data are unnormalized.

Table 3.2. Ranges, means and standard deviations for the LFE-group in the central Lebombo (Table 3.1) and soils data from the Satara area of the Kruger National Park (M. K. Watkeys, pers. comm., 1985; Appendix C). Data is unormalized and total Fe is given as Fe_2O_3.

	LFE-group					Satara soils				
	min.	max.	mean	sd	n	min.	max.	mean	sd	n
%										
SiO_2	46.65	54.06	50.82	1.13	54	48.46	52.32	50.66	1.42	8
TiO_2	2.72	4.07	3.12	.29	54	4.58	5.52	4.97	.33	8
Al_2O_3	10.59	14.00	12.61	.84	54	12.02	12.68	12.39	.22	8
Fe_2O_3t	11.01	12.82	11.86	.44	54	11.58	12.24	11.89	.23	8
MnO	.13	.17	.15	.01	54	.15	.17	.16	.01	8
MgO	3.53	8.50	5.70	.98	54	1.25	1.67	1.46	.17	8
CaO	6.19	9.63	7.91	.83	54	2.06	3.10	2.59	.36	8
Na_2O	1.10	3.85	2.30	.54	54	.59	.81	.69	.08	8
K_2O	.49	3.54	2.10	.68	54	1.71	2.12	1.90	.13	8
P_2O_5	.40	.78	.50	.08	54	.23	.40	.31	.05	8
ppm										
Nb	12.3	35	19.8	5.2	54	30	36	33	1.8	8
Zr	290	517	367	46	54	404	426	412	7.5	8
Y	30	48	36	4.0	54	26	30	29	1.2	8
Sr	402	1290	868	227	54	608	962	744	145	8
Rb	10.0	101	46	18.7	54	41	51	45	4.0	8
Zn	106	139	120	7.3	54	88	101	95	4.4	8
Cu	33	193	80	34	54	113	137	125	9.7	8
Ni	27	278	105	42	54	106	163	141	23	8
Co	39	56	47	3.9	54	47	73	53	8.5	8
Cr	4.5	474	163	108	54	229	316	273	39	8
V	200	276	235	17	54	220	303	237	28	8
CIA	34	44	39	2.2	54	59	67	63	2.8	8

Table 3.3. Mineral mode estimates (vol. %) for "fresh" samples, with estimates of the alteration assemblage (includes kaolinization and sericitization of feldspar, alteration of olivine and the amount of interstitial chlorite present, but excludes glass). 'Other' phases include alteration products of olivine and minor phases such as chlorite, apatite and quartz.

sample	cpx	plag	glass	opaques	other	alteration products
LFE-group						
RSS2	38	55	10	5	2	3
RSS8	35	20	45	-	-	3
RSS26	20	30	45	-	5	20
RSS45	33	57	-	5	5	10
RSS107	20	3	30	6	9	15
RSS138	25	60	10	5	-	8
RSS144	25	60	-	5	10	25
RSS152	38	52	-	5	5	5
RSS157	20	45	20	5	10	20
RSS184	30	-	60	5	5	5
RSV4	13	50	30	6	2	10
RSV14	20	46	20	5	7	15
RSV18	25	45	22	7	1	3
RSV20	25	45	22	7	1	3
RSV31	20	46	20	6	8	8
RSC6	30	60	-	4	6	10
HFE-group						
RSS7	40	52	-	3	-	5
RSS92	20	70	-	10	-	5
RSS147	20	68	-	8	4	4
RSS150	30	64	-	6	-	-
RSS156	37	50	-	8	5	10
RSS160	30	60	3	7	-	2
RSS162	40	55	-	5	-	2
RSS165	35	40	20	5	-	2
RSS168	35	50	5	5	5	10
CL115	30	62	-	5	3	15
N-group						
RSS123	45	50		5	-	3
RSS169	25	60	10	5	-	3
RSS183	42	50	-	3	5	5
RSV11	40	55	-	5	-	5
RSV16	35	55	4	6	-	3
RSV24	40	55	-	5	-	3
RSV35	40	55	-	5	-	2
RSC4	35	60	-	5	-	1
RSC22	45	50	-	3	2	1
RSC32	32	55	-	5	8	30
RSC72	27	50	15	8	-	10
RSC78	30	63	-	2	5	5
RSC79	25	65	-	3	7	15
RSC86	35	60	-	5	-	1
RSC87	45	50	-	5	-	2
CL143	45	50	-	2	3	3
CL356	43	50	-	4	3	5
CL360	50	43	-	4	3	5
CL372	28	60	-	2	10	15

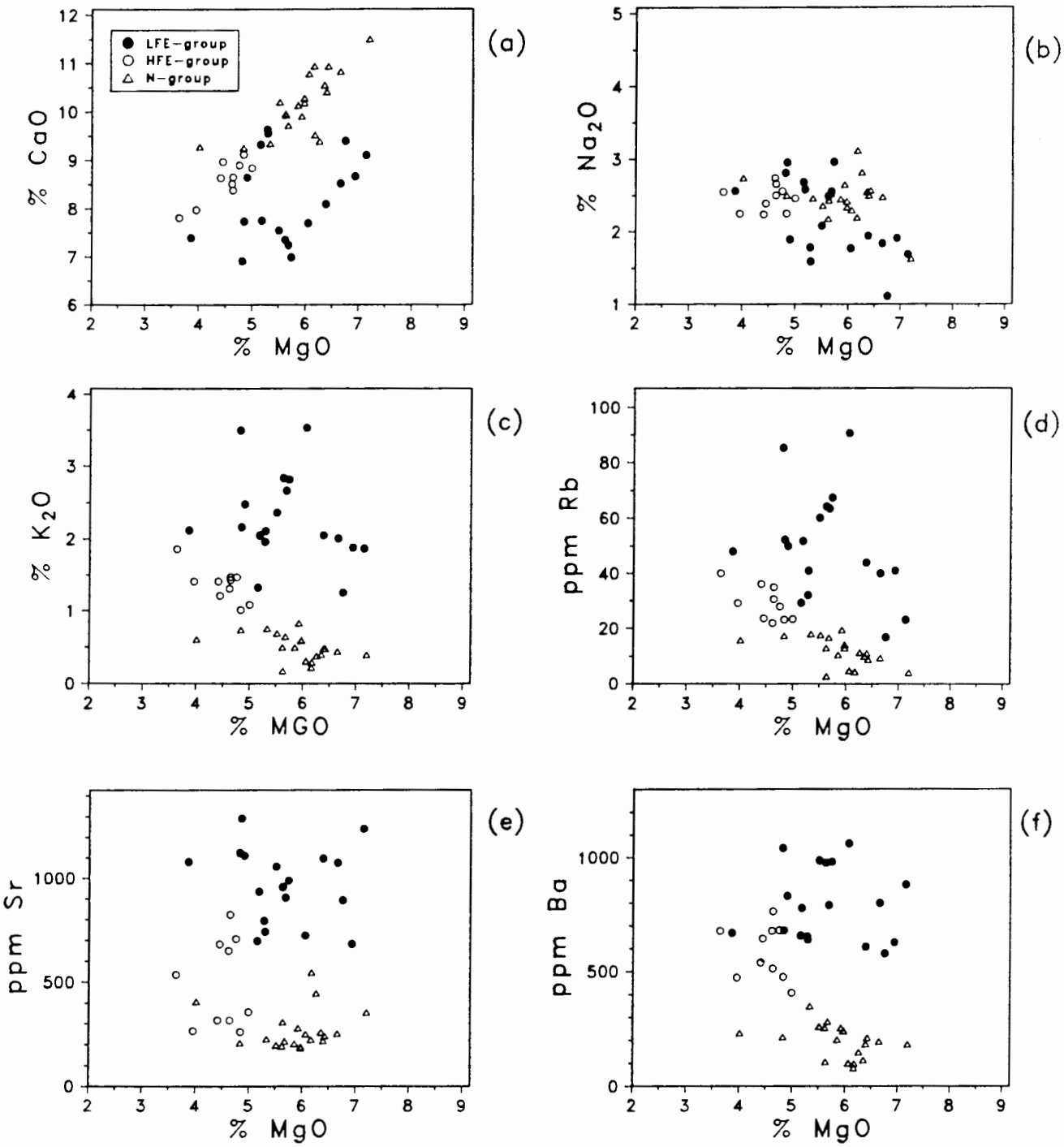

Figure 3.6. Samples are selected for their relative freshness in thin-section (labelled 'F' in Table C1, Appendix C) and data for elements likely to be affected by alteration (Ca, Na, K, Rb, Ba and Sr) are plotted *vs* MgO (n=48). Data are unnormalized.

3.2). Therefore, the CIA index is certainly sensitive to gross alteration effects as these soil samples may be regarded as representing the most extreme case of alteration. The elements most profoundly affected when the soil analyses are compared to the range obtained for the LFE group which they overlie, are Ca and Mg and Na (Table 3.2). Ca and Mg are lost with progressive weathering and deposited elsewhere, potentially in the unconsolidated cover overlying the basalts as calcrete and/or clay minerals. It is likely that Na is easily removed from the soil by solution in groundwaters. All other elements, including mobile elements such as K and Rb, have approximately the same concentration levels when compared to an LFE-group average for the central Lebombo (Table 3.2). This also holds true for Sr, despite the massive loss of CaO with weathering.

An alternative approach is to select the freshest samples on the basis of their appearance in thin-section and compare their chemical variations with variations obtained for the entire data set. These freshest samples selected are denoted by an '(F)' in the sample description in Table C1 (Appendix C). LOI is not used as a selection criterion as no correlations with mobile elements (i.e. LILE), which may indicate the influence of post-extrusion alteration, is observed. The mineralogy of these "fresh" samples is summarized in Table 3.3 along with estimates of the volumes of the altered component (including interstitial chlorite and the alteration products of plagioclase and olivine, but excluding any glass component). Thus, most of the samples in the "fresh" subset are comprised of at least 80% or more pristine mineral phases. The comparative freshness of the dolerites sampled makes them particularly useful in such a comparison and they comprise a substantial component of the "fresh" subset plotted for selected elements in Fig. 3.6. The selection of fresher samples has the effect of constraining the variation of CaO, Na_2O, K_2O, Ba and Rb and excluding samples with higher K_2O, Rb and Ba contents in the N- and HFE-groups.

The increase in Na_2O and decrease in CaO contents, expected as a result of an albitization process, is shown to be a function of the degree of alteration in the N- and HFE-group samples, i.e. Na_2O is constrained to values <3% and CaO has a well-defined positive correlation with MgO for the fresher samples. It is likely too that the alteration of plagioclase feldspar (albitization, kaolinization and sericitization) observed will result in an increase in the D^{plag} for the LILE (K, Rb and Ba). Thus any

exchange of these elements with any post-extrusion circulating (i.e. hydrothermal, groundwater) fluids (potentially the same fluid responsible for the feldspar alteration), will be facilitated.

The LFE group still records a spread in CaO, Na_2O, K_2O, Rb and Ba concentrations with MgO for in "fresh" subset. It is difficult to envisage an alteration process which could produce the spread in the LFE-group and still maintain the trends for these elements in the "fresh" HFE- and N-group samples. The implications of this are discussed below. Sr variations are not changed significantly in any basaltic rock type when just the "fresh" subset is considered (Fig. 3.6e).

Thus the chemical index of alteration (CIA) is of little use in quantifying alteration effects here. A comparison of fresher samples with the whole data set for the N and HFE groups, however, demonstrates a loss of CaO and a gain of Na_2O in the more altered samples - a process linked to the alteration of plagioclase. The increase in LILE (K, Rb and Ba) in some more altered samples of the N and HFE groups is also linked to this alteration (or 'alkalization') of plagioclase. Selection of fresher samples in the LFE group apparently does not change the distribution of CaO, Na_2O or the LILE significantly which implies that the observed spread of concentrations in these elements is similar to the spread before any alteration took place. Thus the effect of alteration cannot be resolved in the LFE group.

3.4 ISOTOPIC VARIATIONS

Isotopic studies on the basaltic rocks of the Lebombo have been conducted by Fitch and Miller (1984, K-Ar and Ar-Ar dating), Allsopp *et al.* (1984, Komatipoort Complex), Bristow *et al.* (1984, Sr-isotope determinations), Betton *et al.* (1984, Pb-isotope determinations) and Hawkesworth *et al.* (1984, a combined Sr- and Nd-isotopic study). Aside from detailed work on specific intrusions, all these studies have been of a regional nature. There was clearly a need to acquire detailed isotopic information on the different basaltic rock types at their juncture in the central Lebombo as part of the present study. The isotopic data given in Appendix C is a compilation of all isotopic data for the central Lebombo.

The majority of data in this study was obtained by the author working at the National Physical Research Laboratory of the Council for Scientific and Industrial Research (CSIR) in Pretoria using techniques described in Appendix A.

As noted previously dolerites are important because of their freshness, and hence several were selected for isotopic analyses. In the case of some LFE-group basalt samples (RSS8, RSS26, RSS184, RSV4, RSV18, RSV20, RSV31) an appreciable amount (>20%) of glass was observed in thin-section. The ease with which glass compositions may be changed by the interaction of groundwaters raises the possibility that the isotopic content of these rocks may have been affected. However, the absence of any correlation between the amount of glass and the measured $^{87}Sr/^{86}Sr$ content of a sample, suggests that no such exchange took place (Table 3.4).

Table 3.4. Mineral mode estimates for LFE-group samples containing glass upon which Sr-isotope determinations have been made (Appendices B and C).

sample	cpx	plag	glass	opaques	other	$^{87}Sr/^{86}Sr_{meas}$	$\delta^{18}O$
		(volume %)					(‰)
RSS2	38	55	10	5	2	.70663	+6.48
CL120	35	40	15	5	5	.70678	+4.65
RSV31	20	46	20	6	8	.70527	+6.17
RSV18	25	45	22	7	1	.70687	+6.17
RSV20	25	45	22	7	1	.70600	
RSV4	13	50	30	6	2	.70642	
RSS8	35	20	45	-	-	.70661	
RSS26	20	30	45	-	5	.70566	
RSS184	30	-	60	5	5	.70650	

(other phases include alteration products of minerals, amygdales, interstitial chlorite, apatite and quartz)

As the LFE-group is allegedly related to the N. Lebombo picrites by continued crystal fractionation (Cox and Bristow, 1984), the existing isotopic data set on these rocks was supplemented in this study by additional analyses on picrite basalts sampled by Bristow (1980) in the N. Lebombo (Appendix C).

Previous O-isotope data were obtained from Erlank (pers. comm., 1986). Reconnaissance analyses of 11 basaltic samples and one granophyre sample (RSS86) for their oxygen isotope content was carried out by H. S. Smith and C. Harris in this department. This data is reported in per-mil (‰) values relative to an international standard (V-SMOW, Appendix A).

The discussion of isotopic data here is limited to reporting observed variations and commenting on any age significance. More detailed interpretive work on petrogenetic implications is dealt with later where relevant.

3.4.1 Rb-Sr systematics

The N-group displays a crude correlation on an Rb-Sr isochron diagram with most data points falling between 380 Ma and 600 Ma reference isochrons when a $^{87}Sr/^{86}Sr$ initial ratio of .7041 is used (Fig. 3.7). This range in age is considerably in excess of the established maximum age of 200 Ma (Allsopp *et al.*, 1984) for the basaltic succession. If these rocks are unaffected by open system processes such as crustal contamination and have not undergone significant Rb/Sr fractionation since their derivation from a mantle source, then this age range (380-600 Ma) reflects the age of separation of such a mantle source from the convecting mantle as a whole.

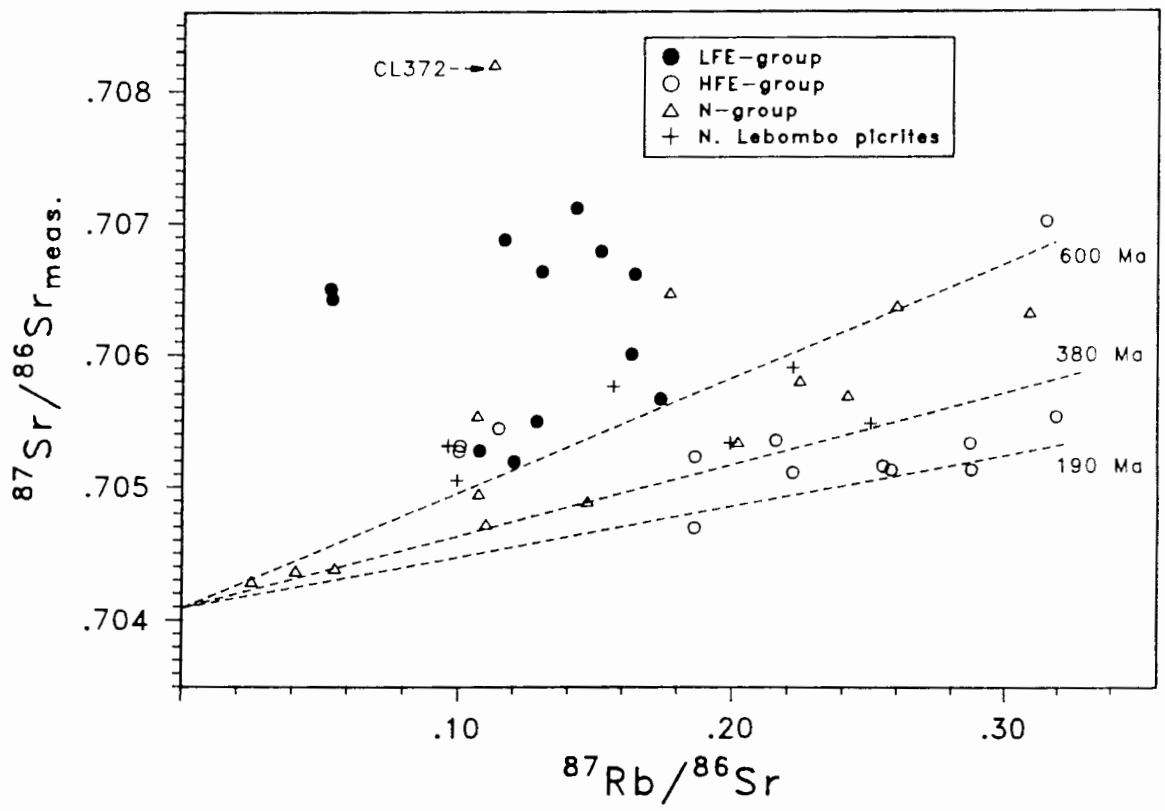

Figure 3.7. Measured $^{87}Sr/^{86}Sr$ ratios *vs* $^{87}Rb/^{86}Sr$, (calculated from whole-rock XRF determinations) for central Lebombo basaltic rocks and N. Lebombo picrites. 190 Ma, 380 Ma and 600 Ma references isochrons are plotted. Data are from this study, Bristow *et al.* (1984) and Hawkesworth, pers. comm. (1987, CL372).

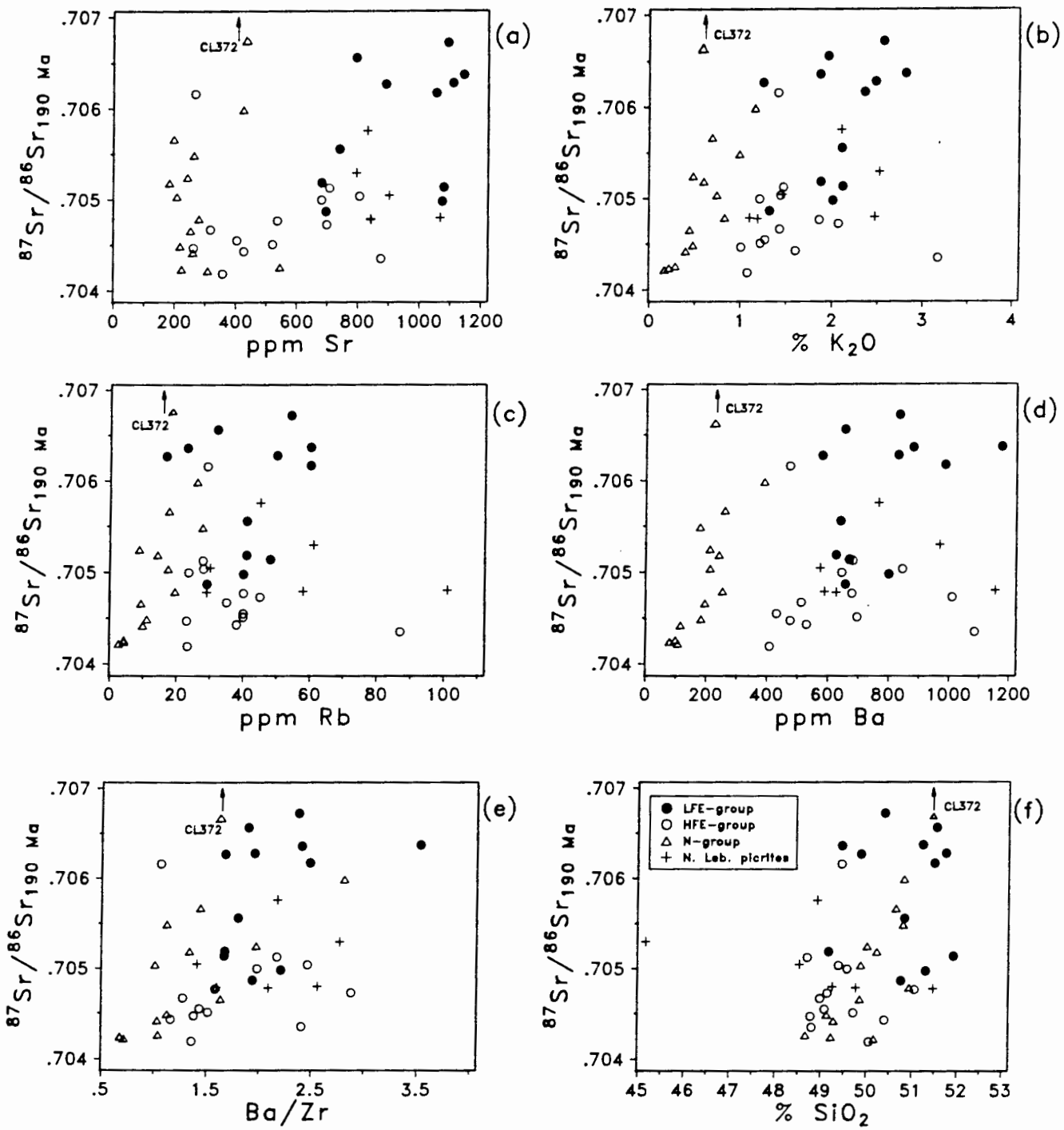

Figure 3.8. Initial $^{87}Sr/^{86}Sr$ ratio (190 Ma) *vs* selected elements for central Lebombo basaltic rocks and N. Lebombo picrites. CL372 (offscale) is a sample of a very plagioclase-phyric basalt from the Komati River section.
Data are from this study, Bristow *et al.* (1984) and Hawkesworth, pers. comm. (1987, CL372).

However, processes such as crustal contamination will bias ages towards the age of the contaminant and therefore no age significance can be attached to the N-group data.

The absence of any correlation of measured $^{87}Sr/^{86}Sr$ with $^{87}Rb/^{86}Sr$ for the LFE group is contrasted by the clustering of the HFE group close to a 190 Ma reference isochron (Fig. 3.7).

There is no correlation of initial $^{87}Sr/^{86}Sr$ ratio (calculated at 190 Ma) with Sr content in the LFE group. There is little change in initial $^{87}Sr/^{86}Sr$ ratio (.70419-.70513) for a considerable range of Sr compositions (with the exception of RSC85) for the HFE group, while the reverse is true for most of the N-group samples (Fig. 3.8). Initial $^{87}Sr/^{86}Sr$ ratios are positively correlated with K_2O, Rb, Ba and SiO_2 content and with Ba/Zr ratio for the N-group samples (Fig. 3.8b-f).

3.4.2 Sm-Nd systematics

The N-group samples have $^{147}Sm/^{144}Nd$ ratios consistently greater than the LFE-group (N. Lebombo and Nuanetsi basic rocks included), while the HFE-group displays little variation in either $^{143}Nd/^{144}Nd$ (measured) or $^{147}Sm/^{144}Nd$ ratios (Fig. 3.9). In contrast to Rb-Sr isotopes, the N-group displays no "age" correlations, which may imply that the process affecting the Rb-Sr isotope systematics of this group is not significant with respect to Sm-Nd isotope systematics.

Fig. 3.10 shows that the LFE group has a range of Sr- and Nd-isotopic compositions similar to that established for Nuanetsi and the N. Lebombo (Hawkesworth *et al.*, 1984). No Nd-isotope determinations exist for N. Lebombo low-MgO volcanics and thus the substantiation of similar ranges for the LFE group (correlated with typical low-MgO N. Lebombo "enriched" basalts) and the picrite data in this study is important as it was suggested (Cox and Bristow, 1984) that the picrites are parental melts to the N. Lebombo low-MgO basalts. The HFE group is characterized by a limited range in $^{143}Nd/^{144}Nd$ initial ratio (calculated at 190 Ma) of .51225-.51249, relative to ranges observed for the other groups (Fig. 3.10). This range becomes even more restricted (.51240-.51249) if CL115 (a HFE-group basalt occurring at a stratigraphic height of *ca* 500 m in the Sabie River

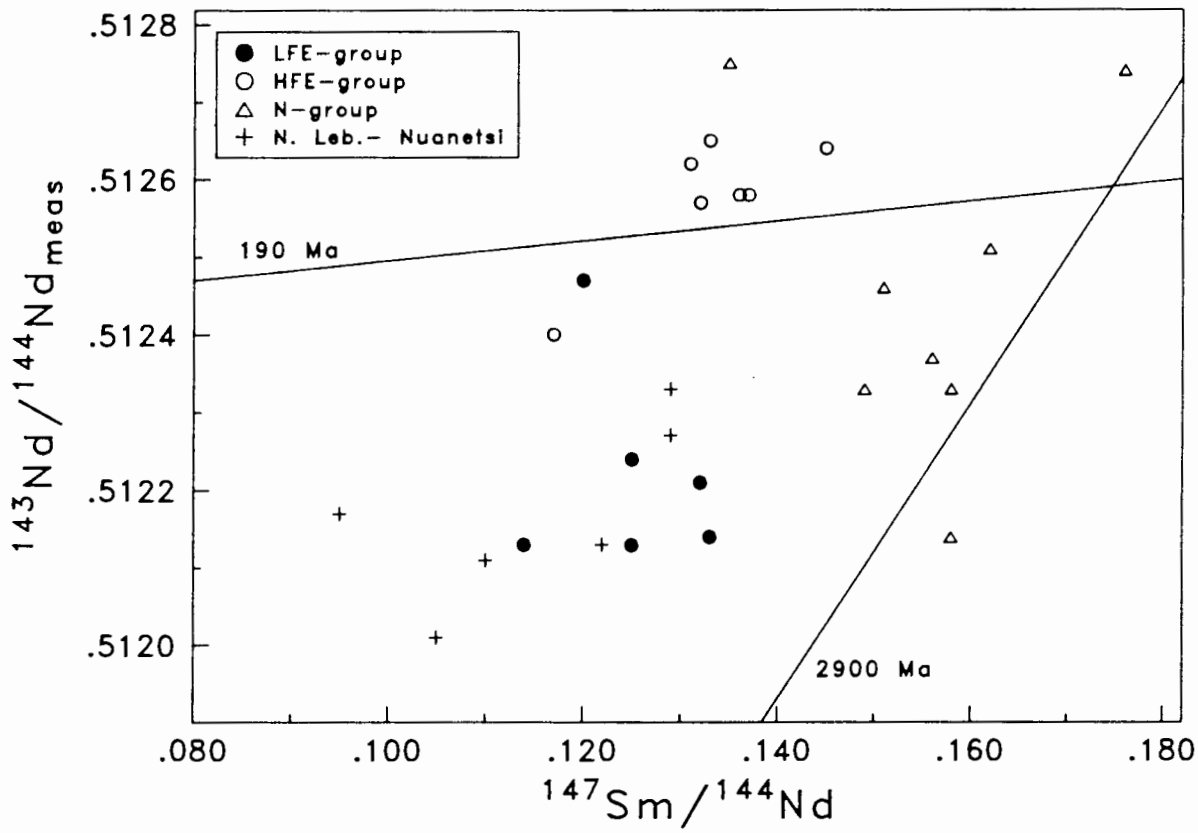

Figure 3.9. Measured $^{143}Nd/^{144}Nd$ *vs* $^{147}Sm/^{144}Nd$ (determined by isotope dilution or spark-source mass spectrography) for central Lebombo, N. Lebombo and Nuanetsi basaltic rocks. 190 Ma and 2900 Ma reference isochrons are shown. Data are from this study, Hawkesworth *et al.* (1984) and Hawkesworth, pers. comm. (1987, CL372).

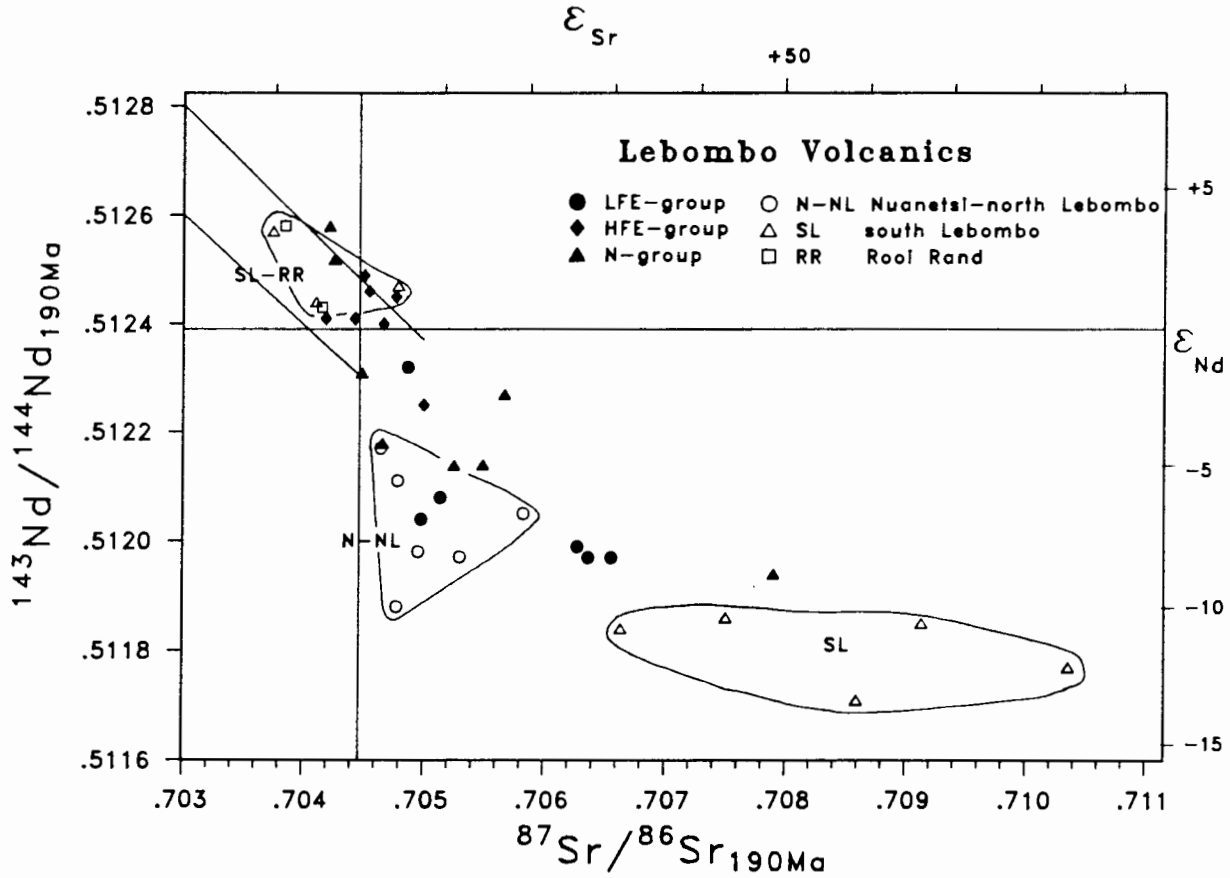

Figure 3.10. ε-diagram at 190 Ma for data from the central Lebombo (filled symbols) and other areas of the Lebombo (open symbols). Data are from this study, Hawkesworth *et al.* (1984) and Hawkesworth, pers. comm. (1987)

section, Appendix D) is excluded. The N-group sample data for the central Lebombo describe an array from ϵ_{Nd} +3.6, ϵ_{Sr} -3.5 (i.e. within the mantle array as defined by MORB and OIB) to approximately ϵ_{Nd} -4.80, ϵ_{Sr} +14.0 (Fig. 3.10). This data fills some of the compositional gap between the two southern Lebombo fields as defined by Hawkesworth *et al.* (1984). The low ϵ_{Nd}-high ϵ_{Sr} southern Lebombo group was supposed by Hawkesworth *et al.* (1984) to be significantly contaminated with continental crust. The possible effects of crustal contamination on basalts of the central Lebombo are examined elsewhere in this study.

3.4.3 U-Th-Pb systematics

Uranium in these rocks is typically below the XRF detection limit (<1ppm, Appendices A and C) which implies a U/Pb ratio of <.20 for the LFE and HFE groups and <.50 for the N group. U and Pb data reported in Betton *et al.* (1984) suggests U/Pb ratios of about .10 for the mafic rocks of the Lebombo in general. Spark-source data for U and Pb for central Lebombo basalts (this study, Appendix C) gives U/Pb ratios of .20-.28 for the HFE and LFE groups and .19-.35 for the N group, consistent with the suggestions above. The low U/Pb ratios make the $^{206}Pb/^{204}Pb$-$^{207}Pb/^{204}Pb$ system insensitive to relatively recent U-Pb fractionation, whether this be petrogenetic or a result of weathering. Furthermore, the relatively young age (190 Ma) coupled with the low U/Pb ratios of these volcanics, ensures that the age correction for the $^{206}Pb/^{204}Pb$ and $^{207}Pb/^{204}Pb$ ratios will be small (Fig. 3.11). Therefore, in the absence of any mixing effects (i.e. crustal contamination, magma mixing), the Pb-Pb isotope system should reflect the source characteristics of these basaltic suites. The problem is to evaluate the extent which the Pb isotopic content has been modified by mixing from original mantle source values.

The $^{206}Pb/^{204}Pb$-$^{207}Pb/^{204}Pb$ isotopic data for all groups plot close to a 2.9 Ga reference isochron (Fig. 3.11). Indeed, 13 of the 17 determinations (RSS2, RSS138, RSC32 and RSC35 excluded) when regressed (using York, 1969), yield an age of 2863 $\pm$270 Ma with an MSUM of 3.3. MSUM is the residual sum of squares, calculated using York (1969), divided by n-2, where n is the number of measurements made. Ideally this index should have a value of unity and Brooks *et al.* (1972) have proposed a value of 2.5 as a cutoff;

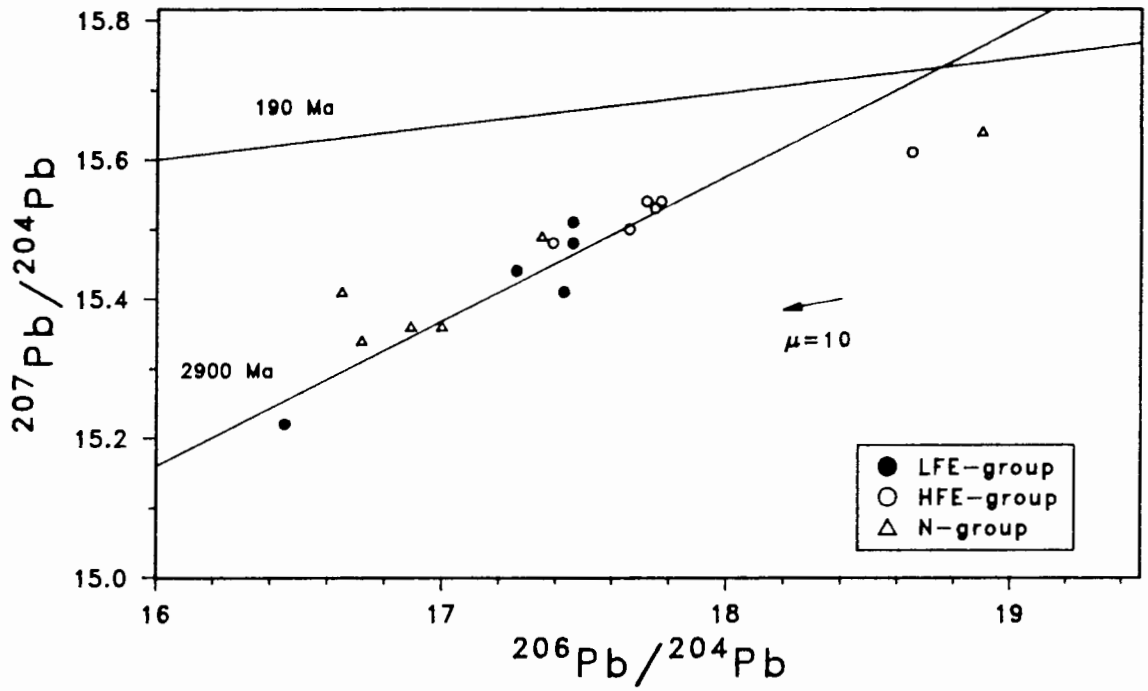

Figure 3.11. $^{206}Pb/^{204}Pb$ *vs* $^{207}Pb/^{204}Pb$ for central Lebombo data. 190 Ma and 2900 Ma reference isochrons are shown. Data are from this study and Betton *et al.* (1984).

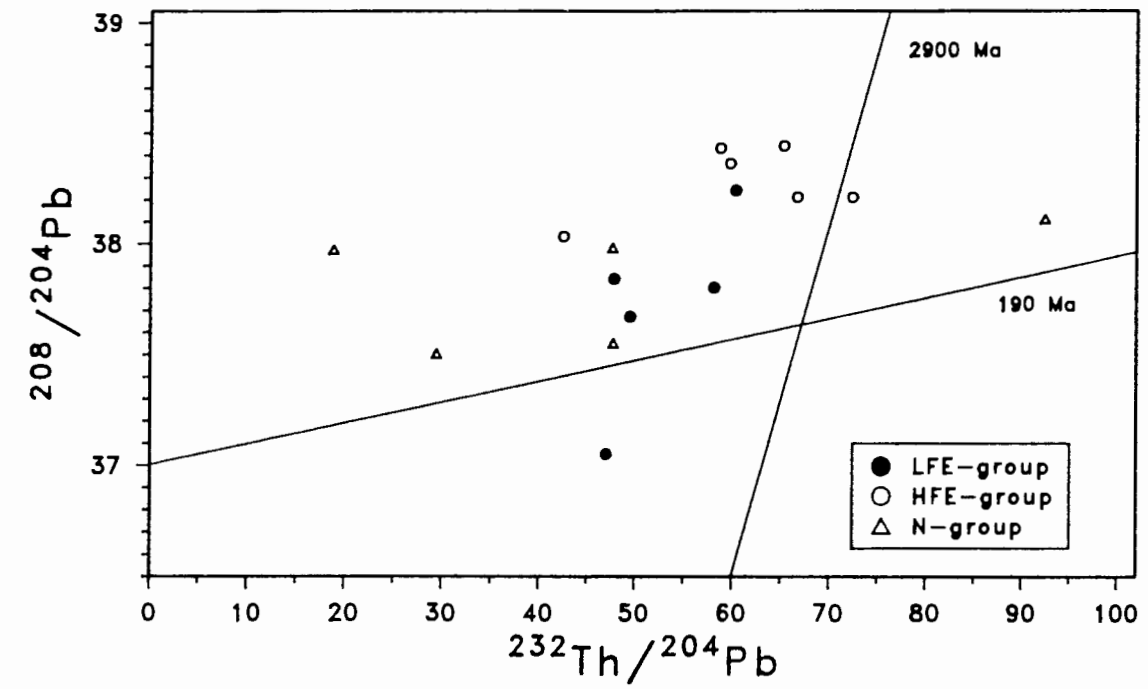

Figure 3.12. $^{232}Th/^{204}Pb$ *vs* $^{208}Pb/^{204}Pb$ for central Lebombo data. 190 Ma and 2900 Ma reference isochrons are shown. Data are from this study and Betton *et al.* (1984).

with higher values indicating that the error in the measurements would be in excess of the experimental error (the excess being geological error). The dispersion of data around this errorchron but not the correlation itself, may be the result of post-eruption U/Pb fractionation (i.e. due to weathering) or variable petrogenetic controls (i.e. fractionation).

Obviously the basaltic rocks are considerably younger and the age suggested by the array does not reflect the age of eruption. The only mechanism of generating such an array in recent time is by mixing between reservoirs with different Pb-isotope compositions.

The measurement of the Th and Pb contents (XRF) of the samples analysed for Pb isotopic ratios enabled the calculation of a $^{232}Th/^{204}Pb$ ratio and plotting of a Th-Pb isochron diagram (Fig. 3.12). The absence of linear arrays on Fig. 3.12 corresponding to those observed on Fig. 3.11, may be a result of the imprecise nature of the Th and Pb XRF data (used to calculate the $^{232}Th/^{204}Pb$ ratio) relative to ratios determined by mass spectrometry.

Obviously any age significance in the Pb-Pb and Th-Pb isotopic systems is conjectural and data is re-examined later in the context of appropriate petrogenetic models.

3.4.4 Oxygen isotope systematics

The $\delta^{18}O$ values for fresh samples fall in the range +5.34‰ to +6.48‰ (Appendix C, Fig. 3.13). RSS40 is an altered N-group basalt and its lower $\delta^{18}O$ (+4.5‰) may be reflecting this alteration, i.e. by interaction with meteoric waters of a lower $\delta^{18}O$ content. Similar interactions have been suggested for the Iceland volcanic pile (Hattori and Muehlenbachs, 1982). The range of values above is indistinguishable from values determined for typical mantle materials (+5 to +7‰) summarized in fig. 2 of Graham and Harmon (1983). Furthermore, the range of $\delta^{18}O$ for fresh samples in the central Lebombo is similar to the estimate of Taylor *et al.* (1986) of +6‰ ±5‰ for terrestrial basaltic rocks in general.

No correlation of $\delta^{18}O$ with $^{87}Sr/^{86}Sr$ initial ratios or Pb-isotopic ratios is observed (Fig. 3.13).

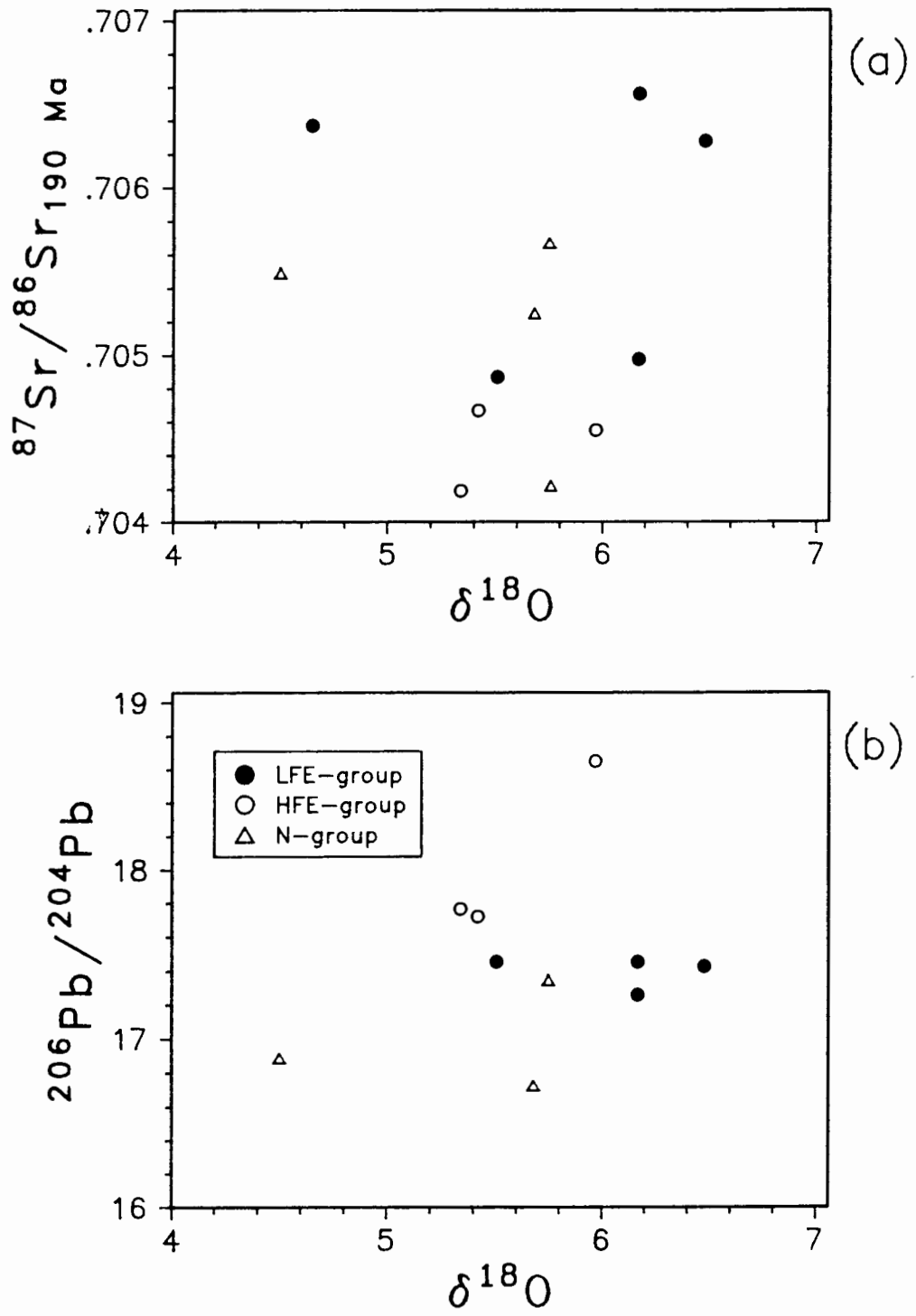

Figure 3.13. Stable (O) and radiogenic (Sr, Pb) isotope data for central Lebombo basaltic volcanics. Data are from this study.

3.5 SUMMARY

All basaltic (<55% SiO_2) samples analysed quantitatively may be divided on the basis of their TiO_2, Zr and Fe_2O_3t contents into "normal" (**N**), low-Fe "enriched" (**LFE**) and high-Fe "enriched" (**HFE**) groups. LFE-group samples are correlated with typical N. Lebombo-Nuanetsi incompatible element enriched types initially defined by Cox *et al.* (1967), while the HFE-type compositions are hithertoe unrecognized elsewhere in the Karoo Igneous Province and may be unique to the central Lebombo. All three basaltic rock-types are represented by dolerite dykes of corresponding geochemical composition.

A comparison between relatively 'fresh' basaltic samples and the whole quantitative data set demonstrated that the N and HFE groups have been affected by a loss of Ca and an increase of Na, K, Rb and Ba with alteration. No alteration effect in the LFE group was resolved and it was concluded that the observed spread in Ca, Na, K, Rb and Ba in this group is representative of at least similar spreads originally present in pristine rocks of this group. Thus there were no consistent variations of these elements with MgO in the LFE group for alteration to disturb and the spread presently observed must be due to petrogenetic and not alteration factors.

Radiogenic isotope ratios of Sr, Pb and Nd do not reflect eruption ages in the case of the LFE and N groups but may do so for the HFE group. It is suggested here and examined later, that the differing sensitivities of Sr, Pb, Nd and O to various petrogenetic processes is responsible for the isotope ratios observed for each system.

4. PETROGRAPHY AND MINERAL CHEMISTRY

4.1 INTRODUCTION

The detailed petrography of individual thin-sections is given in Appendix B and are summarized here for each of the different chemically defined basaltic groups before each mineral phase is considered individually. The objective is to determine whether consistent differences in mineral chemistry exist between the three basaltic groups and what implications such variations might have on the crystallization history of the rocks studied.

A number of textural terms that are utilized require brief elucidation. When the interstices between feldspars are occupied by pyroxene ± olivine ± opaques the texture is termed **intergranular** (Fig 4.1a). If these interstices are partially filled with glass the term **intersertal** is used (Fig 4.1b). The intergranular texture grades into **sub-ophitic** (Fig 4.1c) when pyroxenes begin to mould themselves around the end of feldspars, whilst the intersertal texture grades into **hyalo-ophitic** (Fig. 4.1d) as the proportion of glass increases and begins to envelop either feldspars or pyroxenes. Aggregates of pyroxene and/or feldspar phenocrysts catergorise the **glomeroporphyritic** texture (Fig 4.1d) and where such aggregation is absent, textures are simply **porphyritic** (phyric).

The dolerites typically have sub-ophitic or intergranular textures; the basalts, while rarely sub-ophitic, display the full range of textures described. The only phenocryst phase visible in hand-specimen is feldspar. There is no correlation between the aphyric/porphyritic character of a sample and its intrusive/extrusive nature or the basaltic group with which it is associated. The HFE- and N-group basalts rarely contain appreciable glass whereas glomeroporphyritic clusters of clinopyroxene microphenocrysts in a glass matrix (hyalo-ophitic texture) are often observed in LFE-group basalts.

(a) Intergranular texture (RSS150 - HFE-group dolerite)
(17x magnification, field of view = 6.5 mm)

Figure 4.1. Igneous textures in central Lebombo basaltic rocks. These textures are described in the text. Plane-polarized and polarized photomicrographs are included.
(py = pyroxene; plg = plagioclase; op = opaque oxide and gl = glass)

/Figure 4.1

(b) intersertal (RSS2 - LFE-group basalt)
(17x magnification, field of view = 6.5 mm)

/Figure 4.1

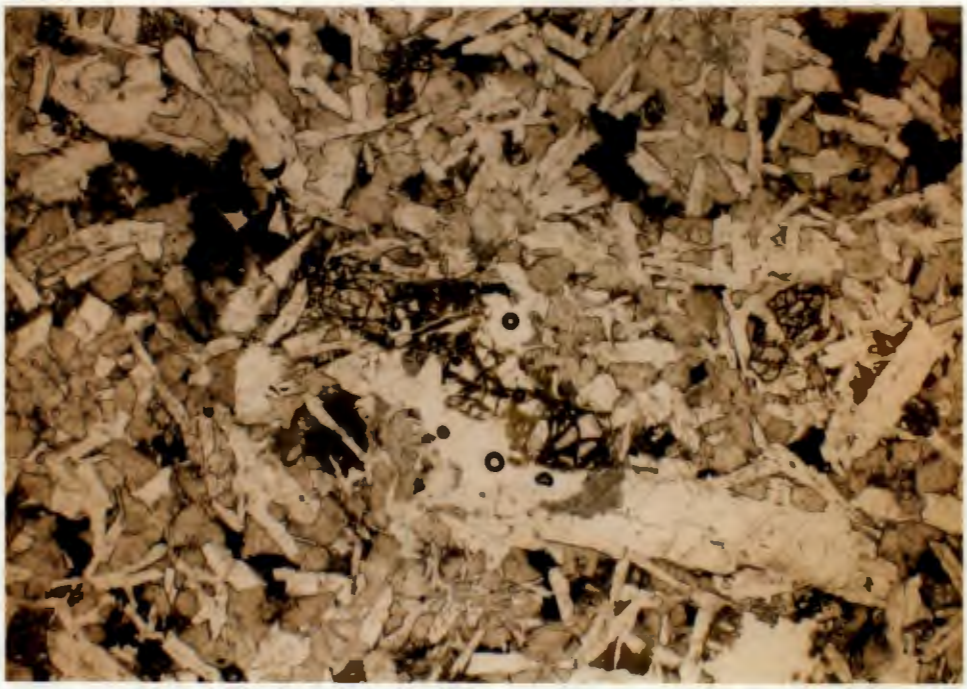

(c) sub-ophitic (RSC22 - N-group basalt)
(17x magnification, field of view = 6.5 mm)

/Figure 4.1

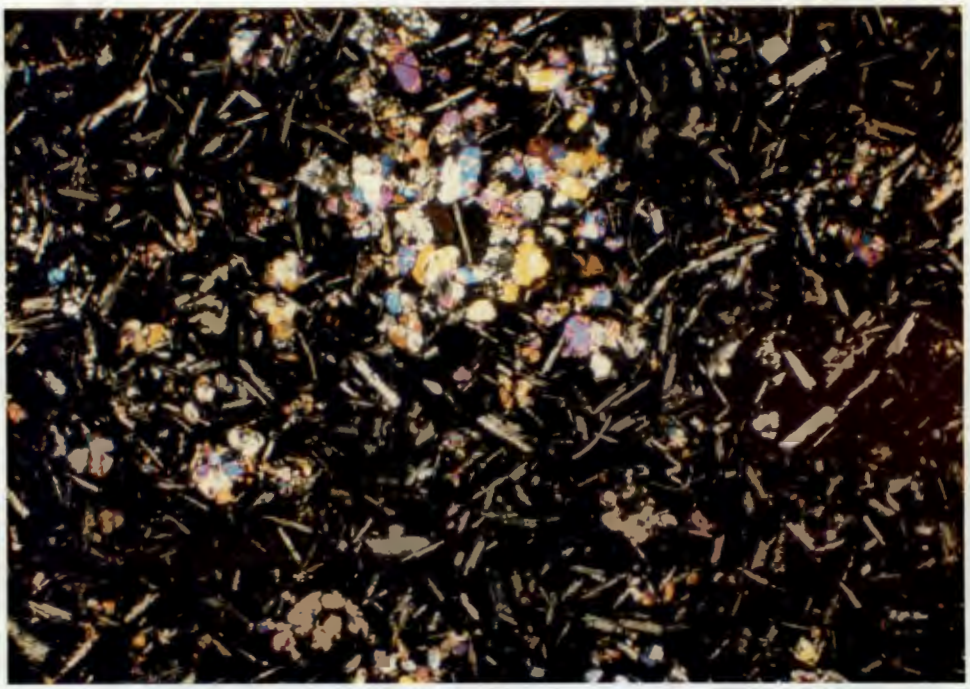

(d) hyalo-ophitic and glomeroporphyritic (RSS8 - LFE-group basalt) showing the aggregation of pyroxene microphenocrysts.
(17x magnification, field of view = 6.5 mm)

4.2 OLIVINE

Olivine in the basalts is always pseudomorphed by serpentine or by chlorite and magnetite. In two dolerites (RSC4 and RSC22) the preservation of some relatively unaltered fragments of olivine is a function of the almost pristine nature of these samples. Selected analyses of olivines from these two samples are given in Table 4.1. With the exception of FV4 (a picrite basalt interbedded with the SRBF about 50 km north of the Sabie River, Appendix D), olivine or pseudomorphs after olivine are nowhere present in greater than 5% (volume) modal abundance. The presence of olivine or pseudomorphs after olivine, does not appear to be restricted to a particular basaltic group or related to the MgO content of a sample.

The range in Fo values for olivines analysed in RSC4 is Fo_{31}-Fo_{56}. The Fo content of an olivine crystallizing from a sample of this whole-rock composition (Mg-number, Mg# = 53, Appendix C) is predicted to be Fo_{79} using Roeder and Emslie's (1970) K_D of 0.30 for the distribution of Fe^{2+} and Mg between a melt and olivine and assuming a whole rock Fe_2O_3/FeO ratio of 0.15. The olivine fragments analysed are remnants of altered grains and it may be that alteration is causing these anomalously low Fo values. Alternatively, if these olivines were phenocrysts their more "evolved" composition relative to the whole-rock host, implies they may be the result of a process such as compensated crystal settling (Cox and Bell, 1972; Krishnamurthy and Cox, 1977), whereby the olivine crystallized in a more Fe-rich portion of a magma chamber (or dyke) and settled into its present position. Similarly, olivines crystallizing in equilibrium with the present batch of magma would have been removed 'downwards'.

Olivine compositions in RSC22 range from Fo_{49} to Fo_{78}. The relatively well preserved nature of olivine 4 in RSC22 made it an ideal site for evaluating zoning patterns across the mineral and these are illustrated in Fig 4.2. Fo content decreases from Fo_{78} in the centre to Fo_{61} and Fo_{72} in each rim. An olivine crystallizing from a liquid of the host whole-rock composition (Mg# = 52) should have a composition Fo_{78} (calculated as outlined above). This value is identical to the composition of the grain centre which implies that the centre of this olivine grain crystallized from a magma of the host rock composition. Although alteration may have had some effect on the olivine composition, the absence of zoning within each unaltered portion of the crystal (Fig. 4.2) means it is more

Table 4.1. Selected olivine analyses (from Appendix C).

	1	2	3	4	5	6
%						
SiO_2	34.55	32.50	35.54	36.90	37.65	37.86
TiO_2						
Al_2O_3			.04	.05		
FeO	37.78	52.07	33.94	28.40	24.31	20.46
MnO	.53	.83	.42	.38	.26	.29
MgO	26.50	14.25	30.05	34.85	37.85	40.50
CaO	.30	.39	.29	.30	.33	.32
Cr_2O_5						.07
NiO			.10	.17	.11	.15
Total	99.70	100.08	100.40	101.07	100.54	99.69
Fo	55.6	32.8	61.2	68.6	73.5	77.9
atomic proportions calculated using 4 oxygens						
Si	.980	.993	.980	.981	.986	.983
Ti						
Al			.001	.002		
Fe2+	.896	1.330	.783	.632	.532	.444
Mn	.013	.021	.010	.009	.006	.006
Mg	1.120	.649	1.235	1.381	1.477	1.567
Ca	.009	.013	.009	.009	.009	.009
Cr						.001
Ni			.002	.004	.002	.003
Sum	3.019	3.007	3.019	3.017	3.014	3.016

values below detection limit are printed as blanks

sample descriptions:

1 : olivine 3 RSC4
2 : olivine 4 RSC4
3 : olivine 4/2B RSC22
4 : olivine 4/2A RSC22
5 : olivine 4/1E RSC22
6 : olivine 4/3A RSC22

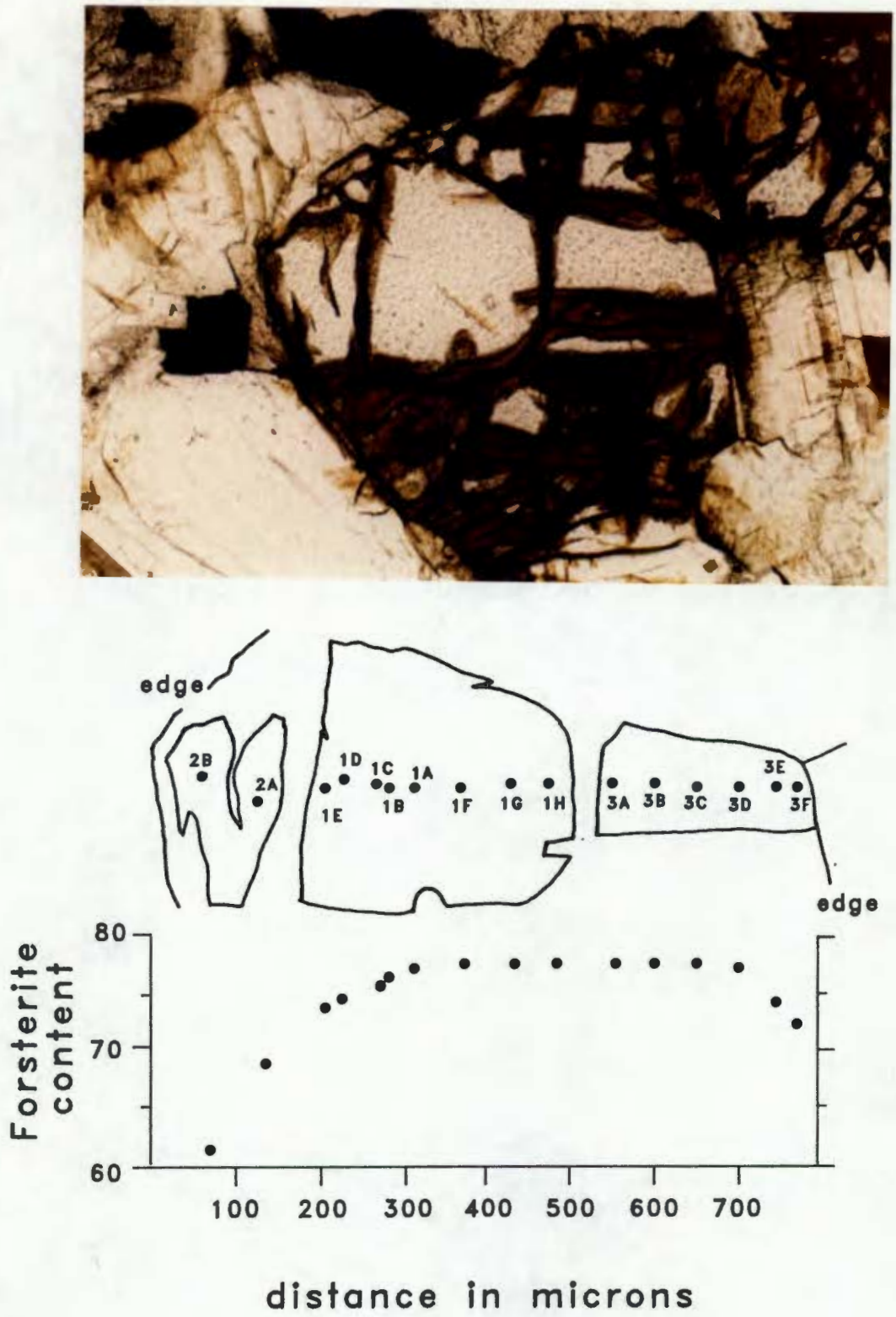

Figure 4.2. Major element zoning in olivine 4 of RSC22.
(photomicrograph magnification x95, field of view = 1.4 mm)

likely that progressive equilibration of the olivine rim with an evolving melt composition is responsible for the normal zoning pattern.

4.3 PYROXENE

Orthopyroxene is only present as a rare microphenocryst in one sample - a LFE-group basalt (RSS167). No mineral chemical data for this occurrence were obtained because of the anticipated difficulty of intersecting such phases in any subsequently prepared polished thin-sections. Orthopyroxene was not observed in the groundmass of any sample.

Clinopyroxene (principally unexsolved augite) is the dominant ferro-magnesian mineral phase in all three basaltic groups (Fig. 4.3). Relative to augite abundance, pigeonite is volumetrically insignificant: it is present in some HFE-group and N-group samples as inclusions in minerals (augite, plagioclase), implying earlier crystallization the host minerals in this case, and as a groundmass phase but is absent altogether in the LFE-group samples examined (Fig. 4.3). Selected clinopyroxene analyses are given in Table 4.2.

Carmichael *et al.* (1974) divide basalts into alkali-olivine basalts and tholeiites on the presence in the groundmass of a Ca-poor pyroxene which is regarded as a mineralogical expression of the reaction

$$Mg_2SiO_2 + SiO_2 = 2MgSiO_3$$

Fo glass clino-enstatite

The above reaction represents a SiO_2 activity (a_{SiO2}) boundary between tholeiitic basalts (with or without olivine) and alkali-olivine basalts which do not show this reaction relationship. The activity (a_i) of species i is defined by

$$a_i = e^{(\mu_i - \mu_o)/RT} \qquad \text{(Levine, 1978)}$$

where the chemical potential (μ_i) of i in the reaction mixture (magma) is some function of T, P and x_n (x_1, x_2..., are the mole fractions of phases in which i occurs). In terms of the pyroxene mineral assemblage observed in these rocks, therefore, the presence of pigeonite in the N and HFE groups is likely to reflect a relative increase in the a_{SiO2} caused by an increase in SiO_2 concentration, decrease in T or decrease in P.

Table 4.2. Selected clinopyroxene analyses (from Appendix C).

	1	2	3	4	5	6	7	8	9
SIO2	51.94	52.00	48.98	50.56	50.26	52.33	50.80	50.19	51.56
TIO2	.97	.92	1.73	1.16	1.27	.56	.92	.46	.57
AL2O3	1.34	1.85	3.84	2.29	2.11	1.53	2.01	.73	1.02
CR2O3	.22	.69	.30	.08		.10			
FEO	9.15	7.08	11.74	12.28	14.04	11.78	14.56	26.82	21.68
MNO	.16	.16	.27	.24	.22	.21	.28	.54	.52
MGO	17.61	17.85	15.25	14.85	13.57	16.07	14.16	15.92	19.87
CAO	18.12	19.35	17.21	17.72	18.31	17.26	17.09	5.00	4.61
NA2O	.20	.25	.28	.26	.25	.19	.26	.07	.09
TOTAL	99.72	100.16	99.61	99.45	100.05	100.04	100.10	99.75	99.94
atomic proportions calculated using 6 oxygens									
SI	1.928	1.913	1.846	1.910	1.906	1.950	1.921	1.950	1.946
TI	.027	.025	.049	.033	.036	.016	.026	.013	.016
AL	.059	.080	.171	.102	.094	.067	.090	.033	.045
CR	.006	.020	.009	.002		.003			
FE2+	.284	.218	.370	.388	.445	.367	.461	.872	.684
MN	.005	.005	.009	.008	.007	.007	.009	.018	.017
MG	.974	.979	.857	.836	.767	.893	.798	.922	1.117
CA	.721	.763	.695	.717	.744	.689	.693	.208	.186
NA	.014	.018	.020	.019	.018	.014	.019	.005	.007
SUM	4.020	4.021	4.026	4.015	4.020	4.006	4.017	4.022	4.019
WO	36.4	38.9	36.2	36.9	38.0	35.4	35.5	10.4	9.38
EN	49.2	50.0	44.6	43.1	39.2	45.8	40.9	46.1	56.2
FS	14.4	11.1	19.3	20.0	22.8	18.8	23.6	43.5	34.4

values below detection limits are printed as blanks

sample descriptions:

1	:	augite - CPX2 RSS2	| LFE-
2	:	augite - CPX4 RSV31	| group
3	:	augite - CPX10 RSS150	
4	:	augite - CPX3 CENTRE RSS160	| HFE-
5	:	augite - CPX3 EDGE RSS160	| group
6	:	augite - CPX3 RSS35	| N-
7	:	augite - CPX20 RSC22	| group
8	:	pigeonite - CPX4 RSS160	| HFE-group
9	:	pigeonite - CPX13 RSC4	| N-group

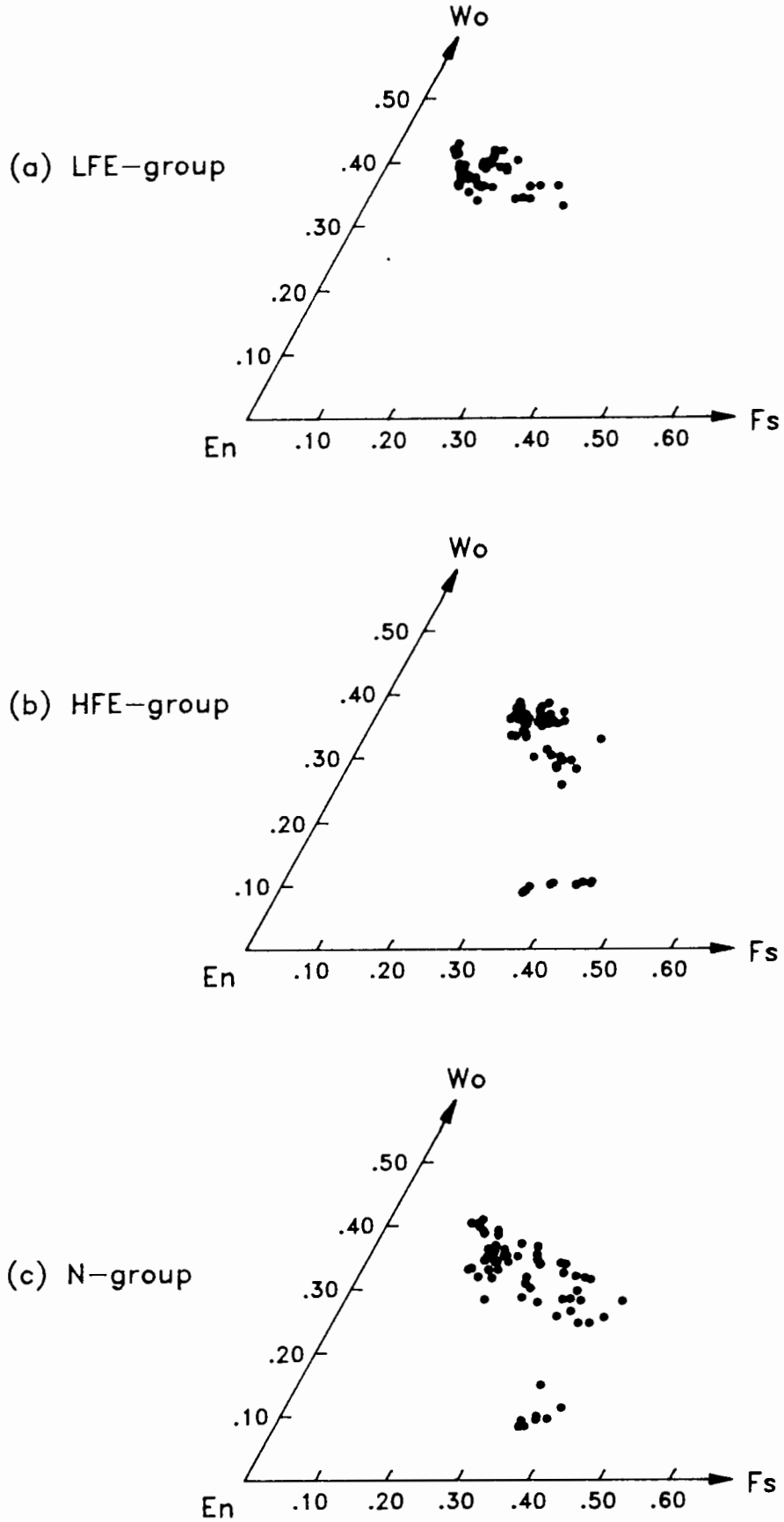

Figure 4.3. Major element content of clinopyroxenes in terms of wollastonite (Wo), enstatite (En) and ferrosillite (Fs) end-members.

Evidence in volcanic rocks generally that the two pyroxenes (subcalcic orthopyroxene/pigeonite + augite) precipitate simultaneously from a melt is elusive (Heubner, 1980). For this reason, pigeonite-augite pairs were not sought for the application of Kretz's (1963) geothermometer. Heubner (1980) states further that there is no conclusive evidence that in natural systems the pigeonite-augite miscibility gap closes with iron enrichment. However, there does appear to be some closure of this gap with iron enrichment in the Lebombo basaltic rocks, particularly in the case of the N-group (Fig. 4.3c) where the augite range is $Wo_{40}En_{50}Fs_{10}$ - $Wo_{25}En_{35}Fs_{40}$ and pigeonite range is $Wo_8En_{57}Fs_{35}$ - $Wo_{12}En_{49}Fs_{39}$. Heubner does concede that such closure has been suggested by experiments at high pressure by Hensen (1973), Mori (1978) and Grover and Lindsley (1972). Similar closures have been found in the clinopyroxenes precipitated from fractionated lunar mare basalt melts (Bence and Papike, 1972; Ross *et al.*, 1973) although Papike *et al.* (1976) maintain that such compositions can also be explained by rapid and metastable crystallization. In conclusion, any case for high pressure fractionation in the N-group, based on the augite-pigeonite miscibility-gap closure, must be regarded as inconclusive.

Microphenocrysts (often glomeroporphyritically clustered) are most typically observed in the LFE-group basalts. Clinopyroxene in all groups is mostly unaltered and zoning was not detected optically. Microphenocrysts analysed in all groups, however, are chemically zoned in a normal fashion to some degree (e.g. cpx3 RSS160 in Table 4.2). In terms of minor constituents, most clinopyroxenes in all groups are also zoned to some degree; up to the extent that the range in composition of a single microphenocryst represents approximately half of the total range in composition for that particular thin-section (Figs. 4.4, 4.5).

The distribution of minor elements (i.e. Ti, Al) with Mg content (ionic) is plotted for each rock type (Figs. 4.4, 4.5). The concentrations of Ti and Al in pigeonite are consistently low and this mineral has been excluded from these plots. Predictably, despite the range of pyroxene compositions within each sample, the values are broadly consistent with the whole-rock geochemistry. For example: (1) in Fig. 4.4a, clinopyroxenes from RSV31 (whole-rock MgO = 6.66%) have generally higher Mg contents than do clinopyroxenes from RSS152 (whole-rock MgO = 5.16%); (2) clinopyroxenes from the HFE-group are both more "evolved" (lower Mg contents) than the LFE-group

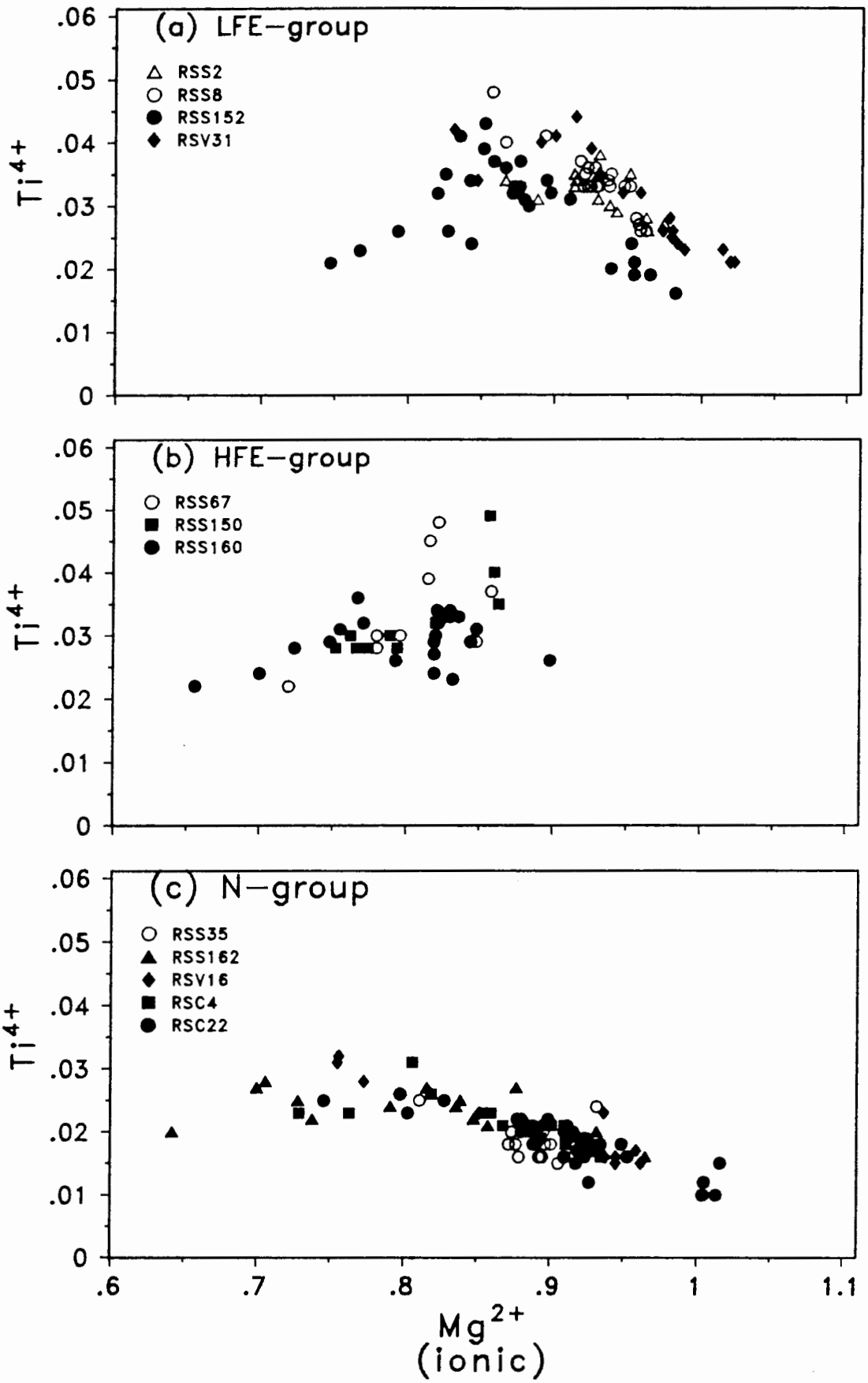

Figure 4.4. Ti (ionic) *vs* Mg (ionic) in calcic clinopyroxenes of the different basaltic groups.

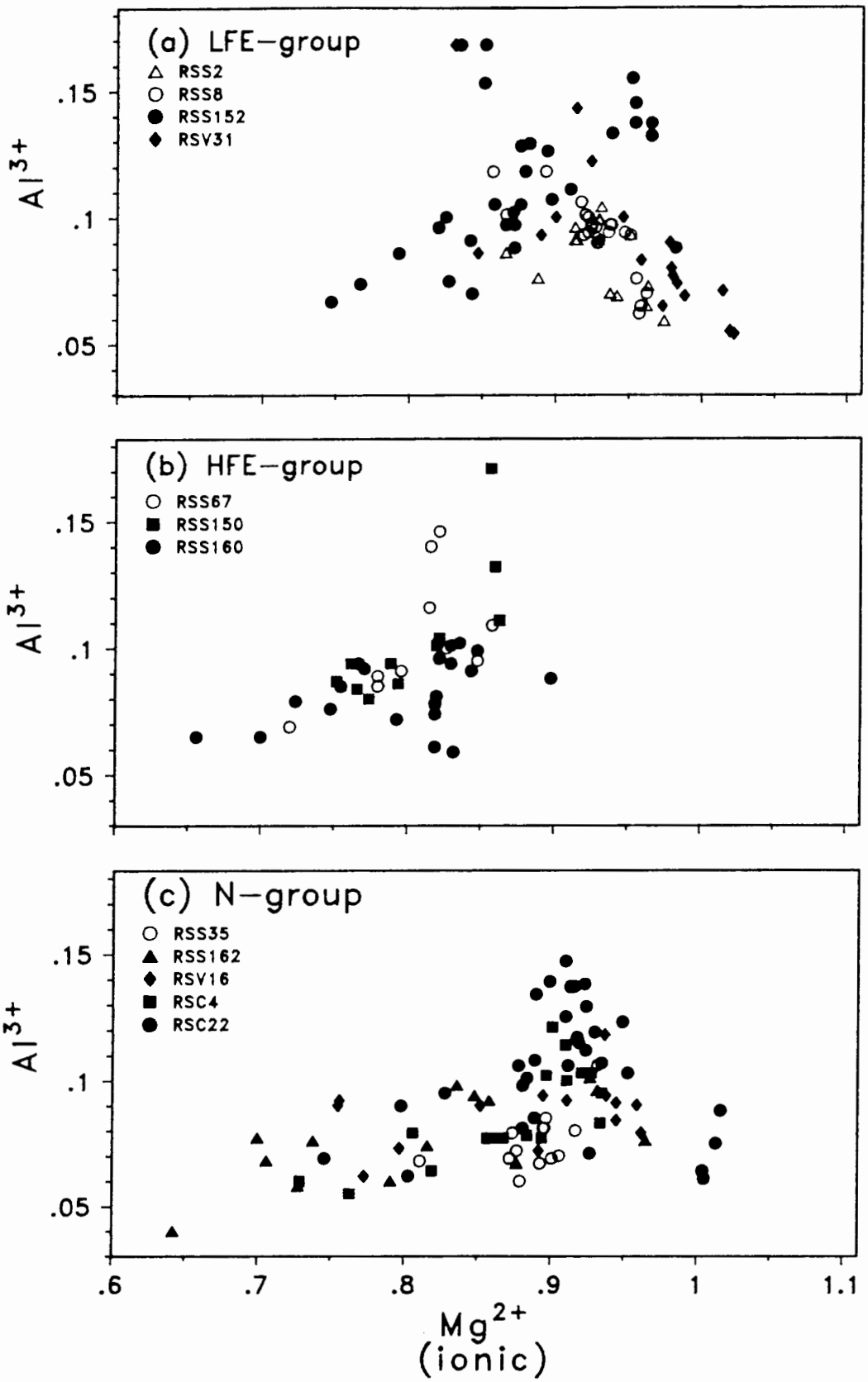

Figure 4.5. Al (ionic) *vs* Mg (ionic) in calcic clinopyroxenes of the different basaltic groups.

and display a broad positive correlation of Ti with Mg (compare Fig. 4.4b with Fig. 3.3b); (3) N-group pyroxenes have both consistently lower Ti concentrations and a gradual increase of Ti with decreasing Mg (Fig. 4.4c); and (4) Al in clinopyroxenes of the N- and HFE-groups decreases with decreasing Mg (Fig. 4.5b, c). The LFE-group pyroxenes display an increase in both Al and Ti content with decreasing Mg content but become positively correlated at lower Mg contents (Fig. 4.5a). This positive correlation is defined primarily by RSS152 (a dolerite dyke) which contains pyroxenes of a lower Mg content than the basalts. In the case of RSS152 the reversal of the variations of these minor components is probably a result of the appearance of plagioclase and ilmenite/magnetite on the liquidus at lower temperatures as the rocks crystallized. It is suggested that crystallization of pyroxenes reflecting these more evolved melts is facilitated by the slower crystallization of RSS152 (a dolerite) compared to the more rapid crystallization in the basalts all of which contain a substantial glass component (Table 3.3).

4.4 FELDSPAR

Plagioclase is the most common mineral phase present in the groundmass and sometimes as phenocrysts in both HFE- and N-group rocks. It is sometimes absent in LFE-group basalts although, without exception, LFE-group basalts with MgO <5% contain plagioclase phenocrysts. Plagioclase and rarely alkali feldspar, are the only phenocryst phases easily visible in hand specimen. Selected feldspar compositions are given in Table 4.3.

Alkali feldspar phenocrysts/xenocrysts (?) are present in a N-group basalt sample (RSS63, Fig. 4.6) and as a groundmass phase in another (RSS67, a HFE-group basalt). The alkali feldspars in RSS63 are coarsely perthitic and have compositions ranging from almost pure orthoclase to pure albite with little or no anorthite component (Table 4.3). Carmichael *et al.* (1974) report examples of the co-crystallization of sanidine and plagioclase in 2 shoshonitic basalts. However, in the case of RSS63, the host rock belongs to the N group, relatively lower in K_2O than the HFE or LFE groups. The unresorbed nature of both alkali and plagioclase feldspars in a micro-crystalline groundmass suggests that these minerals are in equilibrium

Table 4.3. Selected feldspar analyses (from Appendix C).

	1	2	3	4	5	6	7	8	9	10	11	12	13	14	15	16	17
SIO2	55.29	54.92	53.58	64.75	53.33	56.17	54.79	58.89	65.23	66.46	67.44	53.61	55.75	55.03	52.99	50.60	52.07
AL2O3	28.00	27.88	29.16	18.55	28.53	26.64	28.57	25.57	18.62	19.57	21.04	29.08	27.15	28.13	29.26	30.95	29.87
FEO	.53	.60	.99	.24	.77	.67	.70	.60	.10	.01	.01	.49	.85	.57	1.18	.48	.53
MGO	.11	.08	.14	.01	.12	.06	.11	.04	.01	.01	.01	.16	.23	.11	.30	.23	.21
CAO	11.44	11.17	12.58	.01	11.90	10.02	11.35	8.00	.01	.46	1.72	12.67	10.66	11.99	12.54	14.24	13.12
NA2O	4.23	4.41	4.00	.04	4.10	5.17	4.52	6.23	.27	5.13	10.37	3.94	5.07	4.32	3.85	3.05	3.74
K2O	.63	.56	.33	16.15	.41	.60	.32	.73	15.35	8.66	.06	.11	.23	.26	.18	.09	.15
TOTAL	100.23	99.62	100.78	99.75	99.16	99.33	100.36	100.06	99.59	100.30	100.65	100.06	99.94	100.41	100.30	99.64	99.69
atomic proportions calculated using 8 oxygens																	
SI	2.493	2.491	2.417	2.997	2.439	2.550	2.468	2.637	3.007	2.978	2.932	2.426	2.519	2.478	2.403	2.314	2.374
AL	1.488	1.491	1.551	1.012	1.538	1.425	1.517	1.350	1.012	1.034	1.078	1.551	1.446	1.493	1.564	1.668	1.605
FE2+	.020	.023	.037	.009	.029	.025	.026	.022	.004			.019	.032	.021	.045	.018	.020
MG	.007	.005	.009	.001	.008	.004	.007	.003	.001	.001	.001	.011	.015	.007	.020	.016	.014
CA	.553	.543	.608		.583	.487	.548	.384		.022	.080	.614	.516	.579	.609	.698	.641
NA	.370	.388	.350	.004	.364	.455	.395	.541	.024	.446	.874	.346	.444	.377	.338	.270	.331
K	.036	.032	.019	.954	.024	.035	.018	.042	.903	.495	.003	.006	.013	.015	.010	.005	.009
SUM	4.966	4.973	4.992	4.976	4.986	4.982	4.980	4.979	4.951	4.976	4.968	4.974	4.987	4.971	4.990	4.990	4.993
AN	57.6	56.4	62.2	.0520	60.1	49.9	57.0	39.7	.0530	2.29	8.37	63.6	53.0	59.6	63.6	71.7	65.4
AB	38.6	40.3	35.8	.375	37.5	46.6	41.1	56.0	2.60	46.3	91.3	35.8	45.6	38.9	35.3	27.8	33.7
OR	3.78	3.36	1.94	99.6	2.47	3.56	1.91	4.31	97.3	51.4	.348	.657	1.36	1.54	1.09	.539	.890

values below detection limit are printed as blanks

sample descriptions:

1	: PLAG2 CENTRE RSS36	LFE	
2	: PLAG2 EDGE RSS36	-group	
3	: PLAG4 CENTRE RSS152		
4	: GMASS ALK-FELD2 RSS67		
5	: PLAG3 RSS150	HFE	
6	: PLAG8 RSS150	-group	
7	: PLAG8 CENTRE(A) RSS160		
8	: PLAG8 EDGE(B) RSS160		
9	: MACRO-PHENO ALK-FELS2A RSS63	N	
10	: MACRO-PHENO ALK-FELS2C RSS63	-group	
11	: MACRO-PHENO ALK-FELS2K RSS63		
12	: MACRO-PHENO PLAG17C RSS63		
13	: GMASS PLAG18 RSS63	N	
14	: PLAG4 EDGE RSV16	-group	
15	: PLAG3 CENTRE RSC22		
16	: PLAG8 CENTRE RSC22		
17	: PLAG10 CENTRE RSC22		

(a)

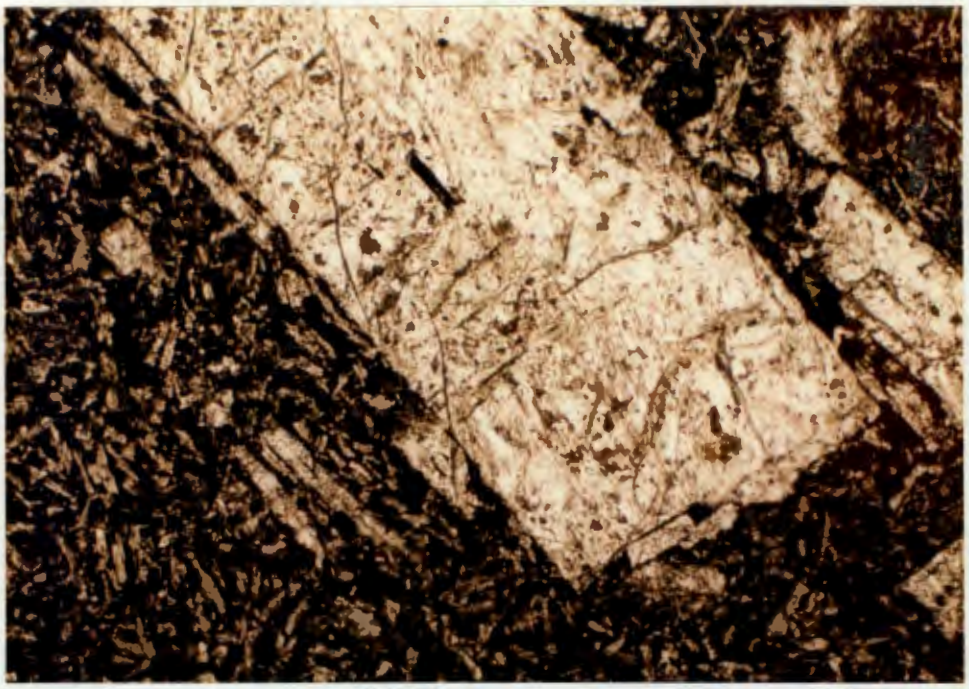

(b)

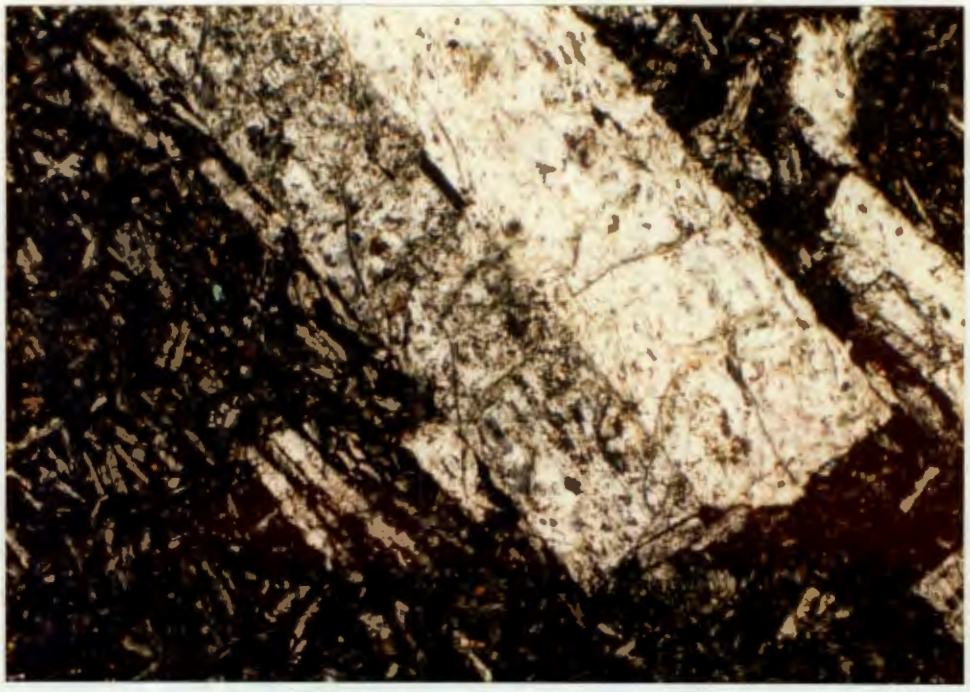

Figure 4.6. Photomicrograph of a large alkali feldspar (ab/or) phenocryst in RSS63 (feldspar 3, Appendix C) under plane polarized light (a) and cross-nicols (b) (17x magnification, field of view is 6.5 mm).

with a melt of the host rocks' (RSS63) composition and that both mineral phases are not xenocrysts. Alternatively, if crystallization in RSS63 was fast (implied by the micro-crystalline groundmass), resorption of xenocrystic feldspars, may have been inhibited. The development of alkali feldspars in igneous rocks has been considered in three stages by Parsons and Brown (1984): magmatic, involving crystal growth from the melt; subsolidus or post-magmatic, involving coherent exsolution and development of regular strain controlled crypto- or microperthites; and deuteric or hydrothermal growth involving feldspar-fluid interactions which give rise to irregular coarse micro-perthites. The occurrence of plagioclase in the groundmass (*ca* An_{55}) and plagioclase phenocrysts (up to An_{64}) in the same thin-section (plag17C and plag18C from RSS63, Table 4.3) rules out post-magmatic deuteric alteration of plagioclase as a **primary** cause of formation of the alkali feldspars as any alteration process should have affected plagioclase equally. However, the irregular and coarse nature of the perthitic exsolutions may represent the final (deuteric) stage of modification which an original magmatic and subsequently exsolved (subsolidus) alkali-feldspar has undergone. Thus, if not xenocrystic, the occurrence of what are probably original primary magmatic alkali feldspars in a N-type basalt (i.e. generally lower K_2O than the "enriched" basaltic groups), is enigmatic.

Plagioclase occurring in the groundmass of basalts is often albitized while any phenocrysts present are usually relatively unaffected by such a process. Post-magmatic fluids may be the agent of this alteration and would be afforded an easy passage by the fine-grained groundmass of such basalts. The equilibrium reaction can be written (Lagache,1984):

$$2NaAlSi_3O_8 + CaCl_2 = CaAl_2Si_2O_8 + 2NaCl + 4SiO_2$$

In the presence of a saline fluid and dissolved silica, the reaction equilibrium is shifted to the left. The altered groundmass feldspars typically have a dusting of kaolinite, which may provide a depository for at least some of the Ca leached by this process. Undoubtedly, however, the Ca lost and the Na gained by feldspars in this albitization process must be reflected in the whole-rock composition and this appears to be the case (Chapter 3.1.3).

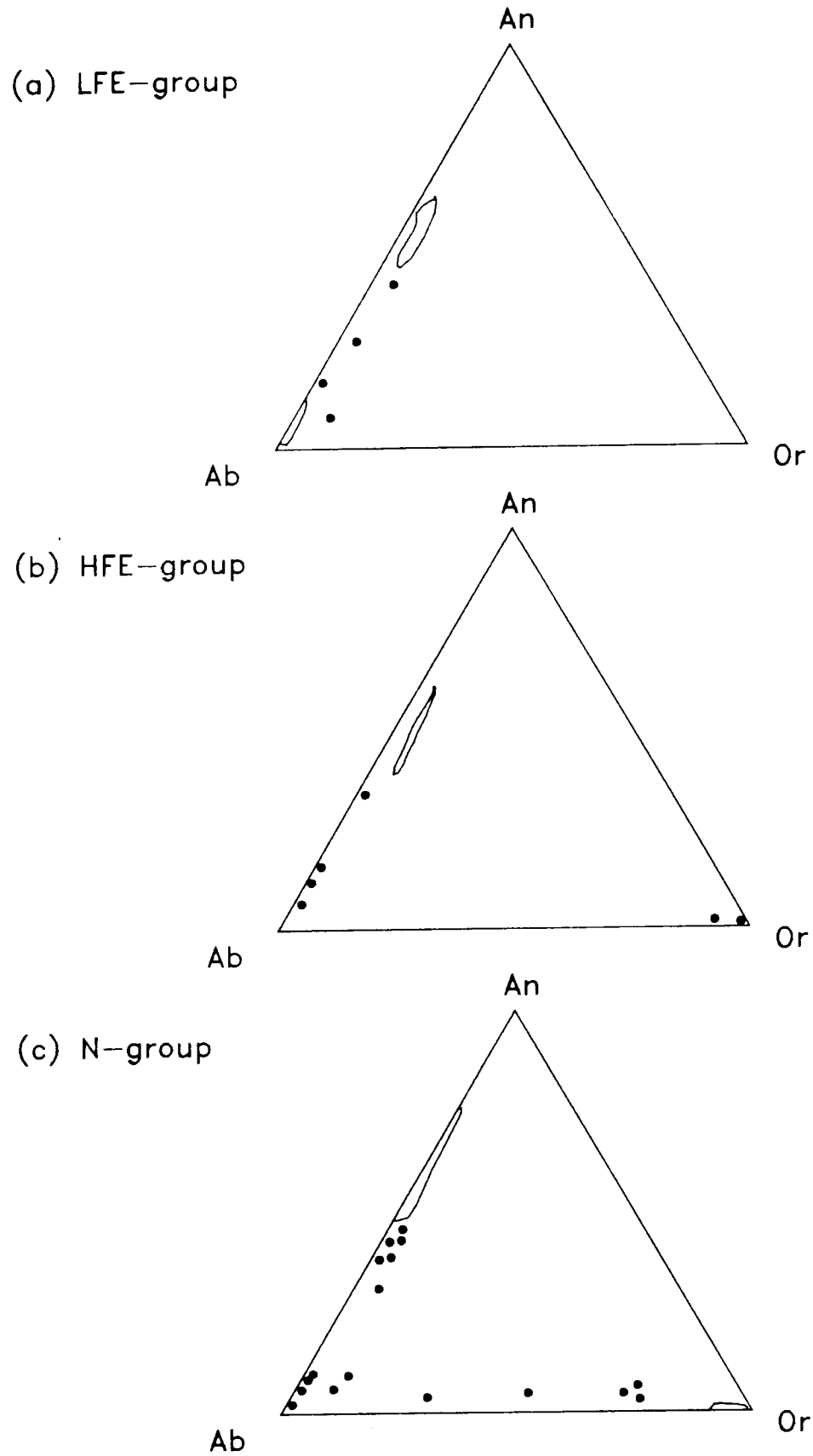

Figure 4.7. Feldspar compositions for all samples in terms of anorthite (An) albite (Ab) and orthoclase (Or) end-members.

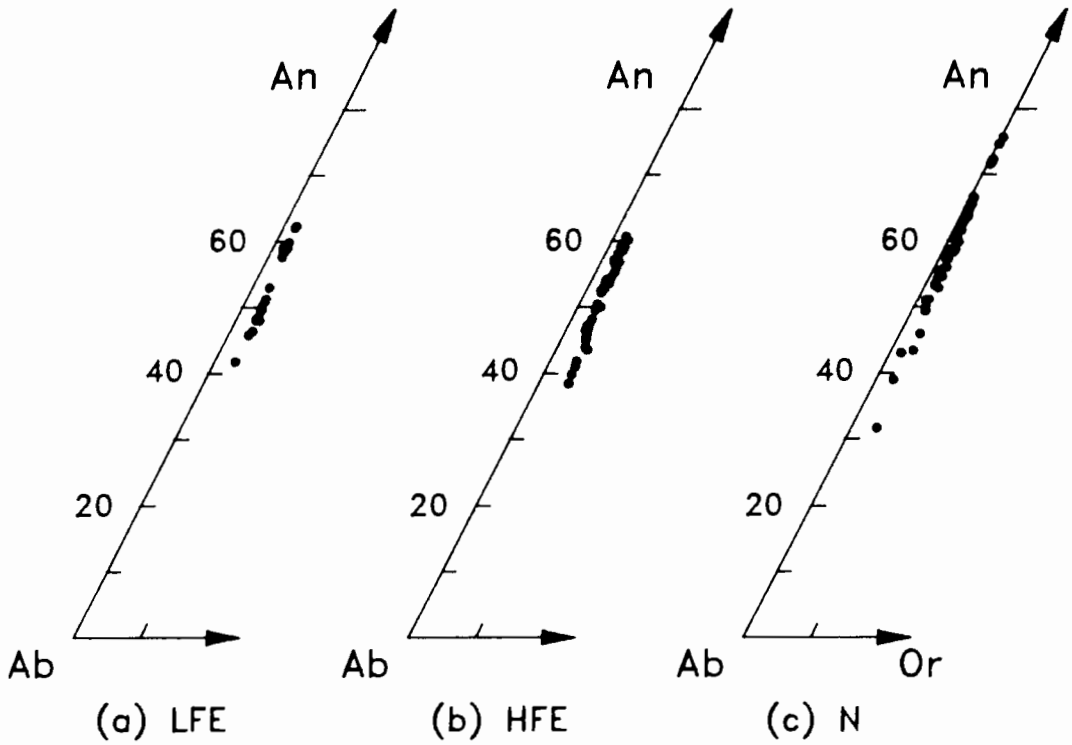

Figure 4.8. Feldspar compositions in dolerites (i.e. relatively unaltered) only.

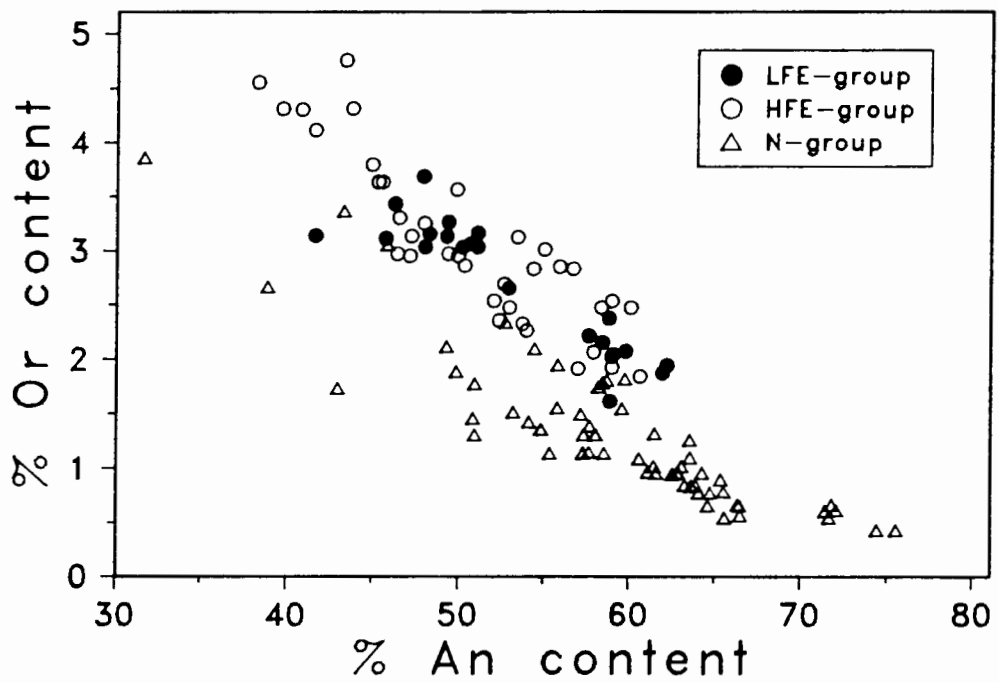

Figure 4.9. Orthoclase (Or) *vs* anorthite (An) contents of plagioclases from central Lebombo dolerites only. Illustrated is the greater orthoclase component in LFE- and HFE-group plagioclases relative to N-group plagioclases.

Plagioclase in dolerites is generally unaltered and usually displays prominent normal zoning patterns from core to edge in all three basaltic groups (a maximum decrease of An_{17} is observed from core to rim, plag8 from RSS160, Table 4.3). Exceptions are the plagioclase phenocrysts analysed in RSS36 (LFE-group) which are unzoned and have a constant composition (*ca* An_{57}, Table 4.3).

All feldspar compositions are plotted in Fig. 4.7. To eliminate possible variations induced by alteration, only feldspars analysed from unaltered dolerites are plotted in Fig. 4.8. For this "fresh" subset, the different basaltic groups have the following ranges:

LFE	(RSS152)	An_{42} - An_{64}
HFE	(2 samples)	An_{39} - An_{61}
N	(4 samples)	An_{32} - An_{77}

The greater Or content of the "enriched" (HFE- and LFE-groups) samples relative to N-group samples, reflects their generally greater whole-rock K_2O content (Fig. 4.9).

4.5 OPAQUE MINERALS

4.5.1 Introduction

Aside from the infrequent and minor occurrence of small pyrite blebs in these rocks, the major opaque phases present belong to the spinel and ilmenite groups and their associated oxidation products.

The classification of oxide minerals into various solid solution series adopted by Haggerty (1976) is used here. With the exception of rutile the oxides are divided into 3 solid-solution series: magnetite-ulvospinel; ilmenite - hematite; and the pseudobrookite series.

The ratio of primary ilmenite/primary spinel is affected by fO_2 and a_{SiO2} (Haggerty,1976). The ratio of primary ilmenite/primary spinel varies considerably with basaltic rock type in the central Lebombo to the point of exclusion of one or the other as a primary phase in some samples. This variation may be affected by fO_2 and a_{SiO2} but also appears to be related to the TiO_2 concentration in the melts from which these rocks crystallized.

Oxide phases are prone to post-crystallization effects such as oxidation and exsolution. It is important, therefore, that these processes are considered as they may change the primary mineralogy considerably. For this purpose the classification scheme of Haggerty (1976) is used, i.e. progressive oxidation is indicated on a scale of 1 to 7 for spinels (C1 - C7) and ilmenites (R1 - R7).

4.5.2 Oxidation conditions

Whether oxidation of both magnetite and ilmenite solid-solution series occurs with magma cooling (fO_2 $\pm 10^{-12}$ atm.) or conditions of deuteric oxidation (fO_2 $\pm 10^{-6}$ atm.) or both, is difficult to ascertain in the absence of detailed sampling profiles across flows. When considering opaque oxides in fresh dolerite, however, deuteric oxidation as a significant mechanism of mineral modification can be excluded.

The petrographic characteristics for each group are summarized here and given in more detail in Appendix B. Selected opaque oxide analyses are given in Table 4.4 and all the data is plotted in Fig. 4.10.

4.5.2.1 LFE-group

Dominant ilmenite and lesser magnetite are present in the rocks of this group. Five (all basalts) of the seven samples considered contain only ilmenite or pseudomorphs after ilmenite. In the remaining two samples, a basalt (RSS36) contains both minerals in about equal proportions whilst a dolerite (RSS152) has a preponderance of ilmenite (estimated ilmenite/magnetite ratio of 70/30). This difference in assemblage may reflect the more 'evolved' nature of the basalt (MgO = 3.94%) compared to the dolerite (MgO = 5.16%), implying that magnetite replaces ilmenite as the dominant opaque phase at more evolved compositions. However, one of the basalts containing only ilmenite (RSS2) has a MgO content intermediate between these two (MgO = 4.94%). This apparent anomaly may be a function of higher fO_2 conditions in the dolerite (RSS152) and/or the higher TiO2 (3.14% *vs* 2.87%) content of RSS2. Thus, there is a suggestion that the TiO_2 concentration may be playing a part in the crystallization of ilmenite in preference to magnetite. Usp-mt_{ss} ranges from usp_{38}-usp_{46} in this rock type and ilmenite compositions fall in the range ilm_{93}-ilm_{98}.

Table 4.4. Selected analyses of opaque oxides (from Appendix C)

	1	2	3	4	5	6	7	8
SIO2	.07	.35		.05		.09	.09	
TIO2	97.36	15.30	50.18	55.18	51.59	24.50	22.77	50.24
AL2O3	.12	1.79		.20	.07	2.17	1.56	.04
CR2O3				.04		.06		
FE2O3	.67	35.30	3.70	20.63	1.69	14.43	19.00	3.22
FEO		44.51	44.55	20.71	45.51	53.23	52.60	44.50
MNO		.51	.71	.16	.44	1.49	1.04	.46
MGO		.11	.35	.05	.63	.01	.05	.43
CAO	.58	.01	.01	.13	.03	.04	.01	.07
ZNO	.01	.32	.01	.01	.01	.79	.01	.01
V2O5	.88		.48	1.03	.44	1.15	1.06	.45
TOTAL	99.73	98.21	100.02	98.19	100.43	97.96	98.20	99.44

atomic proportions calculated on the basis of number of oxygens:

	2	4	3	5	3	4	4	3
SI	.001	.013		.002		.003	.003	
TI	.978	.439	.952	1.645	.972	.698	.650	.958
AL	.002	.081		.009	.002	.097	.070	.001
CR				.001		.002		
FE3+	.007	1.014	.070	.615	.032	.412	.543	.061
FE2+		1.421	.940	.686	.953	1.687	1.670	.943
MN		.0	.0	.0	.0	.0	.0	.0
MG		.006	.013	.003	.024	.001	.003	.016
CA	.008			.006	.001	.002		.002
ZN		.009				.022		
V	.008		.008	.027	.007	.029	.027	.008
SUM	1.005	3.000	2.000	3.000	2.000	3.000	3.000	2.000
IL/US		46.4	95.1		96.0	77.2	70.5	95.3
GK/MT		53.6	1.33		2.38	22.8	29.5	1.64
HM			3.56		1.61			3.11

FE3+/FE2+ proportions are calculated to satisfy cation stoichiometric proportions. Values below detection limit are printed as blanks.

samples descriptions:

1 : rutile - OXIDE4 RSS2
2 : magnetite - OXIDE6 RSS152
3 : ilmenite - OXIDE13 RSS152
4 : pseudobrookite - OXIDE 3 RSV31
5 : ilmenite - OXIDE11B RSS160
6 : magnetite - OXIDE13A RSS160
7 : magnetite - OXIDE1 RSC4
8 : ilmenite - OXIDE4 RSC4

LFE-group

HFE-group

N-group

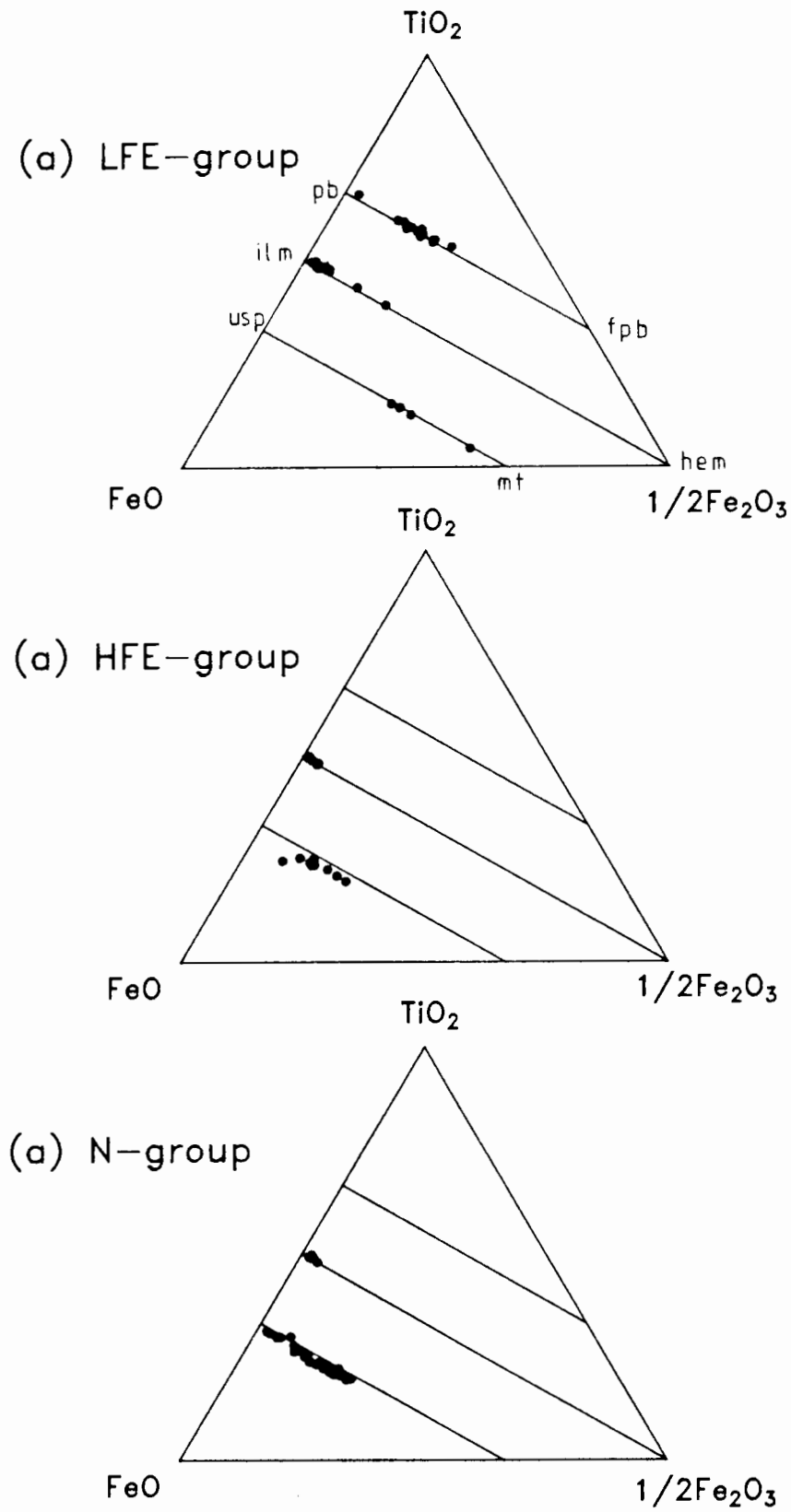

Figure 4.10. Opaque oxide mineral chemistry in mol% of the major oxides for the three solid-solution series ferropseudobrookite-pseudobrookite, ilmenite-hematite and ulvospinel-magnetite for the three basalt groups.

The magnetite in the basalt (RSS36) is optically homogeneous (C1 stage) and contains none of the ilmenite lamellae (C2, C3) present in the magnetites of the dolerite (RSS152). This is probably a function of their different cooling conditions - the basalt is chilled quickly while the slower cooling in the dolerite permits the development of these lamellae.

Ilmenite oxidation states vary from homogeneous unoxidised ilmenite (R1) in RSS2 and RSS14, to ilmenites almost completely replaced by pseudobrookite (R7) in RSV31 (Fig. 4.11). In Fig. 4.11, the confinement of remaining ilmenite to grain boundaries is typical of the latter sample. This confirms that the alteration of these ilmenites is an oxidation effect due to changing temperature and fO_2 conditions and not a result of deuteric oxidation, i.e. oxidation proceeds at a faster rate in the hotter central portions of the grain than at the edges which would have been preferentially affected if deuteric water was responsible for increasing fO_2. The ilmenites of one basalt (RSS36) do occasionally exhibit some rutile exsolution (R2), while ilmenites of RSS41 (basalt) have a range of oxidation stages from R4 (ferrian ilmenite) to R7 (pseudobrookite). The analyses of an ilmenite microphenocryst in RSS2 (Oxide 1A - 1F, Appendix C) revealed no zoning.

4.5.2.2 HFE-group

Both ilmenite and magnetite are present in approximately equal proportions in the three dolerites considered. Ilmenite characteristically occurs as acicular unoxidised (R1, optically homogeneous) grains which have a range in compositions from $ilm_{94}hem_2$ - $ilm_{98}hem_1$ (Appendix C). Magnetite contains both sandwich and trellis lamellae (C3, with compositions $ilm_{93}hem_7$ to $ilm_{97}hem_3$). The exsolved magnetites have a range in compositions from usp_{64} to usp_{84}. Microprobe scans across ilmenites in RSS150 (oxide 8) and RSS160 (oxide 9) showed these minerals to be chemically homogeneous (Appendix C).

4.5.2.3 N-group

Magnetite is the dominant oxide mineral in this group. In the five thin-sections studied, one contains ilmenite only in composite intergrowths with magnetite (RSS162, dolerite) and in only one sample (RSC4, dolerite) is ilmenite present as discrete grains in addition to composite intergrowths with magnetite.

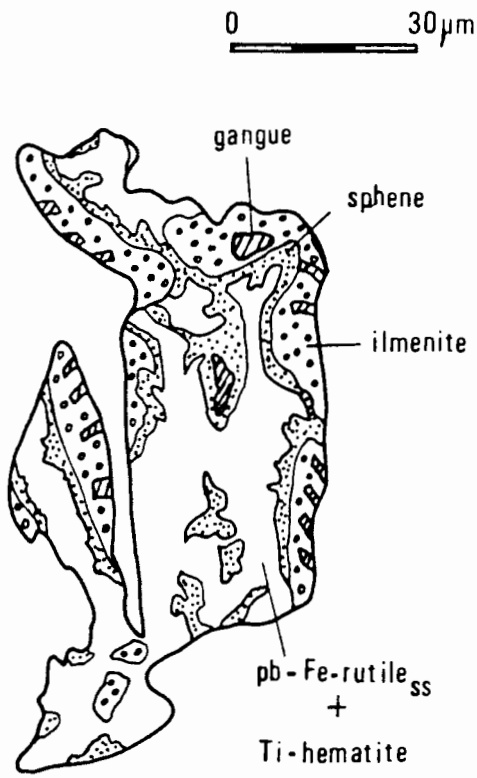

Figure 4.11. Sketch of the distribution of phases in an ilmenite from RSV31 showing the development of pseudobrookite (pb) and Fe-rutile solid-solution + Ti-hematite, typical of the R6-R7 oxidation state of Haggerty (1976). Note that the ilmenite is most oxidised in the grain center rather than at the edge, thereby excluding deuteric alteration as a means of oxidation.

Samples exhibit a range of oxidation states from C1, C2 (RSC4, RSC32) to C3 (RSC22, RSS162, RSV16) containing abundant trellis and sandwich ilmenite lamellae ($ilm_{74}hem_{23}$ - $ilm_{97}hem_{2}$). In the magnetites containing 'exsolved' ilmenite (RSC22, RSS162, RSV16) the compositional range is usp_{64} - usp_{84}, while in samples containing largely homogeneous magnetite (RSC4, RSC32) the range is usp_{61} - usp_{86}. Thus, predictably, a greater upper limit of ulvospinel content is apparent in magnetites containing no exsolution.

Where ilmenite is present as discrete grains, it is optically homogeneous (R1) and has a similar compositional range in all the rock types: $ilm_{93}hem_{3}$ - $ilm_{97}hem_{2}$.

4.5.2.4 Summary of oxide compositions

The typical compositional ranges for primary (i.e. unexsolved) ilmenite analysed in all basaltic rock types is similar, i.e. ilmenite-hematite: $ilm_{93}hem_{6}$ - $ilm_{98}hem_{2}$. The compositions of LFE- and N-group spinels are different, with N-group spinels having a higher ulvospinel content. This is superficially anomalous as LFE-group samples have higher whole-rock TiO_2 contents. The Ti content of liquids from which the LFE-group rocks crystallized, however, may have been sufficiently high to ensure the crystallization of ilmenite as a separate phase while the ilmenite component in N-group rocks is absorbed into the magnetite as an ulvospinel component.

4.5.3 Geothermometry

Buddington and Lindsley (1964) first calibrated an iron-titanium oxide geothermometer and oxygen barometer. Their method of calculation utilises the compositions of co-existing mt-usp_{ss} and ilm-hem_{ss} pairs in the system FeO-Fe_2O_3-TiO_2 (O-Fe-Ti) (expressed as mole fractions of ilmenite and ulvospinel). This model of Buddington and Lindsley's (1964) based on experimental data was revised thermodynamically by Spencer and Lindsley (1981) and it is this latter model that is applied here. The Spencer and Lindsley (1981) model has reproduced experimental data in the range 600-1300°C (bounded by Ni-NiO and wustite-magnetite buffer curves). Uncertainties quoted by Spencer and Lindsley (1981) in T and fO_2 (2 s.d.) are 40-80°C and 0.5-1.0 log units fO_2 assuming $\pm$1% uncertainties in

usp_{ss} and ilm_{ss} compositions. Lamellae and apparent crystallization conditions suggested by composite ilmenite/magnetite grains are given in Tables 4.5 and 4.6.

Aside from three lamellae giving anomalously high temperatures and fO_2 values (1100-*ca*1350°C) the remainder of the lamellae fall in the range: 650-980°C and 10^{-20} - $10^{-12.5}$ atm. (Table 4.5). These conditions are considered representative of the range in T and fO_2 in which these lamellae formed. In oxide 3 of RSS162 similar temperatures and oxidation conditions are obtained for both the lamellae and the composite ilmenite-magnetite intergrowth.

For Spencer and Lindsley's (1981) geothermometer to reflect conditions of their crystallization, it is necessary that equilibrium be established between co-existing magnetite and ilmenite pairs. Obviously an ilmenite which occupies the centre of a magnetite grain may have been a nucleation point for the later crystallization of the magnetite in which case the pair do not represent an equilibrium system. Composite ilmenite-magnetite pairs thought to be in equilibrium reflect a range in physical conditions: temperature 850-920°C and fO_2 $10^{-15.5}$ - $10^{-13.2}$ atm. (Table 4.6). This range, more restricted than the lamellae range, approximates the 2 standard deviation error for the geothermometer and oxygen barometer quoted by Spencer and Lindsley (1981). The use of magnetite-ilmenite pairs in which the magnetite composition has been modified by ilmenite exsolution will produce erroneous results. Only in oxide 6 in RSS162 and the oxide pairs in RSC4 (Table 4.6) was magnetite free of ilmenite exsolution. However, even if only these three grains are considered, then the range in physical conditions changes little from that quoted above (850-910°C; $10^{-13.2}$ - $10^{-14.5}$ atm). The temperatures predicted by this geothermometer are considerably lower than those liquidus temperatures predicted by experimental data for basaltic rocks in general. For instance, the prediction by the model of Nathan and Van Kirk (1978), based on a compilation of experimental data, indicates liquidus temperatures of 1150-1200°C for these basalts.

Thus, the geothermometry does not reflect likely liquidus temperatures of these basalts but values do fall close to the lower limit of the range of likely solidus temperatures (950-1020°C) gauged to be 180-200°C below the liquidus temperatures of basaltic melts at 0-5 kbar (Yoder, 1976). This is to be expected if these minerals crystallized late in the basalt cooling

Table 4.5. Calculated temperatures and oxygen fugacities for magnetite using ilmenite lamellae (morphology indicated) and host magnetite pairs using the model of Spencer and Lindsley (1981)

sample			ilm_{ss}	usp_{ss}	log fO_2 (atm.)	temperature (°C)
RSS150	oxide 1	lamellae	93.1	62	-13.0	900
	oxide 4	lamellae	95.5	70	-15.2	840
	oxide 5	lamellae	96.8	67(2)	-18.7	710
RSS160	oxide 10	lamellae	94.9	76	-13.5	930
	oxide 13	lamellae	96.6	75(2)	-16.6	800
RSC22	oxide 3	lamellae	93.1	68	-10.0	1080
			89.7	68	-6.0	>1300
	oxide 4	lamellae	82.2	77	-7.0	>1300
	oxide 5	lamellae	95.5	61	-16.0	780
	oxide 6	lamellae	94.3	74	-13.5	920
	oxide 8	lamellae	93.1	71	-12.5	980
	oxide 10	lamellae	93.1	65(2)	-12.7	930
RSS162	oxide 1	sandwich	91.1	74	-10.0	1100
		trellis	95.1	74	-14.0	900
	oxide 3	trellis	96.1	76	-15.6	840
RSV16	oxide 1	sandwich	97.0	64	-20.0	660
		sandwich	97.0	76	-18.0	750
	oxide 2	sandwich	96.3	46	-20.0	650
	oxide 3	sandwich	96.7	79	-16.0	830
	oxide 7	sandwich	96.9	74	-18.0	750

(bracketed numbers indicate multiple determinations)

Table 4.6. Calculated temperatures and oxygen fugacities for ilmenite/magnetite pairs using the model of Spencer and Lindsley (1981). Uncertain composite intergrowths are queried (?).

sample		ilm_{ss}	usp_{ss}	log fO_2 (atm.)	temperature (°C)
RSS160	oxide 11 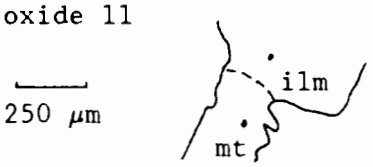	96.0	81	-14.5	920
RSC22	oxide 7 ? 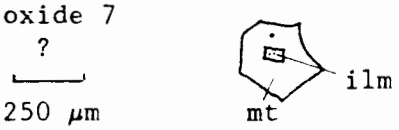	94.4	69 (2)	-14.0	880
RSS162	oxide 2 ? 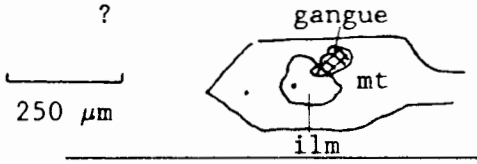	97.4 (2)	79	-19.7	700
	oxide 4 oxide 3 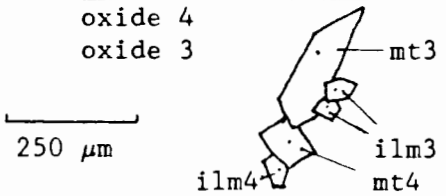	96.7 96.1 (2)	82 76	-15.5 -15.5	860 850
	oxide 5 ? 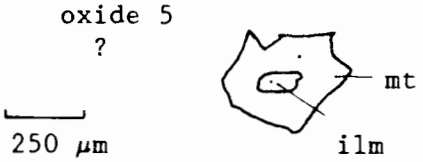	95.9	76	-15.0	860
	oxide 6 	95.7	79	-14.0	900
RSC4	oxide 2 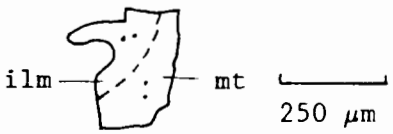	93.8 (2)	66 (2)	-13.2	910
	oxide 6 ? 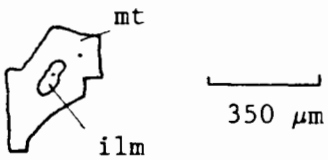	94.3	64	-14.5	850

history. In the case of the HFE group, however, the large decrease of TiO_2 with MgO (Fig. 3.3b) is probably induced by the crystallization of an opaque phase in which case the geothermometer is not reproducing even likely magma solidus temperatures. Therefore, it seems that equilibration of oxides in the HFE-group occurred under sub-solidus conditions and it is unlikely that oxides from the N and LFE groups escaped such equilibration. The homogeneous nature of a LFE-group ilmenite microphenocryst (oxide 1 RSS2), when contrasted with the zoning observed in other mineral species analysed, is further support for sub-solidus equilibration.

4.6 MISCELLANEOUS PHASES

The LFE-group basalts are often characterized by a glass matrix. Analysis showed that the matrix glass typically contains appreciable Ti and K (Table 4.7).

Phases occupying vesicles include zeolites, quartz, calcite, chlorite and epidote. Minor quartz occasionally occurs in the matrix of some basalts. Minor apatite is particularly conspicuous in the groundmass of the HFE-group samples. Specific occurences of these minor phases in individual samples are given in the petrographic descriptions in Appendix B.

4.7 SUMMARY

Primary minerals in the basaltic rocks of the three groups are: plagioclase and pyroxene, lesser olivine and opaque oxides and accessory quartz and apatite. There is no evidence in the mineral assemblage or mineral chemistry for high-pressure fractional crystallization. Oxide mineral geothermometry indicates temperatures closer to the basalt solidus and not the liquidus of their host melts, and it is likely that some equilibration occurred under sub-solidus conditions.

Normal geochemical zoning is present in varying degrees in olivines, clinopyroxenes and plagioclases analysed. Furthermore, the range in mineral chemistry for all mineral species analysed in a single thin-section is considerable, which is evidence against equilibrium crystallization.

Table 4.7. Selected glass analyses (from Appendix C).

	1	2	3	4	5	6
%						
SiO_2	29.41	29.55	51.18	56.22	56.06	51.78
TiO_2	nd	nd	8.93	2.42	6.29	15.22
Al_2O_3	16.48	16.86	14.28	16.61	15.20	7.50
FeO	33.17	33.41	3.60	3.48	1.56	3.41
MnO	.14	.11	.10			
MgO	9.59	9.34	1.24	1.14	.43	.66
CaO	.50	.57	9.13	4.82	7.04	14.63
Na_2O	.05	.04	2.50	1.80	2.53	.84
K_2O	.19	.20	5.63	9.21	8.07	2.98
Cr_2O_5						
P_2O_5			.68	1.80	.64	
Total	89.54	90.09	97.27	97.50	97.82	97.11

values below detection limit are printed as blanks

sample descriptions:

1 : glass 1 RSS2
2 : glass 3 RSS2
3 : glass 11 RSS8
4 : glass 1/2 RSS8
5 : glass 1/3 RSS8
6 : glass 1 RSV31

5. DISTRIBUTION OF BASALTIC ROCK TYPES

5.1 GEOGRAPHICAL DISTRIBUTION

The geographical distribution of the "normal" (N), low-Fe "enriched" (LFE) or high-Fe "enriched" (HFE) groups in the central Lebombo is given in Figs. 5.1 and 5.2. Only areas of known basalt chemistry are shaded and incorporate most of the observable outcrop and all of the outcrop suitable for geochemical sampling. The limitation of reasonable outcrop to major rivers and some streams is obvious. While all samples analysed quantitatively are classified into the three groups, less precise data obtained from the analysis of rock slabs where quantitative data is not available, has resulted in some overlap between the groups. For example, samples with slabs containing Zr >270 ppm, TiO_2 >2.7% and Fe_2O_3t between 13.5% and 14.5% may belong to either the LFE or HFE groups. Thus the few samples of ambiguous geochemical affinity (unclassified in the slab data table on microfiche in Appendix C) were not included in maps and sections defining the distribution of the basaltic groups.

Immediately obvious is the dominance of LFE-group basalts in the west, HFE-group basalts in the east and N-group basalts in the central portions of the mapped area. Also apparent is the increase in N-group basalts and the decrease in LFE-group basalts southwards. All three basalt groups are interbedded in the Sabie River area but only the N- and HFE-groups are interbedded in the Crocodile/Komati River area (within the limits of the sampled outcrop).

It has been suggested in earlier chapters on geological and geochemical grounds that the dolerites in the area represent at least some of the feeders to the basalt succession. The distribution of the dykes is consistent with this suggestion - only 4 N-group dykes in the east of the Sabie River area (Fig. 5.1) have no sampled extrusive equivalent. LFE-group dolerites in the Sabie River area are less common than N- or HFE-group dolerites and no LFE-group dykes were sampled in the Crocodile/Komati River area which is consistent with the less voluminous nature of the LFE-group basalt type in the south.

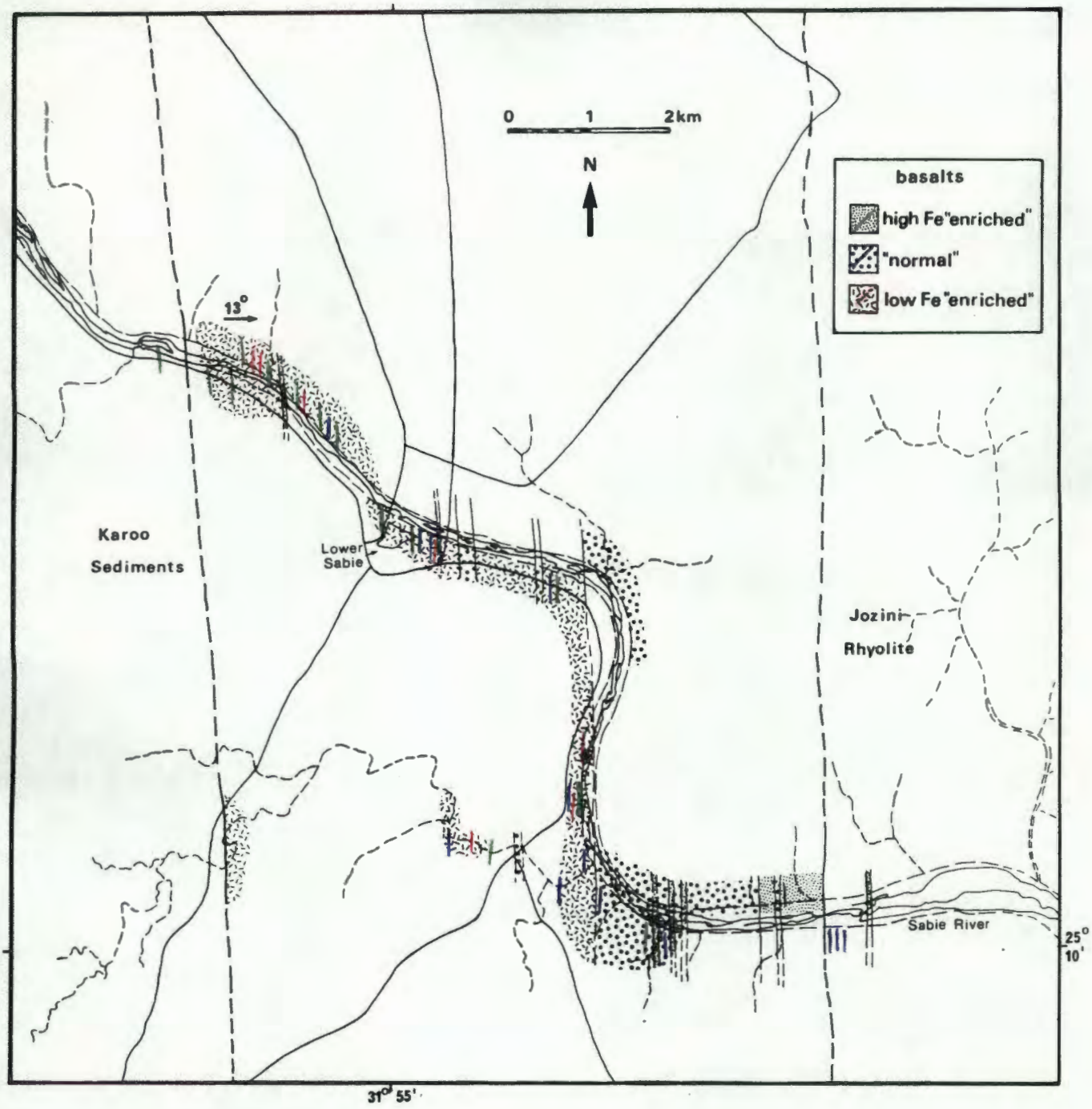

Figure 5.1. Basaltic rock-types in the Sabie River area. Only outcrop wherein the basalt-type is known is shaded. Dolerite dykes belonging to the three basalt groups are represented by coloured lines.

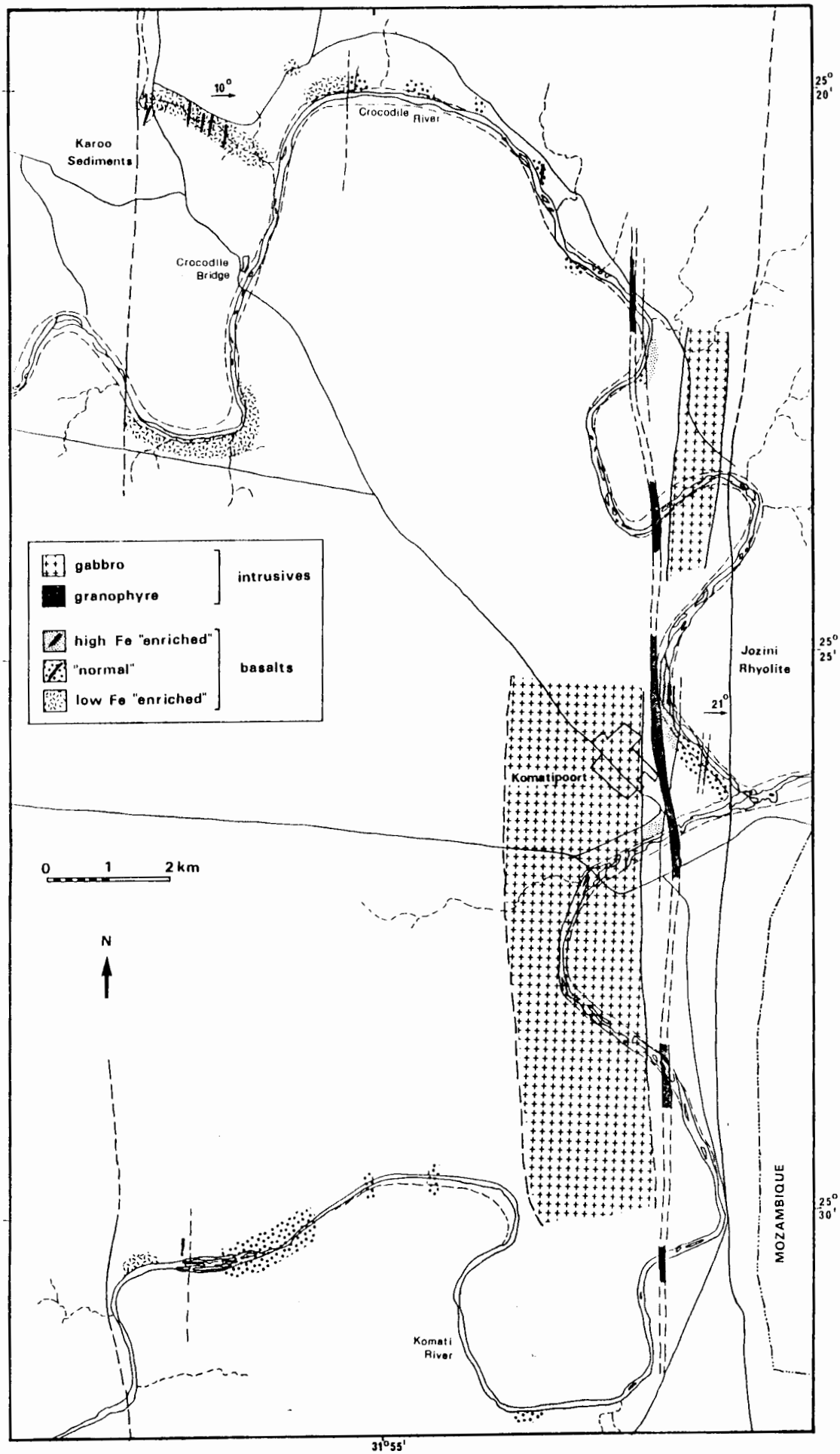

Figure 5.2. Basaltic rock-types in the Crocodile River area. Only outcrop wherein the basalt-type is known is shaded. Dolerite dykes belonging to the three basalt groups are represented by coloured lines.

5.2 STRATIGRAPHIC VARIATIONS

Variations in basalt chemistry with stratigraphic height in the major river sections are given in Fig. 5.3 for the different groups. These sections are summarized in Fig. 5.4. Quantitative data are plotted when available, otherwise samples are represented by semi-quantitative "slab data" (Appendix C). The sample stratigraphic sections in Appendix D show the distribution of quantitative and semi-quantitative samples. An average dip of 18° to the east was used to compute the stratigraphic height measured from the base of each section for each sample. The thickness of the Sabie and Crocodile/Komati stratigraphic sections are 2200 and 2800 metres respectively. The apparently greater thickness of the Crocodile/Komati River sections is due to the intrusion of the 600 m thick Komatipoort Complex in the upper portions of the section.

The basalt flows in the lowermost 1000 m of the Sabie River section, with two exceptions, are exclusively LFE-group basalts. The uppermost LFE-group basalt occurs at a stratigraphic height of 1420 m in this section. There is a preponderence of HFE-group basalts at the top of the section (1900-2200 m) and N-group basalts in the interval 1400-1900 m (Figs. 5.1 and 5.3). In the Crocodile River section LFE-group basalts are confined exclusively to the lowermost 950 m, N-group basalts predominantly to the mid-section (950-2300 m) and the uppermost portions (2600-2800 m) and the HFE-group exclusively near the top of this section (Figs. 5.2 and 5.3). In this section the only interbedding observed occurs between N- and HFE-group basalts near the top of the section. The Komati River section shows a dramatic decrease in the amount of LFE-group basalt (the only two LFE-group samples occur in the interval 0-500 m) in the section when compared to the base of the Crocodile River section merely 12 km to the north. The bulk of the Komati River section is composed of N-group basalts with some interbedded HFE-group basalts at the top of the section. It is expected that the top of this section should be similar to the Crocodile River section as the two rivers come to a confluence at the juncture of the SRBF and the Jozini Rhyolite.

It may be noted from Fig. 5.4 that there is no correlation between basalt type and the presence or absence of phenocrysts (plagioclase) observable in hand-specimen although the lowermost LFE-group basalts in the Sabie (<1000 m), and all LFE-group basalts sampled in the Crocodile (<900 m)

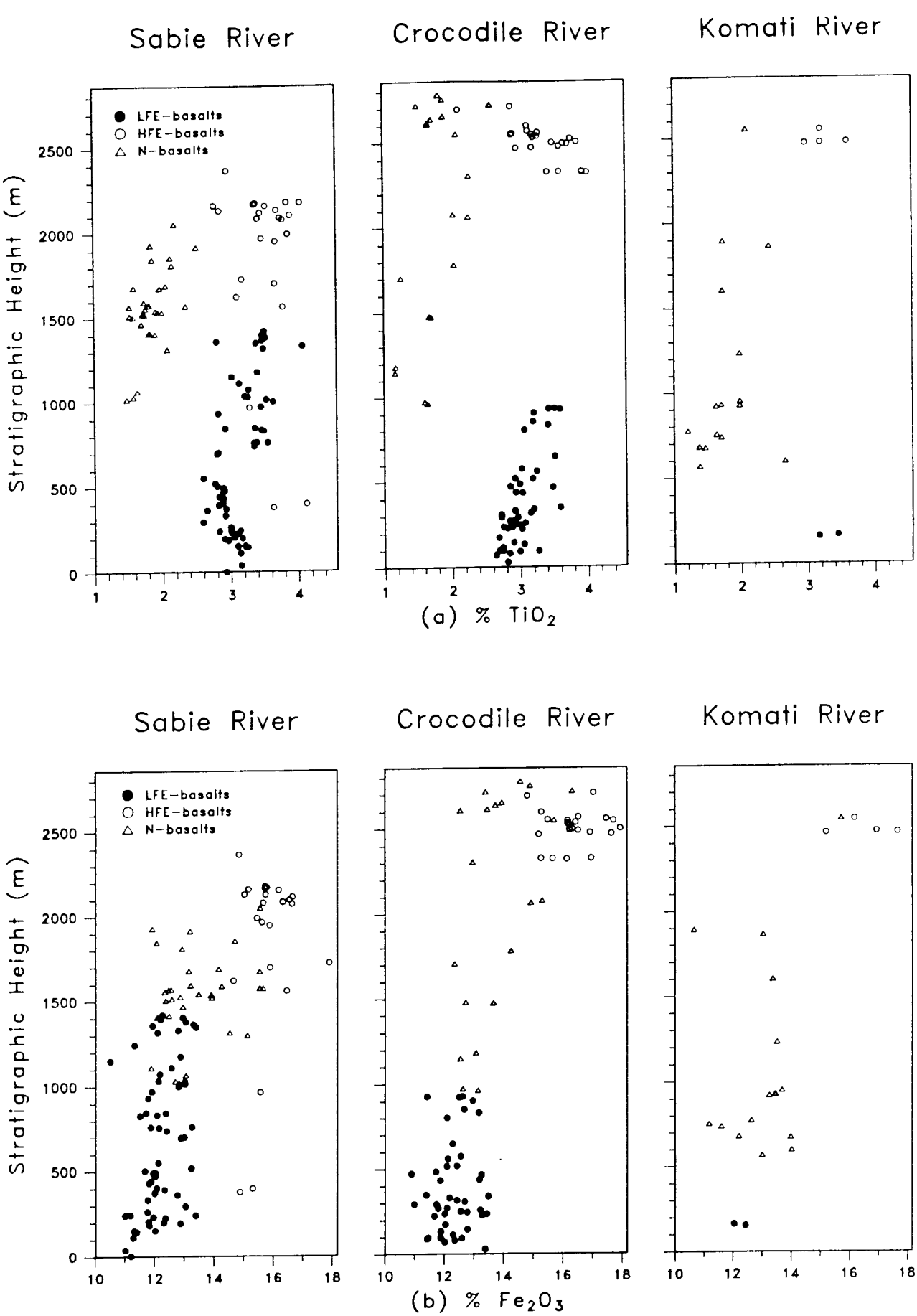

Figure 5.3. Variation of geochemistry with stratigraphy. With the exception of $^{87}Sr/^{86}Sr$ initial ratios (g), only elements analysed by the semi-quantitative slab-technique (Appendix A) are included. Quantitative data are plotted when available.

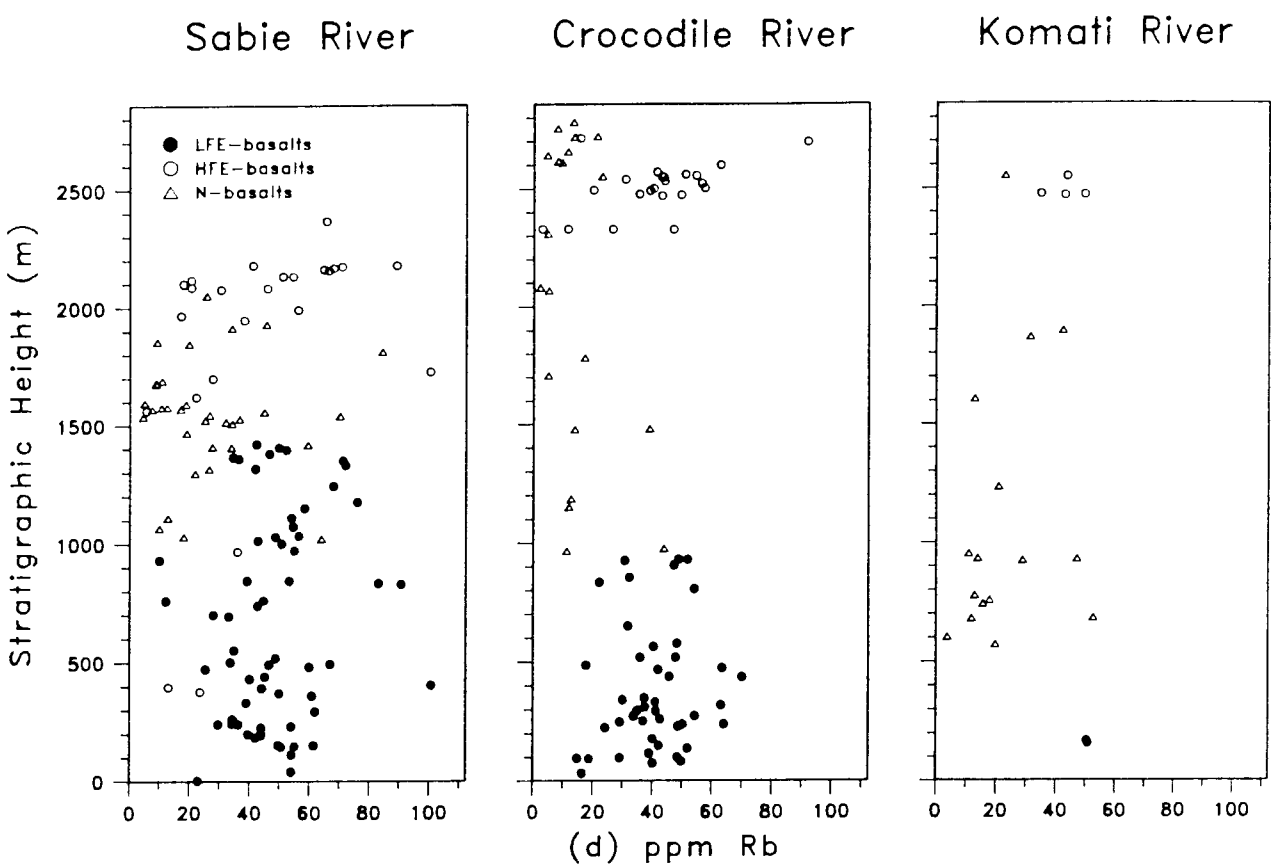
Sabie River
Crocodile River
Komati River
LFE–basalts
HFE–basalts
N–basalts
Stratigraphic Height (m)
0
500
1000
1500
2000
2500
0 20 40 60 80 100
(d) ppm Rb

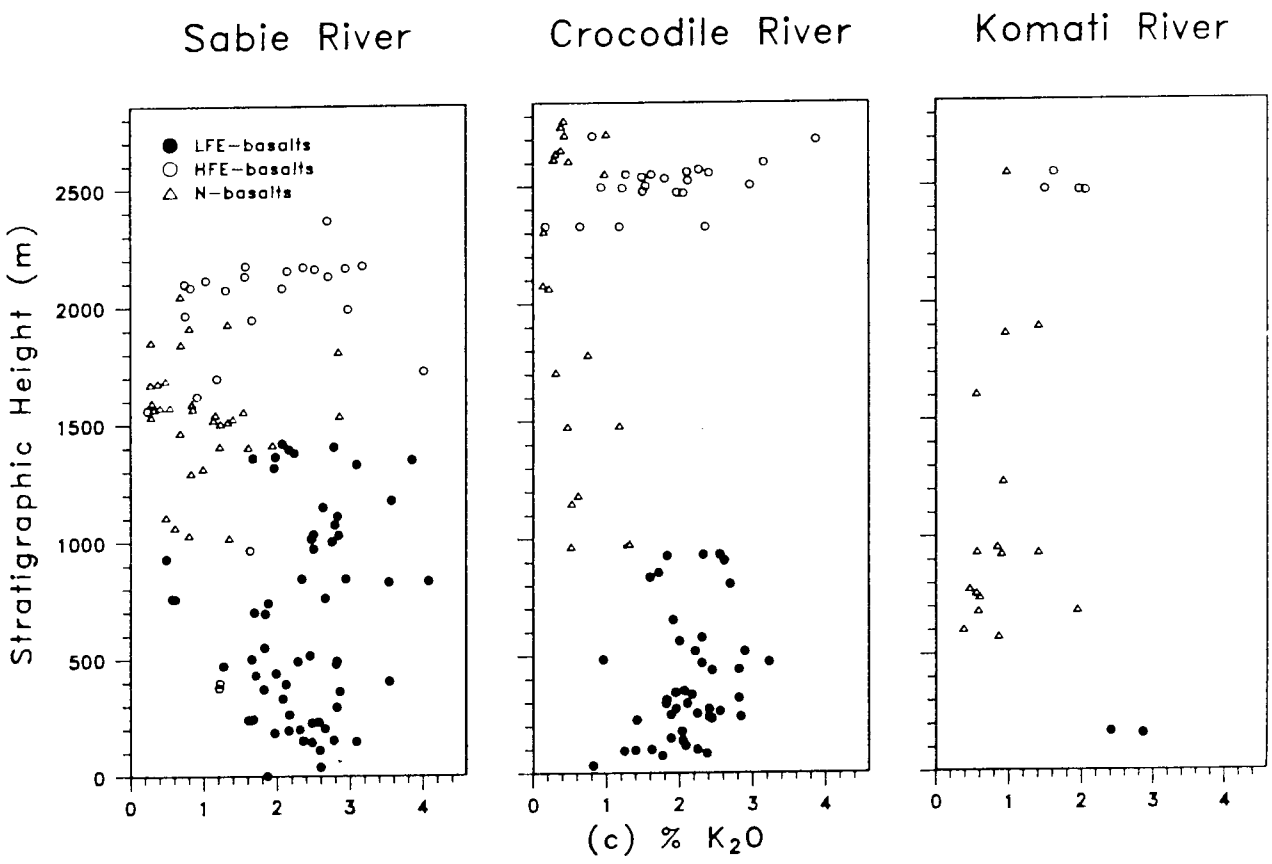
Sabie River
Crocodile River
Komati River
LFE–basalts
HFE–basalts
N–basalts
Stratigraphic Height (m)
0
500
1000
1500
2000
2500
0 1 2 3 4
(c) % K_2O

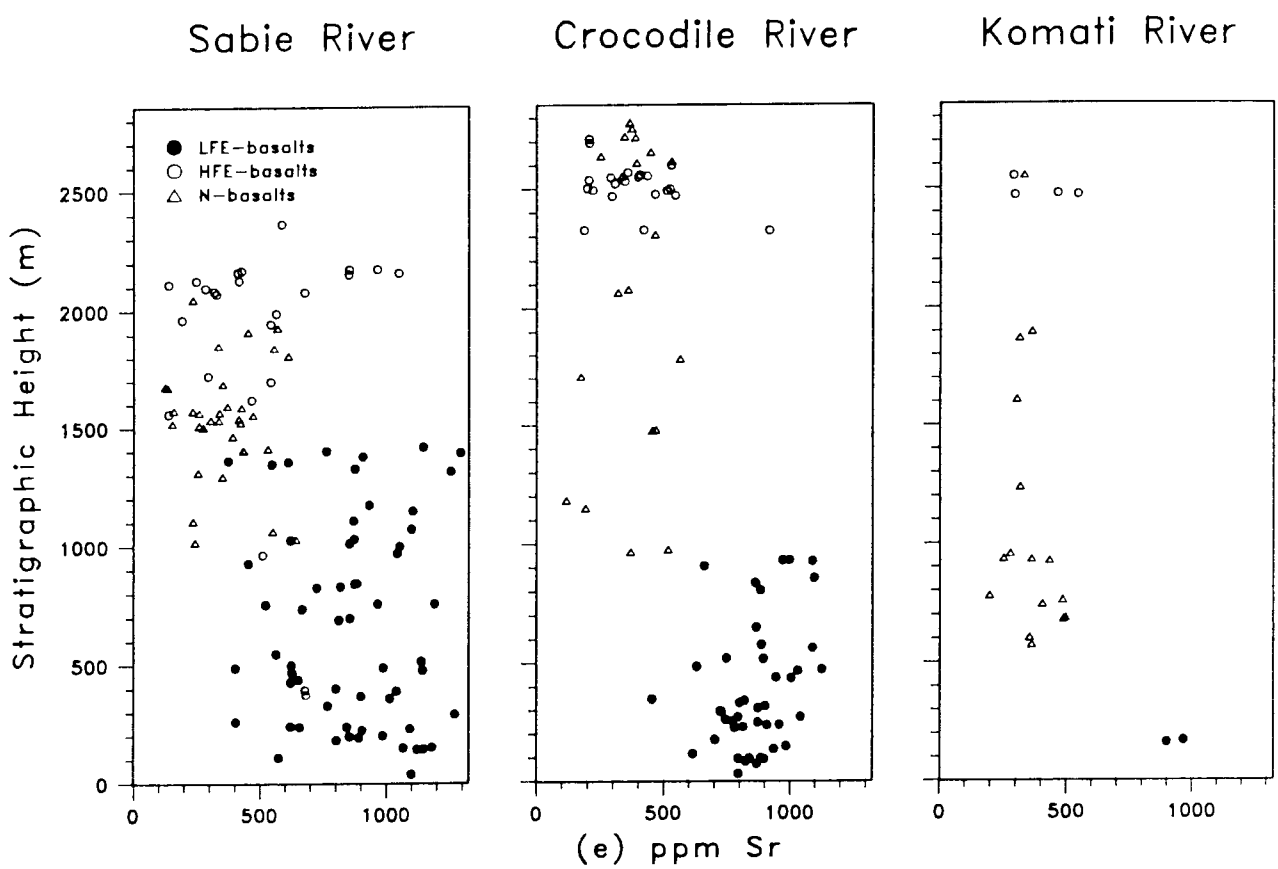
Sabie River
Crocodile River
Komati River
LFE-basalts
HFE-basalts
N-basalts
Stratigraphic Height (m)
0
500
1000
1500
2000
2500
(e) ppm Sr

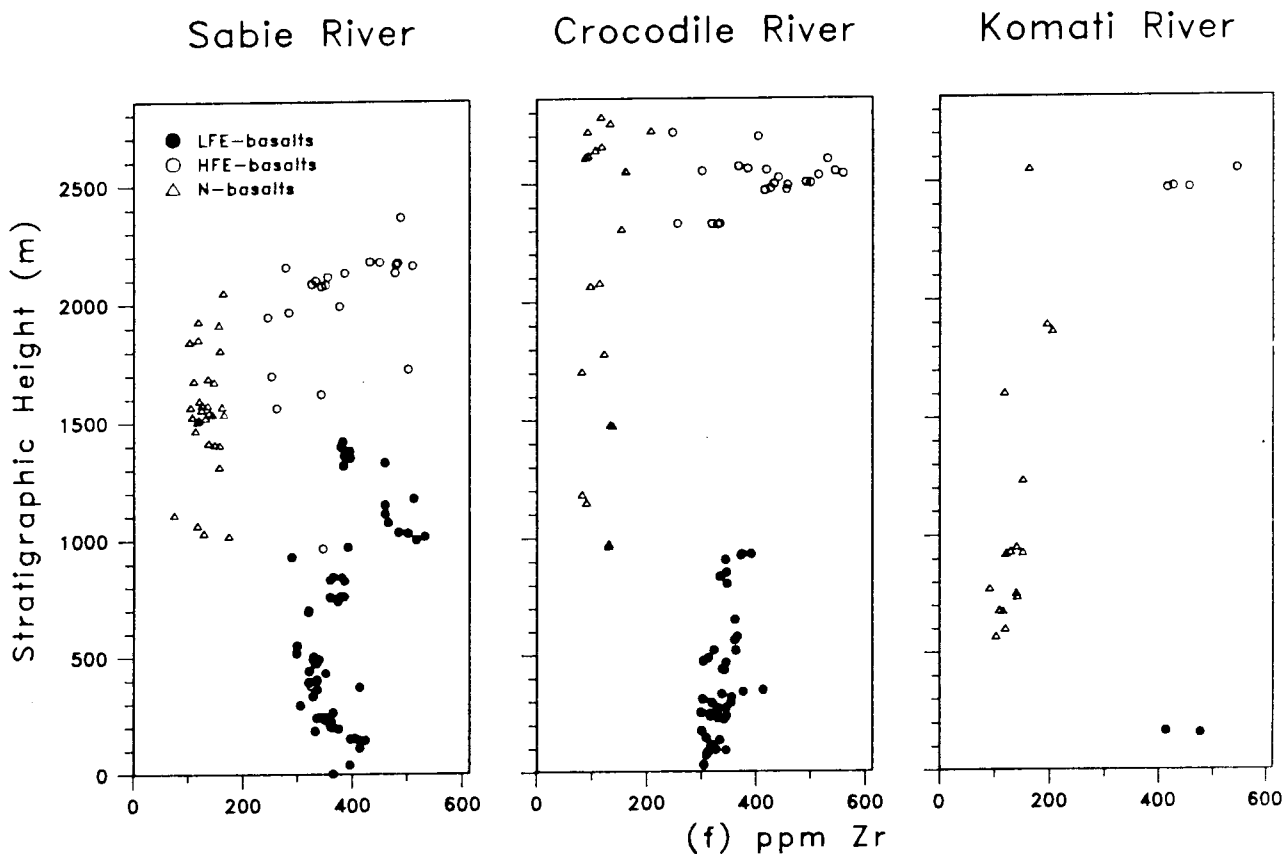
Sabie River
Crocodile River
Komati River
LFE-basalts
HFE-basalts
N-basalts
Stratigraphic Height (m)
0
200
400
600
(f) ppm Zr

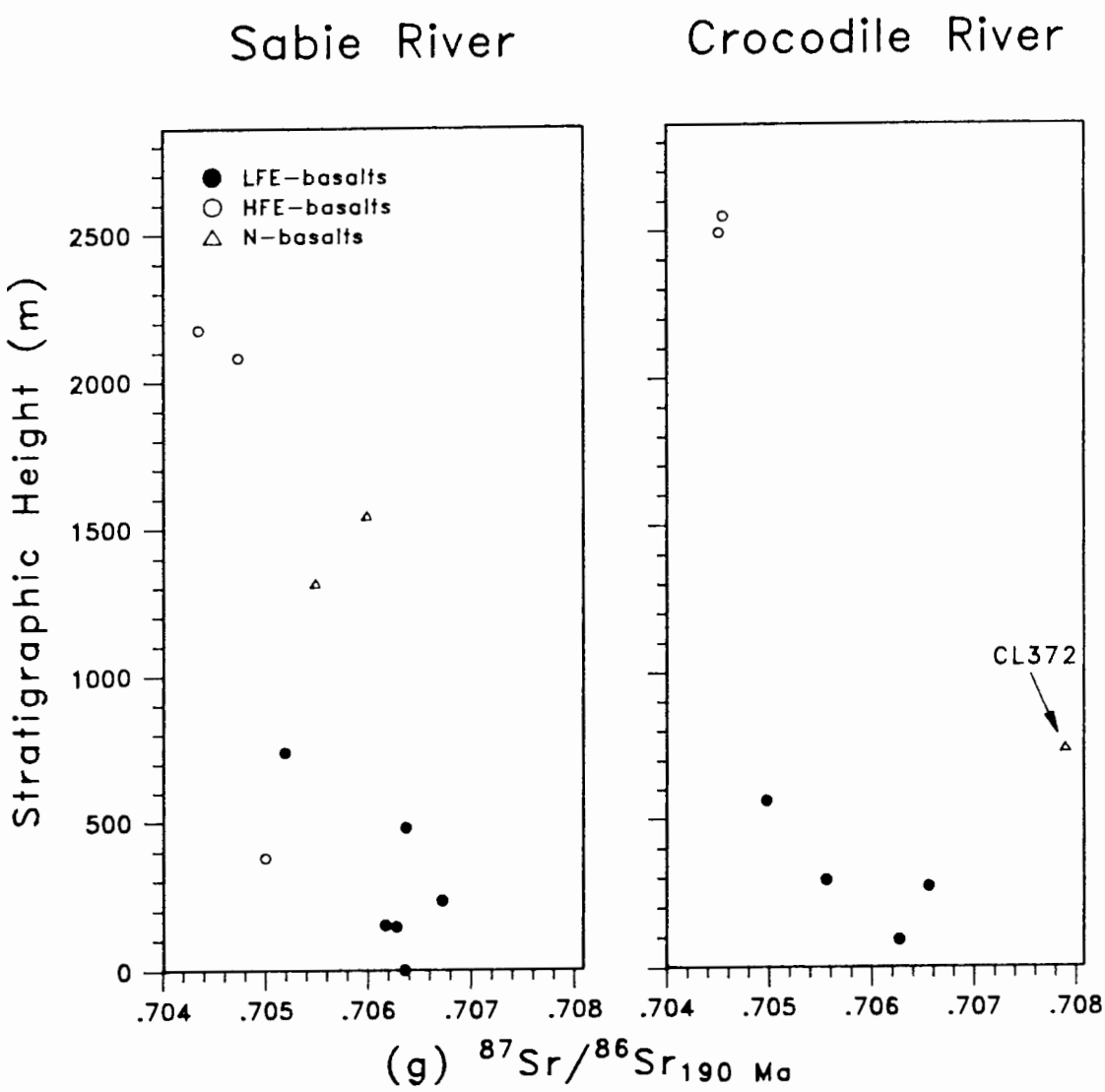
Sabie River
Crocodile River
LFE–basalts
HFE–basalts
N–basalts
Stratigraphic Height (m)
2500
2000
1500
1000
500
0
.704
.705
.706
.707
.708
CL372
(g) $^{87}Sr/^{86}Sr_{190\ Ma}$

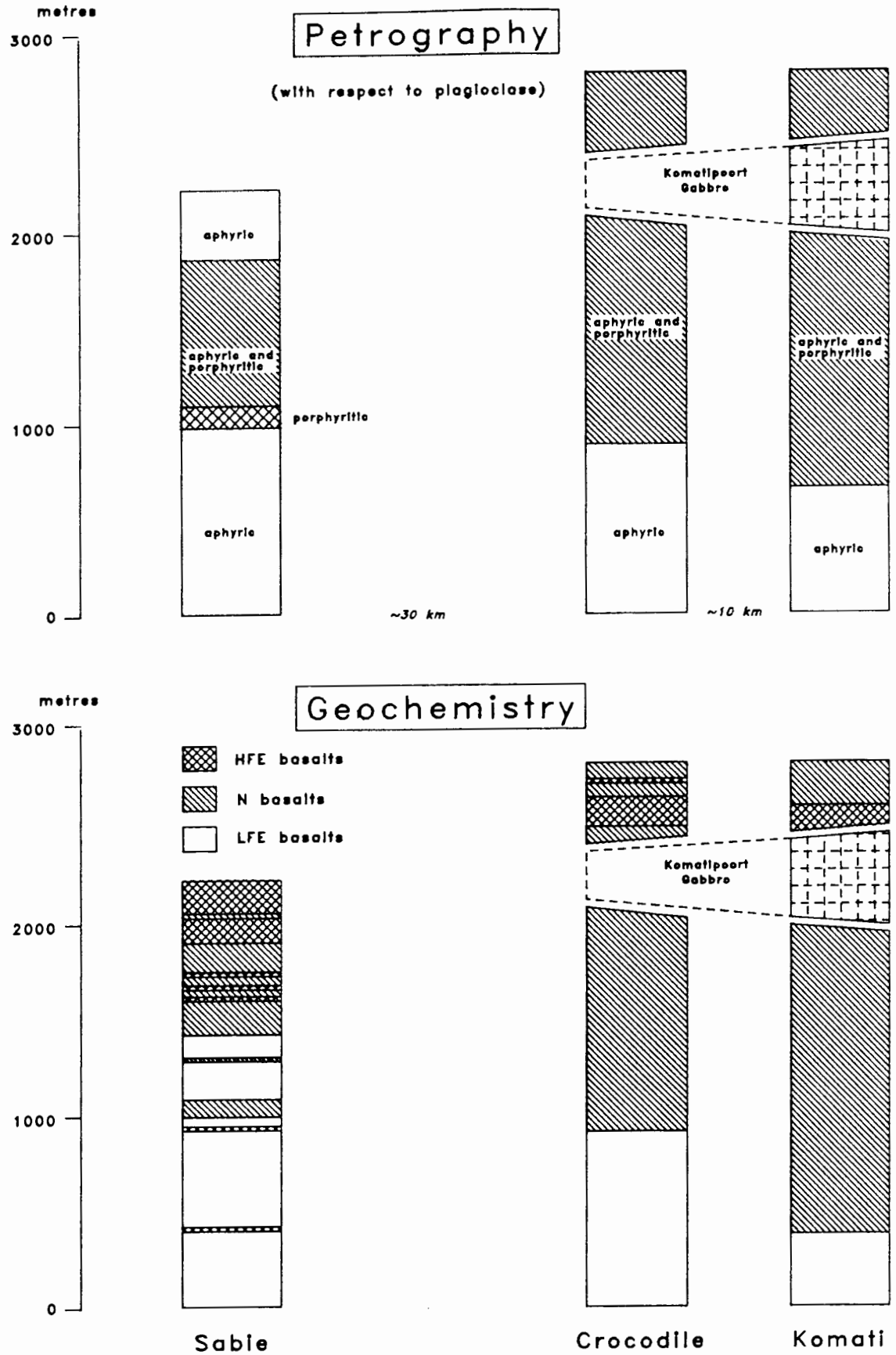

Figure 5.4. Sketch summarizing the geochemical and petrographic stratigraphy in the SRBF of the central Lebombo.

and Komati River (<300 m) sections are exclusively aphyric.

There is a systematic distribution of some elements within each basalt type with stratigraphic height. In the Sabie River section Zr, and to a lesser extent TiO_2, concentrations initially decrease and then increase with stratigraphic height in the LFE group whereas concentrations increase with height in the Crocodile River section (Fig. 5.3a, f). Sr concentrations do not show any systematic variations with height for any of the basalt groups (Fig. 5.3e). There is a tendency for LFE-group basalts with higher initial $^{87}Sr/^{86}Sr$ ratios to occur at the base of the Sabie and Crocodile sections (Fig. 5.3g).

5.3 CONCLUSIONS

It is likely that the complete replacement of LFE- with N-group basalts takes place within a north-south distance of about 60 km. This may be a continuation of the progressive onlap situation (Fig. 5.5) outcrop pattern typical of the various basic rock types of the Lebombo (Cox and Bristow, 1984; Duncan *et al.*, 1984b).

It may be argued that these basalt types originated from areas considerably distant from one another and flowed for great distances to their present locations. The dykes, however, imply that the mantle source regions and/or crustal magma chambers for the three groups were probably separated laterally by distances less than *ca* 50 km. Furthermore, the spread of data stratigraphically even for elements with data having restricted ranges (e.g. Ti and Zr in the LFE group), argues against eruption of residual liquids from simple closed-system magma chamber(s) feeding the basalt sequences. Thus some petrogenetic mechanism must be sought to explain the absence of any time dependent geochemical variations in the three basaltic groups.

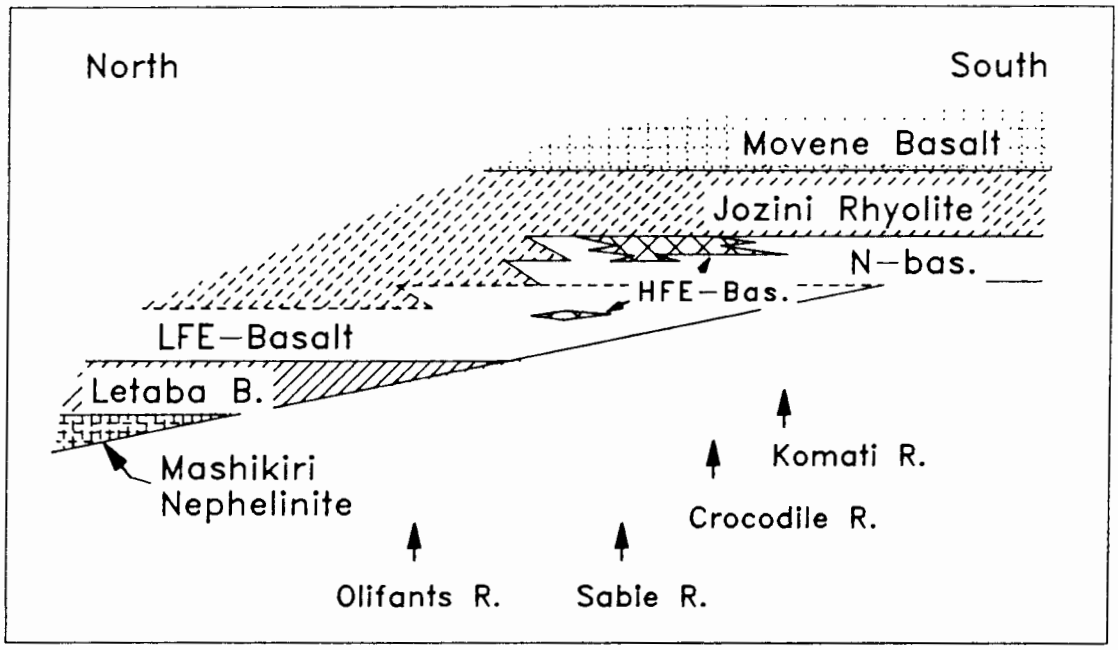

Figure 5.5. Schematic N-S cross section of the Lebombo showing the preponderance of LFE-group basalt at the base, N-group basalt in the mid- and upper-sections, and HFE-group basalt almost exclusively near the top of the central Lebombo sections.

6. CLOSED-SYSTEM FRACTIONAL CRYSTALLIZATION

6.1 INTRODUCTION

In this study if material is added to a fractionating magma chamber the system is regarded as 'open', while material removed in the form of cumulates is still regarded as part of the system and the system is considered to be closed. In open systems material may be introduced by assimilation of wall-rocks and/or the introduction of new magma. These more complex models are examined in following chapters.

Closed-system fractional crystallization (CSF) models are examined in terms of variations "between" and "within" groups. The manner in which some HFSE variations (Zr, La, Ce, Nd) in the HFE group 'straddle' the low MgO end of the LFE group trend (Fig. 3.3) suggests that these two groups cannot be related by continued fractionation. For example, Zr in the LFE group varies between 300-400 ppm over the interval 7-5% MgO, whearas Zr in the HFE group increases from 250 ppm to 500 ppm with MgO decreasing from 5% to 3% (Fig. 3.3i). In contrast, most HFE-group and N-group samples form a continuum of compositions for many elements (Fig. 3.3) and the HFE group may be result of continued fractional crystallization of a N-type composition.

It is stressed that in modelling "within-group" variations, any single liquid line of descent model cannot account for much of the dispersion of data around trends observed when elements are plotted against MgO. The approach here is to test whether closed-system fractional crystallization can produce the general changes observed between primitive and evolved samples from each group.

6.2 MODELS

6.2.1 Major Elements

The magmatic crystallization models of Nathan and Van Kirk (1978) and Nielsen and Dungan (1983) and Nielsen (1985) are compared below. How well these models reproduce observed major element variations (numerically modelled using Le Maitre, 1976) is discussed for each group.

The formulation of Nathan and Van Kirk (1978) given a whole-rock composition (assumed to approximate a liquid composition) as input, calculates the crystallization temperature of basaltic minerals based on a compilation of experimental data obtained at 1 atm. pressure. The mineral with the highest crystallization temperature is considered to be the primary phase on the liquidus and any minerals with a crystallization temperature within 10°C of this temperature are considered secondary phases in the liquidus assemblage. The phase assemblage so derived is then subtracted in specified increments (e.g. 2-4%) from a starting composition until the predicted model phase assemblage changes and adjustments to the fractionating assemblage have to be made.

Nielsen and Dungan (1983) and Nielsen (1985), use a two-lattice (network formers and network modifiers) melt activity model to predict a liquidus phase assemblage. The distribution of major elements between minerals and melt is determined using distribution coefficients to approximate equilibrium constants. These distribution coefficients are calculated by the application of a two-lattice melt model based on the models of Nielsen and Drake (1979), Drake (1976) and Bottinga and Weill (1972). In the two lattice model, the melt is assumed to be made up of network formers (molecules of SiO_2, $NaAlO_2$ and $KAlO_2$) and network modifiers (composed of the free oxides of Ca, Mg, Fe, Al, Ti, Mn, Ni and Cr). The relationship between these distribution coefficients and temperature for all major and some minor components in olivine, plagioclase, high Ca pyroxene, spinel and ilmenite is defined by regression of an experimental data set (at 1 atm.) (Nielsen and Dungan, 1985). Using a whole-rock composition (as representative of a liquid) as input, the composition of mineral phases and temperature is calculated using an iterative technique ensuring that mass-balance and stoichiometry is satisfied (Nielsen, 1985). The phase(s) with the highest calculated temperature is then the designated liquidus phase. This phase is then subtracted from the whole-rock composition in specified increments (0.2% recommended by Nielsen, 1988), is used here . The value for fO_2 has been set at 1 log unit below the quartz-fayalite-magnetite (QFM) buffer in all Nielsen's (1985) models applied in this chapter.

An important difference between these two magmatic process models as applied here, is that *observed* (analysed) mineral compositions are fractionated in the case of the Nathan and Van Kirk (1978) (NVK) model, while

Table 6.1. Mineral compositions used in petrological models. Compositions are all normalized to 100% with all Fe as FeO and are given in Chapter 4 except where otherwise indicated.

	ol* KP111	ol* KP101	ol* KS3	ol4A RSC22	ol4E RSC22	opx* KS47
SiO_2	40.28	39.88	38.56	38.19	37.60	55.73
TiO_2	.00	.00	.05	.00	.00	.35
Al_2O_3	.04	.00	.00	.00	.00	.36
FeOt	10.90	14.15	19.27	20.64	24.27	10.58
MgO	48.55	45.68	41.81	40.85	37.80	30.61
CaO	.23	.29	.31	.32	.33	2.33
Na_2O	-	-	-	-	-	.04
Fo	89	85	79.5	78	74	

	cpx4 RSV31	cpx2 RSS2	cpx10 RSS150	cpx3 RSS35	cpx20 RSC22	mt13A RSS160	il11B RSS160
SiO_2	52.36	50.41	49.36	52.48	50.91	.10	.00
TiO_2	.93	1.43	1.85	.56	.92	26.39	51.93
Al_2O_3	1.86	2.28	3.88	1.53	2.01	2.33	.07
FeOt	7.13	11.51	11.85	11.81	14.59	71.14	47.34
MgO	17.98	15.51	15.40	16.12	14.19	.00	.63
CaO	19.49	18.64	17.38	17.31	17.12	.04	.03
Na_2O	.25	.22	.28	.19	.26	-	-
K_2O	.00	.00	.00	.00	.00	-	-

	plag4 RSS152	plag3 RSS150	plag8 RSC22	plag10 RSC22	plag4 RSV16	plag3 RSC22	plag8 RSS150
SiO_2	53.17	53.79	50.78	52.24	54.80	54.32	56.56
Al_2O_3	28.93	28.77	30.82	29.96	28.02	28.41	26.82
FeOt	.98	.78	.69	.53	.57	.89	.67
MgO	.14	.12	.17	.21	.11	.13	.06
CaO	12.48	12.00	14.34	13.16	11.94	11.12	10.09
Na_2O	3.97	4.13	3.10	3.75	4.30	4.90	5.20
K_2O	.33	.41	.10	.15	.26	.23	.60
An	62	60	72	65	60	55	50

* from Bristow (1980)

Table 6.2. Mineral/melt partition coefficients used for trace element modeling (selected from a compilation in Appendix E). Bracketed values are estimates as these elements are essential structural constituents in these phases.

(a) "Typical" mineral/melt partition coefficients:

	olivine	opx[+]	cpx	plag	ilmenite	magnetite
Ti	.0350	.1000	.7000	.0300	(50.0)	(30.0)
P	.0100	.0100	.0100	.0100	.0500	.0500
Zr	.0350	.0050	.4000	.0300	.5000	2.0000
Nb	.1500	.0700	.1000	.1000	5.0000	.4000
Y	.1300	.2000	.5500	.1500	.4000	.8000
La	.0010	.0005	.0400	.1500	.0980	.0150
Ce	.0010	.0009	.0800	.1200	.1100	.0150
Nd	.0010	.0019	.1600	.0800	.1400	.0260
K	.0100	.0100	.0100	.2000	.0100	.0430
Rb	.0100	.0250	.0300	.0700	.0100	.0040
Ba	.0200	.0140	.0100	.3000	.0100	.4000
Sr	.0200	.0150	.1000	2.0000	.0100	.6000
Ni	*	3.0000	2.0000	.0800	20.0000	10.0000
Cr	.6000	5.0000	12.0000	.0300	6.0000	50.0000
V	.0800	.5000	1.5000	.0500	12.0000	20.0000
Sc	.1500	.8000	3.0000	.0200	2.0000	2.0000
Co	3.0000	2.0000	1.5000	.0700	2.0000	3.4000
Zn	1.2000	2.1000	.5000	.1100	2.0000	5.0000
Cu	1.0000	.2500	.2000	.3000	1.5000	5.4700

* olivine: D^{Ni} = 124/MgO - .90 (Hart and Davis, 1978).

(b) "Minimum" mineral-melt partition coefficients.

	olivine	opx[+]	cpx	plagioclase	ilmenite	magnetite
Ti	.0300	.1000	.2000	.0200	(50.0)	(30.0)
P	.0010	.0100	.0010	.0010	.0010	.0010
Zr	.0300	.0030	.1420	.0300	.1900	.1000
Nb	.0500	.0400	.0430	.0300	.8100	.4000
Y	.1300	.2000	.2000	.1300	.4000	.2000
La	.0005	.0005	.0200	.0900	.0980	.0150
Ce	.0000	.0009	.0400	.0230	.1100	.0150
Nd	.0000	.0019	.0650	.0230	.1400	.0260
K	.0017	.0080	.0013	.0800	.0010	.0010
Rb	.0023	.0220	.0017	.0294	.0010	.0040
Ba	.0013	.0130	.0016	.1500	.0010	.0010
Sr	.0012	.0104	.0719	1.0400	.0010	.0010

[+] also used for pigeonite

Table 6.3. "Primitive" magma compositions (all composition are normalized to 100%, Fe as FeO) estimated from unevolved compositions of each basaltic group.

	LEPRIM (LFE)	HEPRIM (HFE)	NPRIM (N)
%			
SiO_2	52.50	49.50	51.03
TiO_2	3.00	4.10	1.50
Al_2O_3	11.10	13.50	14.70
FeOt	11.00	14.60	11.08
MgO	9.00	5.00	7.09
CaO	10.00	9.10	11.00
Na_2O	1.94	2.40	2.90
K_2O	1.00	1.20	.35
P_2O_5	.45	.60	.17
Mg#	62.3	40.9	56.4
ppm			
K	8302	9962	2906
Rb	18	19.0	5.0
Ba	490	410	100
Sr	610	240	240
Ti	17985	23897	8993
P	1964	2619	742
Zr	355	270	100
Nb	20	25	5.0
Y	35	40	25
La	36	27	5.0
Ce	85	67	18.0
Nd	62	50	15.0
Ni	230	55	105
Cr	470	80	300
V	250	370	285
Sc	27	37	35
Co	55	49	55
Zn	120	123	95
Cu	100	160	200
$^{87}Sr/^{86}Sr_{190\ Ma}$	.705		.704
$\delta^{18}O$ (‰)			+5.68

in the case of Nielsen's (1985) model, mineral compositions calculated by the program NIELSEN (modified after the program TRACE.FOR, Nielsen, pers. comm., 1987) are used. This is necessary because as yet no facility exists for inputting observed (i.e. analysed) mineral compositions into Nielsen's (1985) model.

Where observed compositions are used for olivine and plagioclase in any fractionating assemblage (e.g. NVK), they are continually monitored to ensure that the mineral composition used would be in equilibrium with a melt from which it is allegedly crystallizing. The equilibrium olivine composition is predicted using the formulation of Roeder and Emslie (1970), assuming a Fe_2O_3/FeO ratio of 0.15 for the magma composition and a Fe/Mg distribution coefficient (K_D) value of 0.30. The composition of plagioclase used is generally consistent with the composition predicted by both Nathan and Van Kirk (1978) and Nielsen (1985). The observed clinopyroxene compositions used within each group is consistent with observed variations in mineral composition (Chapter 4.3). For example cpx4 of RSV31 was used in the initial stages and cpx2 of RSS2 in the latter stages of fractional crystallization models in the LFE-group (Table 6.4a).

Major components considered exclude Mn and P but include Ni and Cr which, because of the different distribution coefficients used for olivine, orthopyroxene and clinopyroxene (Table 6.2), provide a useful constraint on the relative proportions of these minerals in any fractionating assemblage. In all instances models are initiated from the hypothetical 'primitive' compositions: LEPRIM, HEPRIM and NPRIM; in the LFE, HFE and N groups respectively (Table 6.3). These compositions are estimates chosen to generally approximate observed data for the least evolved basaltic rocks of each geochemical group. The compositions of minerals used are given in Table 6.1.

6.2.2 Trace Elements

Trace element fractionation is modelled using the Rayleigh Fractionation Law given in Arth (1976):

$$C_L/C_0 = F^{D-1} \qquad - (6.1)$$

where C_0 is the initial concentration of an element in a magma, C_L the

concentration in the liquid of which the proportion remaining is given by F (predicted by major element models). D is the bulk partition coefficient for an element calculated from individual mineral/melt partition coefficients weighted in proportion to each mineral in the crystallizing assemblage. The partition coefficients used are listed in Table 6.2 and were selected from values available in the literature (Appendix E). Obviously use of single values for distribution coefficients involves the assumption that they do not change with parameters such as temperature and host melt composition. However, this is certainly not true in the case of Sr (e.g. Philpotts and Schnetzler, 1970; Koringa and Noble, 1971; Drake and Weill, 1972 and Sun *et al.*, 1974) and it is stressed that the values used are approximations assumed to be typical for the range of conditions involved (e.g. basaltic melt at 1200-1150°C).

Rayleigh fractionation assumes crystals are effectively and instantaneously removed from the system (e.g. by gravity settling). While this assumption may not be entirely justified, the other "end-member" alternative is equilibrium crystallization (Shaw, 1970), which assumes continuous re-equilibration of a phase with its host melt as crystallization proceeds. An equilibrium model would produce minerals of a singular composition in a particular magma batch and this would certainly be reflected in a single thin-section. The considerable range for analysed mineral compositions within single thin-sections, implies that this is not the case for basaltic samples in the central Lebombo (Chapter 4). Hence any crystallization in the basaltic rocks of the central Lebombo is thought to proceed in a fashion more closely approximated by fractional (Rayleigh) than equilibrium models.

The trace element partitioning between a mineral and melt assumes that Henry's Law is obeyed, i.e. there is proportionality between activity and concentration in the system considered, a condition satisfied by most elements present in trace quantities (Watson, 1985). It is expected that P, which is not a major element in any observed or modelled fractionating phase, will also obey the Rayleigh fractionation equation. Where elements are present as stoichiometric components (essential structural constituents) of minerals (e.g. Ti in ilmenite) which occur in a fractionating assemblage, these elements are modelled by a mass-balance approach, involving calculation of the amount of an oxide in the fractionating assemblage and subtraction from a starting composition.

6.2.3 Isotopes

Radiogenic isotope ratios are not modelled as both fractionation of ratios induced by either instruments measuring these ratios or any geological fractional crystallization process are corrected for in their measurement (Appendix A). However, stable isotopes of oxygen are fractionated by geological processes (O'Neil, 1986a) and the degree of fractionation may be measured. The degree of fractionation generally decreases with temperature and in basaltic systems the difference in O-isotope composition between minerals and melt is small, typically an order of magnitude less than at lower temperatures (O'Neil, 1986b). For example, in the Kiglapait intrusion a $\delta^{18}O$ fractionation of only 0.1‰ occurred during the crystallization of 85% of the total magma (Taylor, 1968; Kalamarides, 1984). Modelling of $\delta^{18}O$ with fractional crystallization is achieved using the experimental data of Kyser *et al.* (1981) to determine Δ-values used in the expression of Taylor and Sheppard (1986) for Rayleigh fractionation and are incorporated by A. R. Duncan in the modelling program DARTS.

Modelling of $\delta^{18}O$ in this study confirmed the insensitivity of $\delta^{18}O$ values to fractional crystallization processes and they did not change by more than 0.03‰ for any model used. This is well within the experimental error ($\pm$0.2‰) for data and therefore $\delta^{18}O$ is not considered further in terms of fractional crystallization models.

6.3 "WITHIN-GROUP" VARIATIONS

The approach adopted is to constrain the fractionating assemblage by considering changes in observed major element composition and how these changes compare to the predictions of some theoretical models available in the literature. The model which best explains the major element variations observed in each group gives a fractionating assemblage and an F-value which are then used in Rayleigh Fractionation models to calculate the trace element composition of derivative melts.

6.3.1 Major Elements

6.3.1.1 The LFE group

Evolved compositions calculated using the models described above are compared to an evolved relatively unaltered LFE-group sample (RSS2) in Table 6.4a. In each instance the sum of squares of percentage differences (ss^2) excluding Na and K should be compared as these elements have a considerable and generally random distribution within this group (Fig. 3.6b, c). Thus an average deviation of 5% from observed compositions for each of the five remaining oxides would result in a model having a ss^2 of 150 for the six major elements used.

The NVK model produces a better fit for the major elements used than NIELSEN but predicts orthopyroxene as a major liquidus phase over the crystallization range covered (Table 6.4a). This is inconsistent with the occurrence of only one phenocryst of orthopyroxene in a single sample of this group (Chapter 4) and it is unlikely that orthopyroxene was removed entirely from fractionating liquids. Furthermore, if included in a least-squares mixing calculation (GENMIX), the proportion of orthopyroxene is negative. The phase assemblage predicted by NVK is also inconsistent with observed Ni and Cr values for the D's used (Table 6.2a), although the Cr content of RSS2 is greater than most evolved LFE-group samples (more typically *ca* 60 ppm, Fig. 3.3t). The Ni and Cr contents of derivative melts using NIELSEN are calculated as major components (network modifiers) and the Rayleigh Fractionation Law is not used. The depletion of Ni and Cr with fractional crystallization using NIELSEN is controlled largely by the crystallization of small amounts of a Cr-spinel early in the fractionation history. This is unlikely to be the case in any of the groups examined as Cr-spinel was not observed in any central Lebombo basaltic rock. However, despite apparent problems with the spinel crystallization temperatures, the phase assemblage predicted by NIELSEN (olivine + clinopyroxene $\pm$ plagioclase) is more consistent with the numerical differences between evolved and primitive compositions as calculated by GENMIX (Table 6.4a).

The proportions of phases selected in the estimated "best-fit" model are chosen to reflect the changing proportions predicted in a stepwise manner (in this case by NIELSEN) and the aggregate assemblage predicted by GENMIX. This "best-fit" assemblage is also consistent with the general spread of data observed between evolved and primitive compositions (Figs. 6.1a, 6.2 and

Table 6.4. Major element (excluding Mn and P) and Ni and Cr content of derivative liquids produced by the magmatic crystallization models (Nielsen, 1985; Nathan and Van Kirk, 1978), least-squares mixing (GENMIX, Le Maitre, 1976) and an estimated best-fit with observed compositions. Models are initiated from LEPRIM, HEPRIM and NPRIM (Table 6.3). Fe is given as FeO and a Fe_2O_3/FeO ratio of 0.15 is used for NIELSEN and NVK models.

(a) LFE group:

	observed	NIELSEN		NVK		GENMIX		est. 'best-fit'	
	RSS2	calc	%diff	calc	%diff	calc	%diff	calc	%diff
%									
SiO_2	53.46	52.92	-1.0	52.53	-1.7	53.55	0.2	53.51	0.1
TiO_2	3.36	3.46	3.0	3.58	6.6	3.56	6.0	3.67	9.2
Al_2O_3	13.33	12.87	-3.5	13.60	2.0	13.44	.8	13.95	4.6
FeOt	10.62	13.01	22.5	11.23	5.7	11.03	3.9	11.19	5.4
MgO	5.07	5.03	-7.9	4.86	-4.1	5.11	.8	4.86	-4.1
CaO	8.93	8.20	-8.2	9.98	11.8	9.15	2.5	8.42	-5.7
Na_2O	1.95	2.38	22.0	2.39	22.7	2.36	21.0	2.47	27.0
K_2O	2.56	1.35	-47.0	1.25	-51.2	1.24	-51.5	1.32	-48.0
ss^2 (all)			3351		3376		3152		3217
ss^2 (excl. Na, K)			658		239		59		184
ppm									
Ni	63	16 (not		133		-		96	
Cr	141(60)	0 Rayleigh)		98		-		44	
F		.72		.80		.81		.76	

Fractionation assemblage: (step ending in F value given)

	mineral proportions in fractionating assemblages (weight %)											
F-end	ol	cpx	sp	plg	ol	opx	cpx		ol	opx	cpx	plg
.96	99	-	1	-	20	80	-		50	10	40	-
.92	50	50	<1	-	15	60	25	ol = 30.84	40	5	55	-
.88	-	100	<1	-	10	40	50	cpx = 69.16	20	-	80	-
.84	-	100	-	-	-	20	80		5	-	95	-
.80	-	90	-	10	-	20	80		-	-	100	-
.76	5	50	<1	45					-	-	90	10
.72	10	35	5	50								

mineral compositions used (from Table 6.1):

F-interval			For F	
1.0 - .96		ol-KP101	= 1.0-.81	ol-KP101
		opx-KS47	olivine	opx-KS47
			= ol-KS3	cpx4-RSV31
.96 - .92		ol-KP101		ol-KS3
		opx-KS47	cpx =	opx-KS47
		cpx4-RSV31	cpx4-RSV31	cpx4-RSV31
.92 - .88		opx-KS47		ol-KS3
		cpx4-RSV31		cpx4-RSV31
.88 - .84		opx-KS47		as above
		cpx2-RSS2		
.84 - .80				cpx2-RSS2
.80 - .76				cpx2-RSS2
				plag4-RSS152

/Table 6.4

(b) HFE group:

	observed RSC38	NIELSEN calc	NIELSEN %diff	NVK calc	NVK %diff	GENMIX calc	GENMIX %diff	est. 'best-fit' calc	est. 'best-fit' %diff
%									
SiO_2	51.49	54.30	5.5	49.13	-4.6	51.51	0.0	51.48	-0.0
TiO_2	3.84	2.21	-42.4	4.56	18.8	3.87	.8	3.63	-5.7
Al_2O_3	12.64	12.55	-.7	13.64	8.0	12.76	.9	12.78	1.1
FeOt	15.39	13.79	-10.4	15.54	1.0	15.42	.2	15.64	1.7
MgO	3.70	3.72	.5	3.78	2.1	3.74	1.1	3.76	1.5
CaO	7.47	7.55	1.1	8.83	18.2	7.50	.4	7.53	.7
Na_2O	3.13	2.79	-10.9	2.50	-20.2	2.59	-17.3	2.59	-17.4
K_2O	1.26	1.83	45.2	1.34	6.3	1.70	35.5	1.70	-34.7
ss^2 (all)			4100		1226		1562		1546
ss^2 (excl. Na, K)			1938		775		3		39
ppm									
Ni	34	2 (not		47		-		22	
Cr	3	0 Rayleigh)		46		-		7.1	
F		.64		.86		.67		.67	

Fractionation assemblage: (step ending in F value given)

	mineral proportions in fractionating assemblages (weight %)							
F-end	sp	cpx	pig	plg	opx	cpx	plg	
.96	55	-	-	45	25	35	40	ol - 3.92 3.9
.92	20	35	-	45	20	30	50	cpx - 38.73 38.7
.88	15	50	-	35	15	25	60	plg - 46.23 46.3
.84	15	45	-	40				mt - 7.58 5.6
.80	15	50	-	35				ilm - 3.54 5.5
.76	15	45	-	40				
.72	15	45	-	40				
.68	10	40	10	40				
.64	10	25	20	45				

mineral compositions used (from Table 6.1):		For F = 1.0 - .67
F-interval		
1.0 - .98	ol4E-RSC22	
	opx-KS47	olivine = ol4E-RSC22
	cpx10-RSS150	cpx = cpx10-RSS150
.98 - .96	ol4E-RSC22	plg = plag3-RSS150
	opx-KS47	mt = mt13A-RSS160
	cpx10-RSS150	ilm = ilm1B-RSS160
	plag8-RSS150	
.96 - .86	as above	
	(-ol)	

/Table 6.4

(c) N group:

	observed	NIELSEN		NVK		GENMIX		est. 'best-fit'	
	RSS169	calc	%diff	calc	%diff	calc	%diff	calc	%diff
%									
SiO_2	50.63	49.78	-1.7	51.74	2.2	51.63	2.0	51.54	1.8
TiO_2	2.62	2.34	-10.7	1.79	-31.5	2.52	-3.8	2.46	-6.0
Al_2O_3	12.72	12.93	1.7	15.49	21.8	12.35	-2.9	13.24	4.1
FeOt	15.81	17.06	7.9	11.17	-29.4	14.74	-6.7	13.88	-12.2
MgO	4.91	4.71	-4.1	4.94	.7	5.26	7.1	5.07	3.3
CaO	9.40	8.93	-5.0	10.67	13.5	8.54	-9.1	8.96	-4.7
Na_2O	2.54	3.15	24.0	3.33	31.1	3.77	48.4	3.65	43.7
K_2O	.75	.59	-21.3	.43	-42.7	.58	-22.7	.57	-24.0
ss^2 (all)		1254		5318		3063		2724	
ss^2 (excl. Na, K)		224		2519		205		238	
ppm									
Ni	47	6 (not		42		-		39	
Cr	45(60)	44 Rayleigh)		118		-		39	
F		.56		.80		.56		.56	

Fractionation assemblage: (step ending in F value given)

	mineral proportions in fractionating assemblages (weight %)											
F-end	ol	cpx	pig	plg	ol	cpx	plg		ol	cpx	plg
.96	-	50	-	50	60	40	-		10	40	50
.92	15	30	-	55	25	45	30	ol = 8.87	10	40	50
.88	5	40	-	55	10	40	50	cpx = 35.45	10	40	50
.80	10	30	-	60				plg = 55.68	10	40	50
.72	5	40	-	55					10	35	55
.64	10	30	-	60					10	35	55
.56	10	25	5	55					10	35	55

mineral compositions used (from Table 6.1):

F-interval			For F=	
1.0 - .96		ol4A-RSC22	1.0-.56	ol4A-RSC22
		cpx3-RSS35		cpx3-RSS35
			ol4A-RSC22	plag8-RSC22
.96 - .92		ol4A-RSC22	cpx3-RSS35	as above
		cpx3-RSS35	plag8-RSC22	
		plag8-RSC22		
.92 - .86		ol4A-RSC22		as above
		cpx20-RSC22		
		plag8-RSC22		
.86 - .80		ol4E-RSC22		as above
		cpx20-RSC22		
		plag8-RSC22		
.80 - .56				ol4E-RSC22
				cpx20-RSC22
				plag10-RSC22

ol = olivine, cpx = high Ca clinopyroxene, opx = orthopyroxene,
pig = low Ca clinopyroxene, sp = spinel, plg = plagioclase,
mt = magnetite, ilm = ilmenite.

Table 6.5. Major element (excluding Mn and P) and Ni and Cr closed-system fractional crystallization model produced for the LFE group when small amounts of ilmenite are included in the fractionating assemblage. Explanation as for Table 6.4.

	observed RSS2	est. 'best-fit' (incl. ilm) calc	%diff
%			
SiO_2	53.46	54.51	2.0
TiO_2	3.36	2.62	-22.0
Al_2O_3	13.33	14.16	6.2
FeOt	10.62	10.54	-0.9
MgO	5.07	5.00	-1.4
CaO	8.93	8.75	-2.0
Na_2O	1.95	2.50	28.2
K_2O	2.56	1.32	-48.4
ss^2 (all)			3671
ss^2 (excl. Na, K)			623
ppm			
Ni	63	67	
Cr	141(60)	47	
F		.76	

Fractionation assemblage: (step ending in F value given)

	mineral proportions in weight %				minerals used (Table 6.1)
F-end	ol	opx	cpx	ilm	
.96	50	10	40	-	ol-KS3, opx-KS47, cpx4-RSV31
.92	40	5	55	-	as above
.88	20	-	70	10	ol-KS3, cpx4-RSV31, i111B-RSS160
.84	5	-	90	10	as above
.76	-	-	90	10	cpx4-RSV31, i111B-RSS160

ol = olivine, cpx = high Ca clinopyroxene, opx = orthopyroxene, ilm = ilmenite.

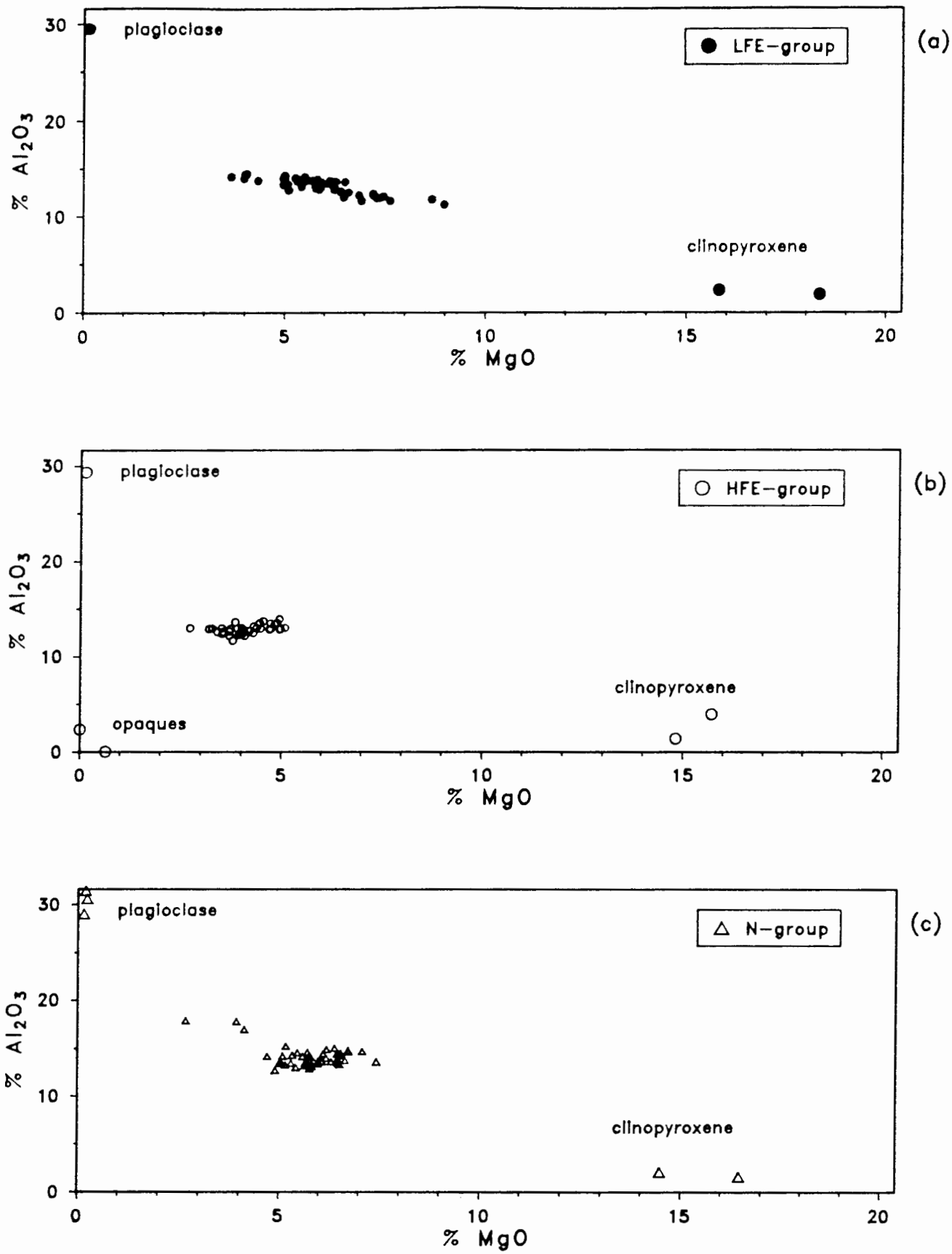

Figure 6.1. Al_2O_3 *vs* MgO with mineral data (from Table 6.1) (normalized to 100% volatile free, Fe as FeO).

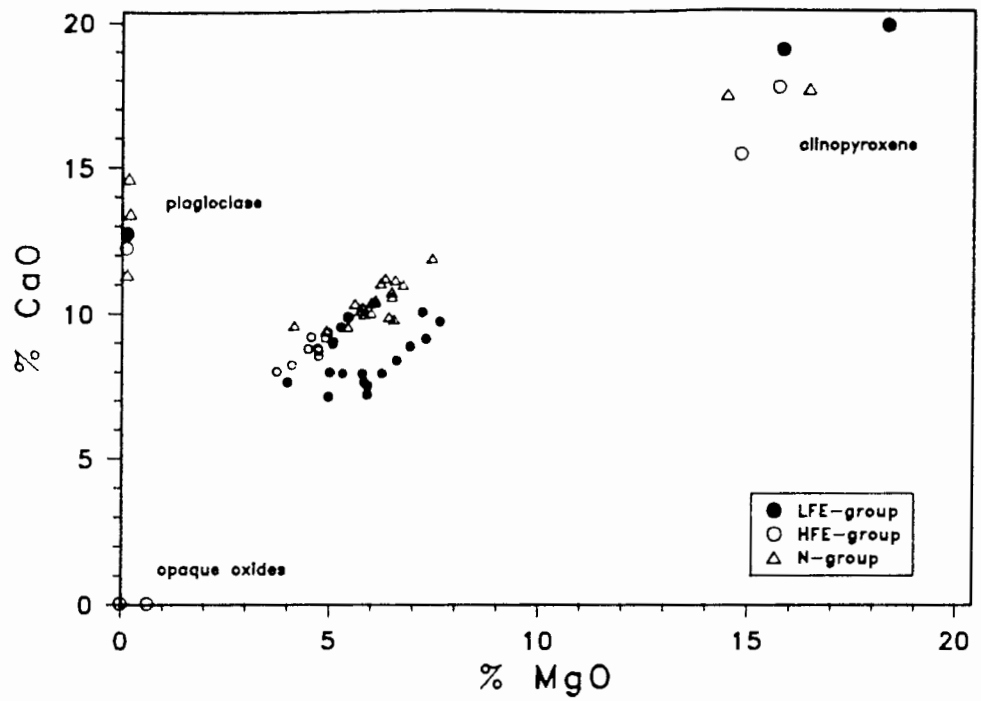

Figure 6.2. CaO *vs* MgO with mineral data (from Table 6.1) (normalized to 100% volaltile. free, Fe as FeO).

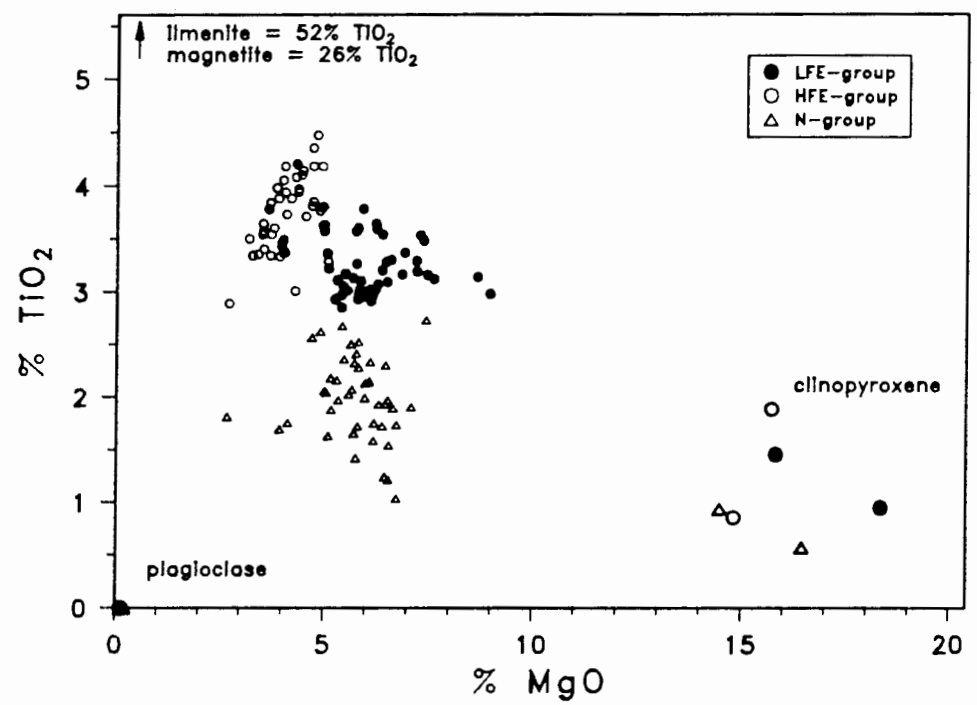

Figure 6.3. TiO_2 *vs* MgO with mineral data (from Table 6.1) (normalized to 100% volatile free, Fe as FeO).

6.3). The increased Al_2O_3 content with decreasing MgO in the LFE group (Fig. 6.1a) implies the absence of plagioclase as a major crystallizing phase and this trend is dominantly controlled by the fractionation of mafic minerals alone. Microphenocryst and intratelluric phases present in the LFE group (Chapter 4) indicate that the only possibility is clinopyroxene + lesser olivine ± orthopyroxene. Orthopyroxene, is only included as a minor fractionating phase at higher MgO contents in the "best-fit" assemblage (Table 6.4a) because of its frequent occurrence in the N. Lebombo picrites which are potentially parent magmas to the LFE group (Cox and Bristow, 1984; Bristow, 1980).

The general decrease in CaO content with decreasing MgO (Fig. 6.2) in the LFE group supports the dominance of clinopyroxene in the crystallizing assemblage. The dominance of clinopyroxene is consistent with its frequent occurrence as the only microphenocryst phase (in glomeroporphyritic clusters) observed to be typical of these rocks for MgO >5% (Chapter 4.3). The calculated fractional crystallization trend illustrated in Fig. 6.4c, however, does not account for the still considerable dispersion of CaO *vs* MgO for LFE-group data. It is unlikely that the dispersion in the data in Fig. 6.2 is a result of alteration as only samples observed to be relatively unaltered in thin-section have been plotted. Variable amounts of olivine or plagioclase fractionation or addition may be the cause of this dispersion.

The appearance of plagioclase on the liquidus at lower MgO contents (Table 6.4) is consistent with the predictions of Nielsen (1985) and observed mineralogy, i.e. all samples with MgO <5% in the LFE-group are plagioclase-phyric. This suppression of plagioclase crystallization in the "enriched" basalts of the northern Lebombo was noted by Cox and Bristow (1980) who concluded that this was a consequence of the higher K_2O contents characteristic of these rocks.

The variation of TiO_2 with MgO (Fig. 6.3) indicates that ilmenite (the primary opaque mineral in the LFE group, Chapter 4.5) is not a major phase in the fractionating assemblage. The spread of TiO_2 contents at MgO <7% may, however, be due to a small and variable ilmenite component in the fractionating assemblage. The LFE-group fractionating assemblage is adjusted in Table 6.5 to include small amounts of ilmenite for from F=.88 to F=.76. Elements most significantly affected are Ti, Fe, Ni and V (dashed line in Figs. 6.4, 6.5c). Thus, variable amounts of ilmenite in the fractionating

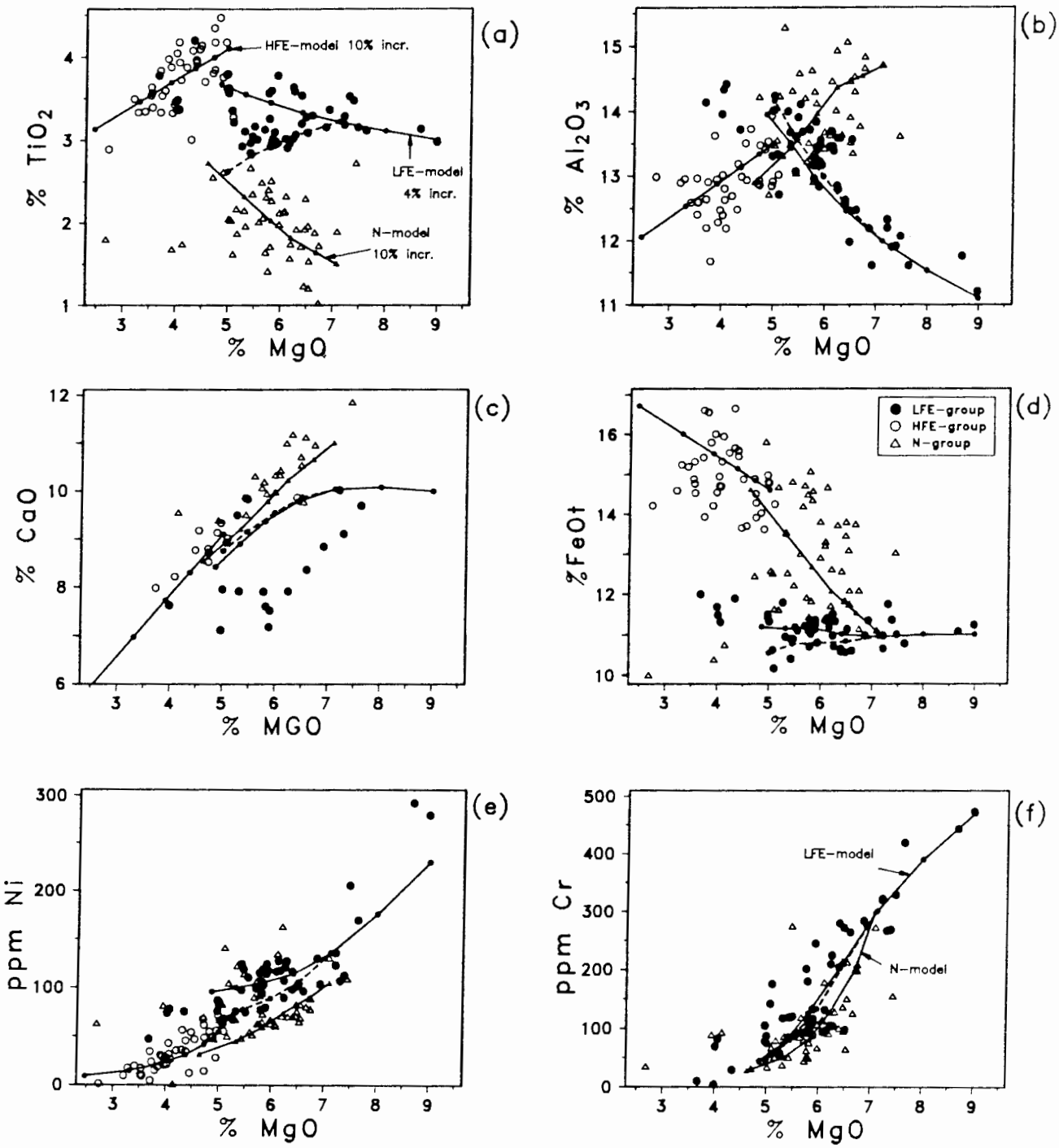

Figure 6.4. Selected major elements *vs* MgO for central Lebombo basaltic rocks and closed-system fractional crystallization model trends. Each point on the model trends represents 4% fractional crystallization increments in the case of the LFE-group model and 10% crystallization in the case of the N- and HFE-group models. The dashed line associated with the LFE-model trend represents the liquid line of descent when ilmenite is added to the fractionating assemblage (after 8% crystallization). (Table 6.5). All data are normalized 100% volatile-free, Fe as FeO.

assemblage could explain the spread in TiO_2, FeO, Ni and V contents with decreasing MgO but have little affect on other element abundances (Figs. 6.4, 6.5).

6.3.1.2 The HFE group

In the HFE group, the most evolved compositions (e.g. RSS112) are unfortunately more altered. The composition used (RSC38) represents the most evolved relatively unaltered HFE-group sample. In the case of the HFE group, magmatic crystallization models (NVK and NIELSEN) are not consistent with parameters calculated numerically using GENMIX (Table 6.4b). Although the NVK model gives a better sum of squares (excluding Na and K) fit than calculations using NIELSEN, it predicts significant orthopyroxene on the liquidus and this mineral is not observed in the mineralogy of this group (Chapter 4). While the assemblage predicted by NIELSEN is closer to that predicted by GENMIX than NVK, a large proportion of spinel (a high alumina spinel enriched in Cr in the initial stages) is included in the early stages of fractional crystallization. This results in too high SiO_2 and too low FeOt and TiO_2 contents of the derivative liquid (Table 6.4b). Thus, the absence of any correspondence between NIELSEN and NVK models leaves GENMIX as the only means of estimating the fractionating assemblage required to account for the major element variations observed. It is acknowledged that this assemblage represents the **aggregate** fractionation of these phases over the interval considered as any melt is unlikely to be multiply saturated with 5 mineral phases simultaneously.

The general decrease in Al_2O_3 and CaO with decreasing MgO for this group is consistent with almost equal proportions of clinopyroxene and plagioclase on the liquidus (Figs. 6.1b, 6.2). Clinopyroxene and plagioclase are also phenocrysts and/or major components of the intratelluric assemblage in this group (Chapter 4). The observed decrease in TiO_2 with decreasing MgO indicates the presence of a TiO_2-bearing phase (ilmenite and/or Ti-magnetite) in the crystallizing assemblage (Fig. 6.3). The approximately equal amounts of ilmenite and magnetite used in the "best-fit" assemblage in Table 6.4b is consistent with petrographic evidence which indicates approximately equal proportions of these minerals in this group (Chapter 4.5). The effect of fractionation of this assemblage, kept constant for 5x10% fractionation increments is illustrated for selected major elements

(Al, Ca, Fe and Ti) and Ni and Cr in Fig. 6.4. The assemblage chosen is generally consistent with these variations although the considerable spread in Al_2O_3 and FeOt contents is unaccounted for. In the case of FeOt this may be a result of changes in the ilmenite/magnetite ratio in the fractionating assemblage to which the FeOt (and TiO_2) content of any derivative melt will be particularly sensitive.

6.3.1.3 The N group

Models are compared to an unaltered evolved N-group sample (RSS169). In the case of the N-group models there is an excellent correspondence between NIELSEN's predictions and the observed numerical (GENMIX) variations, both with respect to whole-rock variations (see ss^2 excluding Na and K) and the predicted mineral assemblage (Table 6.4c). Even NVK predicts a similar assemblage although the proportion of olivine on the liquidus is much greater than NIELSEN or GENMIX predictions. Geochemical variations of Al_2O_3 and CaO with MgO observed for the group generally, are consistent with the aggregate predictions of the numerical modelling and the "best-fit" assemblage used is based on this and the stepwise predictions of NIELSEN, i.e. dominant clinopyroxene and plagioclase with lesser olivine (Figs. 6.1c, 6.2, Table 6.4c).

The greater Al_2O_3 content of 3 samples (Fig. 6.1c) are a result of their plagioclase-phyric character and hence the movement of the whole-rock composition towards the plagioclase mineral composition. The general increase in TiO_2 with decreasing MgO (Fig. 6.3) implies there is no significant Ti-bearing phase in the fractionating assemblage. The fractionating assemblage in Table 6.4 is also consistent with petrographic evidence (Chapter 4).

Model compositions are plotted in Fig. 6.4 for selected elements at 10% fractionation intervals and demonstrate that the broad decrease in CaO and Al_2O_3 and the increase in TiO_2 and FeOt is accounted for, but not the spread in these data. The decrease in Ni and Cr with MgO is also accounted for although some N-group samples have contents elevated from the bulk-trend. This may be a result of cumulus enrichment in olivine and/or clinopyroxene.

6.3.1.4 Conclusions

The estimated assemblages used for each group were selected to satisfy numerical predictions (GENMIX) which reflect the range of data observed (Figs. 6.1-6.4). Generally these assemblages are consistent with the stepwise predictions of NIELSEN, but not with the predictions of NVK. It is emphasized, however, that both models are based on experimental data obtained at one atmosphere and therefore any conclusions as to their effectiveness can only be made assuming one atmosphere crystallization. This may imply, at least in the context of NIELSEN, that fractional crystallization in central Lebombo basic volcanics seems consistent with low-pressure conditions.

For the range in compositions modelled the range in F (amount of liquid remaining) of the "best-fit" models for each group is similar in every instance to F-values calculated by NIELSEN and the least-squares numerical model (GENMIX, Le Maitre, 1976) (Table 6.4). This constraint is important for the modelling of trace element variations in the succeeding section.

6.3.2 Trace Elements

6.3.2.1 The LFE-group

It is emphasized that closed-system fractional crystallization can only be judged for its ability to produce observed chemical variations with respect to elements which show consistent variations in the rock types. The range of K, Ba, Rb and Sr contents in the LFE-group for instance (Figs. 3.6c-f; 6.5d, e) must be accounted for by processes other than closed-system fractional crystallization. The "best-fit" closed-system fractional crystallization model used to account for observed changes in major elements (Table 6.4a) is able to account for the degree of enrichment in HFSE with decreasing MgO in this group with the exception of the LREE in some samples (Figs. 6.5a, b; 6.6). The "envelope" or spread of concentrations observed (Figs. 3.3; 6.5a, b) may be attributed to similar variations in the parent magmas of this suite (dealt with later) and, to a lesser degree, slight variations in fractionating mineral proportions. For example, the trend of LREE concentrations with MgO is relatively flat (Figs. 3.3m, n; 6.5b) for most of the data and the envelope of data around this trend is probably a function of similar variations in the parental magmas (i.e. N. Lebombo picrites, Cox and Bristow, 1984) of this group.

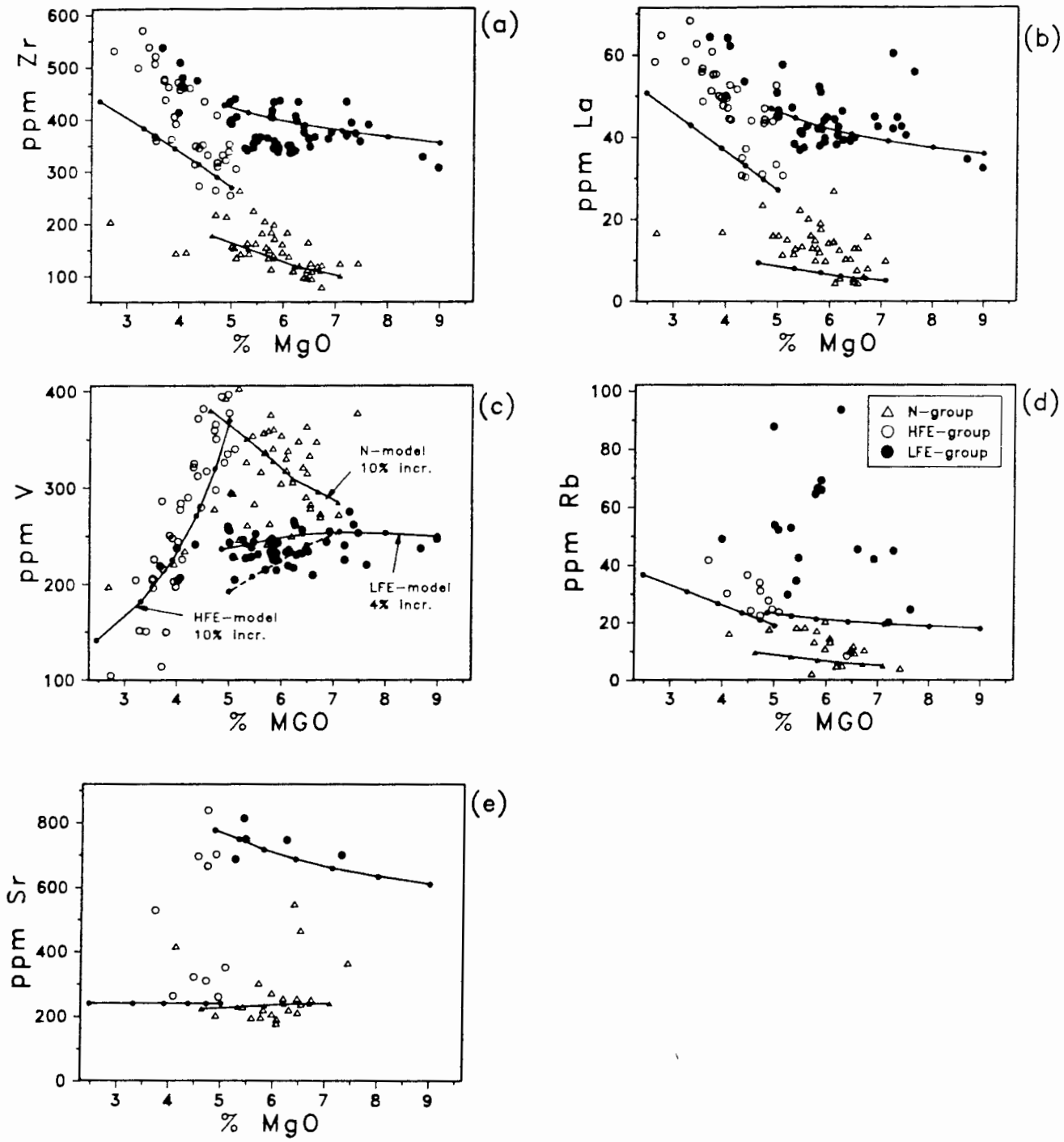

Figure 6.5. Selected trace elements *vs* MgO for central Lebombo basaltic rocks and closed-system fractional crystallization model trends. Each point on the model trends represents 4% fractional crystallization increments in the case of the LFE-group model and 10% crystallization in the case of the N- and HFE-group models. The dashed line associated with the LFE-model trend for V represents the liquid line of descent when ilmenite is added to the fractionating assemblage (after 8% crystallization) (Table 6.5). In the case of Rb and Sr only "fresh" sample data (as in Fig. 3.6, Table C1) are plotted. All data are normalized to 100% volatile-free, Fe as FeO.

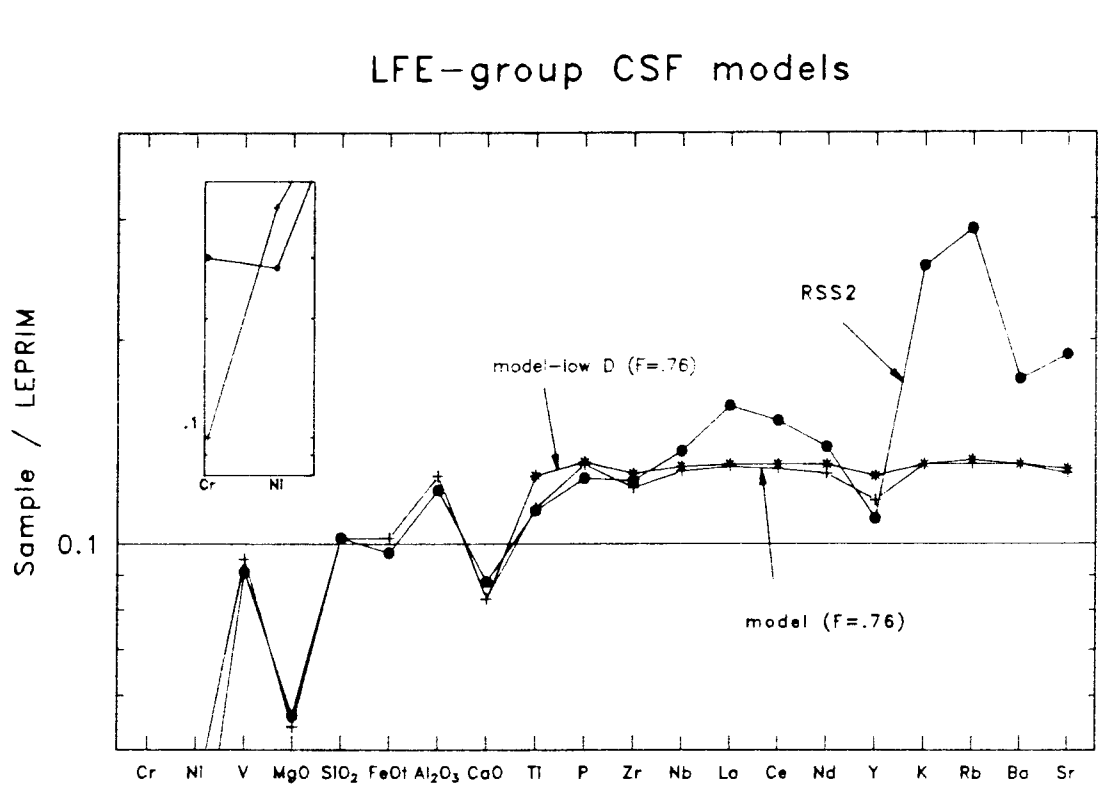

Figure 6.6. LFE-group closed-system fractional crystallization model. All compositions have been normalized to the model starting composition (LEPRIM) and the effectiveness of the model is gauged by the magnitude of the difference between the model and observed (RSS2) compositions.

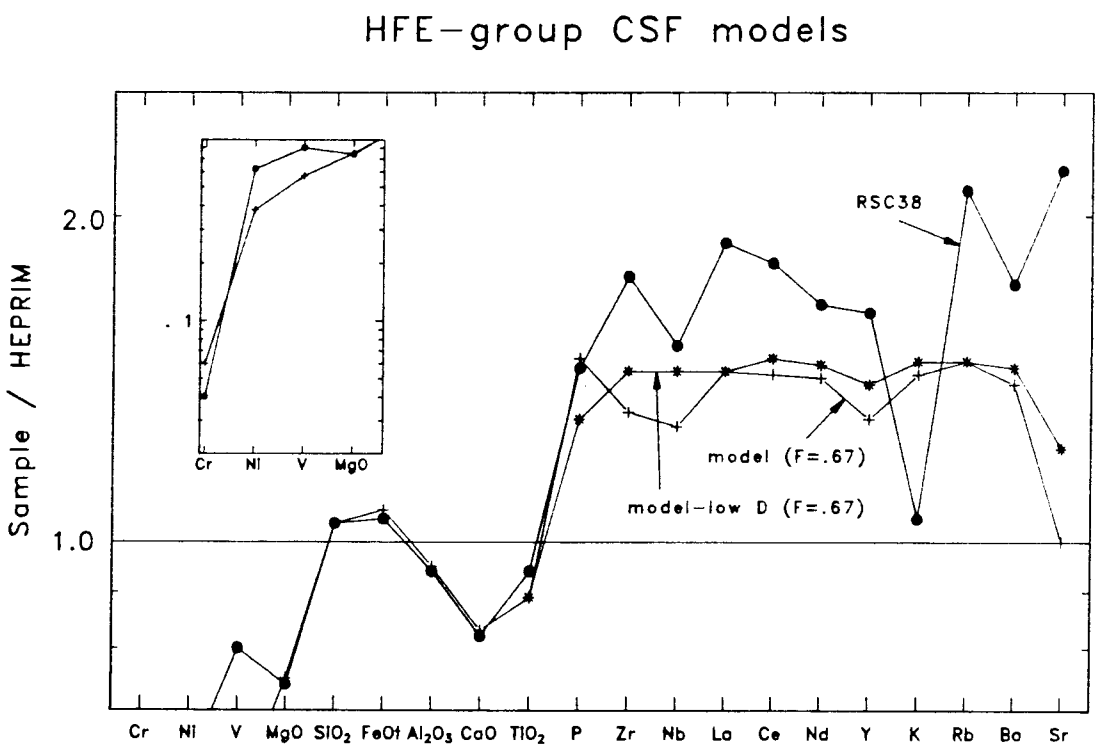

Figure 6.7. HFE-group closed-system fractional crystallization model. All compositions have been normalized to the model starting composition (HEPRIM) and the effectiveness of the model is gauged by the magnitude of the difference between the model and observed (RSC38) compositions.

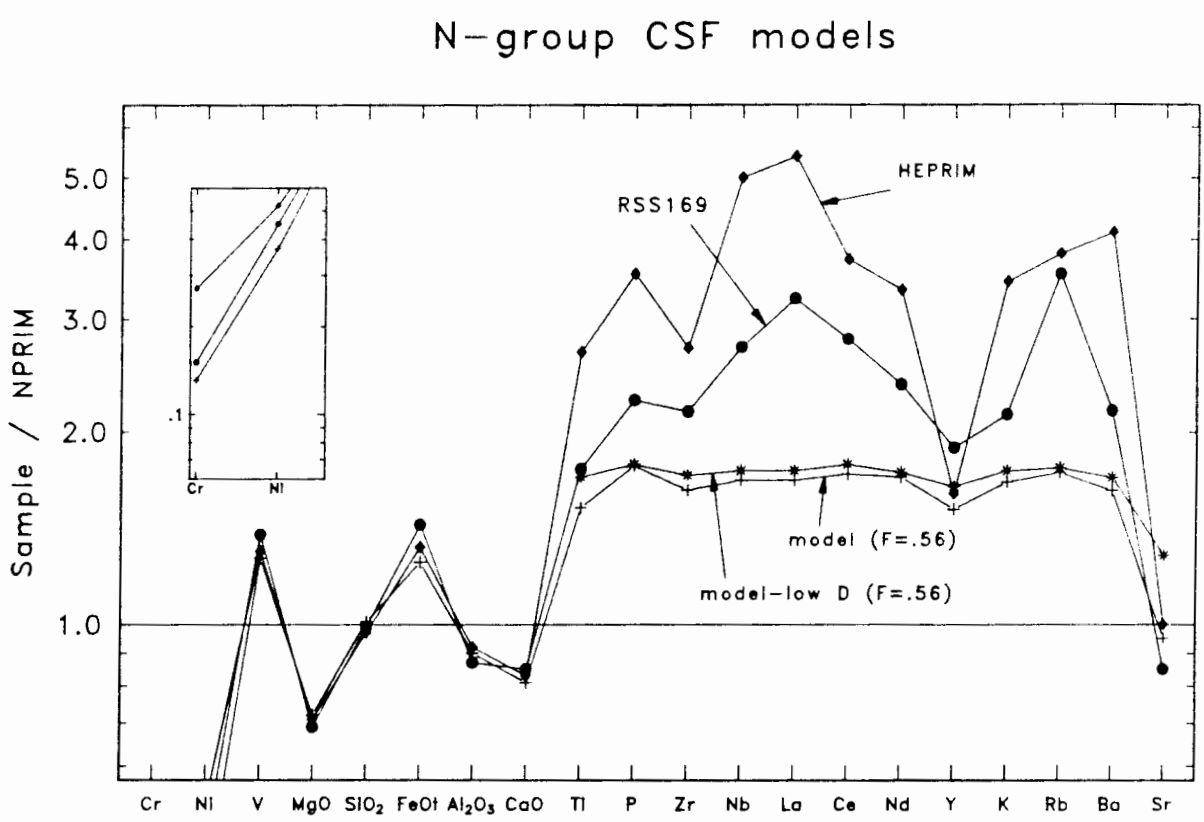

Figure 6.8. N-group closed-system fractional crystallization model. All compositions have been normalized to the model starting composition (NPRIM) and the effectiveness of the model is gauged by the magnitude of the difference between the model and observed (RSS169) compositions.

As mentioned previously, the inclusion of small and variable amounts of ilmenite in the fractionating assemblage of this group (Table 6.5) could account for some of the dispersion in V values observed with decreasing MgO (Fig. 6.5c). This inclusion of ilmenite in the fractionating assemblage does not significantly affect the concentrations of trace elements, other than Ni and V, in closed-system fractionation models.

6.3.2.2 The HFE group

The "best-fit" model constrained by major elements (Table 6.4b) is unable to generate the observed increases in Zr (270-475 ppm), Y, Nb, La (27-50 ppm), Ce and Nd for MgO 5% to 3.7% (Figs. 6.5a, b; 6.7). Even using the lowest possible mineral/melt partition coefficients (Table 6.2b) does not alter this conclusion (Fig. 6.7).

The general increase in K_2O (1.2-2.5%) and Rb (25-42 ppm) and the random distribution of Ba (400-900 ppm) and Sr (200-900 ppm) with MgO (Fig. 3.6c-f) cannot be explained by the models presented (Figs. 6.5d, e; 6.7). As for the HFSE, the levels of enrichment in these elements are not produced when minimum D-values (Table 6.2b) are used (Fig. 6.7). Furthermore, the high LILE (K, Rb and Ba) and Sr content of some samples is clearly outside the maximum degree of enrichment possible using the Rayleigh Fractionation Law (eqn. 6.1); for the F-value indicated for a model matching the major element composition, i.e. for D=0 and F=.67, C_L/C_0 = 1.49.

6.3.2.3 The N group

The "best-fit" model (Table 6.4c) cannot produce the increase in Zr (100-215 ppm), La (5-16 ppm) or the other HFSE (Nb, Ce, Nd and Y) with decreasing MgO (Figs. 6.5a, b; 6.8). There is a considerable spread in Y content with MgO and the Y content of RSS169 (Fig. 6.8) does not represent the maximum values observed (Fig. 3.3k). The increase in the LILE content of some samples with decreasing MgO (Figs. 3.6c-f; 6.5d) are also unexplained by this model (Fig. 6.8). HFSE and LILE enrichments are not explained even when the lowest possible D-values (Table 6.2b) are used (Fig. 6.8). Even if D=0, the Rayleigh Fractionation Law predicts a maximum C_L/C_0 of 1.7 for F=.56 and most incompatibles (with the sole exception of Y) for the evolved N-group sample (RSS169) used here show greater degrees of enrichment (Fig. 6.8). Furthermore, the degree of incompatible element enrichment predicted by the

model does not even approach the enrichment observed in the HFE group (HEPRIM, Fig. 6.8) with which the N-group has consistent variations with decreasing MgO for many elements (Chapter 3).

The Sr content of the N group, with the exception of a few high values, is consistently lower than that of the "enriched" groups (Fig. 6.5e). The high-Sr sample containing about 4% MgO (Fig. 6.5e) may be explained by its plagioclase-phyric nature if the plagioclase phenocrysts are cumulate (i.e. $D_{Sr}^{plag} \simeq 2$, Table 6.2a). The high Sr values in the other N-group samples are impossible to explain by closed-system fractional crystallization. The spread of Sr concentrations in the bulk of the N-group samples (200-300 ppm), similar for any MgO interval, may represent a similar spread in magmas parental to this group.

6.4 "BETWEEN-GROUP" VARIATIONS

The preceding discussion indicates that the HFE group cannot be related to the N group by continued closed-system crystal fractionation alone. The possibility of the LFE and HFE groups being related has been discounted in section 6.1. The question of whether the LFE and N groups have a common **parent** magma composition and if not, how their **primary** compositions differ will now be examined.

6.4.1 Primary melts - a definition

A melt which is still in equilibrium with its mantle source composition is considered primary in character. The question of whether basaltic rocks of continental flood basalt provinces are primary or whether they are generally derived from picritic parent melts has been reviewed by Cox (1980) who argues strongly in favour of the latter alternative. Cox (1980) notes that the olivine phase field contracts at higher pressures (i.e. mantle melting) while the orthopyroxene field expands, giving rise to a melt that will be more magnesian than a melt derived under low-pressure conditions. The alternative view (e.g. Wilkinson and Binns, 1981) is that basalts are derived from a more Fe-rich source to produce melts much lower in MgO. Fe-rich lherzolite xenoliths are very rare in southern African kimberlites

(Gurney and Harte, 1980). Assuming such xenoliths are representative of mantle compositions beneath southern Africa, then an Fe-rich source region for Karoo basalts seems improbable.

For mantle-derived magmas to be primary in nature, they should be in equilibrium with mantle olivine compositions as this mineral is both ubiquitous and voluminous in mantle assemblages. The olivines in common mantle modules brought up by southern African kimberlites have a range of compositions: Fo_{88}-Fo_{95} (Gurney and Harte, 1980). If a magmatic Fe_2O_3/FeO ratio of 0.15 and a Fe/Mg K_D value of 0.30 is assumed for olivine (Roeder and Emslie, 1970), then magmas in equilibrium with olivines of this composition would have Mg-numbers in the range 68-85. The basalts of the central Lebombo have a range of Mg-numbers 31-62, which implies they have undergone substantial fractionation from possible parent magmas.

6.4.2 LFE-group "primary" melts

The hypothetical "primitive" composition LEPRIM (Table 6.3) was chosen as representative of an unevolved LFE-group composition. Two back-calculations of this composition to higher MgO values are conducted and compared:
(1) using Nathan and Van Kirk (1978) predictions (i.e. assuming low pressure fractional crystallization) and
(2) using a high-pressure phase assemblage.

Although the equations of Nathan and Van Kirk (1978) did not have great success in predicting liquidus phase assemblages in the previous section, they are applied here as a first approximation to low-pressure fractional crystallization. The predicted liquidus assemblage was then added incrementally to the whole-rock major element composition (initially LEPRIM, Table 6.3) in likely proportions. In this instance (MgO range 9-15%) the inclusion of some orthopyroxene in the fractionating assemblage is consistent with petrographic observations for the N. Lebombo picrites (Bristow, 1984). Successive increments were tested using the Nathan and Van Kirk (1978) equations for any changes in the liquidus assemblage. This incremental addition of material and testing to see what phases constitute the liquidus assemblage was repeated until a composition was reached which is considered to be in equilibrium with a mantle assemblage. Phases and compositions used

along with temperatures predicted by the Nathan and Van Kirk (1978) equations are given in Table 6.6. Olivine compositions used in this calculation are continually changed to ensure that an approximate equilibrium is maintained between the liquid and crystallizing compositions. Trace element compositions are calculated using the Rayleigh fractionation law. Back-calculated major and trace element compositions (LFE primary (1)) are summarized in Table 6.9.

As seen in the previous section, however, the Nathan and Van Kirk (1978) predictions are not always consistent with major element and petrographic evidence an is restricted to low pressures. Cox and Bristow (1984) and Bristow (1980) maintained that shoshonitic and absarokitic basalts (LFE here) of the SRBF were generated by fractionation from picritic magmas similar to those erupted within the Letaba River Formation in the N. Lebombo.

Bristow (1980, 1984) recognized two parageneses in the Lebombo picritic basalts and dolerites:

PI : olivine (group I) + orthopyroxene mantled by clinopyroxene.

PII : olivine (group II) + clinopyroxene ± unmantled orthopyroxene.

Group I olivines have a higher mean Fo content (Fo_{87}) than group II olivines (Fo_{79}, Bristow, 1980). These two parageneses are interpreted by Bristow (1980) to represent two distinct crystallizing environments:

PI : - where mineral compositions are similar to mantle olivines and orthopyroxenes, implies high-pressure crystallization,

PII : - low pressure crystallization by analogy to other low pressure assemblages (Thompson *et al.*, 1972; Cox and Jamieson, 1974; Cox, 1987).

High-pressure fractionation for the PI assemblage is confirmed by the experimental work of Cox and Jamieson (1974) which revealed that pressures of 6-12 kb (corresponding to depths of 18-36 km) are necessary to stabilize orthopyroxene as a major crystallizing phase on the liquidus in the MgO interval concerned. Cox (1987) describes two textural forms of orthopyroxene within the high-pressure assemblage, one interpreted as a high-pressure crystallate and the other as a mantle restite phase recognized by the

Table 6.6. Calculation of a LFE-group "primary" composition under low pressure crytallization conditions (using NVK). Mineral compositions are taken from Table 6.1. Also given are Mg#'s and the olivine composition in equilibrium with such a melt (calculated using Roeder and Emslie, 1970, assuming Fe_2O_3/FeO = 0.15 and Fe/Mg K_D = 0.30).

Addition of phases						
Phases	ol-KP101	50%	70%			
	ol-KP111			90%	100%	
	opx-KS47	50%	30%	10%		
%+	LEPRIM	+5%	+10%	+15%	+20%	
SiO_2	52.50	52.31	51.94	51.46	50.93	
TiO_2	3.00	2.87	2.74	2.61	2.49	
Al_2O_3	11.10	10.57	10.08	9.60	9.14	
FeOt	11.00	11.05	11.14	11.12	11.11	
MgO	9.00	10.38	11.85	13.52	15.19	
CaO	10.00	9.59	9.18	8.76	8.35	
Na_2O	1.94	1.85	1.76	1.68	1.60	
K_2O	1.00	.95	.90	.86	.82	
P_2O_5	.45	.43	.41	.39	.37	
Mg#	62.3	65.5	68.3	71.1	73.4	
eqm.ol(Fo)	84.6	86.4	87.8	89.1	90.2	
NVK ol	1210*	1231*	1253**	1277**	1301**	
temps opx	1215**	1232**	1249*	1265	1280	
cpx	1204	1215	1225	1237	1249	

NOTE:
+ all Fe as FeO, normalized volatile free. Fe_2O_3/FeO = 0.15 for all calculations.
* indicates phases on the liquidus (within a 10°C range) where '**' is the dominant phase.

Table 6.7. Calculation of LFE-group "primary" composition under high pressure conditions.
Mineral compositions are taken from Table 6.1. Also given are Mg#'s and the olivine composition in equilibrium with such a melt (calculated using Roeder and Emslie, 1970, assuming Fe_2O_3/FeO = 0.15 and Fe/Mg K_D = 0.30).

Addition of phases						
Phases	ol-KP101	30%	40%			
	ol-KP111			50%	60%	70%
	opx-KS47	70%	60%	50%	40%	30%
%[+]	LEPRIM	+5%	+10%	+15%	+20%	+25%
SiO_2	52.50	52.39	52.25	52.03	51.76	51.44
TiO_2	3.00	2.95	2.82	2.70	2.58	2.47
Al_2O_3	11.10	10.57	10.08	9.61	9.16	8.73
FeOt	11.00	11.02	11.07	11.06	11.05	11.04
MgO	9.00	10.24	11.49	12.83	14.19	15.57
CaO	10.00	9.60	9.22	8.84	8.47	8.10
Na_2O	1.94	1.85	1.76	1.68	1.60	1.52
K_2O	1.00	.95	.90	.86	.82	.78
P_2O_5	.45	.43	.41	.39	.37	.35
Mg#	62.3	65.3	67.7	70.1	72.2	74.1
eqm.ol(Fo)	84.6	86.3	87.5	88.7	89.9	90.5

[+] all Fe as FeO, normalized volatile free. Fe_2O_3/FeO = .15 for all calculations.

existence of a distinct fabric. The PII olivines are out of equilibrium with a magma of their host's whole-rock composition and may represent the "last-stage" crystallization of an interstitial melt. The observation that these lower-Fo olivines and clinopyroxenes are generally confined to the groundmass in these rocks (Bristow, 1980) supports this explanation. Alternatively the more Fe-rich olivines may be inherited by accumulation from "above" in a zoned magma chamber by crystallization from a more evolved melt (a process called "compensated crystal settling" by Cox and Bell, 1972).

Bristow (1980, table 8.16) demonstrates using a least-squares modelling technique (Bryan *et al.*, 1968) that orthopyroxene dominates the fractionating assemblage for the fractionation step 12-9% MgO:

step	opx/ol ratio
18 - 15% MgO	1.6
15 - 12% MgO	1.3
12 - 9% MgO	3.1

A primary major element composition is calculated accordingly, with the parameters used and results given in Table 6.7. Calculated trace element contents are given in Table 6.9 (LFE primary (2)).

6.4.3 N-group "primary" melts

The procedure for the "back-calculation" here is identical to that outlined in the previous section using Nathan and Van Kirk (1978) for low-pressure fractional crystallization; NPRIM is selected as a primitive N magma composition (Table 6.3) and the compositions assumed for the fractionating minerals are consistent with the Nathan and Van Kirk (1978) predictions. The parameters used are presented in Table 6.8 and the results of the back-calculation summarized in Table 6.9. Unfortunately the N-group basaltic rocks have no high-MgO equivalent in the Lebombo or the Karoo in general, so estimates of the extent of fractionation and the pressure at which it occurs, cannot be made. The similarity of the back-calculated results for the LFE primary (1) and LFE primary (2) (Table 6.9), however, indicate that such a consideration would not produce very different primary chemical compositions.

Table 6.8. Calculation of a N-group "primary" composition under low pressure conditions (using NVK). Mineral compositions are taken from Table 6.1. Also given are Mg#'s and the olivine composition in equilibrium with such a melt (calculated using Roeder and Emslie, 1970, assuming Fe_2O_3/FeO = 0.15 and Fe/Mg K_D = 0.30).

Addition of phases						
Phases	ol-KS3	80%				
	ol-KP101		100%	100%		
	ol-KP111				100%	100%
	cpx3-RSS35	20%				
%+	NPRIM	+5%	+10%	+15%	+20%	+25%
SiO_2	51.03	50.67	50.16	49.69	49.23	48.80
TiO_2	1.50	1.44	1.37	1.30	1.24	1.18
Al_2O_3	14.70	14.04	13.37	12.73	12.12	11.54
FeOt	11.08	11.42	11.55	11.68	11.65	11.62
MgO	7.09	8.49	10.26	11.94	13.69	15.35
CaO	11.00	10.68	10.18	9.71	9.26	8.83
Na_2O	2.90	2.77	2.64	2.51	2.39	2.28
K_2O	.35	.33	.31	.30	.29	.28
P_2O_5	.17	.16	.15	.14	.13	.12
Mg#	56.4	60.1	64.2	67.4	70.4	72.8
eqm.ol(Fo)	81.2	83.4	85.7	87.3	88.8	89.9
NVK ol	1201**	1222**	1248**	1272**	1297**	1320**
temps opx	1169	1187	1207	1225	1243	1259
cpx	1196*	1206	1219	1231	1243	1254
NVK Fo	81.2	83.4	85.7	87.3	88.8	89.9

+ all Fe as FeO, normalized volatile free. Fe_2O_3/FeO = .15 for all calculations.

* indicates phases on the liquidus (within a 10°C range) where '**' is the dominant phase.

6.4.4 Conclusions

The back-calculated LFE-group "primary" compositions may be compared to the average composition for the N. Lebombo picrites (Duncan *et al.*, 1984b) to which they are allegedly related (Table 6.9). Most of the back-calculated LFE-group concentrations area within 1 s.d. and are all within 2 s.d. of the N. Lebombo mean. Elements such as K, Rb, Ba and Sr exhibit a wide range of values within the picrites and do not vary consistently with MgO content (Fig. 6.9) and it is likely that similar distributions in these elements in the LFE group reflect this dispersion. The calculated LFE-group "primary" compositions for these elements are at the lower end of the range exhibited by the picrites. Elements such as Al_2O_3, Y, Ni and Cr, however, exhibit constrained variations with MgO content in the picrites. The calculated Al_2O_3, Y and Ni concentrations for the LFE-group are consistent with values observed for the picrites at these MgO contents (Fig. 6.9). The back-calculated Cr composition in LFE primary (2) (high pressure fractionation) is more compatible with Cr contents observed in picrites of this MgO content than the Cr content of LFE primary (1) (Fig. 6.9h). Thus, under closed-system fractional crystallization conditions, the LFE group may be derived from the N. Lebombo picrites. Furthermore, the differences between the N and LFE groups persist back to primary magma compositions.

6.5 SUMMARY

The element dispersions and enrichments which are not accounted for by a closed-system fractional crystallization model are summarized in Table 6.10. In any specific model it is difficult to produce the compositional variations which may be directly compared to the dispersion of the observed data. It is likely that the latter reflects a range of compositions in the parental magmas of each group. In some instances a closed-system fractional crystallization model may explain the "enrichment" but not the dispersion, e.g. FeO in the HFE and N groups (Fig. 6.4c) and the HFSE in the LFE group (Fig. 6.4a, b). If closed-system fractional crystallization cannot produce the "within-group" abundances in the N and HFE groups, it is unlikely that the HFE group evolved from a N-type basaltic rock solely by this petrogenetic process. Quite clearly some process is acting to decouple the major and incompatible trace elements in the N and HFE groups. The identification of

Table 6.9. Summary of "primary" whole-rock compositions calculated for the LFE- and N-groups.

	LFE-group primary (1) (low press.)	(2) (high press.)	N-group primary	N. Lebombo picrites+ mean	s.d.	n
SiO_2	50.93	51.44	48.80	50.65	1.25	19
TiO_2	2.49	2.47	1.18	3.11	.41	19
Al_2O_3	9.14	8.73	11.54	8.33	1.27	19
FeOt	11.11	11.04	11.62	10.97	.75	19
MgO	15.19	15.57	15.35	15.73	3.51	19
CaO	8.35	8.10	8.83	7.17	1.08	19
Na_2O	1.60	1.52	2.28	1.45	.53	19
K_2O	.82	.78	.28	2.13	.91	19
P_2O_5	.37	.35	.12	.46	.09	19
Mg#	73.4	74.1	72.8	74.4	4.6	19
K*	6952	6508	2433	17683	7555	19
Rb	14.9	14.2	4.1	56	22.8	17
Ba	404	385	82	930	351	17
Sr	503	479	198	1014	272	17
Ti*	14918	14300	7488	18644	2458	19
P*	1645	1540	621	2008	393	19
Zr	293	279	83	408	84	17
Nb	16.8	16.1	4.1	19	7.4	17
Y	30	28	21	28	3.4	17
La	30	28	4.1	-		
Ce	70	67	14.8	-		
Nd	51	48	12.3	-		
Ni	814	742	1048	838	299	17
Cr	529	730	310	815	140	17
V	212	210	241	207	31	17
Sc	23	24	30	21	3.0	16
Co	78	79	80	82	15.5	17
Zn	130	141	98	112	7	17
Cu	96	91	198	84	12.2	17

+ from Duncan *et al.* (1984b).

* calculated using the Rayleigh Fractionation Law.

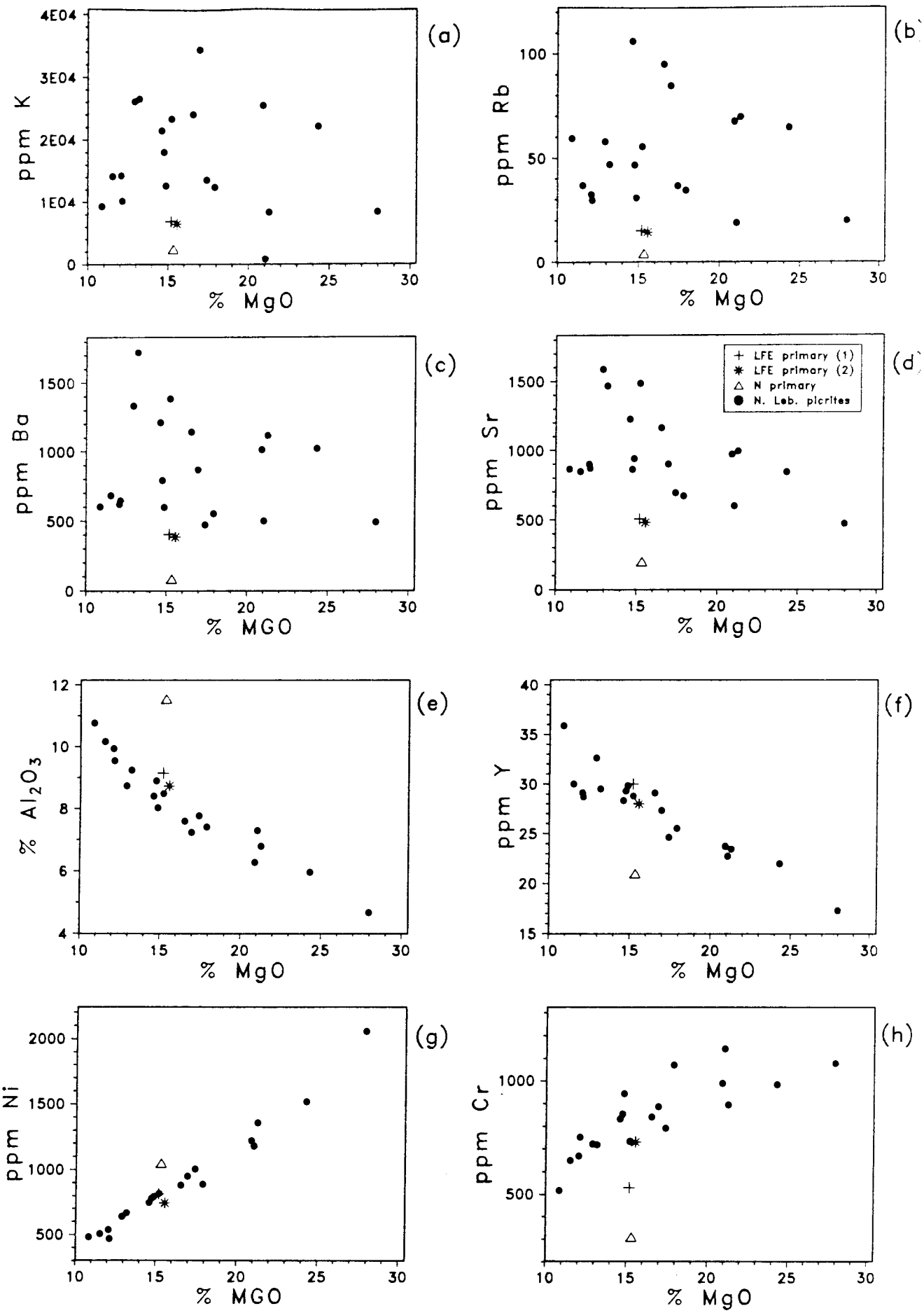

Figure 6.9. Selected N. Lebombo picrite data (from Bristow, 1980) with calculated LFE- and N-group "primary" compositions (Table 6.9) (normalized 100% volatile free, Fe as FeO).

this process is attempted in later chapters. A striking feature of the data (Table 6.10), however, is the similarity of element variations in the HFE and N groups which cannot be attributed to closed-system fractional crystallization. Thus, the process producing these variations is likely to be common to both the HFE and N groups and the possibility of a relationship between the two still cannot be discounted.

A "primary" composition calculated assuming closed-system fractional crystallization at elevated pressures for rocks parental to the LFE group is consistent with the derivation of this group from a N.Lebombo picritic parent. Differences between the LFE and N groups persist back to primary magma compositions.

Table 6.10. Element dispersions and enrichments not accounted for by closed-system fractional crystallization models alone.

	dispersion	enrichments
LFE group	LILE, Sr	LILE, Sr
	(HFSE)	
HFE group	FeOt	Zr, Nb, La, Ce, Nd
	Y	P, (Y)
	Ba, Sr	Ba, Sr, Rb, K
N group	FeOt	Zr, Y, Nb, La, Ce, Nd
	V, Y	P, (Y)
	(Sr)	Ba, Sr, Rb, K

7. CONTAMINATION WITH GRANITIC CRUST

7.1 INTRODUCTION

It is considered unlikely that the volumes of magma which the Lebombo volcanics represent were able to pass through approximately 40 km of dominantly granitic continental crust without being affected to some extent by contamination. It is emphasized that crustal contamination is only considered in terms of a granitic contaminant as basement rocks exposed west of the basalts are dominantly granitic (examined later in greater detail). Two questions are posed:
(1) what variables measured are most susceptible to granitic contamination, and
(2) how significant is such contamination.

Field evidence indicating significant granitic contamination is not substantial. Felsic xenoliths were recorded in only two samples (both dolerites: RSS145, a LFE-group sample, and RSS168, HFE-group sample), where they were infrequent and reached a maximum dimension of 15 cm. However, it may also be argued from the rarity of field evidence that the assimilation of felsic material, if it has occurred, was efficient, creating a homogeneous end-product. Thus, the possiblity of granitic contamination must still be examined from a geochemical viewpoint.

Two styles of **bulk** contamination which produce significantly different results are examined:

(1) Contamination accompanied by fractionation, which is considered to occur in magma chambers where the latent heat released by crystallization contributes to the melting and assimilation of wall rock. Alternatively the heat differential between a basic melt and acidic wall rocks may be sufficient to cause assimilation, which will then decrease the magma temperature and promote crystallization. A model for coupled **assimilation - fractional crystallization** (AFC) was proposed by De Paolo (1981) and is examined here.

(2) Where contamination is greatest in the more basic, and therefore the hottest, magmas, **conduit contamination** is dominant. This style of

contamination (i.e. in conduits to the surface) is examined in terms of models proposed by Huppert and Sparks (1985).

The problem is to determine which of these styles of bulk contamination are dominant, if any, and to what extent selective contamination must be invoked to explain observed variations. AFC, conduit contamination and selective contamination models are discussed and then considered in terms of variations observed in the LFE-, HFE- and N-groups.

7.2 THE MODELS

7.2.1 Coupled Assimilation-Fractional Crystallization (AFC)

7.2.1.1 Equations

De Paolo (1981) derives equations for trace element and isotopic variations in a magma chamber where the mass assimilation rate (M_a) is an arbitrary fraction (r) of the fractional crystallization rate (M_c). De Paolo (1981) integrates these rates, M_a and M_c, with respect to time to become total mass assimilated and total mass fractionated (or crystallized) respectively. Two cases are considered, when $M_a=M_c$ and $M_a\neq M_c$ ($r=M_a/M_c$). For r=1:

$$C_m/C_m^0 = (C_a/DC_m^0)[1 - \exp(-DM_a/M_m)] + \exp(-DM_a/M_m)$$

(equation 3 of De Paolo, 1981)

where M_m = mass of magma, C_m^0 = starting concentration in the magma, C_m = concentration of an element in the magma and D = bulk solid/liquid partition coefficient.

For $r\neq 1$

$$C_m/C_m^0 = F^{-z} + [r/(r-1)](C_a/zC_m^0)(1-F^{-z})$$

(equation 6a of De Paolo, 1981)

where $F = M_m/M_m^0$ (or amount of liquid remaining) and $z = (r+D-1)/(r-1)$.

In the case of radiogenic isotopes De Paolo's (1981) equation 13a for r=1 and equation 15a for r≠1, are used. For oxygen isotopes equation 17 (r=1) and equation 18 (r≠1) from De Paolo (1981) are used. These expressions are incorporated by A.R. Duncan in the program DARTS to model trace elements and isotope ratios. Major elements are modelled by a mass-balance approach, i.e. the concentration of an oxide in the fractionating assemblage is calculated depending from its measured concentration in the constituent phases and subtracted from the starting composition (A. R. Duncan, pers. comm., 1986).

7.2.1.2 Important aspects of the model

De Paolo (1981) points out that the model becomes a simple binary mixing model by setting M_c=0 (i.e. as r tends to infinity) or when an element mineral-melt partition coefficient is 1. The isotopic and trace element "mixing" trends generated, however, can be very different from binary mixing, especially for r <1. This is important, particularly in the models used later in this chapter, where it is considered that r will most likely be constrained to values less than 1. This is suggested from heat budget considerations, i.e. the mass of material crystallized will most likely only supply sufficient heat for a maximum equivalent mass of granitic material to be assimilated. Taylor (1980) estimated an upper limit of .3 for r, for thermal balance between cold country rock (150°C) and hot basalt (1150°C) to be preserved. An analogous calculation for country rock at 1000°C (e.g. lower crust in regions of active volcanism), results in an upper limit for r of about 1.0 (De Paolo, 1981). Furthermore, there is a "volume problem" in the magma chamber if $M_a > M_c$ (i.e. if r >1). Another important conclusion of De Paolo's (1981) model is that the change in concentration in the residual magma is dependent not on the concentration difference between magma and wallrock, but on the concentration difference between wallrock and cumulates.

Generally an AFC model predicts that a magma with the longest residence time in a chamber (nominally the most fractionated) will also be the most contaminated. Assuming a granitic contaminant, this will result in enhanced negative correlations between MgO (a fractionation index) and elements relatively more concentrated in granitic rocks (e.g. Si, K, Rb and Ba) than closed-system fractional crystallization can produce.

7.2.1.3 The choice of a contaminant

The nature of potential contaminants in the central Lebombo must be resolved. Fig. 7.1 is reproduced from Jackson and Robertson (1983, fig. 1) and gives the distribution of the various crustal components in the region of the extensively studied Barberton Greenstone Belt. This area is approximately 50-100 km west of the central Lebombo as depicted in Fig. 2.1. The dominant crust in this region is essentially bimodal in nature, consisting of the older (3.0-3.5 Ga) tonalitic gneisses (e.g. Ancient Gneiss Complex of Swaziland, Kaap Valley and Nelshoogte Plutons) and the more recent (2.7-3.2 Ga) potassic granites (e.g. Nelspruit, Lochiel granite). Typical chemical data for these granitoids are given in Table 7.1 along with $^{87}Sr/^{86}Sr$, calculated at 190 Ma, from Barton *et al.* (1983). Potassic granites dominate the Archaean crust observed in this region (and worldwide, Sutton, 1977) and thus the "typical" composition of a composite crust (Table 7.1, composition 9) is biased towards that of a potassic granite. It is appreciated that these crustal suites probably represent upper crust at the time of basalt eruption, but in the absence of any reasonable constraint on lower crust compositions (the rocks are not observed) this approximation is justified.

It is assumed that the prime site of assimilation will be in the region of the magma chamber where the heat flux is greatest (i.e. the roof) while the floor and sides of such a chamber will probably be quickly sealed off by "chilled" magma. It is likely that the incorporation of crustal material by a mafic melt will involve melting of less refractory crustal material. Thus, in the AFC models, the contaminant used is a calculated partial melt of composition (9) ("typical crust") in Table 7.1. The degree of partial melting used is arbitrarily set at 20%. The compositions of constituent minerals from granitic rocks are selected from Deer *et al.* (1966) and normalized to 100% (Table 7.2). The mineral mode of the "typical crust" was calculated (Table 7.3) using a least-squares technique based on that of Le Maitre (1976). The plagioclase composition (plag-I) was determined by initially using An and Ab "end-members" in the model and calculating the composition of an "ideal" feldspar (plag-I) from the relative proportions of each in the resulting "mix". The weight fractions of each phase entering the melt (Table 7.4) reflect the eutectic melting of a granitic rock (Hanson, 1978).

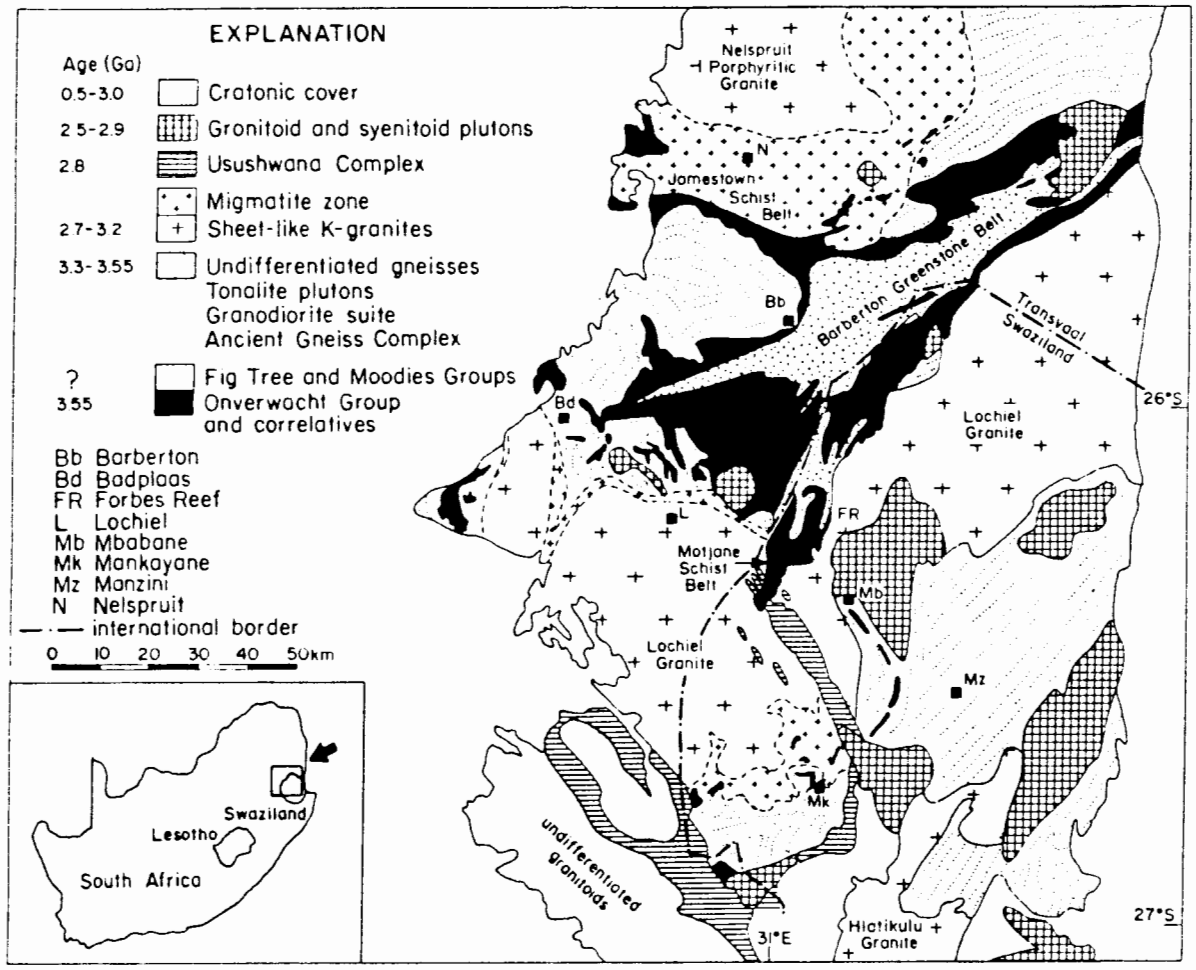

Figure 7.1. Simplified geological map of north-western Swaziland and south-eastern Transvaal about 50-100 km to the west of the central Lebombo (from Jackson and Robertson, 1983).

Table 7.1. Composition of granitoid rocks of the crust in the vicinity of the central Lebombo: Barberton area and Swaziland (total Fe as FeO, normalized to 100% volatile-free).

	(1)*	(2)*	(3)	(4)	(5)	(6)*	(7)*	(8)	(9)
%									
SiO_2	70.50	70.00	66.10	71.49	70.44	71.80	77.09	67.00	71.00
TiO_2	.30	.40	.46	.30	.32	.33	.25	.52	.35
Al_2O_3	14.50	15.00	15.50	14.83	14.98	14.91	11.41	15.36	14.80
FeOt	2.60	2.50	4.00	2.27	2.53	2.40	3.37	4.28	2.70
MgO	1.40	1.50	2.50	1.46	1.34	.89	.59	2.36	1.40
CaO	2.00	2.10	4.30	3.60	3.01	3.06	1.67	4.32	2.10
Na_2O	3.90	4.30	5.40	4.52	5.72	4.83	3.64	4.41	4.00
K_2O	4.60	4.10	1.38	1.52	1.66	1.63	1.88	1.53	3.50
P_2O_5	.20	.10	.16	-	-	.11	.03	.14	.15
ppm									
Rb	186	114	56	69	52	55	52	57	100
Ba	800	700	350	186	380	528	178	315	650
Sr	338	463	574	237	544	392	496	418	400
Zr						154	531	185	300
La						27.6	61	31.0	40
Ce						46.9	119	59.5	70
Nd						18.9	69.3	24.0	35
Cr				22	18	16	4	50	15
$R_{190\ Ma}$	.881		.709						.730
$\delta^{18}O$									9.0

* areally dominant rock types,
$R_{190\ Ma} = {}^{87}Sr/{}^{86}Sr$ calculated at 190 Ma,
blank spaces indicates data not available.

(1) Typical composition of the Mpuluzi Granite (Lochiel Granite) in the Barberton area (Anhaeusser and Robb, 1983). Sr-isotope ratio is from Barton *et al.* (1983) calculated at 190 Ma.
(2) Typical composition of the Nelspruit Granite in the Barberton area (Anhaeusser and Robb, 1983).
(3) Typical composition of the Kaap Valley Pluton in the Barberton area (Anhaeusser and Robb, 1983). Sr-isotope ratio is from Barton *et al.* (1983) calculated at 190 Ma.
(4) ave. of tonalitic diapirs (Condie and Hunter, 1976).
(5) ave. of Ancient Gneiss Complex (Condie and Hunter, 1976).
(6) ave. of Archaean Bimodal Suite type A, Ancient Gneiss Complex (Hunter *et al.*, 1984).
(7) ave. of Archaean Bimodal Suite type B, Ancient Gneiss Complex (Hunter *et al.*, 1984).
(8) ave. of Tswela Gneiss, Ancient Gneiss Complex (Hunter *et al.*, 1984).
(9) suggested estimate for typical crust, reflecting the greater abundance of potassic varieties over tonalitic types. The value for $R_{190\ Ma}$ is also an empirical estimate. The value of $\delta_{18}O$ is presumed representative of a typical granitic rock in this area (H. S. Smith, pers. comm., 1987).

Table 7.2. Composition of mineral phases occurring in granitic rocks (Deer *et al.*, 1966, normalized to 100%)

	(1)	(2)	(3)	(4)	(5)
SiO_2	64.54	68.57	44.54	62.46	41.27
TiO_2	-	-	-	.01	4.50
Al_2O_3	18.57	19.86	35.24	23.76	13.81
FeOt	.13	.05	.58	.01	17.60
MgO	-	.04	-	.01	13.44
CaO	.17	-	18.79	5.00	1.73
Na_2O	.49	11.19	.79	8.55	.74
K_2O	16.09	.29	.05	.23	6.91

(1) microcline (micro-D), Deer *et al.* (1966)
(2) albite end-member (ab-D), Deer *et al.* (1966)
(3) anorthite end-member (an-D), Deer *et al.* (1966)
(4) 'ideal' plagioclase composition (plag-I)
(5) biotite composition (biot-D), Deer *et al.* (1966)

Table 7.3. Least-squares mixing model for determining the mineral mode of composition (9), Table 7.1.

	Whole-rock Composition composition (9)				
%	Observ.	Calc.	Difference	minerals used	calculated modes
SiO_2	71.00	71.00	.00	quartz	: 28.2%
TiO_2	.35	.60	.25	plag-I	: 43.1%
Al_2O_3	14.80	14.80	.00	micr-D	: 15.5%
FeOt	2.70	2.35	-.35	biot-D	: 13.2%
MgO	1.40	1.78	.38		
CaO	2.10	2.10	.00	Total	100.0%
Na_2O	4.00	4.00	.00		
K_2O	3.50	3.50	.00		
Total	99.85	99.71			

Residual sum of squares = .33

Table 7.4. Granitic melting model parameters

Distribution coefficients (Appendix E)

	quartz	oligoclase (plag-I)	microcline (micr-D)	biotite (biot-D)
Rb	.010	.041	.340	3.200
Ba	.050	.308	6.400	6.500
Sr	.010	4.400	3.800	.120
P	.010	.100	.060	1.500
Zr	.070	.100	.060	1.500
La	.010	.300	.060	1.020
Ce	.010	.270	.044	1.210
Nd	.010	.210	.025	1.250
Cr	.010	.010	.010	7.000

Parameters describing source

	initial wt. fraction	wt. fraction entering liquid (1)
plag-I	.43	.33
quartz	.28	.33
biot-D	.13	.01
micr-D	.16	.33

Melting parameters - simple equilibrium melting

final degree of melting = 20%

Melt composition

wt %		ppm	
SiO_2	75.57	P	1500
TiO_2	.05	Rb	152
Al_2O_3	14.00	Ba	371
FeOt	.22	Sr	184
MgO	.13	Zr	668
CaO	1.48	La	89
Na_2O	3.09	Ce	152
K_2O	5.46	Nd	79
		Cr	13.6

Major elements are modelled as oxides by a mass-balance approach, i.e. the concentration of an oxide in a mineral is multiplied by the proportion of that mineral in the melt.

Trace element concentrations in the melt are calculated using the simple equilibrium melting model given in Shaw (1970), since with the approximations made here (e.g. starting composition), more complex models are not warranted.

$$C_L/C_0 = 1/[D + F(1-P)] \qquad - (7.1)$$

where the liquid phase remains in equilibrium with the residual solid phase until it is removed. Symbols are:

F = weight fraction of melt relative to original parent

C_L = concentration of a trace element in the melt

C_0 = original concentration of a trace element in the source

P,D = bulk solid-liquid partition coefficients and

$D = \sum X^i.D^i$

$P = \sum P^i.D^i$

where D^i = mineral-liquid partition coefficient for phase i

X^i = weight fraction of phase i in the solid

P^i = fractional contribution of phase i to the liquid

The model parameters used are summarized with the resultant melt compositions in Table 7.4.

K is an essential structural constituent in microcline and biotite and while these minerals remain in the source (and melting) assemblage, K is modelled using a mass balance approach (defined earlier). The same is true of Ti in biotite.

Elements such as Zr may be almost totally concentrated in zircon (i.e. 60% Zr in ZrO_2 corresponds to a whole rock Zr content of 300 ppm when the modal proportion of zircon is .07%). This is supported by the experimental work of Watson (1979) who concluded that partial melting of any regions of the Earth's crust that contain zircon and more than 100 ppm Zr will produce magmas whose Zr contents are buffered (by zircon in the restite) at constant low values (<100 ppm). It is likely that the same is true of P in apatite and the LREE which tend to partition strongly into zircon, apatite and other refractory phases. These refractory phases are unlikely to be extensively involved in any melting and are thus likely residual phases. For

these reasons it is suggested that the predicted concentrations of Zr, P and LREE in the melt (Table 7.4) are exaggerated.

The radiogenic isotope ratios of primary melts at the sites of melt segregation are assumed to be the same as that of the source. The oxygen isotope content of each melt has also been set as that of the source, although this is an approximation as small fluctuations of $\delta^{18}O$ may be expected depending on the individual mineral-melt Δ-values.

It is accepted that the use of a constant 20% melt and the initial granitic crust composition, are grossly simplifying assumptions. However, it is suggested that AFC models using an assimilant composition derived in this more selective fashion are more realistic than assuming simple bulk contamination.

7.2.2 Conduit Contamination

Contamination of magmas en-route to the surface in the conduits is considered in terms of the bulk contamination model of Huppert and Sparks (1985). These authors present calculations for cooling, crystallization and contamination during the turbulent ascent of a komatiite, a picrite basalt and a tholeiitic basalt. Contamination is postulated to take place through the rapid transfer of heat to the wall rocks which melt and are then assimilated into the magma. Huppert and Sparks (1985) also state that for such contamination to occur, the flow rate must be sufficient to ensure turbulent rather than laminar flow, and they assume such a physical state for their model. They point out that conduit contamination will produce trends on geochemical diagrams which are opposite to those produced by AFC. Thus, indices of crustal contamination (e.g. initial $^{87}Sr/^{86}Sr$ ratio and LILE concentrations) will be greatest in magmas with high MgO contents. They also point out that thermal erosion rates are proportional to the difference between magma temperature and the fusion temperature of the wall rock. Basalts are thus less likely to be contaminated during turbulent ascent than komatiitic or picritic magmas.

Huppert and Sparks (1985) present calculations which predict 2.5% wall rock assimilation by a tholeiitic dyke 2.9 m wide with a flow rate of 25 m^2/s or 5.0% assimilation for a dyke 1.6 m wide with a flow rate of 10

m^2/s. Dolerite dykes in the central Lebombo generally exceed 2.9 m width and where smaller dykes are encountered they most typically utilize passages previously forced by larger dykes and are therefore effectively "insulated" from the crust. Thus, it is likely that conduit contamination is restricted to values less than 2.5% for the low-MgO Sabie River basalts.

The potential geochemical effect of conduit contamination is sketched in Fig. 7.2; AFC enhances enrichments in elements such as Rb, relative to closed-system fractional crystallization (CSF) predictions and the vectors illustrating conduit contamination superimposed on a CSF trend become shorter at lower MgO values, resulting in a "flattening" of correlations relative to CSF.

7.2.3 Selective Contamination

Selective contamination in the present context concerns the chemical interaction between molten basalt and granitic continental crust. It may be that the styles of contamination supposed above (AFC and "conduit contamination") are inadequate models for assessing the sensitivity of some elements (e.g. LILE relative to the HFSE) to crustal contamination processes. The experimental work of Watson (1982) and Watson and Jurewicz (1984) is considered in detail to determine which elements are affected, and to what degree, by selective contamination with felsic material.

Watson (1982) conducted a number of diffusion experiments placing felsic material in a basaltic melt and recorded the results under various experimental conditions (i.e. varying temperature and time). Synthetic granite and basalt and an oceanic tholeiite were used in these experiments to calculate the diffusivities of the various species involved (table 1, Watson, 1982) the values of which were specific to the rate of stirring used. Work by Watson and Jurewicz (1984) dealt with the alkalies (Na, K) only but supports the conclusions of Watson (1982) regarding basalt/granite interdiffusion. These are summarized below:

(1) When mantle-derived basaltic magmas induce local melting of crustal rocks the assimilation process becomes one of liquid-state interdiffusion.

(2) The varying diffusivities of ions and their differing preferences for silicic relative to basaltic melts can produce marked selective contamination

effects. The selective contamination of ascending basaltic magmas is particularly likely in the case of K_2O. The "selectivity" of such a process is illustrated by fig. 11 of Watson (1982), reproduced here as Fig. 7.3. For example, a basalt containing 10% molten felsic "xenoliths" of radius 50 cm for 1000 years will have the composition:

	basalt	xenolith	contaminated basalt
SiO_2	50%	70%	51% (2% increase)
K_2O	0.1%	2.5%	0.3% (200% increase)
La	3.3 ppm	33 ppm	5 ppm (50% increase)
Sr	200 ppm	200 ppm	200 ppm
$^{87}Sr/^{86}Sr$	0.703	0.712	0.7044 (0.2% increase)

The concentrations used for the basalt and xenolith end-members are those chosen by Watson (1982) to construct fig. 11 (Fig. 7.3 here). Diffusivities of $3x10^{-10}cm^2/s$ for SiO_2, $5x10^{-7}cm^2/s$ for K_2O, $1x10^{-8}cm^2/s$ for La and $5x10^{-8}cm^2/s$ for ^{87}Sr and ^{86}Sr were used by Watson (1982). No diffusion of Sr is anticipated as concentrations are equal in basalt and xenolith and Watson (1982) considers the transition equilibrium partition coefficient to be close to 1. The change in $^{87}Sr/^{86}Sr$ of the basalt is caused by a net flux of ^{87}Sr from xenoliths to basalt and vice-versa for ^{86}Sr (Watson, 1982).

Therefore, K_2O appears to be the most susceptible to granitic contamination and it is reasonable to expect Rb to behave in a similar manner. Watson (1982) maintains on the basis of experimental doping of granite with Sm that the diffusivity of this element is greater than SiO_2 and then extrapolates this conclusion to the high charge cations: REE, Zr and Nb. The diffusion of high charge cations into the basaltic melt from the felsic end-member will therefore occur more quickly than the diffusion of SiO_2, i.e. abundances of REE, Zr and Nb may be enhanced relative to SiO_2 in any basaltic melt subjected to selective contamination effects. However, Watson (1982) does not take into account that these high charge cations may be residing in highly refractory phases (i.e. zircon, apatite) - an extremely likely situation in granitic rocks, although earlier work (Watson, 1979) did show that partial melts of granites containing zircon will be buffered to low Zr values (see section 7.2.1.3). Furthermore, if Zr, REE and Nb are not enriched in crustal melts relative to their original unmelted parent composition ((9), Table 7.1), then the assumption by Watson (1982) that the

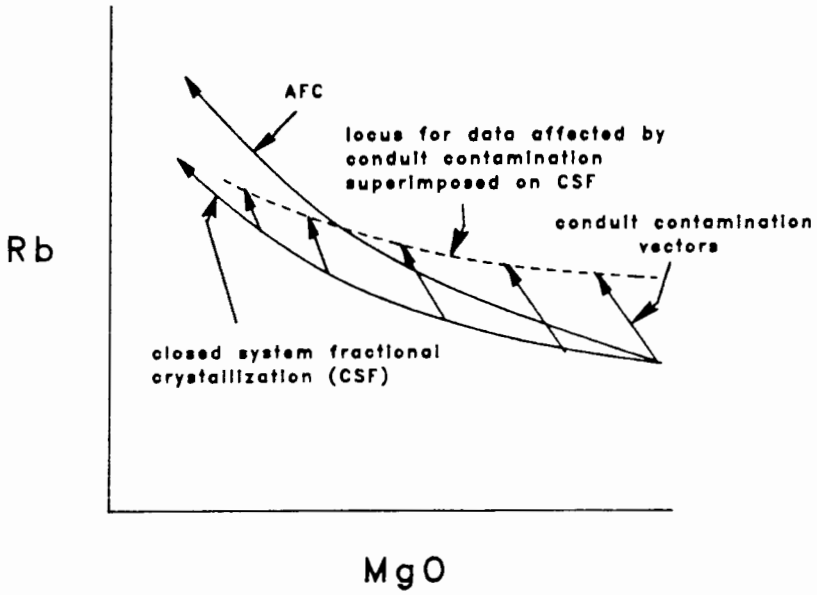

Figure 7.2. Sketch of the likely effect of CSF, AFC and conduit contamination on the distribution of Rb with MgO. Note that conduit contamination vectors when combined with CSF effects, result in a "flattening" of Rb trends with MgO.

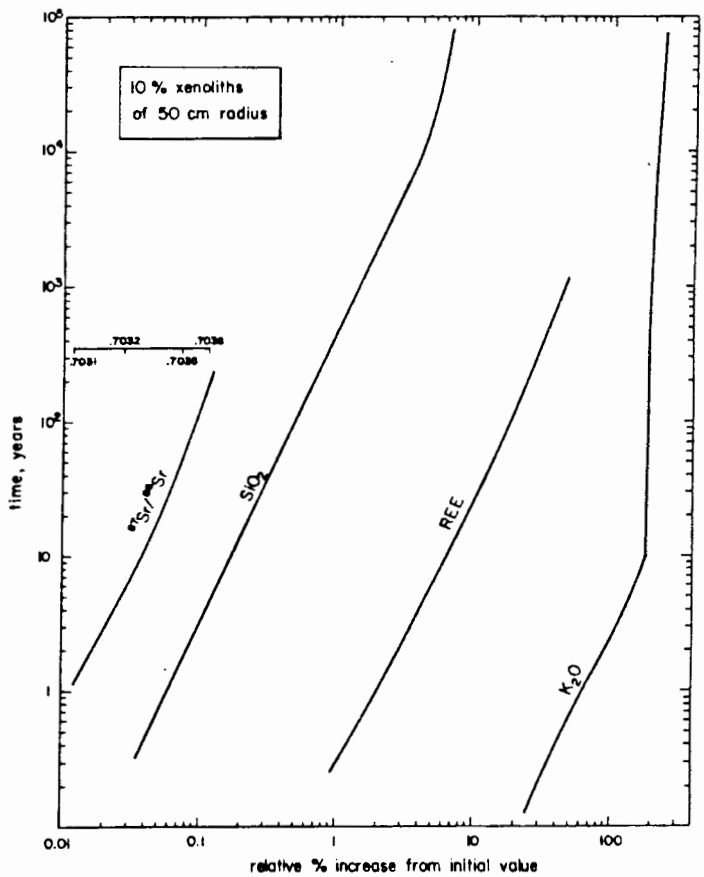

Figure 7.3. Comparison of selective contamination effects on SiO_2, K_2O, REE and $^{87}Sr/^{86}Sr$ for a case of 10% felsic molten xenoliths of 50 cm radius (from fig. 11 of Watson, 1982; see text for discussion).

a^{REE} in felsic melts > a^{REE} in basaltic melts may not hold true as activity (a) is a function of P, T and concentration. For example, the concentration of Zr, REE and Nb is greater in the LFE-group than typical granitic compositions (compare Tables 3.1 and 7.1).

(3) The absence of an activity gradient between basalt and granite for Na_2O buffers this element against re-distribution. K_2O is buffered against further increases once it reaches a certain concentration level in the basaltic melt (e.g. the near vertical trend in Fig. 7.3 once time >10 years). Any increase in K_2O beyond this "limiting value" must involve extensive bulk incorporation of xenolithic material which would presumably show up in SiO_2 content of any resulting magma. Watson (1982) suggests that this limiting value is *ca* 1/3 the K_2O content of the felsic melt.

Although subsequent experimental work (Watson and Jurewicz, 1984) showed that the diffusivity of K is lower than the value used above (new value of $3x10^{-8}cm^2/sec$), the new value is still high enough to qualitatively confirm the conclusions of Watson (1982) summarized above. Thus, K_2O (and by association Rb) is viewed as the element most sensitive to crustal contamination.

7.2.4 Approach

Each basaltic group is examined to see whether it is possible to resolve effects of the contamination mechanisms outlined above. The correlations observed between $^{87}Sr/^{86}Sr$ initial ratio and LILE and SiO_2 for the N group (Fig 3.9) make it the most likely candidate for granitic contamination, and discussions concentrate on this group.

7.3 THE N GROUP

7.3.1 Introduction

A number of the features of N-group geochemistry cannot be explained by closed-system fractionation models:

(1) correlation of $^{87}Sr/^{86}Sr$ initial ratio with LILE and SiO_2;

(2) spread in SiO_2, TiO_2 and FeOt contents with MgO;

(3) the enrichments observed and the general spread in HFSE and LILE contents with decreasing MgO; and
(4) the relatively random distribution of Sr with MgO.

One problem with resolving the effects of granitic contamination is alteration as the two processes may produce similar geochemical results (Chapter 3). However, it is stressed that the variations enumerated above persist even when just "fresh" samples are considered (Chapter 3). Granitic contamination is examined successively in terms of AFC, conduit and selective models.

7.3.2 Coupled Assimilation-Fractional Crystallization (AFC)

7.3.2.1 Parameter selection

The composition of a hypothetical melt produced at 20% melting (Table 7.4) is used as the assimilant. Mineral compositions most frequently used in the fractionating assemblages for closed-system models (Table 6.4c) are used here: ol4A-RSC22; cpx3-RSS35 and plag8-RSC22 (Table 6.1). This assemblage is consistent with the results of NIELSEN which predicts olivine, clinopyroxene and plagioclase typically in the proportions 10:35:55, for a range of r-values (.1 to .5) for the MgO interval 7-5%. This range of r-values (.1 to .5) is consistent with most likely values based on heat budget calculations of Taylor (1980) and De Paolo (1981) (see earlier). All N-group models are initiated from a primitive N-group composition (NPRIM, Table 6.3) and individual mineral/melt partition coefficients are given in Table 6.2a.

7.3.2.2 Models and geochemical variations.

The range in compositions generated is represented by the shaded area on Fig. 7.4. This area may be compared with two evolved (MgO *ca* 5%) N-group samples, RSS40 and RSS169. RSS40 (a basalt) is altered , however, and it is impossible to determine whether the increase of LILE (K, Rb and Ba) in RSS40 relative to RSS169 (a fresh dolerite) is a function of alteration (Chapter 3) or greater (i.e. r=.5) contamination. What is more difficult to accept is that the lower Ti, P, Zr and La concentrations (immobile elements) in RSS40 are a result of depletion by alteration, although Hellman *et al.* (1979) maintain that REE are mobilized during conditions of low grade burial metamorphism of basic volcanics. This, however, would still leave the

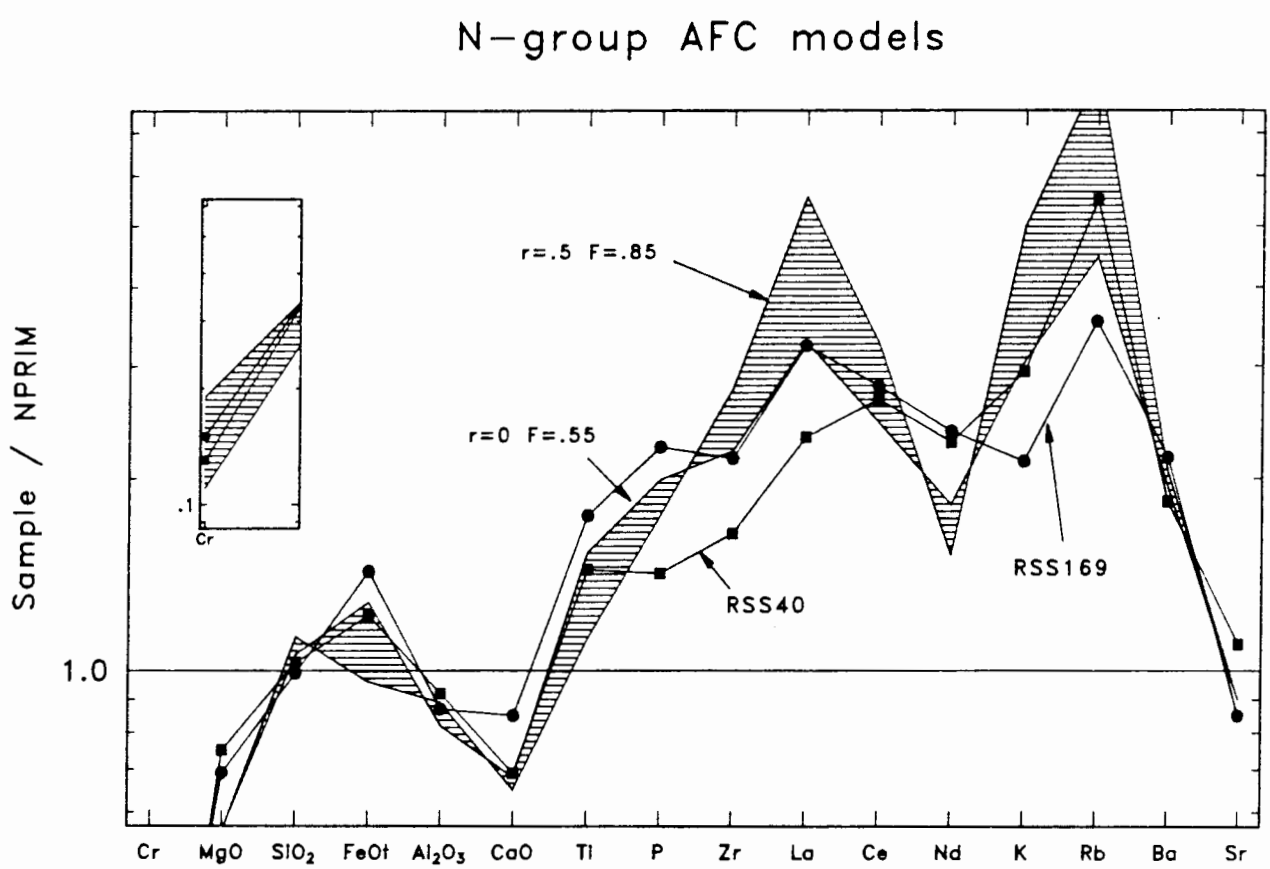

Figure 7.4. Spidergram for N-group AFC models, with calculated derivative liquids and N-group samples normalized to the model starting composition (NPRIM, Table 6.3). A measure of the effectiveness of the model is the closeness of fit between the shaded area (defined by derivative liquids containing *ca* 5% MgO, for the parameters r=0, F=.55 and r=.5 and F=.85) and the two samples (RSS40, RSS169), representing the range of compositions for evolved (*ca* 5% MgO) N-group samples.

similar Ce and Nd (both LREE) concentrations in RSS140 and RSS169 unexplained, and movement of the HFSE due to alteration is considered unlikely in this instance. However, in light of the ambiguity between alteration and contamination with respect to LILE (and Sr), "fresh" sample data (as used on Fig. 3.6) are plotted separate from the whole data set.

Selected variables unlikely to be significantly affected by alteration (except $\delta^{18}O$) are shown *vs* MgO on Fig. 7.5. Also shown with AFC models are closed-system fractional crystallization (CSF) predictions using the same fractionating assemblage. The assumption that the proportions of minerals in this fractionating assemblage is constant over the entire fractionation range is consistent with the CSF models presented for the N group in Chapter 6. The variation of SiO_2 with MgO seems consistent with variable degrees of contamination from r=0 (i.e. CSF) to r=.5 (Fig. 7.5). Furthermore, the range in observed SiO2 concentrations is almost completely accounted for if models are initiated from a more primitive (i.e. lower SiO_2 and higher MgO) composition. Similarly, the spread in both FeO and Ti (modelled as a trace element) contents are also consistent with such a variable contamination model (Fig. 7.5b, c).

A range of $\delta^{18}O$ values also result from variable contamination effects (Fig. 7.5.d). Unfortunately low-temperature alteration can affect $\delta^{18}O$ data to a significantly greater degree than the range generated by CSF or AFC (Chapter 6) and, coupled with the small number of determinations available, limits the usefulness of this data. One general conclusion, however, is that mixing either through isotopic exchange during alteration, contamination or source mixing, is required to change $\delta^{18}O$ values substantially.

The changes in the HFSE (Fig. 7.4 and Zr and La in Fig. 7.5e, f) predicted by this AFC model must be viewed with caution as the concentrations of these elements calculated for a granitic partial melt (e.g. Zr is 668 ppm Table 7.4) may be unrealistically high (discussed earlier). Thus, the spread of HFSE data predicted by models on Figs 7.4 and 7.5e and f, for variable degrees of granitic contamination, may not be real. For instance if Zr is buffered to values <100 ppm with zircon as a restite phase, as Watson (1979) supposes, then fractional crystallization and assimilation effects will act in an opposite sense and tend to reduce any spread with decreasing MgO in derivative melts.

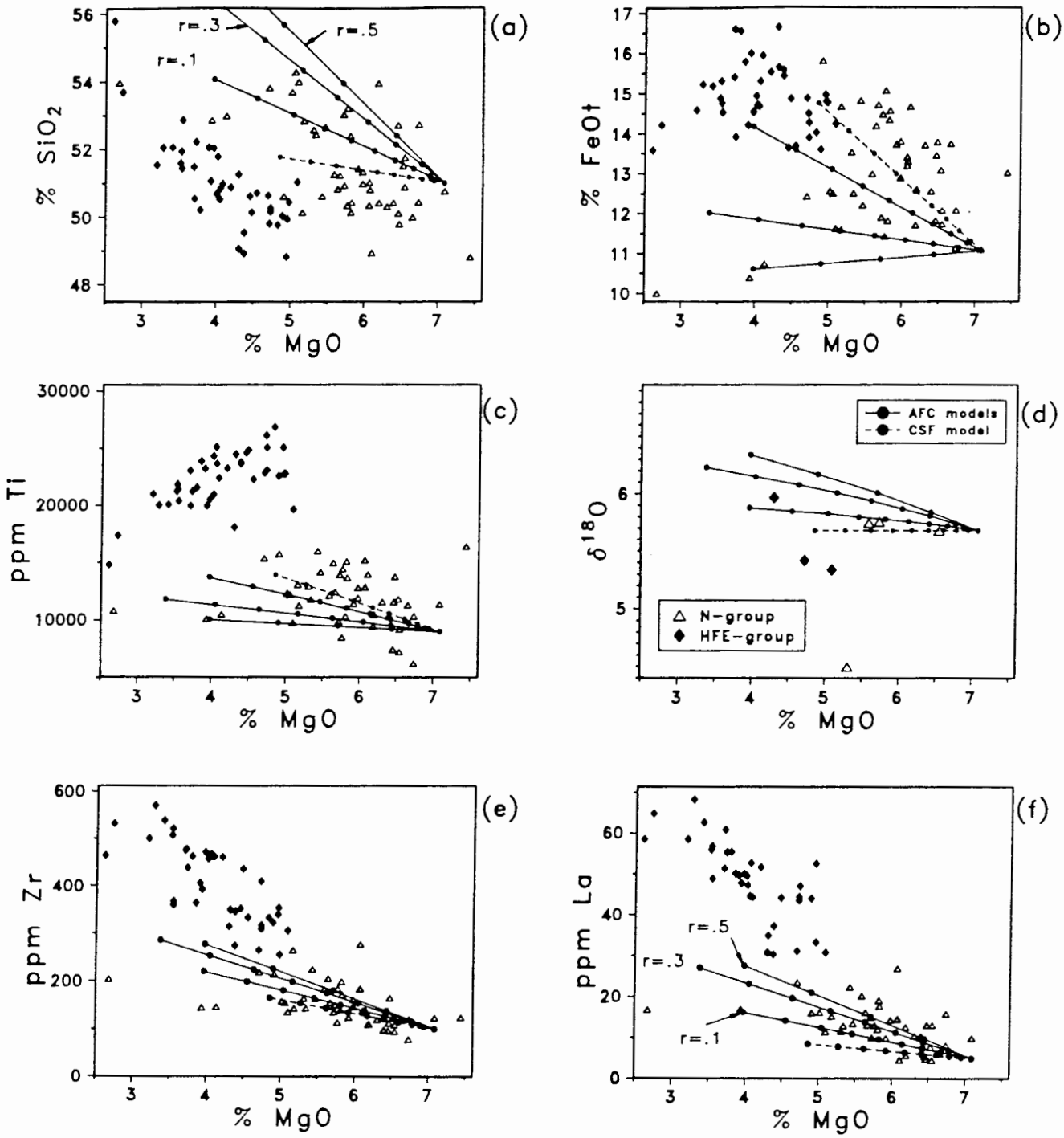

Figure 7.5. AFC (solid line) and CSF (dashed line) models for selected major element oxides, HFSE and $\delta^{18}O$ *vs* MgO. Each dot on the model curves represents a 5% crystallization increment for the assemblage olivine + clinopyroxene + plagioclase in the respective proportions 10:35:55. All data is normalized volatile-free and Fe reported as FeO.

In the case of variables which may be affected by alteration the "fresh" sample subset used in Fig. 3.6 is plotted against MgO along with the whole data set for the N- and HFE-groups in Fig. 7.6. The discussion concentrates on variations observed in the "fresh" subset in an effort to exclude confusion between alteration and granitic contamination effects. The variation of K (modelled as a trace element), Rb, Rb/Sr ratio and initial $^{87}Sr/^{86}Sr$ ratio with decreasing MgO for the "fresh" subset, are consistent with models varying the degree of granitic contamination from r=0 (CSF) to r=.5 (Fig. 7.6). Initiating models from a more primitive N-group composition (e.g. higher MgO and lower K and Rb contents may account for some samples which have concentrations of K and Rb (and lower Rb/Sr ratios) outside the range bounded by CSF and AFC (r=.5) trends.

Of particular note in Fig. 7.6 is the fact that Ba and Sr concentrations in derivative melts are not significantly changed from CSF trends (only AFC for r=.5 shown in Fig. 7.6c, d) by variable degrees (e.g. r=.1 to .5) of granitic contamination. This is the result of the buffering of both these elements to values similar to NPRIM (initial model composition) abundances, by feldspar in the granitic melt used as a contaminant (Table 7.4). Thus the Ba (100-300 ppm) and Sr (100-400 ppm) abundances observed in fresh samples from the N group cannot be explained by AFC models using the most likely set of parameters.

It was suggested earlier that the correlation in the N group of $^{87}Sr/^{86}Sr$ initial ratio with elements relatively more concentrated in a granitic crust or the melt of such a crust, is strong evidence for contamination (Fig. 7.7). Fortunately the relatively fresh nature of many N-group samples results in only a few data being excluded on the "fresh" diagrams. The point made earlier with respect to the initiation of models from a more primitive N-type (i.e. higher MgO) composition is especially valid in this case. Models would then have lower SiO_2, K, Rb, Ba and Rb/Sr initial values which would enable the array of model curves in Fig. 7.6a, b, c and f to encompass most of the data and certainly explain the general positive correlations of these elements with $^{87}Sr/^{86}Sr$ initial ratio.

As pointed out in Fig. 7.6, the change in Sr and Ba contents with varying degree of contamination is not significantly different from CSF trends (Fig. 7.6d and e). To produce the range of Ba concentrations in the "fresh" N-group samples (10-300 ppm) by AFC, the granitic parent would have

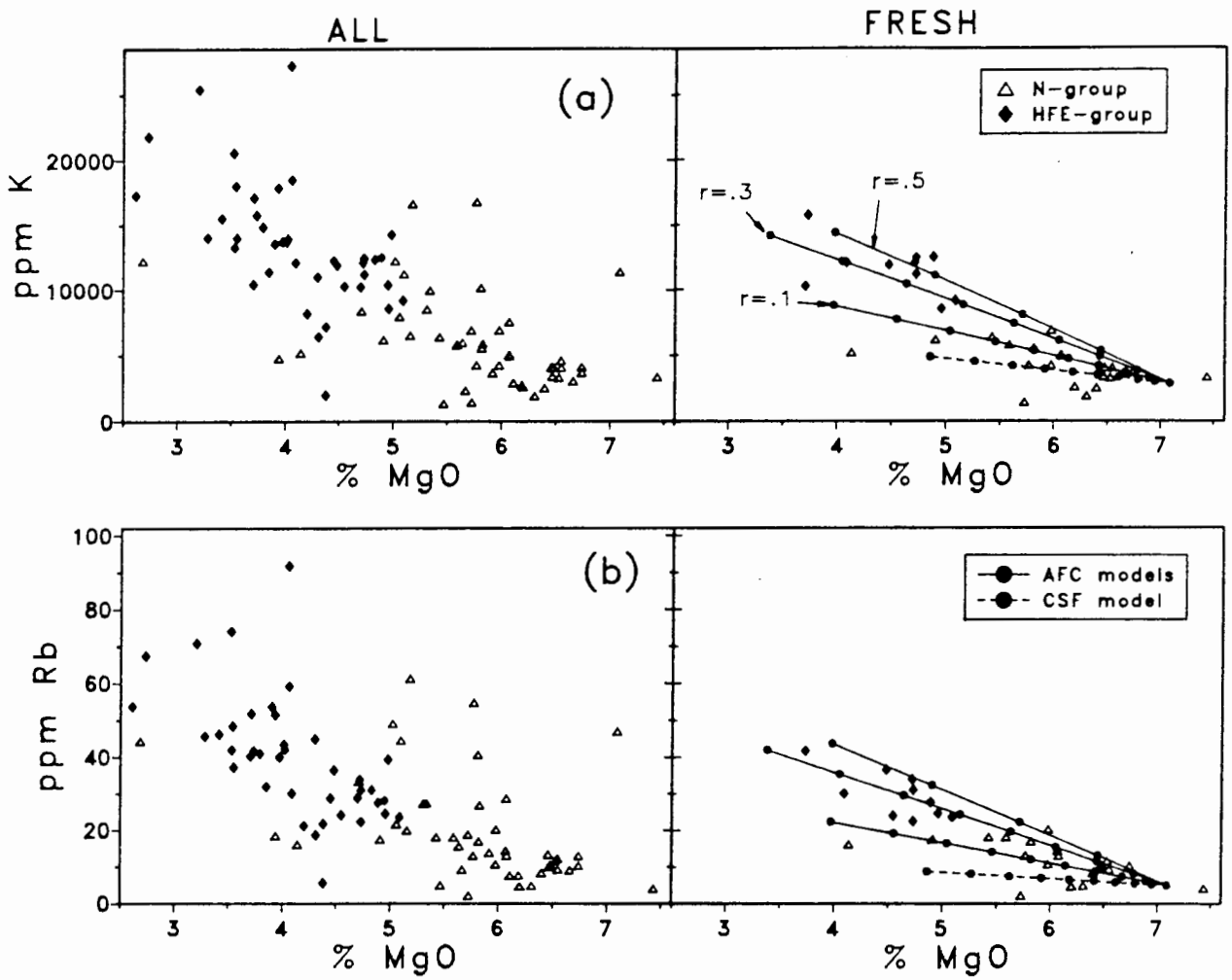

Figure 7.6. All and "fresh" (normalized volatile free, Fe as total FeO) N- and HFE-group data for LILE, Sr and $^{87}Sr/^{86}Sr$ initial ratio *vs* MgO. Each dot on the model trends (CSF-dashed; AFC-solid) represents a 5% crystallization increment for the assemblage given in Fig. 7.5. Note, however, in the case of Ba and Sr, only the AFC model curve for r=.5 is shown as all other model curves are coincident along this trend.

/Figure 7.6

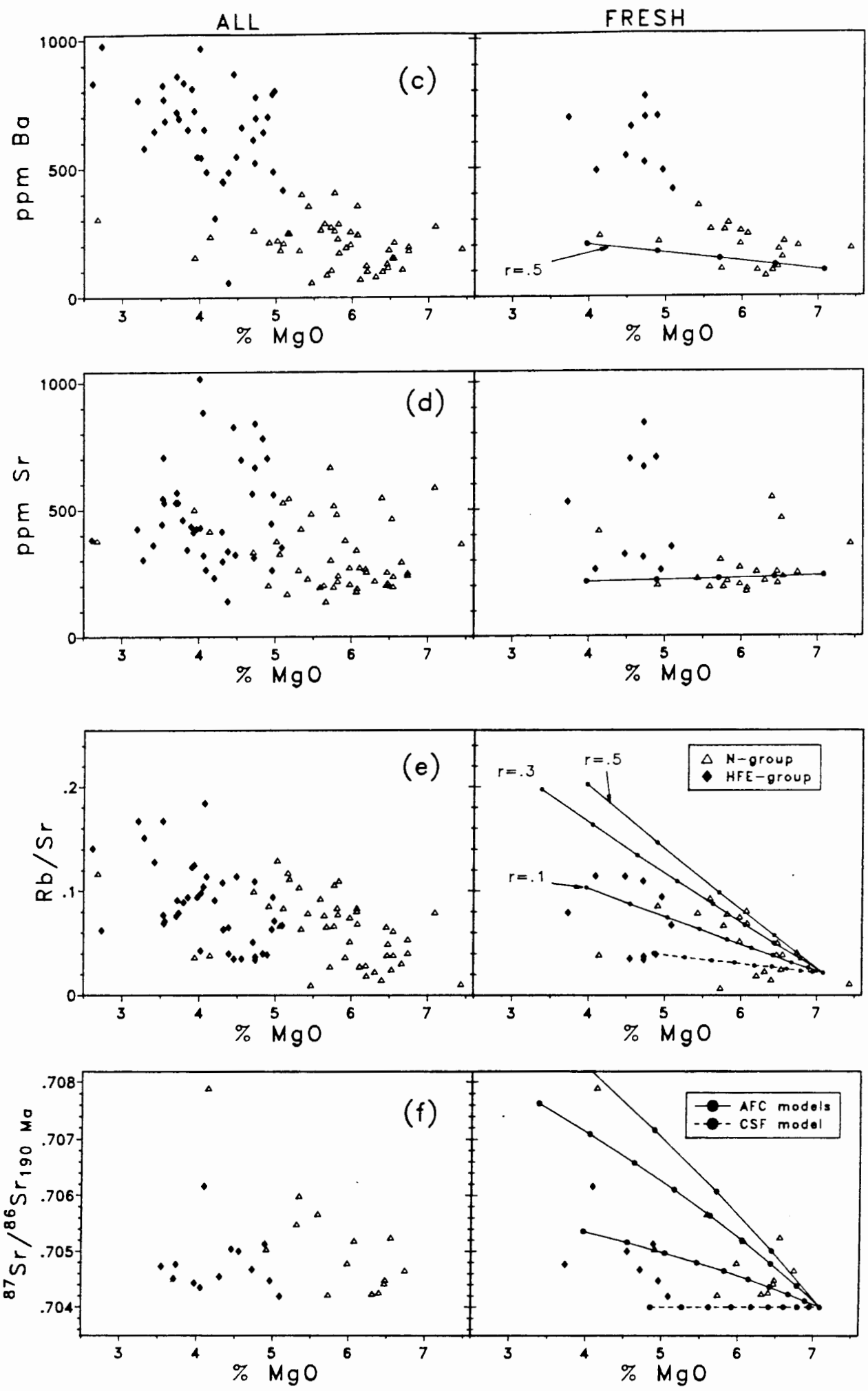
ALL
FRESH
(c)
ppm Ba
1000
500
0
r=.5
% MgO
(d)
ppm Sr
(e)
Rb/Sr
.2
.1
r=.3
r=.5
r=.1
N-group
HFE-group
(f)
$^{87}Sr/^{86}Sr_{190\ Ma}$
.708
.707
.706
.705
.704
AFC models
CSF model
3
4
5
6
7

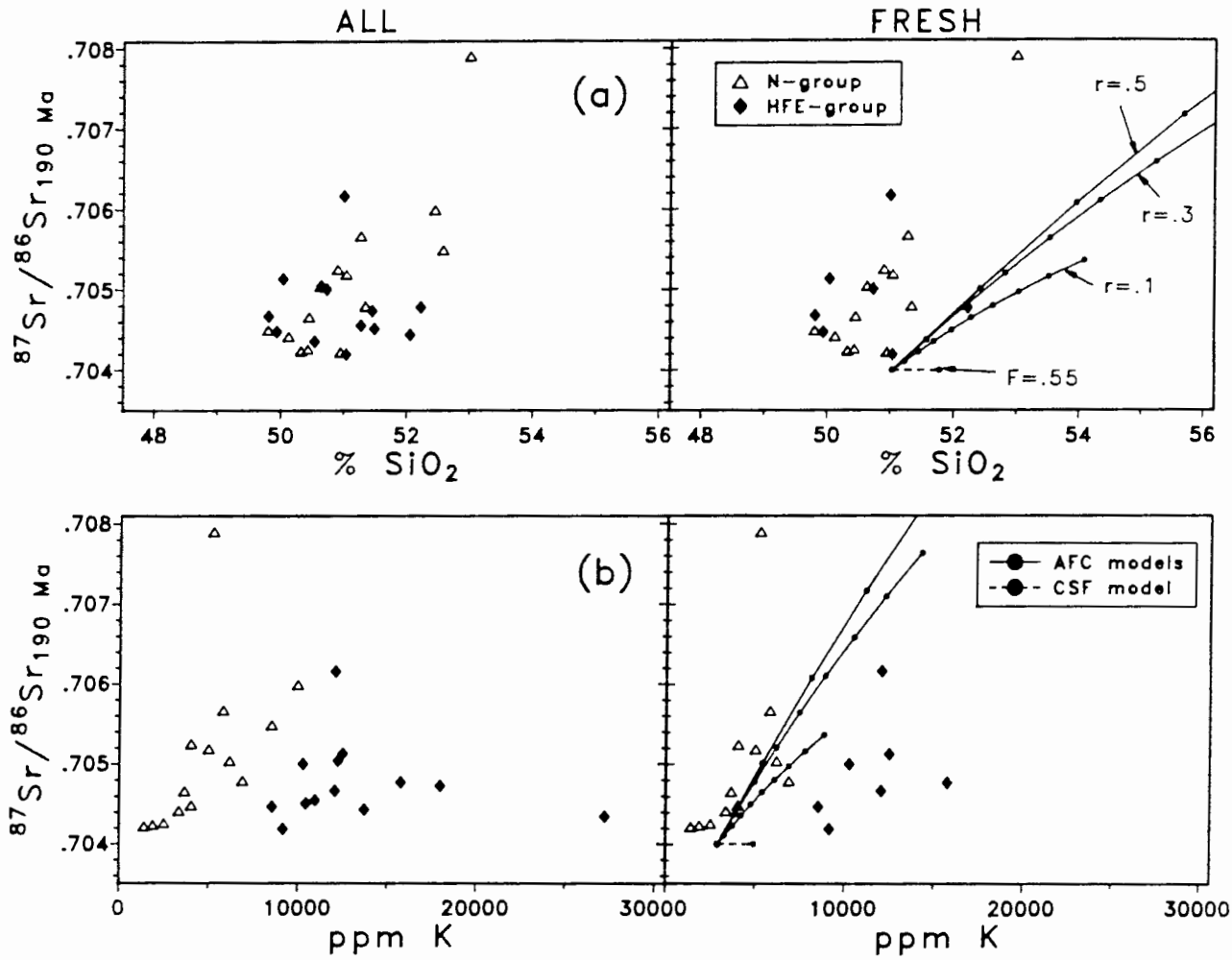

Figure 7.7. All and "fresh" (normalized volatile free, Fe as total FeO) N- and HFE-group data for $^{87}Sr/^{86}Sr$ initial ratio *vs* selected elements. Each dot on the model trends (CSF-dashed; AFC-solid) represents a 5% crystallization increme nt for the assemblage given in Fig. 7.5. Note, in the case of Sr, only the AFC model curve for r=.5 is shown as all other model model curves are coincident along this trend.

/Figure 7.7

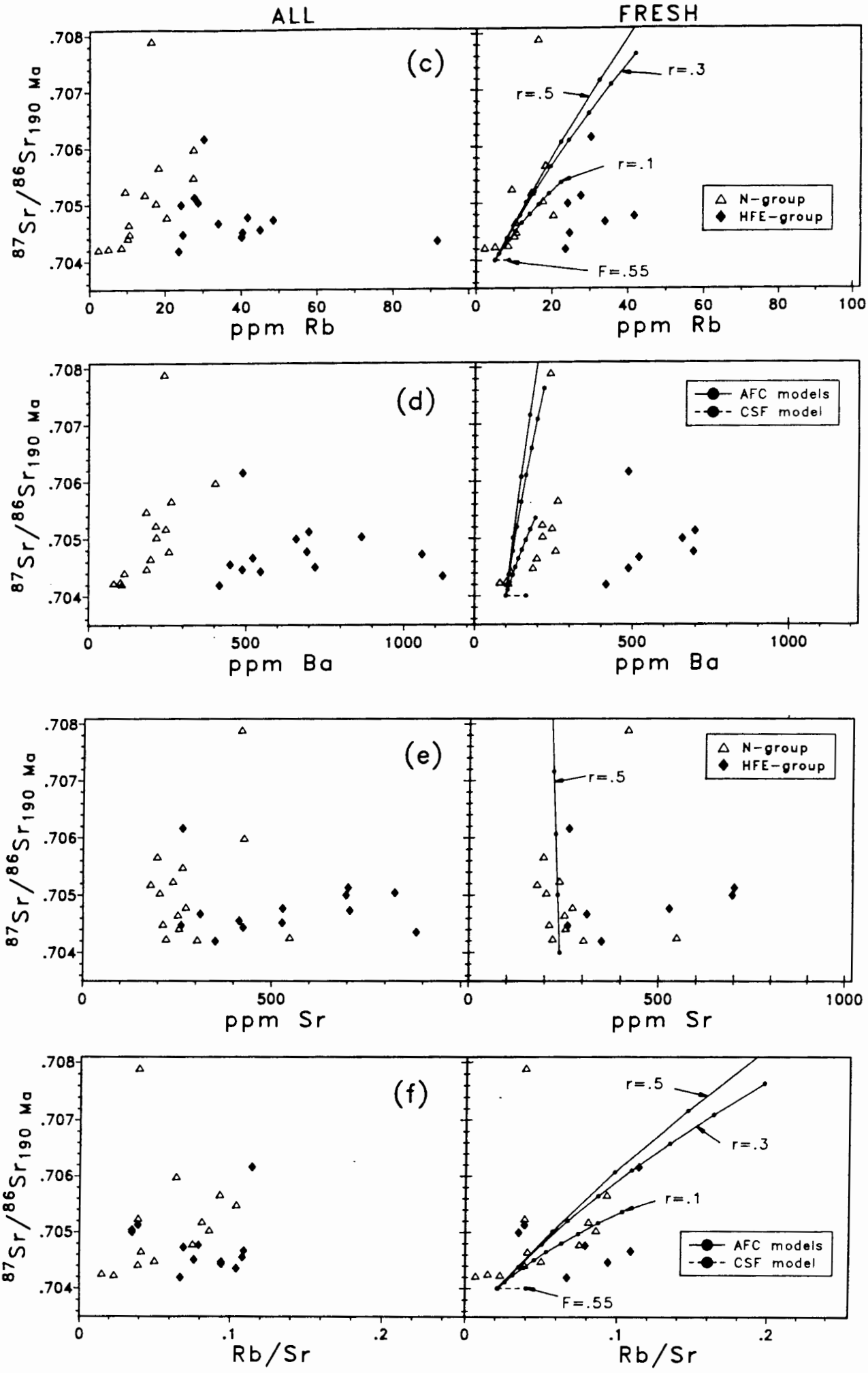
ALL
FRESH
(c)
(d)
(e)
(f)
$^{87}Sr/^{86}Sr_{190\ Ma}$
ppm Rb
ppm Ba
ppm Sr
Rb/Sr
r=.5
r=.3
r=.1
F=.55
N-group
HFE-group
AFC models
CSF model

to contain in excess of 1000 ppm Ba to produce a melt (assimilated) sufficiently enriched in Ba. The concentration of Ba in the granitic rocks underlying the central Lebombo is clearly not sufficient to satisfy this condition (Table 7.1). This is also the case for Sr which is even more effectively buffered to low values (by both K-feldspar and plagioclase) than Ba in any granitic melting regime. Thus the ranges in Ba and Sr in the N group remain unexplained.

The range of possibilities with respect to Sr- and Nd-isotopes is given by the shaded area in Fig. 7.8. Thus Sr- and Nd-isotope data in the N-group, with the exception of CL372 (a very plagioclase-phyric basalt sample in the Komati River Section; $^{87}Sr/^{86}Sr_{190\ Ma}$ = .70790), may be explained by assuming end-members illustrated in Fig. 7.8. However, it is more likely that these basalts will be affected by granitic crust with $^{87}Sr/^{86}Sr$ (190 Ma) >.720 and that Nd contents (along with Zr and other LREE) will be buffered to low values by refractory minerals such as zircon and apatite in any melting of such a crust. Thus, the more likely model would probably approximate the high $^{87}Sr/^{86}Sr$ (190 Ma) and low Nd (20 ppm) end-member in Fig. 7.8. This, coupled with the fact that some southern Lebombo samples do not fall close to the "permissible" field in Fig. 7.8, suggests that the N-group has been influenced by a component containing low $^{143}Nd/^{144}Nd$ and high $^{87}Sr/^{86}Sr$ initial ratios. As no such crust of such a composition is known in this region this is assumed to represent variations in the mantle source area of the N-group.

The Pb-isotope ratios determined for all three groups together define a single array, implying that the process responsible for the array is common to all three groups. Thus it is more appropriate to discuss Pb-isotopes once each group has been examined in terms of granitic contamination.

7.3.3 Conduit Contamination

The discussion above indicated that AFC is a significant process in the N-group. It is difficult to examine conduit contamination in such a quantitative fashion except to note the conclusion in section 7.2.2. that it is probably restricted to values less than 2.5% for the low-MgO Sabie river basalts. This conclusion is directly applicable to N-group samples as the tholeiite composition used by Huppert and Sparks (1985) is not too different

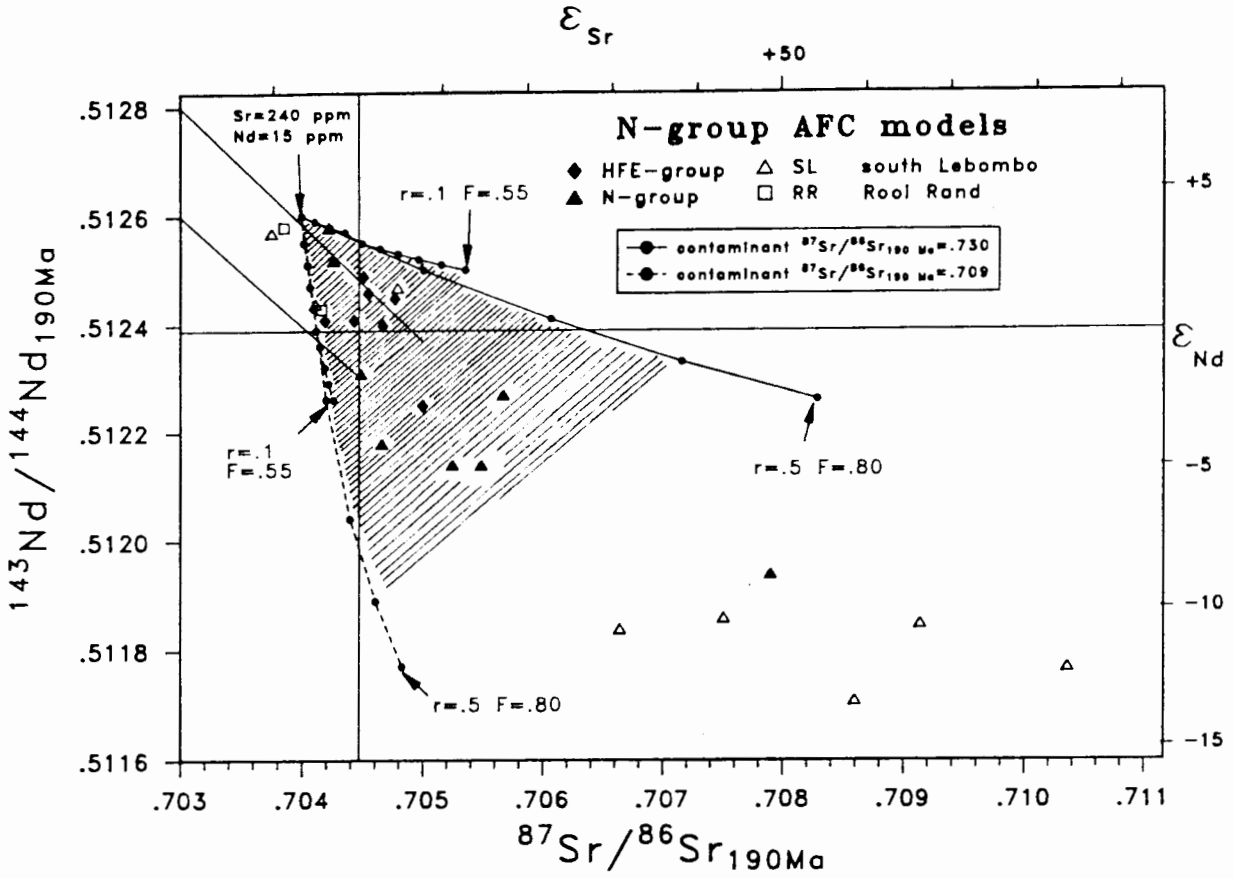

Figure 7.8. The potential influence of AFC models on Sr- and Nd-isotope variations in the central Lebombo (solid symbols) and southern Lebombo (open symbols) N-type compositions. Two contaminants are considered to represent the range observed (Table 7.1; Carlson *et al.*, 1983; Harris *et al.*, 1987) for any melts derived from granitic crust:
(1) where $^{87}Sr/^{86}Sr$ (calculated at 190 Ma) = .730 and Nd = 20 ppm; and
(2) where $^{87}Sr/^{86}Sr$ (calculated at 190 Ma) = .709 and Nd = 79 ppm (from Tables 7.1 and 7.4).
Nd-isotope data on the basement rocks in south-east Africa are limited to determinations by Carlson *et al.* (1983) on the Bimodal Suite of the Ancient Gneiss Complex of Swaziland (Fig. 7.1; .51029-.51110) and the Bulai and Sand River Gneisses of the Limpopo Mobile Belt (Harris *et al.*, 1987; .51013-.51122) much further to the north. A value of .5110 is used in both the end-member models as representative of the $^{143}Nd/^{144}Nd$ ratio in the assimilant 190 Ma ago. It is assumed that the Sr will be buffered to consistently low values in any granitic melt (184 ppm used, Table 7.4). The shaded area represents the region in which N-group compositions may be explained by the AFC models presented in Figs 7.5 to 7.7.

from the primitive N-group composition (NPRIM) from which models are initiated:

	H + S tholeiite	NPRIM
%		
SiO_2	50.3	51.03
TiO_2	1.8	1.50
Al_2O_3	16.1	14.70
FeO	11.1	11.08
MgO	6.9	7.09
CaO	9.7	11.0
Na_2O	3.0	2.90
K_2O	1.1	.30
P_2O_5	-	.22

Furthermore, contamination in conduits with granitic crust results in the "flattening" of some incompatible element trends (e.g. Rb, K) MgO (Fig. 7.2) when it is desirable to explain the enrichments of these elements in some samples (see AFC models in the previous section). If granitic contamination produced the negative correlations between $^{87}Sr/^{86}Sr$, LILE and SiO_2 with MgO in most N-group samples then the dominant process must be AFC. Conduit contamination of the style suggested by Huppert and Sparks (1985), therefore, is not significant in the N-group of the central Lebombo although such a process may have induced some of the spread in the data.

7.3.4 Selective Contamination

AFC models explain the geochemical variation of variables likely to be most affected by granitic contamination (e.g. $^{87}Sr/^{86}Sr$ initial ratio, SiO_2, K and Rb) although Ba and Sr data remain unaccounted for. Watson (1982) concluded that K was most sensitive to selective contamination effects and thus, if a bulk assimilation model such as AFC can explain the variation in K, there is no justification for invoking selective contamination to explain Ba and Sr data.

It is important to stress that bulk assimilation (e.g. AFC) and selective contamination models are not mutually exclusive but rather the former is a progression of the latter. Watson (1982) stated: "Previous discussions of magma contamination by crustal materials (most recently, that

of De Paolo 1981) implicitly regard the process as one of "congruent" solution - that is the dissolving component is considered to be a mineral or combination of minerals. It is clear from the experiments on feldspar/basalt and "granite"/basalt interdiffusion, however, that if **melting** of country rock or xenoliths occurs prior to or at the beginning of interaction with the magma, and if the assimilation process does not go to completion the resulting contamination may be more complicated". Thus in the case of the N-group, the applicability of the AFC-models suggest that the assimilation process has gone to completion.

7.3.5 Conclusions

Many of the geochemical variations in the N-group unexplained by closed-system fractional crystallization are explained by AFC models with varying degrees of contamination, i.e. r=0 (or CSF) for 45% crystallization to r=.5 for 15% crystallization. Amongst the variations explained are observed correlations of $^{87}Sr/^{86}Sr$ initial ratios with Rb, K, Rb/Sr and SiO_2; and the spread in these variables and TiO_2 and FeOt with decreasing MgO. Still unexplained are the spread and enrichments in Ba and Sr and, potentially, in the HFSE (Zr, La, Ce, Nd and P).

Conduit contamination is not significant relative to the postulated AFC processes and the absence of selective contamination effects implies that the assimilation process has gone to completion.

7.4 THE HFE GROUP

The uniformity of Sr-, Nd- and, to a lesser extent, Pb-isotopes (Figs 3.11, 7.8), and the absence of well-developed positive correlations of the LILE with $^{87}Sr/^{86}Sr$ initial ratios (Fig. 7.7), strongly suggest that the HFE-group has not interacted significantly with granitic continental crust by an AFC process.

It may be argued that a combination of AFC and conduit contamination have obliterated any correlations. However, the conclusions reached for the N group in the previous section may be extrapolated to the HFE group. If

conduit contamination is not significant in the N group, it is likely to be even less significant in the more evolved (cooler) HFE group. Furthermore, of all three groups, the HFE group approximates most closely to 190 Ma reference isochrons for Sr, Nd and Pb isotopic systems (Figs 3.7, 3.9, 3.11 and 3.12).

Selective contamination may be responsible for some variation in the HFE-group, particularly with respect to K (and Rb) as the element most sensitive to such effects. Watson (1982) maintains that K_2O contamination is limited to *ca* 1/3 of the contaminant. Thus for a granitic contaminant containing 3.5% K_2O (29055 ppm, composition 9 in Table 7.1) selective contamination could account for 1.16% (9700 ppm) K_2O in the basaltic magma. However, such effects would still be accompanied by some increase in $^{87}Sr/^{86}Sr$ initial ratio which is not observed, while CSF models explain the increase of SiO_2 with decreasing MgO in this group (Chapter 6).

The Nd- and Sr- isotope composition of most HFE-group samples approximate N-group compositions unaffected by granitic contamination (Fig. 7.8). This is also the case for other geochemical data. For example, if N-group models were initiated from more primitive (e.g. higher MgO and lower SiO_2) compositions the closed-system fractional crystallization model illustrated on Fig. 7.5 would be able to generate SiO_2 and FeO contents similar to primitive members of the HFE-group. However, the levels of enrichment in HFSE, LILE and Ba necessary to derive the HFE-group from the N-group, are still not attained.

7.5 THE LFE GROUP

In the LFE group, like the HFE group, there are no positive correlations between $^{87}Sr/^{86}Sr$ initial ratios and the LILE. However, the spread in Sr- and Nd-isotope ratios are greater (Fig. 3.10) and models are considered to examine how much of this variation may be due to granitic contamination.

7.5.1 Coupled Assimilation - Fractional Crystallization (AFC).

A number of simplifying assumptions are made. The assimilant composition at 20% partial melting of "typical" granitic crust used for modeling contamination in the N group is also used here (Table 7.4). Mineral compositions most commonly used in the closed-system fractional crystallization (CSF) models (Table 6.4) are used throughout (ol-KS3 and cpx4-RSV31, Table 6.1). Constant mineral proportions represent the aggregate fractionation assemblage over the range 9-5% MgO estimated for CSF are used, i.e. the olivine:clinopyroxene ratio is 30:70. Models are initiated from a primitive LFE-group composition (LEPRIM, Table 6.3) for varying degrees of granitic contamination (r=0 to .5) in the MgO range 9-5%. Mineral/melt partition coefficients used are given in Table 6.2a.

The range in compositions generated in derivative melts of *ca* 5% MgO by varying degrees of contamination (r=0, F=.8 to r=.5, F=.92) is illustrated in Fig. 7.9. This area may be compared with an evolved relatively "fresh" LFE-group composition (RSS2). In light of the general spread in many element abundances in this group, however, it is more realistic to consider the models on variation diagrams (selected elements plotted *vs* MgO on Fig. 7.10). Part of the spread in SiO_2, FeOt and Ti may be accounted for by AFC models, while the considerable spread in Rb and Sr (still indicated if only "fresh" samples are plotted, Fig. 3.6), does not conform to model predictions (Fig. 7.10e, f). The small Zr range predicted by such varying degrees of granitic contamination is a function of the Zr content supposed in the melt (Table 7.4) and subject to ambiguity (see earlier discussion). Indeed if the Zr content in the assimilant were lower (e.g. *ca* 100 ppm) progressive contamination models (e.g. r=.5) would record a decrease in the Zr concentration of derivative melts, and this may then explain some of the spread with decreasing MgO to lower values in some LFE-group samples (Fig. 7.10d).

On the basis of combined Sr- and Nd-isotope systematics, the shaded area of Fig. 7.11 represents the range of possibilities for the two end-member situations described for Fig. 7.8. This diagram shows convincingly the insensitive nature of the LFE-group Sr- and Nd-isotopic compositions to granitic contamination. This insensitivity is a direct result of the greater Sr and Nd contents (ppm) of this group and it is likely that the range of isotopic ratios observed is a direct consequence of mantle source heterogeneity.

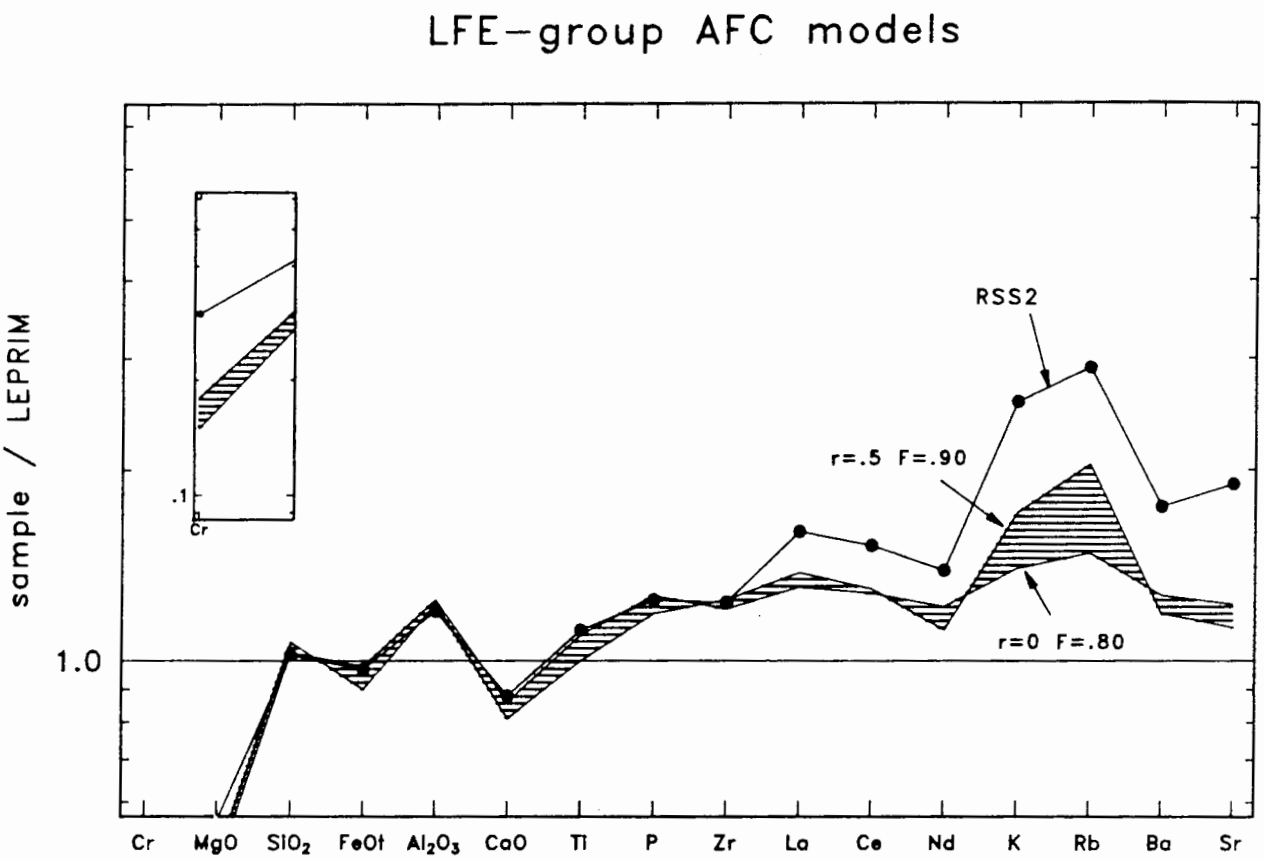

Figure 7.9. Spidergram for LFE-group AFC models, with calculated derivative liquids normalized to the model starting composition (LEPRIM, Table 6.3). A measure of the effectiveness of the model is the closeness of fit between the shaded area (defined by derivative liquids containing *ca* 5% MgO, for the parameters r=0, F=.80 and r=.5 and F=.90) and the evolved LFE-group sample (RSS2). The fractionating assemblage used was ol-KS3 30% and cpx4-RSV31 70% (Table 6.1).

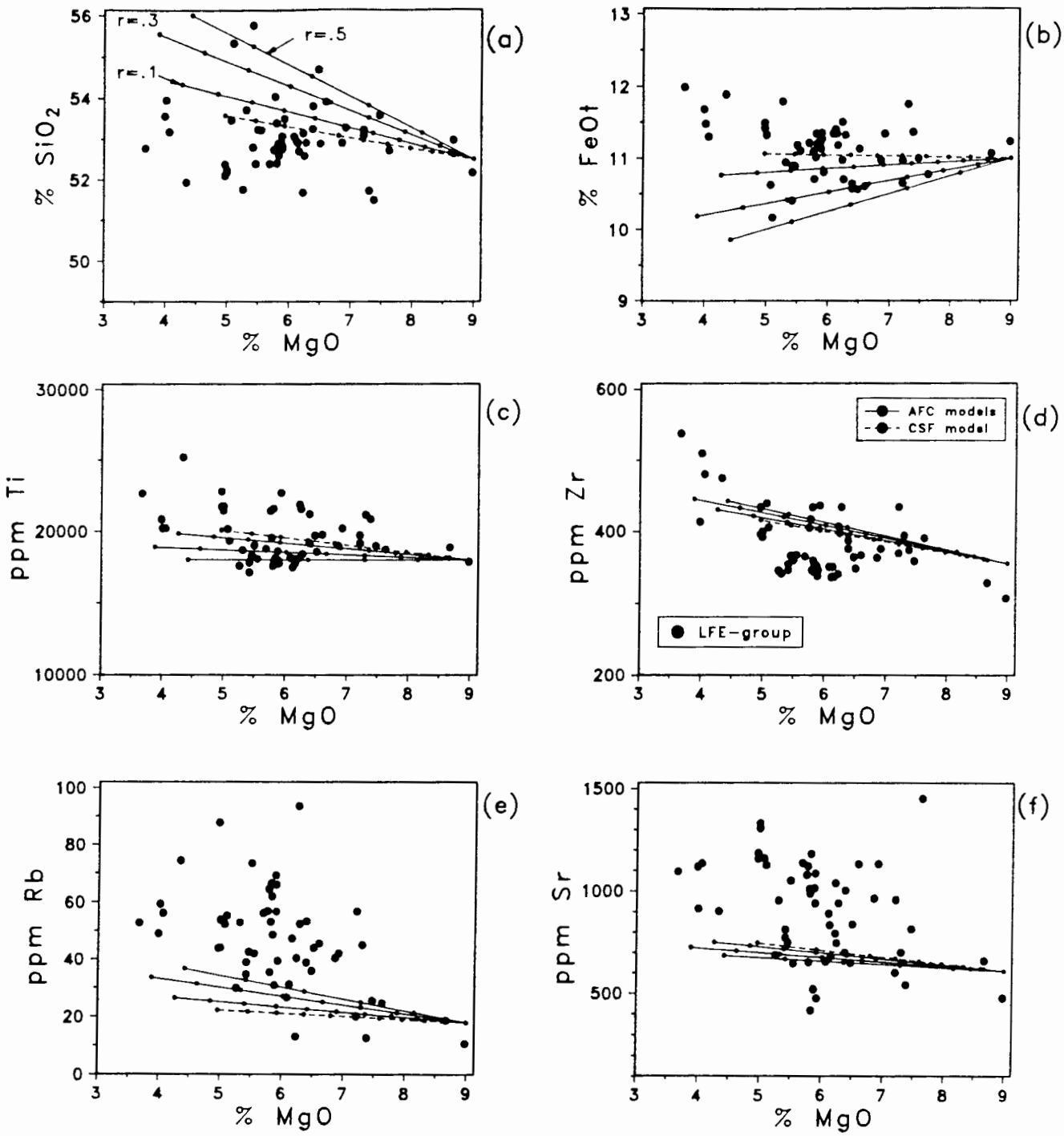

Figure 7.10. AFC (solid line) and CSF (dashed line) models for selected elements initiated from a LFE-group primitive (LEPRIM, Table 6.3) composition. Each dot on the model trends represents 2% crystallization increments for the assemblage given in Fig. 7.9. All data is normalized volatile free with Fe as total FeO.

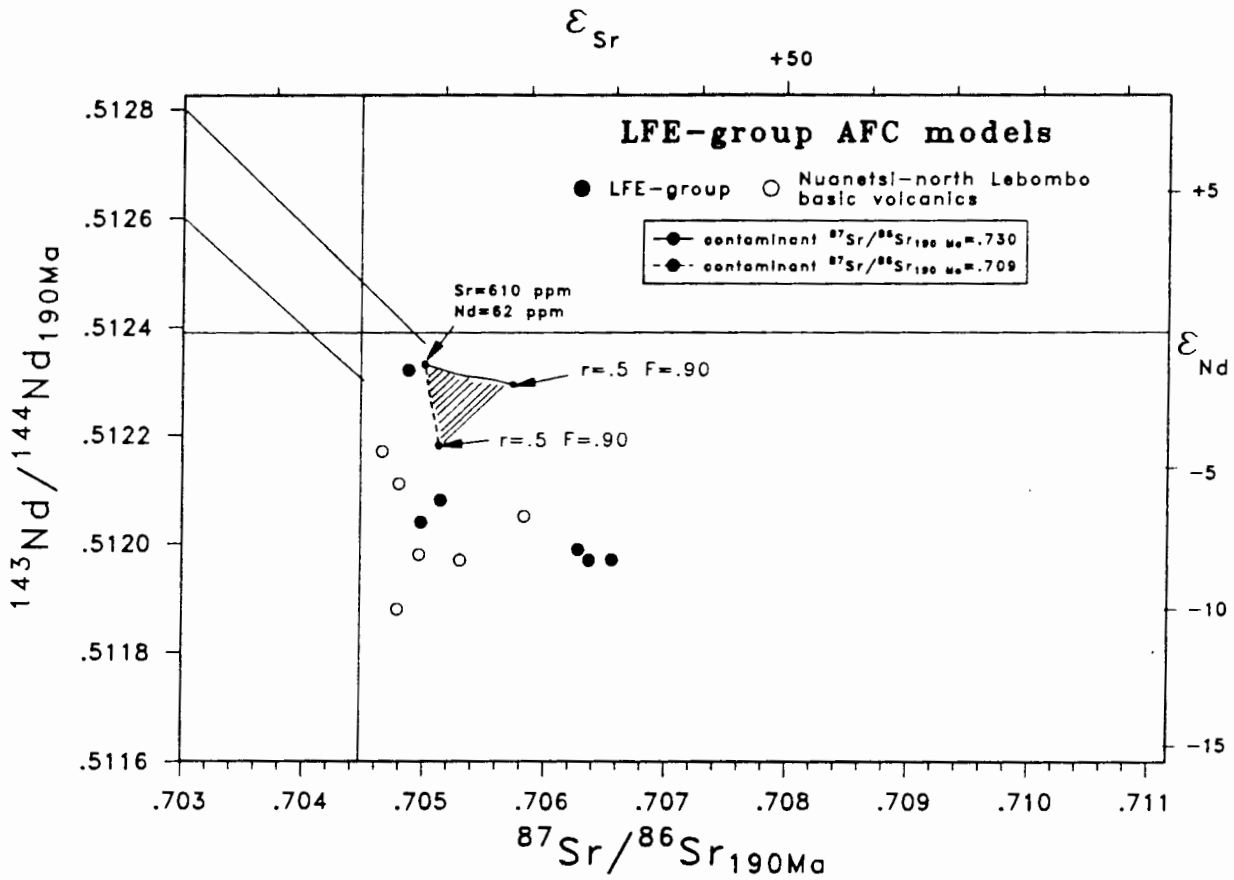

Figure 7.11. The influence of AFC models on Sr- and Nd-isotope variations in central Lebombo (filled) LFE-group samples and samples correlated with this group to the north (N. Lebombo and Nuanetsi basic volcanics, data from this study and Hawkesworth *et al.*, 1984). The two end-member models described in Fig. 7.8 are illustrated here with the shaded area representing the range of possibilities.

7.5.2 Conduit Contamination

A characteristic of the LFE-group mentioned above is the absence of any well developed correlation between $^{87}Sr/^{86}Sr$ initial ratio and LILE, SiO_2 (Fig 3.8) or any other element. It may be that a combination of AFC and conduit contamination is producing the apparently random variation of $^{87}Sr/^{86}Sr$ initial ratio and LILE with MgO in this group. The fact that picritic magmas generally may be affected to a greater degree by conduit contamination (see above) and the random LILE variations in both the LFE-group and the N. Lebombo picrites (Fig. 6.9) to which they are allegedly related (Chapter 6 and Cox and Bristow, 1984), may not be entirely fortuitous. Obviously, such contamination would then have to affect the LILE preferentially relative to major elements and HFSE. The likelihood of such a selective process is examined below.

7.5.3 Selective Contamination

If selective contamination, either in conduits or a magma chamber, is invoked to explain the random $^{87}Sr/^{86}Sr$ initial ratios, LILE and Sr variations with MgO in the LFE-group, the question as to why only one magma-type should be affected arises. Perhaps a partial explanation is the relationship of the LFE-group to parental picrites (mentioned above) and the greater ability of these "hot" picritic magmas to interact with crust relative to lower MgO magmas, that may have enhanced the selective contamination effects. By implication, possible picritic parents to the N group did not traverse continental crust, a supposition bourne out by the absence of such erupted magmas in the southern Lebombo. Extrapolating the results of Watson (1982; section 7.2.3 above) to a basaltic composition containing a greater initial K_2O abundance (e.g. 1%), suggests an increase to a maximum of 3%. However, Watson (1982) also states that K_2O is likely to be buffered to values <1/3 the composition of the contaminant, i.e. 1.2% in the case of composition 9 (Table 7.4).

7.5.4 Conclusions

Granitic contamination in the LFE-group may only be significant if selective, which, unfortunately can only be tested in a qualitative manner.

However, it is unlikely that even selective contamination was responsible for a major part of the spread in K (and Rb) data, and cannot be responsible for Sr and Ba variations.

7.6 PB-ISOTOPES

Pb-isotopes are considered separately as they define a broad array in $^{207}Pb/^{204}Pb$ and $^{206}Pb/^{204}Pb$ (and $^{208}Pb/^{204}Pb$, not shown) for all groups together, without the restriction of any one group to a particular part of the array (Fig. 7.12). Thus any process explaining this variation affects all groups without bias. Explanations of such any array may be divided into mixing (crust-mantle mixing considered here) and mantle source heterogeneities (essentially mantle-mantle mixing).

I. Crust-Mantle Mixing

Central Lebombo $^{207}Pb/^{204}Pb$ and $^{206}Pb/^{204}Pb$ data appears to straddle fields occupied by typical crust (from the Barberton area, Fig. 7.1) and mantle data (sub-oceanic and Parana data) plotted on Figs 7.12 and 7.13. Furthermore, the preservation of an array in the basalts is suggested to be a function of similarly orientated arrays in possible crust and mantle end-members. This broad classification into crust and mantle signatures also corresponds to Newsom *et al.*'s (1986) estimates for lower crust and upper mantle respectively (Table 7.5, Figs 7.12 and 7.13), although it is not certain whether granitic rocks of the Barberton area are representative of lower or upper crustal values.

Table 7.5. Pb-isotopic mass-balance for the Earth (from Newsom *et al.*, 1986).

	Mass (10^{24}kg)	Pb ppm	$^{206}Pb/^{204}Pb$	$^{207}Pb/^{204}Pb$
Upper mantle	2000	.04	18.40	15.49
Upper crust	8	15	18.76	15.66
Lower crust	18	7.5	15.96	15.03
Whole crust	26	10	17.23	15.32
System (bulk-earth)	2026	.163	17.51	15.36

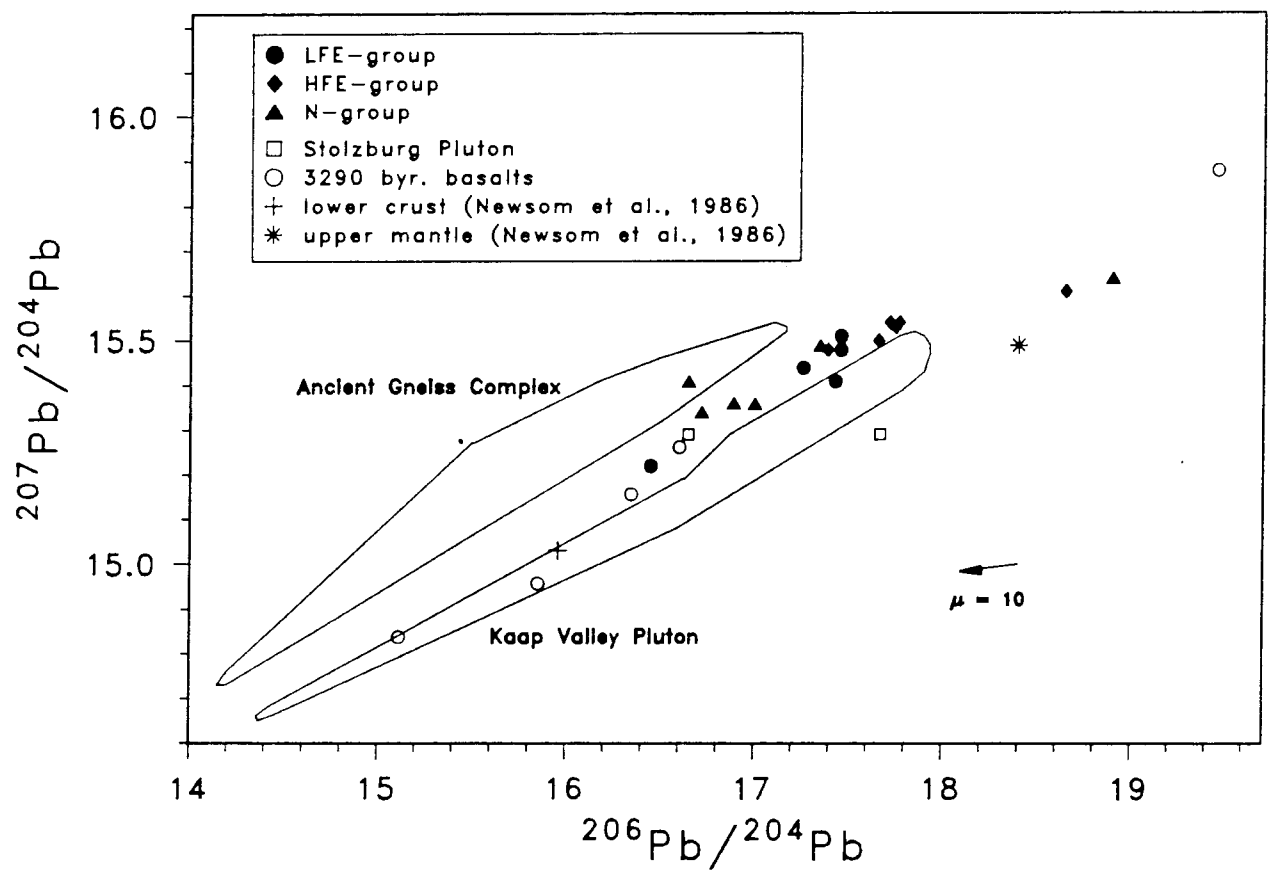

Figure 7.12. Central Lebombo Pb-isotope (present day) data (filled symbols), with available data for granitic rocks occuring 50-100 km to the west (see Fig. 7.1; granite data from Robb *et al.*, 1986). Also included are basalt data from the Barberton Mountainland (Sinha, 1972) and Newsom *et al.*'s (1986) estimates of upper mantle and lower crust. The age correction at 190 Ma for a typical central Lebombo basaltic μ-value is shown.

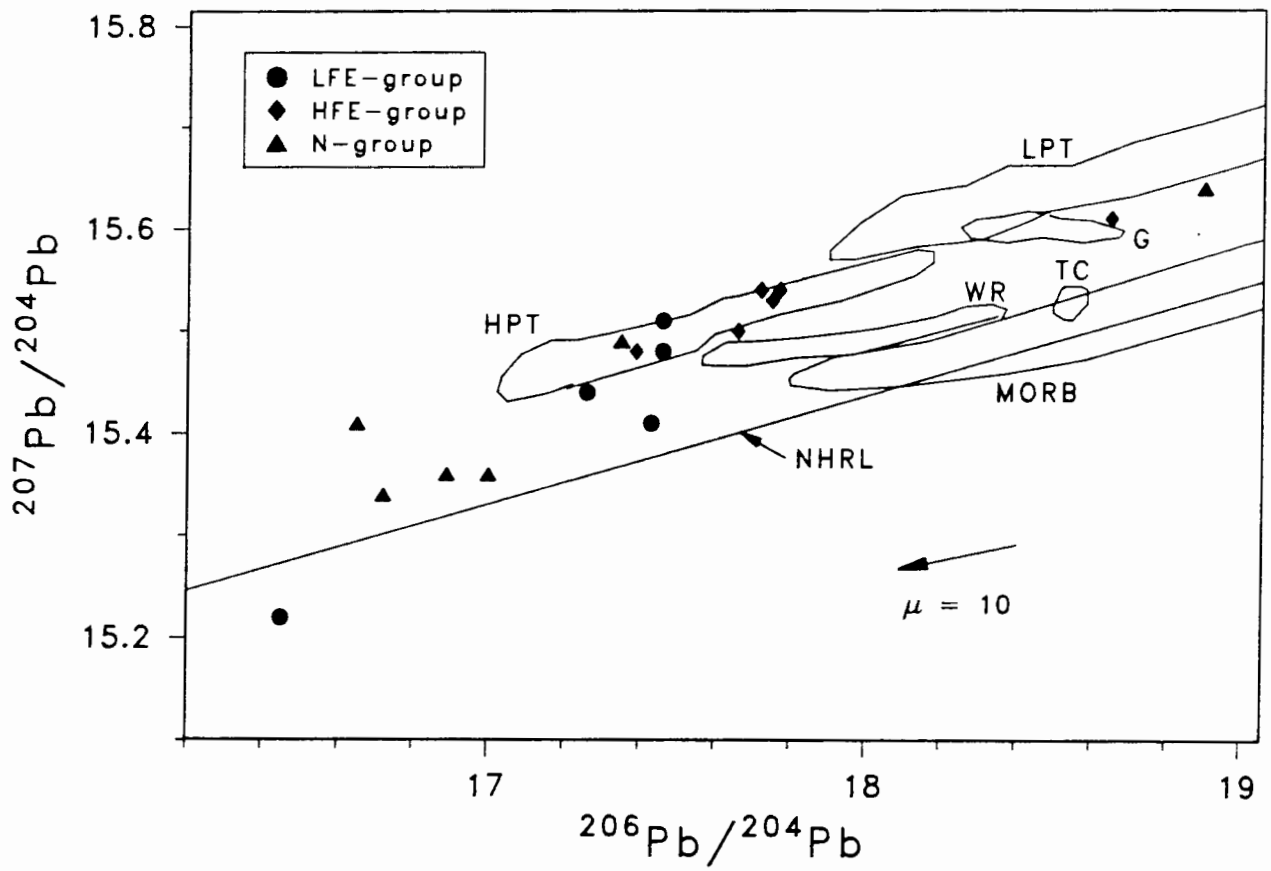

Figure 7.13. Pb-isotope data (present day) for central Lebombo basaltic volcanics plotted with fields described by MORB, the Walvis Ridge (WR), Gough (G), Tristan da Cunha (TC) and the high- (HPT) and low- (LPT) phosphorous titanium Mesozoic basalts of the Parana basin (from Hawkesworth *et al.*, 1987). The northern hemisphere reference line (NHRL) is from Hart (1984).

Nonetheless, if the array of Pb-isotope data in central Lebombo basalts is a function of such crust-mantle mixing, the implication is that this mixing is decoupled from both $^{87}Sr/^{86}Sr$ ratios (Fig. 7.14) and the absolute abundances of Pb and Th (Fig. 7.15). Thus mixing cannot be due to bulk assimilation of granitic crust (e.g. AFC) and must be highly selective for all groups. This would imply that Pb-isotopes are most sensitive to crustal contamination.

II. Mantle Source Heterogeneity

The observed Pb-isotope array may represent the range of values which exist in the mantle source(s) to all the basalt types. A similar spread of data for 3290 Ma basalts from Barberton (Fig. 7.12; Sinha, 1972) assuming no interaction with crust, would imply that such heterogeneities have been in existence for a long time. Such a model would explain decoupling of Pb-isotopes and Pb and Th abundances, i.e. Pb-isotopes would preserve the source signatures, while Pb and Th contents could be affected by a variety of petrogenetic processes (e.g. degree of partial melting and fractional crystallization).

In conclusion, it seems that mantle source heterogeneity is a more effective mechanism for explaining the data observed given the data available. However, it is likely, that the two models above may be superimposed in which case the situation becomes complex.

7.7 SUMMARY OF CONCLUSIONS

Varying degrees of fractional crystallization and assimilation (AFC) may account for most N-group data, notably the correlation of $^{87}Sr/^{86}Sr$ initial ratio with SiO_2, K and Rb. The high Ba and Sr contents of some samples, however, are still unaccounted for, and may be a function of the primary magma composition. The spread and enrichment of HFSE (Zr, La, Ce, Nd and P) with decreasing MgO may be accounted for if these elements are not buffered to low values in a partial melt by refractory phases (i.e. zircon and apatite) in the granitic parent. The domininance of AFC processes over selective contamination effects in this group implies that assimilation has gone to completion.

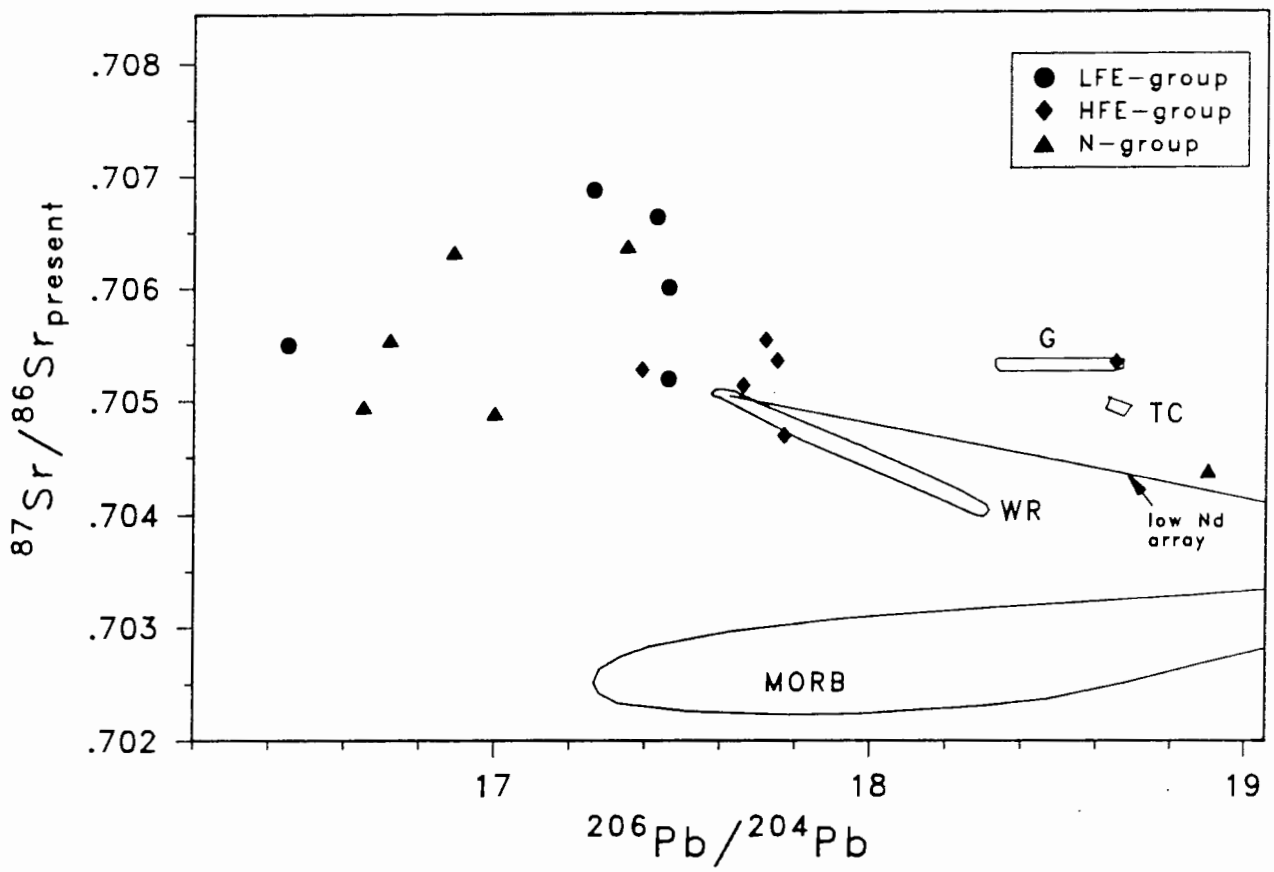

Figure 7.14. $^{206}Pb/^{204}Pb$ and $^{87}Sr/^{86}Sr$ ratios (present day) for central Lebombo basaltic volcanics plotted with fields described by MORB, the Walvis Ridge (WR), Gough (G), Tristan da Cunha (TC) (from data compiled in Zindler *et al.*, 1982) The northern hemisphere reference line (NHRL) is from Hart (1984).

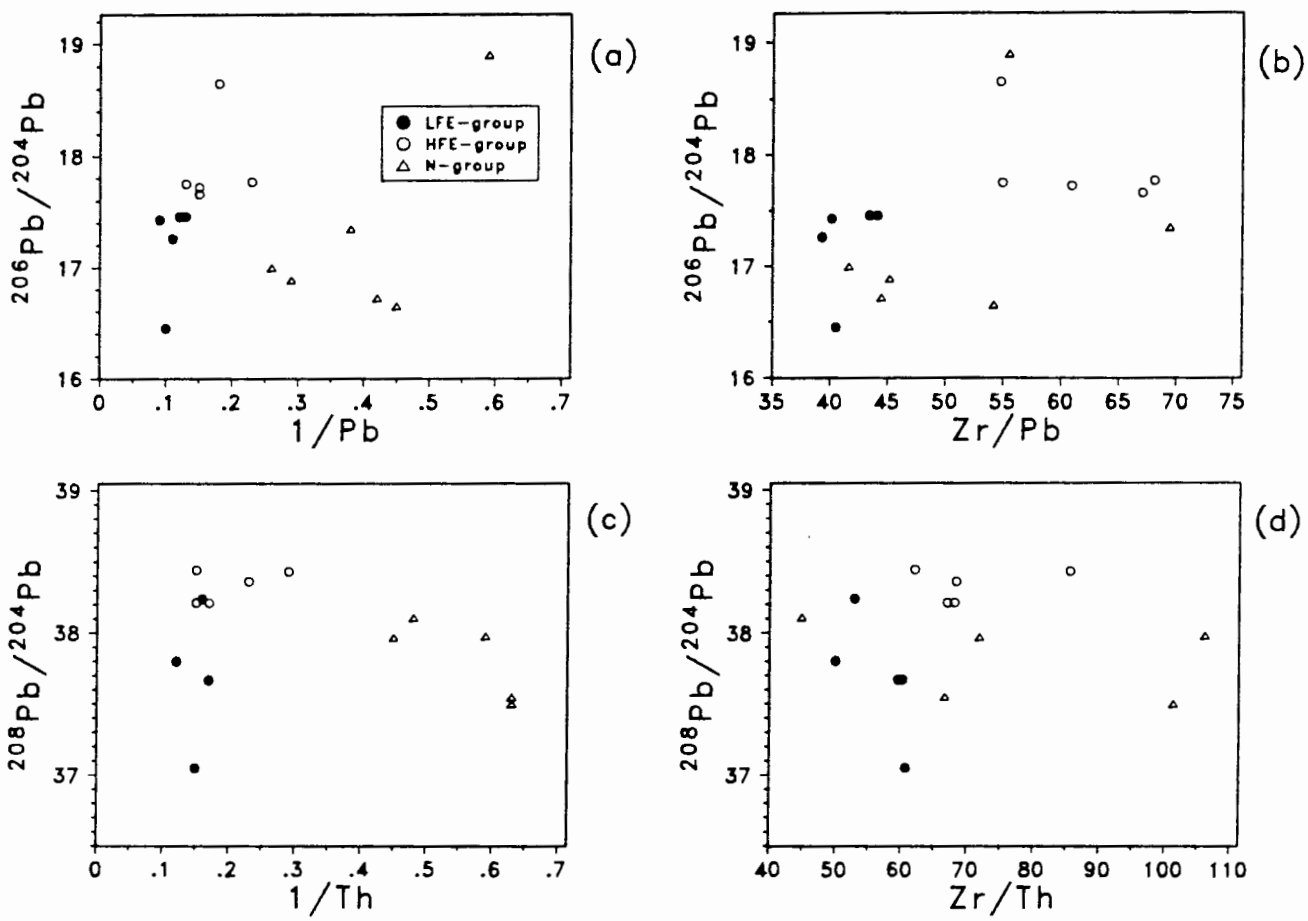

Figure 7.15. $^{206}Pb/^{204}Pb$ *vs* 1/Pb and Zr/Pb, and $^{208}Pb/^{204}Pb$ *vs* 1/Th and Zr/Th for central Lebombo basaltic volcanics.

Contamination of the HFE-group magmas with granitic crust is not significant for any of the contamination models considered, although selective effects may account for some of the spread in K and Rb abundances. It is suggested that the HFE group may be related to a N-type parent composition unaffected by granitic contamination. Given the much greater overall degree of fractionation in the HFE group (i.e. their more evolved nature), however, it is surprising that AFC processes were not significant. One explanation may be that the HFE-group magma chambers were not sited in granitic crust.

It is unlikely that bulk contamination (AFC and conduit contamination) has affected LFE-group geochemistry significantly, while selective contamination may be causing some of the spread in K and Rb abundances in this group. The insensitivity of the LFE-group to granitic contamination is considered to be largely a function of greater abundances of elements such as LILE, Sr, Nd and Zr, in the primary magmas of this group relative to those of the N group.

Thus, the most convincing evidence for granitic contamination in the central Lebombo is in the N group. The higher $^{87}Sr/^{86}Sr$ and lower $^{143}Nd/^{144}Nd$ initial ratios obtained for southern Lebombo N-type Sabie River basalt compositions (Fig. 7.8) were interpreted by Hawkesworth *et al.* (1984) as being the result of granitic contamination. However, the point made for the N-group in the central Lebombo is still valid in this instance: while higher $^{87}Sr/^{86}Sr$ initial ratios may be more easily generated by granitic contamination than low $^{143}Nd/^{144}Nd$ initial ratios, it is improbable that the total spread in both isotope ratios is solely the result of granitic contamination affecting this group. It is suggested that some additional high-ϵ_{Sr} and low-ϵ_{Nd} component (e.g. in the mantle source) is still required.

8. REPLENISHED, TAPPED AND FRACTIONATED MAGMA CHAMBERS

8.1 INTRODUCTION

Two important justifications for considering the replenished, tapped and fractionated chamber model (RTF) of O'Hara (1977) and O'Hara and Mathews (1981) exist:

(1) Their model predicts considerable changes of incompatible element concentrations for small variations in major element composition This could potentially explain the degrees of enrichment of some incompatibles (e.g. Zr, Y, La) with decreasing MgO content in the N and HFE groups hitherto unexplained by either closed-system fractional crystallization (CSF) or coupled assimilation-fractional crystallization (AFC).

(2) Given the large number of flows in the area, comprising a total thickness of *ca* 2000 m, a replenished, tapped and fractionated magma chamber is more realistic than a fractionating chamber closed to periodic replenishment. Furthermore, the volumes of basalt observed require a magma chamber to be much larger in the case of closed-system fractional crystallization than a periodically replenished, tapped and continuously fractionated chamber where the same volume of magma may be cycled through a considerably smaller chamber for the same geochemical effect.

8.2 O'HARA'S RTF MODEL

8.2.1 The Equations

O'Hara (1977) first suggested this model and followed it with a more rigorous treatment in O'Hara and Mathews (1981). These authors derive a general expression for the calculation of element concentrations in a magma chamber undergoing periodic replenishment, tapping and continuous fractionation using a mass-balance approach:

$$ {}_{n+1}C_M = \frac{1}{M_{n+1}} \cdot \left[{}_0C_M . M_0 \prod_{q=0}^{q=n} (1-x_q-y_q).(1-x_q)^{D_q-1} + \sum_{q=0}^{q=n} ({}_qC_w . w_q + {}_qC_z z_q) \times \frac{\prod_{q=0}^{q=n} (1-x_q-y_q)(1-x_q)^{D_q-1}}{\prod_{q=0}^{q=q} (1-x_q-y_q)(1-x_q)^{D_q-1}} \right] \qquad - (8.1) $$

where symbols are from O'Hara and Mathews (1981):

x = mass fraction crystallized

y = mass fraction which escapes as lava

z = absolute mass of replenishing magma

w = absolute mass of contaminant

n = number of cycles of successive replenishment, crystallization, contamination and extrusion

${}_0C_M$ = initial concentration of an element

${}_{n+1}C_M$ = concentration of an element in the mixed magma at the beginning of the n+1 cycle (or end of the n^{th})

C_w = concentration of an element in the contaminant

C_z = concentration of an element in the replenishing magma

D = bulk distribution coefficient

M_0 = initial mass of magma in the chamber

M_{n+1} = mass of mixed magma at beginning of n+1 cycle (or end of the n^{th} cycle), and is calculated below

$$M_{n+1} = M_0 \cdot \prod_{q=0}^{q=n} (1-x_q-y_q)$$

$$+ \sum_{q=0}^{q=n} (w_q+z_q) \cdot \frac{\prod_{q=0}^{q=n} (1-x_q-y_q)}{\prod_{q=0}^{q=q} (1-x_q-y_q)} \qquad - (8.2)$$

It was noted during this study that in equation 9 of O'Hara and Mathews (1981), repeated here as equation 8.1 above, the term ${}_0C_M$ is omitted and z_q is mislabelled z_0. Rigorous derivations of these equations are given in O'Hara and Mathews (1981) and are not repeated here. The derivation of O'Hara and Mathews (1981) steady-state equation is repeated below (eqns. 8.3 to 8.7).

At any stage the residual (or erupted if y>0) liquid composition (C_B) is:

$${}_{n+1}C_B = {}_{n+1}C_M \cdot (1-x_{n+1})^{D_{n+1}^{-1}} \qquad - (8.3)$$

O'Hara and Mathews (1981) initiate their RTF model in the zeroth cycle, hence the C_M and C_B values are calculated for the zeroth cycle, i.e. the C_M and C_B values are calculated for the n+1 cycle using the equations above. A n-value of 10 therefore actually reflects 11 cycles, i.e. 11 eruptions of magma if y is non-zero.

These authors then derive special case equations by assuming a number of constant parameters: M_0=1, x, y, z and D are all constant, $C_z = {}_0C_M$ (constant) and no contamination takes place (w=0). Equation 8.1 becomes

$$\frac{{}_{n+1}C_M}{{}_0C_M} = \frac{[(1-x-y)(1-x)^{D-1}]^n}{M_{n+1}} +$$

$$+ \frac{z}{M_{n+1}} \cdot \left[\frac{1-[(1-x-y)(1-x)^{D-1}]^n}{1-(1-x-y)(1-x)^{D-1}}\right] \qquad - (8.4)$$

and equation 8.2 becomes

$$M_{n+1} = (1-x-y)^{n+1} + z.\left[\frac{1-(1-x-y)^{n+1}}{1-(1-x-y)}\right] \qquad - (8.5)$$

Furthermore as n become large $M_{n+1} = z/(x+y)$ (eqn. 8.5) and because (1-x-y) and (1-x) are both less than unity, eqn. 8.4 tends to the limit

$$\frac{{}_{ss}C_M}{{}_0C_M} = \frac{(x+y)}{1-(1-x-y)(1-x)^{D-1}} \qquad - (8.6)$$

and combining with eqn. 8.3 gives the so-called steady-state composition of the erupted magma:

$$\frac{{}_{ss}C_B}{{}_0C_M} = \frac{(x+y)(1-x)^{D-1}}{1-(1-x-y)(1-x)^{D-1}} \qquad - (8.7)$$

This is the equation which O'Hara (1977) uses to predict the generation of considerable ranges in incompatible element concentrations, to exploit small differences in bulk D between two incompatible elements to change their ratio significantly, and markets as describing a mechanism which decouples major from trace elements in an RTF magma chamber. A useful aspect of this equation is that it is independent of any estimation of magma chamber mass (M_{n+1}), mass of replenishing magma (z) and element concentration in that magma (C_z). It is of paramount importance, however, to stress that the application of this equation is conditional on the assumptions made in its derivation holding true. This is discussed below.

8.2.2 Assumptions: are they valid?

(1) The steady-state assumption.

Equation 8.7 is based on the assumption that a magma chamber has undergone a sufficiently large number of cycles to ensure that a 'steady-state' has been achieved. This effectively means that the term '$(1-x-y)^{n+1}$' (implicit in assuming that M_{n+1} tends to $z/(x+y)$) and the

product '$[(1-x-y)(1-x)^{D-1}]^n$' (in the simplification of eqn. 8.4) should approach zero. The approach of these two terms to zero may therefore be used as a measure of the justifiability of the steady-state assumption. For example, for fig. 3 (Fig. 8.1) of O'Hara (1977) to be valid (i.e. for the above terms to be less than .001) for the parameters x=.01, y=.001, D=.01, n must have a value greater than 4144 cycles. Some control over the value of n is gained by the actual number of lavas observed providing the magma tapped from the chamber in each cycle reaches the surface. For an average flow thickness of 10 m, therefore, 4144 cycles implies a lava pile in the region of 40 km thick - unreasonable for any volcanic province.

It may be argued that this steady-state RTF model could operate for a number of cycles without extrusion (y=0) to generate tremendous incompatible enrichments (i.e. up to $1000xC_0$, fig. 4, O'Hara and Mathews, 1981; reproduced here as Fig. 8.2) before extrusion takes place. The problem here is that, not only does the magma chamber need $\pm 10^5$ cycles to reach a steady-state under these conditions (x=.1, y=0, D=.001), but once extrusion does occur (y=.01) a further 10^3 cycles are required to achieve a new steady-state and then the enrichment levels have 'decayed back' to a value of about $10xC_0$.

(2) A constant C_z (= $_0C_M$), and z?

Most magmas derived by partial melting of a mantle source will typically have a similar (picritic?) major element chemistry with progressive (or successive) partial melting. This high-MgO magma which is fed into a chamber occupied by magma which has evolved to lower-MgO compositions will not mix until the density contrast between the two is minimized (Huppert and Sparks, 1981) by, for instance, fractional crystallization of the incoming magma. Obviously as a magma chamber evolves to lower MgO values, more crystallization of the replenishing magma will be needed to minimize this density contrast. Therefore, to keep z (taken here as the mass of replenishing magma which actually mixes) constant necessitates progressively larger liberations of melt from the mantle - a very fortuitous situation. Furthermore, the degree of evolution in the replenishing magma necessary to facilitate mixing will change considerably for **large** ranges of MgO content in the resident magma and therefore it is unlikely that $C_z = {}_0C_M$.
O'Hara and Mathews (1981) do mention the problem of mixing two melts of different density, but retain the above assumptions and still do not take

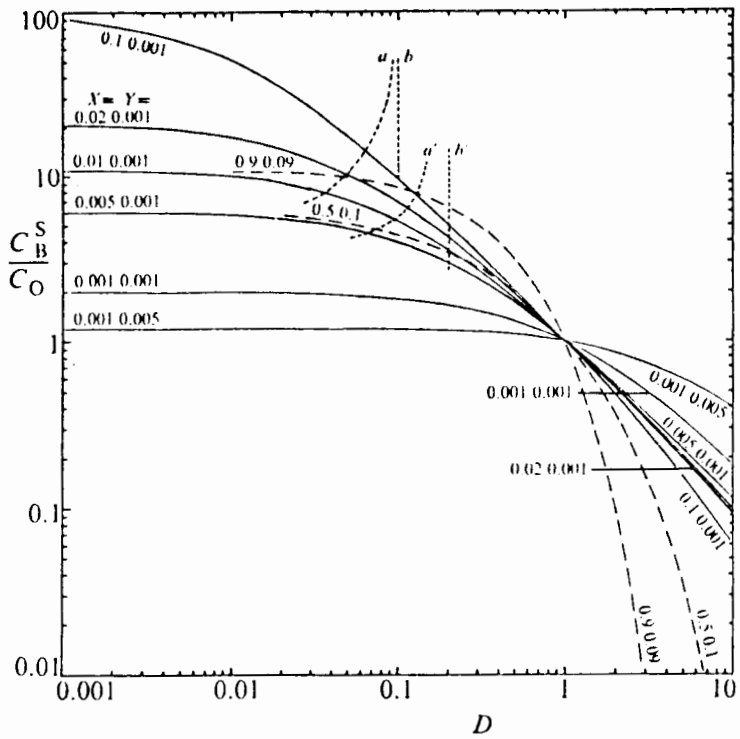

Figure 8.1. Variation of the relative concentration of an element as a function of D for a selection of x and y values using the steady-state equation (8.7). At values of D along curves *a*, *a'* the concentration of an incompatible element is 1.5 times that at the values of D given on *b*, *b'*, for all curves with y=.001 (from O'Hara, 1977, fig. 3).

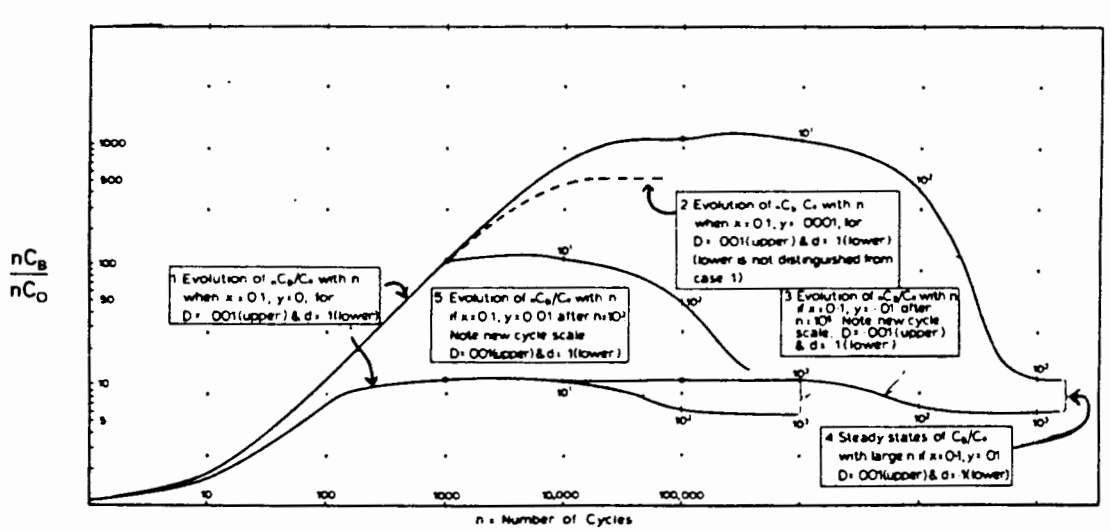

Figure 8.2. The evolution of incompatible elements (D=.001 and D=.1) as a function of the number of cycles. Cases 1 and 2 show how concentrations increase, then stabilise when y=0. Case 3 shows how the steady-state in case 1 will decay to a new steady-state taking many cycles to do so when y>0. Case 4 illustrates a direct approach to this latter steady-state while case 5 shows how case 1 would have been modified if a steady state had not been achieved when eruption continued (from O'Hara and Mathews, 1981, fig. 4).

this problem into account in their conclusions.

(3) Major elements.

O'Hara and Mathews (1981) do not model major elements in their RTF magma chamber beyond a rudimentary consideration of FeO and MgO variations using mineral/melt distribution coefficients. The modelling of major elements is especially critical when the fractionating assemblage is not gabbroic, i.e. where there is a significant change in major element content of a fractionating magma.

8.3 AN ALTERNATIVE SIMPLIFICATION

It would be useful to derive a simplification of O'Hara and Mathews (1981) general expression in which the steady-state assumptions are not necessary and in which there was no requirement for a constant z or C_z. Such a procedure would also be used for modelling the behaviour of major elements. Although this would then require estimates for the abovementioned parameters to be made, their magnitude would be useful in evaluating the feasibility of magma chamber dynamics. The definition of 'z' to be the absolute mass of magma which actually mixes in the chamber will enable the requirement for similar densities, as detailed in Huppert and Sparks (1981), to be satisfied. The ability to vary C_z would also be useful when evaluating the combined effect on liquid compositions of introducing magma derived by variable degrees of partial melting into a chamber.

Symbols used here are consistent with those used in O'Hara and Mathews (1981) and the treatments of major and trace elements and isotopic ratios described are those incorporated into the RTF subroutines in the modelling program 'DARTS' (written by A. R. Duncan, with the exception of subroutines pertaining to RTF processes) extensively used in the modelling carried out in this thesis.

8.3.1 Major Elements

The modelling of major elements in a RTF magma chamber involves a relatively simple mass-balance approach for each cycle:

$$C_B = \frac{C_c - x.C_x - y.C_c + z.C_z}{M} \qquad - (8.8)$$

where C_c is the concentration of an element in a chamber and is equal to ${}_0C_M$ at the beginning if the initial cycle and C_x is the concentration of an element in the crystallate. Note that C_c is analogous to C_M of the trace element equations. C_B is the residual or erupted concentration and becomes C_c of the next cycle. As mentioned in a preceding section, the initiation of fractionation in the 0^{th} cycle means that for a given n value this calculation must be repeated n+1 times. The mass of a magma chamber at the onset of each cycle is set equal to 1, so the M calculated here is a relative mass only, calculated for each cycle (i.e. n=0) using eqn. 8.5 (preceding section).

8.3.2 Trace Elements

As previously: M_0=1, x, y, z, D are assumed constant, as is C_z (but not = ${}_0C_M$) for a designated number of cycles and w=0 (no contamination). O'Hara and Mathews (1981) general expression then becomes:

$$ {}_{n+1}C_M = \frac{1}{M_{n+1}} \left[{}_0C_M[(1-x-y)(1-x)^{D-1}]^n + C_z.z \; \frac{1-[(1-x-y)(1-x)^{D-1}]^n}{1-(1-x-y)(1-x)^{D-1}} \right] \qquad - (8.9)$$

Except for the addition of C_z this is identical to eqn. 8.4. M_{n+1} is given by eqn. 8.5. Combining eqns. 8.9 and 8.3 gives the erupted or residual liquid composition:

$$ {}_{n+1}C_B = \frac{(1-x)^{D-1}}{M_{n+1}} \left[{}_0C_M[(1-x-y)(1-x)^{D-1}]^n + C_z.z. \; \frac{1-[(1-x-y)(1-x)^{D-1}]^n}{1-(1-x-y)(1-x)^{D-1}} \right] \qquad - (8.10)$$

and the erupted mass ($_{n+1}M_y$) is:

$$_{n+1}M_y = M_{n+1} \cdot y_{n+1} \qquad - (8.11)$$

8.3.3 Isotopes

Techniques for measuring radiogenic isotope ratios routinely correct for any fractionation (instrumental) between the isotopes of any ratio and changes which may be induced by fractional crystallization processes Thus the only way to change the measured Sr-, Pb- or Nd-isotopic ratios in a magma chamber is if the isotopic content of the replenishing magma is not the same as that of the resident magma. The case then becomes one of evaluating the mixing relationships that occur.

O'Hara and Mathews (1981) do not model the variations expected to occur in either stable or radiogenic isotopes in RTF magma chambers. Equations derived by De Paolo (1981) are used (Chapter 7) where the replenishing magma composition replaces the assimilant composition - a possibility suggested by De Paolo (1981). De Paolo's (1981) 'r' is therefore given by z/x. There is no facility, however, in De Paolo's (1981) equations for the reduction in mass of a magma chamber by the mass of magma extruded (y). This means that the mass of the magma chamber given by eqn. 8.5 (M_{n+1}) is **not** directly comparable to De Paolo's (1981) M_m; rather M_m is given by

$M_m = 1-x+z$ (i.e. no y)

In summary the following equations of De Paolo (1981) are cycled n+1 times to model the evolution of isotopic ratios in a RTF magma chamber:

Radiogenic Isotopes: R=1, De Paolo eqn. 13a
R=1, De Paolo eqn. 15a

Stable Isotopes: R=1, oxygen, De Paolo eqn. 19
other, De Paolo eqn. 17
R=1, oxygen, De Paolo eqn. 20
other, De Paolo eqn. 18

Oxygen Δ-values required to estimate the individual melt-crystal exchange using De Paolo's (1981) equations were obtained from the experimental work on basaltic systems of Kyser *et al.* (1981).

8.4 A COMPARISON WITH STEADY-STATE PREDICTIONS

O'Hara's (1977) steady-state equation (eqn. 8.7 here) predicts large degrees of incompatible element enrichment depending on the x and y (principally x) values used (Fig. 8.1). Obviously eqn. 8.10 may also produce the same levels of enrichment if n (the number of cycles) is sufficiently large. By setting $C_z = C_0$ (also assumed in O'Hara's steady-state equation), eqn. 8.10 may be solved for various values of n, x, and y. The value of z is set equal to x+y, thereby not changing the magma chamber mass (M_{n+1}=1). The predicted levels of incompatible element enrichment using eqn. 8.10 are given in Fig. 8.3 for D=.001 and D=.1. The x and y values used duplicate those used in Fig. 8.1. In both instances (Fig. 8.3a, b) the tendency of C_B/C_0 to approach a constant value after a number of cycles reflects the achievement of a steady-state in the system concerned. Therefore a system attains a steady-state once the rate of change of C_B/C_0 relative to n becomes negligible: i.e. $d(C_B/C_0)/dn \simeq 0$.
The number of cycles required (n-req.), given opposite each curve, to achieve this steady-state is the n-value for which both the expressions '$(1-x-y)^{n+1}$' and '$[(1-x-y)(1-x)^{D-1}]^n$' are less than or equal to .001 (i.e. approach 0, section 8.2.2). The steady-state enrichment (the value towards which these curves tend at large n) is given in brackets opposite each curve.

The enrichments predicted by O'Hara's (1977) steady-state equation are thus only possible when n is relatively large, e.g. generally >1500 cycles for the two examples illustrated in Fig. 8.3. When y is non-zero and if these cycles are matched by an eruption of magma, 1500 eruptions of flows each 5 m thick, would imply a section thickness of 6 km. Even allowing for some cycles (e.g. one third or 500 in the example above) to be represented by intrusives only, the achievement of a steady-state would still imply a section thickness in excess of 4 km, twice the thickness of the basaltic section observed in the central Lebombo (*ca* 2 km). However, by setting y=0

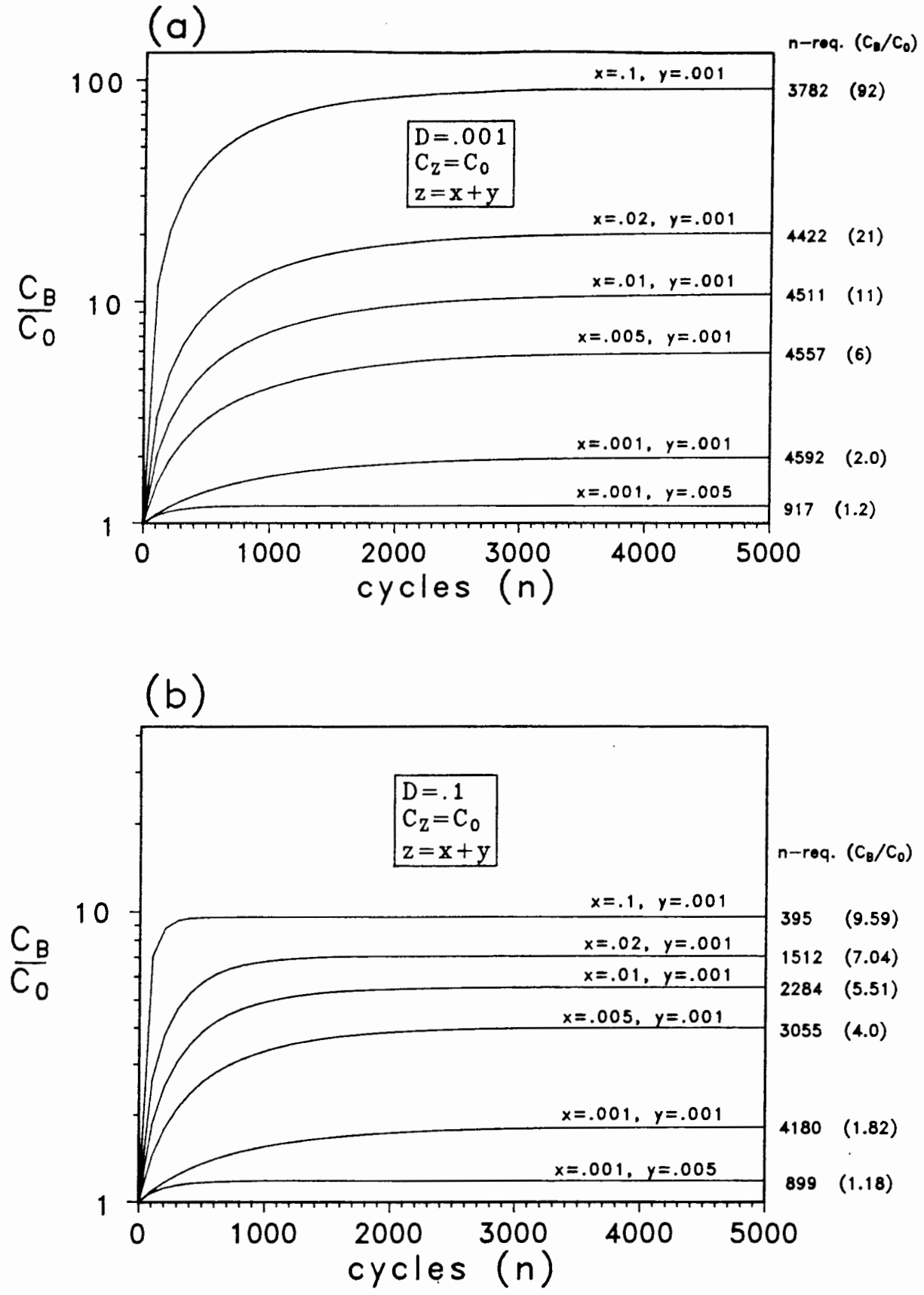

Figure 8.3. The effect of n (number of cycles) on C_B/C_0 for illustrated x and y values (where y>0) predicted using equation 8.10 for:
(a) D = .001 and
(b) D = .1.
A steady-state is reached when the curves reach a plateau. The number of cycles needed to reach this state is shown opposite each curve (n-required) along with the steady-state C_B/C_0 (enrichment) value (bracketed).

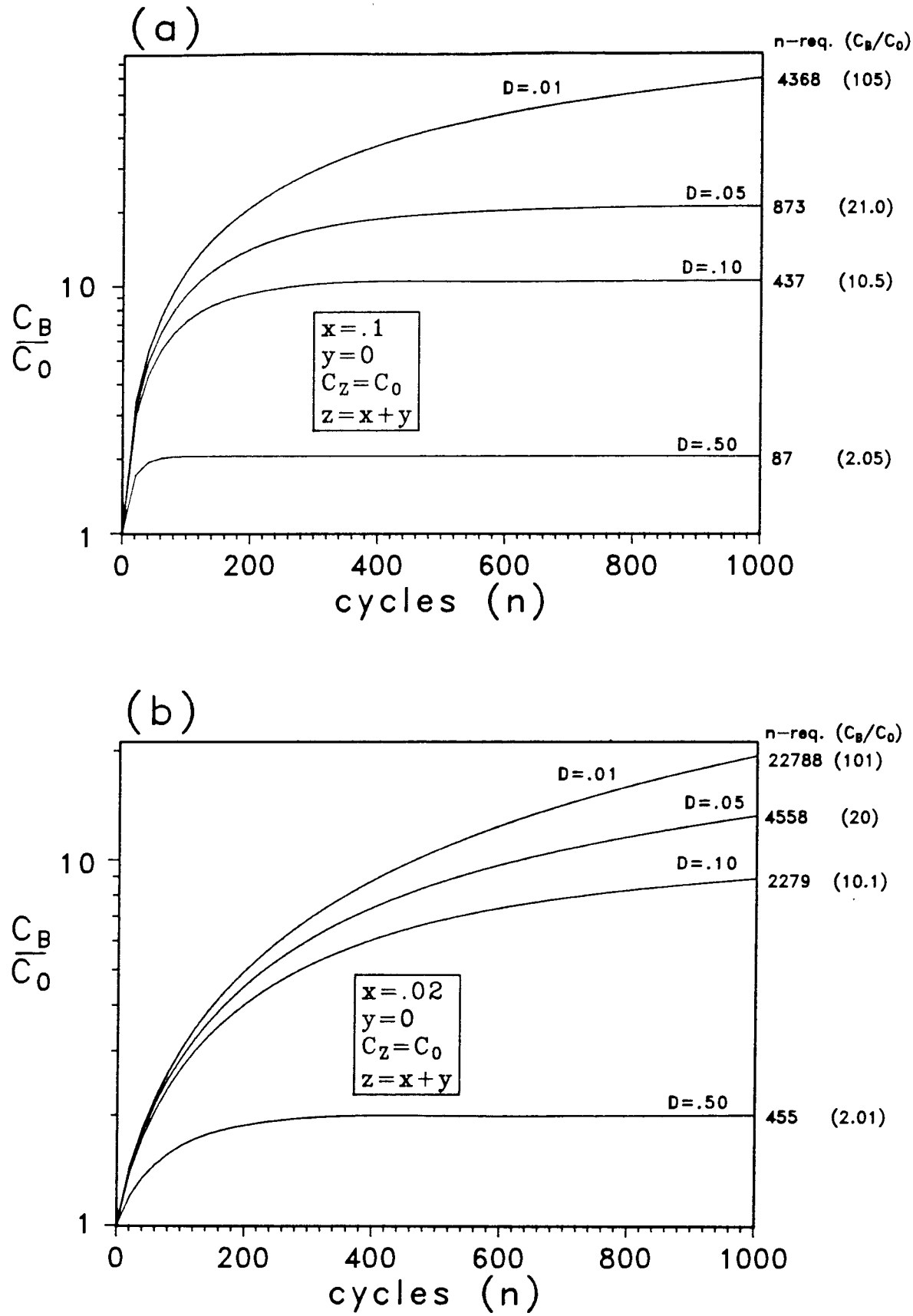

Figure 8.4. The effect of n (number of cycles) on C_B/C_0 for illustrated D values (where y=0) predicted using equation 8.10 for:
(a) x = .1 and
(b) x = .02.
A steady-state is reached when the curves reach a plateau. The number of cycles needed to reach this state is shown opposite each curve (n-required) along with the steady-state C_B/C_0 (enrichment) value (bracketed).

for a number of cycles there is no need no match each cycle with an eruption (or intrusion) and the levels of incompatible element enrichment are improved,

e.g. for D=.1: when x=.02, y=.001, z=x+y then C_B/C_0=7.03

: when x=.02, y=0, z=x+y then C_B/C_0=9.93

Fig. 8.4 shows the variation of C_B/C_0 with n for varying D's and x values for y=0. In most magma chamber systems, cycles of crystallization and replenishment are unlikely to exceed 1000 cycles without any eruption - hence n is only plotted in Fig. 8.4 for 0-1000 cycles.

Thus, **providing** the major element content of an evolving magma chamber is buffered (i.e. composition melt $\simeq$ composition crystallizing assemblage), the levels of enrichment predicted in Figs. 8.3 and 8.4 are possible. Although estimates of n and z are necessary in this model, it does not have the limitations which the assumptions of O'Hara's (1977) steady-state model imply.

There is no difference between O'Hara and Mathews' (1981) RTF model and that postulating a series of alternating fractional crystallization and magma-mixing (with replenishing magma) steps (Fig. 8.5). For example, if x=.2, y=.01 and z=.21 for one cycle in the RTF case the results are duplicated by fractional crystallization with F=.8 followed by magma-mixing with the mixed-magma containing 79% of the fractionated composition. Such a model effectively predicts liquid compositions intermediate between the 'end-member' RTF and closed-system fractional crystallization models and therefore may be an effective mechanism for explaining the spread of compositions typically observed in many magma suites (Fig. 8.5). The RTF model of O'Hara and Mathews (1981) as given in section 8.3, however, provides a convenient calculation of the maximum incompatible element enrichment in the residual liquid at the end of a series of fractionation and mixing increments, and monitors magma chamber mass which is dependent on the parameters x, y and z.

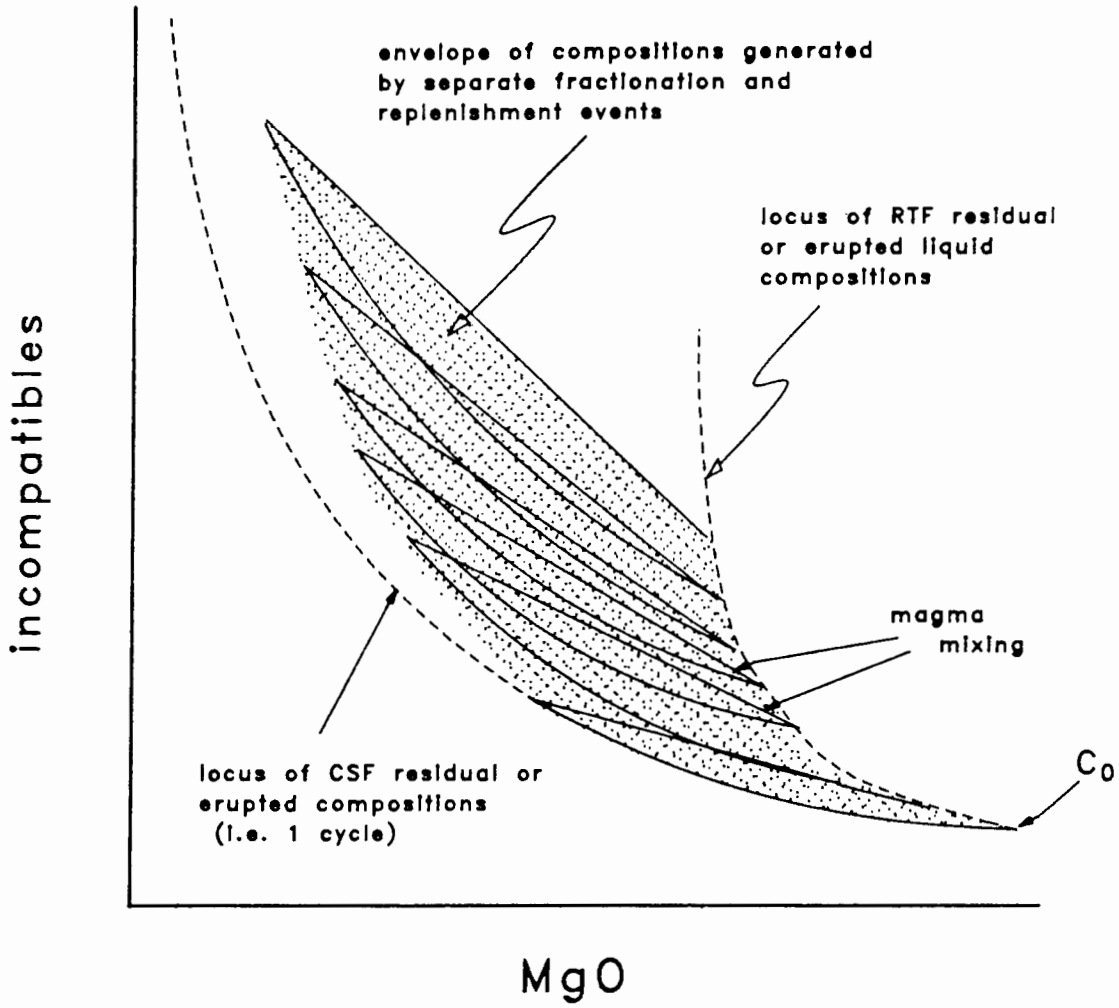

Figure 8.5. A sketch of evolution possibilities in a magma chamber. CSF predicts the least amount of enrichment of any incompatible element and RTF the most. Discrete cycles of fractionation (concave upward curves) and magma-mixing (straight lines) with a replenishing magma of composition C_0, could produce an envelope of compositions (shaded).

8.5 APPLICATION TO THE LFE GROUP

A model describing closed-system fractional crystallization for the LFE group is consistent with most of the geochemical variations observed (Chapter 6). Exceptions are K, Rb, Ba and Sr which have a random distribution in this group and are not accounted for by any model advocating a liquid line of descent (e.g. CSF, AFC, RTF). The random variation of K and Rb with MgO may be due in part to selective granitic contamination, but Ba and Sr concentrations and Nd- and Sr-isotope ratios are not significantly influenced by these processes (Chapter 7). Pb-isotope data are ambiguous and may reflect crust-mantle or mantle-mantle mixing (Chapter 7). RTF model parameters are sought to duplicate the geochemical results of closed-system fractional crystallization models which explained most general trends in the data (Chapter 6). Field evidence (e.g. section thicknesses observed) are also used to constrain the RTF parameters n, x, y and z which define the magma chamber dynamics.

A conclusion reached in Chapter 6 was that this suite of low-MgO basalts may be related to the northern Lebombo picrites by a closed-system fractional crystallization process. The likelihood of such a relationship prompts the inclusion of the picrites in an RTF model. There is strong evidence (reviewed in Chapter 6) to suggest that the picrites have undergone substantial high-pressure fractionation. The high-pressure "primary" composition (LFE primary 2, Table 6.9) is therefore used as the composition from which the model is initiated. This is not a circular approach as the intention is to duplicate the closed-system fractional crystallization variations. The fractionation assemblage selected for this compositional range (MgO 15.5-10.4%) is consistent with high pressure conditions (e.g. orthopyroxene is stabilized as a major phase on the liquidus, Cox and Jamieson, 1974). The parameters used for the LFE-group RTF model are given in Table 8.1. The fractionating assemblage adopted in high-MgO and low-MgO intervals is consistent with high- and low-pressure crystallization discussed in Chapter 6. The model proceeds incrementally from the "primary" composition LFE primary 2, i.e. the residual melt represented by increment 1 (MgO=14.51%) is produced by the fractionation of ol-KP101 (70%) + opx-KS47 (30%) (mineral compositions from Table 6.1). This stepwise approach (in 0.5-1.0% MgO steps) enables the crystallizing assemblage and RTF parameters to be changed between increments. The selection of RTF parameters given in Table 8.1 is described below. M_{rel} and M_y are then calculated using

Table 8.1. Stepwise RTF model for picrites and the LFE group.

incr.	%MgO	RTF parameters x	y	z	n	M_{rel}	M_{abs}	M_y	minerals and proportions (%)
LFEPR2 - 1	15.57	.004	.02	.0300	10	1.059	1.059	.021	ol-KP111 70 opx-KS47 30
1 - 2	14.51	.004	.02	.0262	10	1.022	1.081	.020	ol-KP111 60 opx-KS47 40
2 - 3	13.45	.004	.02	.0230	10	.990	1.071	.019	ol-KP111 50 opx-KS47 50
3 - 4	12.40	.004	.02	.0191	10	.952	1.020	.019	ol-KP111 40 opx-KS47 60
4 - 5	11.36	.004	.02	.0158	10	.920	.938	.018	ol-KP101 30 opx-KS47 70
5 - 6	10.37	.004	0	.0128	5	1.052	.987	0	ol-KP101 70 opx-KS47 30
6 - 7	9.65	.004	0	.0098	5	1.035	1.021	0	ol-KP101 60 opx-KS47 20 cpx4-RSV31 20
7 - 8	9.00	.001	.005	.0071	40	1.040	1.062	.005	ol-KP101 50 opx-KS47 10 cpx4-RSV31 40
8 - 9	8.13	.001	.005	.0091	40	1.114	1.183	.005	ol-KP101 40 opx-KS47 5 cpx4-RSV31 55
9 - 10	7.38	.001	.005	.0088	40	1.101	1.302	.005	ol-KS3 30 opx-KS47 5 cpx4-RSV31 65
10 - 11	6.73	.001	.005	.0063	40	1.011	1.317	.005	ol-KS3 10 cpx4-RSV31 90
11 - 12	6.23	.001	.005	.0046	40	1.001	1.318	.005	cpx4-RSV31 100
12 - 13	5.88	.001	.005	.0038	40	.921	1.214	.004	cpx4-RSV31 100
13 - 14	5.51	.001	.005	.0023	40	.867	1.052	.004	cpx4-RSV31 100
14 - 15	5.11	.001	.005	.0014	40	.834	.877	.004	cpx4-RSV31 80 plag4-RSS152 20
15	4.81								

(mineral compositions given in Table 6.1)

equations 8.5 and 8.11.

The sequence of picrite basalts becomes progressively thicker as the northern edge of the Kaapvaal Craton is approached (Fig. 1.4), attaining a maximum thickness of 4 km (Bristow, 1980). The average stratigraphic thickness for the picrite basalt sequence (Letaba Formation) is estimated to be 2000 m. Thus, in a model which proceeds incrementally, the 5 increments from 15.57% MgO (LFE primary 2) to 10.37% MgO (Table 8.1) may correspond to 50 eruptions of flows 20 m thick if n=10 for each step and y is non-zero. This assumes that the MgO range 15.5-10.4% is representative of approximately half the number of observed picrite basalt compositions. This is reasonable as the median of the 19 northern Lebombo picrite analyses (Duncan *et al.*, 1984b) is about 15.5% MgO (10 samples <15.5% MgO and 9 samples >15.5% MgO).

Similarly the 7 low-MgO increments (9-5% MgO, Table 8.1) may represent 280 eruptions (for n=40 and y>0 in each increment). An average flow thickness of 4.3 m is then required to fill the stratigraphic thickness of 1200 m estimated for the LFE-group (section 8.1.2). This is similar to the measured average of 4.9 m (Chapter 2) for flows in the central Lebombo. Although no estimates for picrite basalt flow thickness on the N. Lebombo are available, their greater thickness relative to low-MgO flows implied by this model is consistent with the field observations of Bristow (pers. comm., 1986).

It remains to select values for x, y and z which are consistent with magma chamber dynamics, estimated eruption volumes and geochemical variations. There is a distinct compositional gap in Lebombo basic rocks between MgO 10.4-9.0% (Fig. 8.6) and, therefore, the RTF magma chamber is modelled as closed to eruption (y=0) in this interval. This reduced activity is likely to be reflected by a reduction in the number of cycles (n) in each increment (decreased from 10 to 5 for MgO 10.4-9.0%, Table 8.1). Thus for the intervals where y>0 (15.5-10.4% MgO and 9-5% MgO) the continued eruption of magma is sustained by a chamber increasing in size. This change in size from increment to increment is manipulated by changing the x, y and z values (principally z here) which are used to calculate M_{rel} (eqn. 8.5) where M_{rel} is the magma chamber mass calculated relative to M_0=1 for each increment only and a magma chamber is increasing in size when $M_{rel}>1$. When eruption ceases $M_{rel}<1$ (MgO 10.4-9.0%, Table 8.1); and where eruption rates are greatest the observed lava volumes are greatest. M_{rel} is plotted

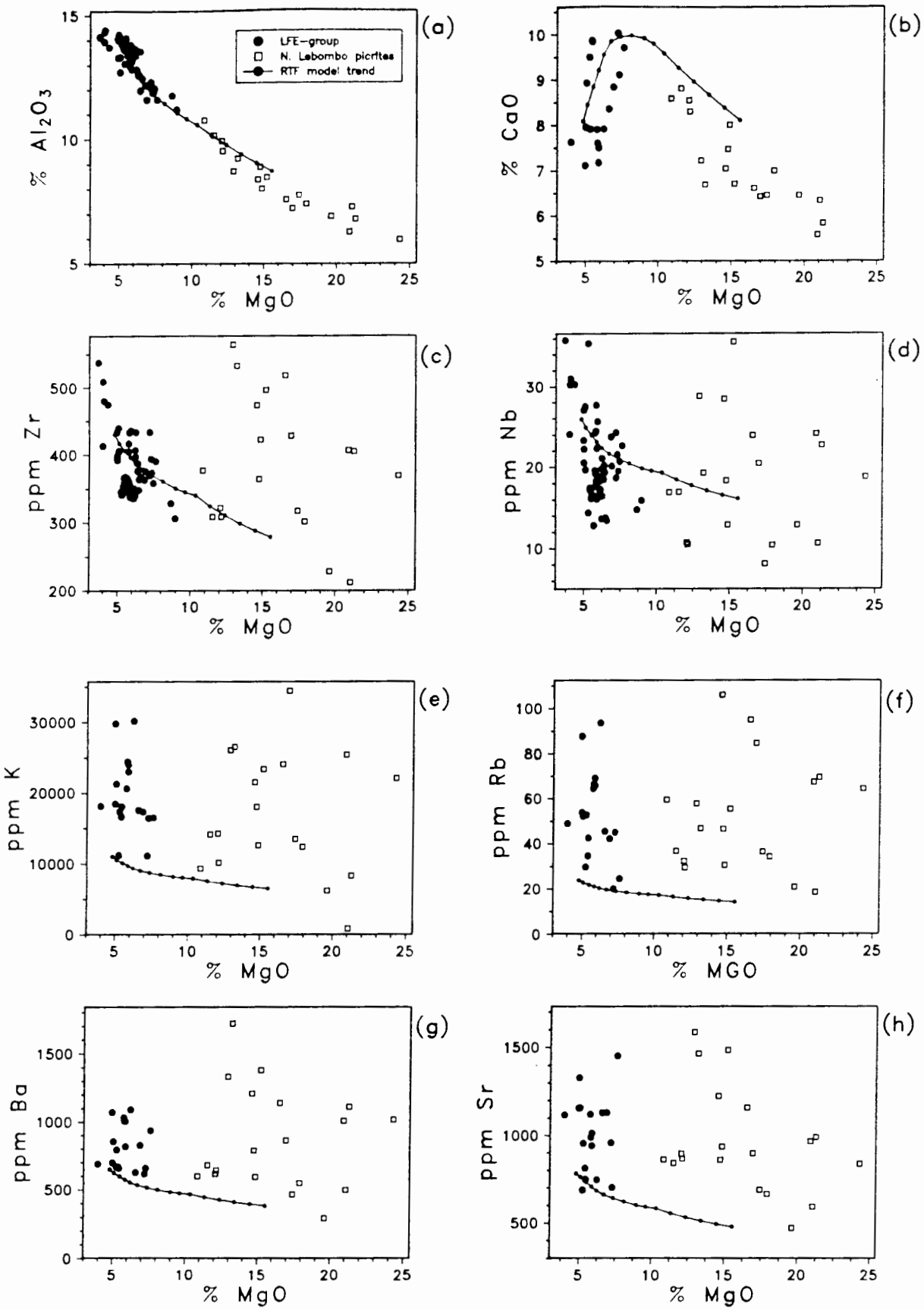

Figure 8.6. RTF model variations for selected elements in N.Lebombo picrite (from Duncan *et al.*, 1984a) and LFE-group data. Increments plotted (dots on model trends) correspond to parameters given in Table 8.1 for each step. The model is initiated from the LFE primary 2 composition in Table 6.9 and is fractionated to evolved LFE-group compositions (Fe as total FeO, data are normalized to 100% volatile-free).

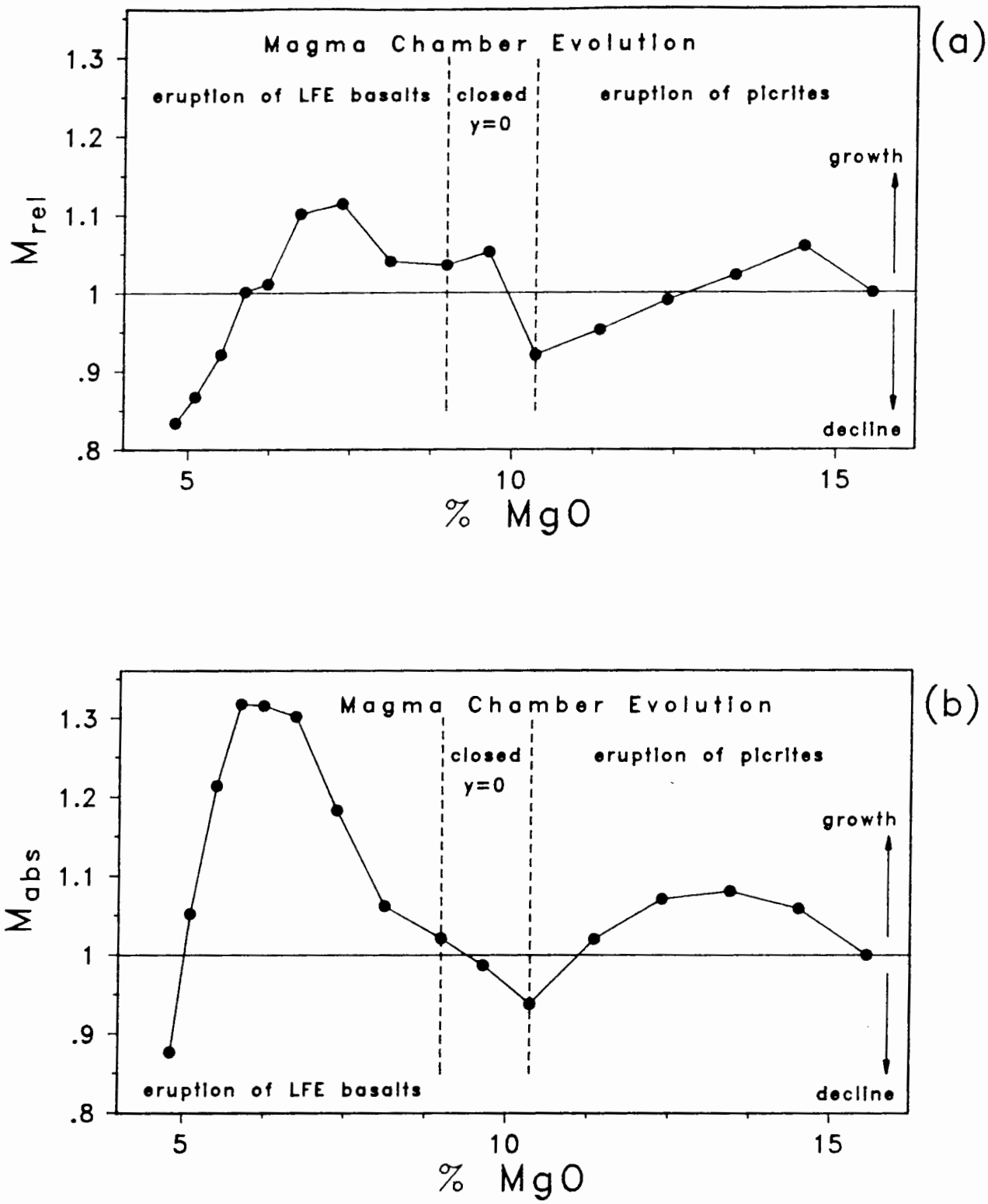

Figure 8.7. RTF model for magma chamber evolution in the LFE-group and the N. Lebombo picrites. M_{rel} (a) monitors the relative change in magma chamber mass between successive cycles. M_{abs} (b) is the cumulative (absolute) change in magma chamber mass. If $M_{rel} > 1$ eruption is sustained while M_{abs} gives the observed change in chamber mass relative to a starting value of 1. Increments plotted correspond to those labelled in Table 8.1.

vs MgO in Fig. 8.7a and M_{abs} monitors the absolute change in magma chamber mass with degree of evolution (Fig. 8.7b).

The magnitude of x and y are set relative to M_0=1 (see section 8.2) and along with the calculated M_y (erupted mass, equation 8.11), may be used to test whether a 'reasonable' magma chamber volume will result in 'reasonable' flow volumes. RTF parameters are, however, defined in mass units. The density of two basaltic samples of different MgO contents (data normalized volatile-free with Fe as FeO) from the Lebombo was measured and the MgO content of any intermediate sample was extrapolated from:

RSK10 (plag-phyric basalt) MgO=2.68%, density=2.44 g/cm^3

FV4 (picrite basalt) MgO=19.63%, density=2.74 g/cm^3

For the picrite basalt series M_y is typically .02 (Table 8.1). Thus a magma chamber of dimensions 4 (height) x 10 x 10 km containing magma of density 2.62 g/cm^3 (average MgO = 13%), gives rise to a flow of dimensions 20 m (thick) x 20 km x 20 km (Fig. 8.8a). For the LFE group M_y=.005 (Table 8.1) which for a magma chamber of dimensions 4 (height) x 10 x 10 km containing magma of density 2.52 g/cm^3 (average MgO = 7%), gives rise to a flow of dimensions 4.3 m (thick) x 20 km x 23 km (Fig. 8.8b). Therefore, the selected RTF parameters correspond to reasonable magma chamber and flow volumes.

The relatively small MgO range covered by each increment (i.e. 0.5-1.0%, Table 8.1) ensures that there is a mimimal difference in MgO content between resident and replenishing magmas (i.e. $C_z = C_0$ in each increment). It is suggested that this will satisfy the equivalent density requirements of Huppert and Sparks (1981) and therefore magma mixing between resident and replenishing magmas will be ensured. The increments labelled in Table 8.1 correspond to the liquid compositions plotted in Fig. 8.6. Considering the widely varying incompatible element concentration in the picrites, the relatively restricted range of, and the preservation of any consistencies in, the HFSE concentration with MgO in the LFE group is surprising. The RTF model is able to account for the general trend of HFSE abundances with MgO in the LFE group. The RTF model composition with a MgO content similar to an evolved LFE-group sample (RSS2) is normalized to the model starting composition (LFE primary 2) and are plotted in Fig. 8.9. With the exception of K, Rb, Ba and Sr the model is in good agreement with observed variations. These elements which have a random distribution with MgO in the LFE group

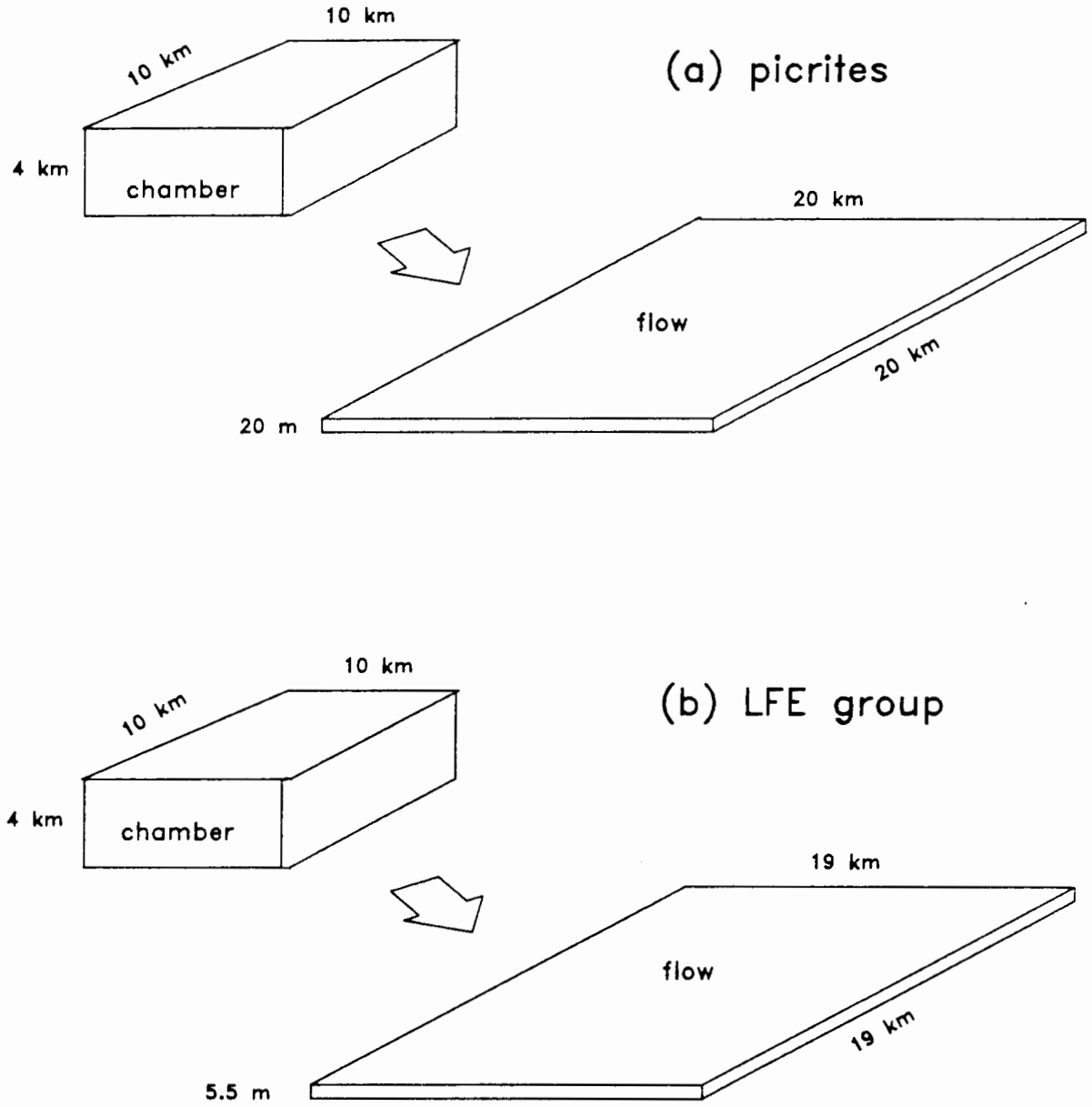

Figure 8.8. A schematic diagram showing the flow volumes expected for a magma chamber of the given size and the RTF model parameters (principally y) chosen:
(a) N. Lebombo picrites; (b) LFE group.

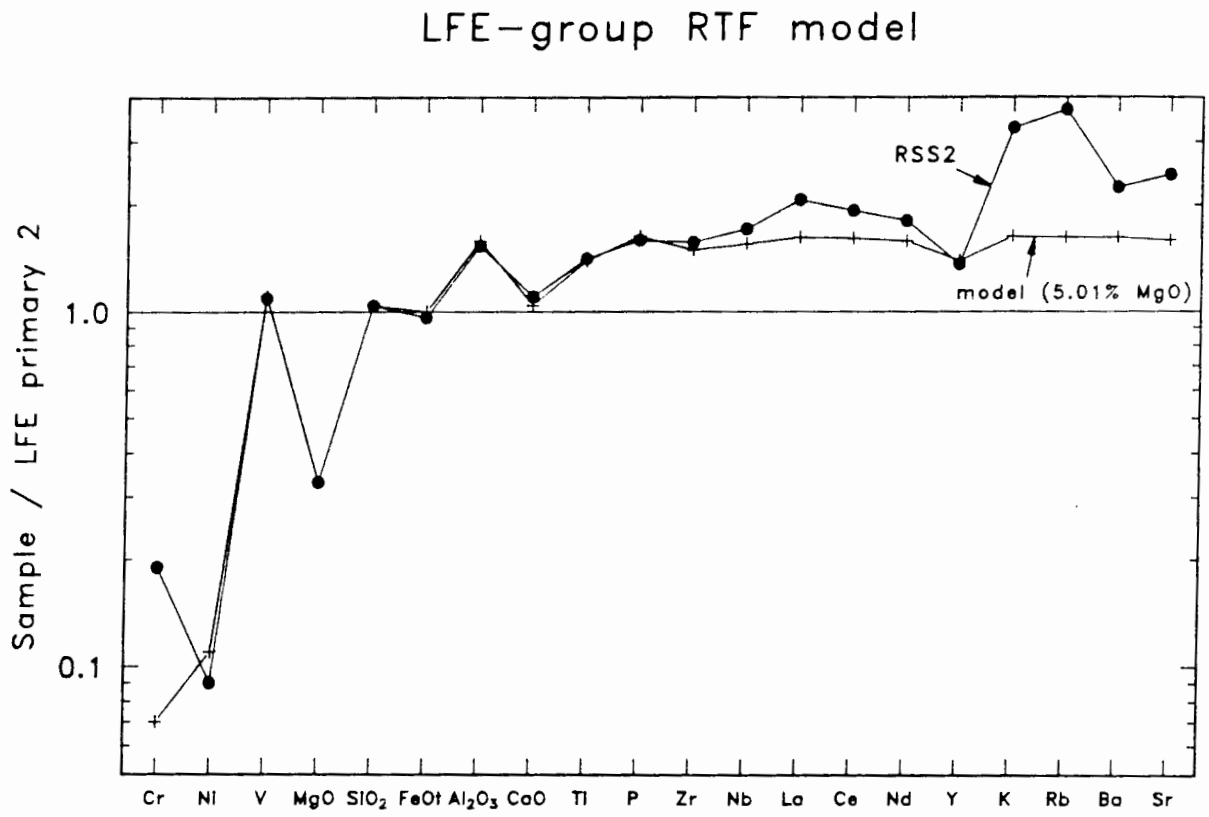

Figure 8.9. Spidergram for LFE-group RTF models, with calculated derivative liquids and an evolved LFE-group sample (RSS2) normalized to the model starting composition. Model parameters are given in Table 8.1. The model shows the consistency of the model composition with the abundances observed in RSS2 with the exception of K, Rb, Ba and Sr.

reflect a similar distribution in the picrites (Fig. 8.6e-h). This distribution is not fully accounted for by any petrogenetic model examined thusfar (e.g. CSF, AFC, RTF) and may reflect a source heterogeneous with respect to these elements (following chapter). In the RTF model chosen, $C_z - C_0$, so Sr-, Pb- and Nd-isotope ratios are unchanged throughout the evolution of a magma chamber. If $C_z - /C_0$ then a heterogeneous source with respect to these ratios is implied.

8.6 APPLICATION TO THE N AND HFE GROUPS

The N and HFE groups characteristically display greater ranges of incompatible element enrichment for similar ranges in MgO than the LFE group. Closed-system fractional crystallization (CSF) models examined were unable to account for these variations, whearas, when coupled with variable granitic assimilation (AFC), the ranges in K_2O, Rb, Sr, SiO_2 and $^{87}Sr/^{86}Sr$ initial ratio in some of the N-group samples were explained (Chapter 7). The range in HFSE (specifically Zr, P and LREE) concentrations observed in the N-group was only accounted for by AFC models if minerals such as zircon and apatite were not residual phases in any granitic melting model (the assimilant). The general increase in HFSE with decreasing MgO in the HFE group is unexplained by petrogenetic models examined thusfar. Furthermore, it was suggested in Chapter 7 that the HFE group may be related to an uncontaminated N-type parent by continued fractionation. Thus it is important to examine whether the differences between the N and HFE groups (specifically for the HFSE) may be explained by RTF mechanisms.

8.6.1 N Group

The estimated thickness of this group in the Sabie River section (500 m) is taken as representative of the average stratigraphic thickness in the central Lebombo. For an average flow thickness of 5 m in the central Lebombo (Chapter 2), this would correspond to n=100 if y is non-zero. Thus, assuming the fractionating assemblage can be manipulated such that major element variations correspond to those observed (e.g. MgO 7-5%) for this group, the incompatible element enrichments predicted for x=.1, y=.001 (z=x+y) and n=100

for various bulk partition coefficents (D) in an RTF magma chamber are:

D	.001	.005	.01	.05	.10	.5
C_B/C_0	11.6	11.3	11.0	8.9	6.9	2.0

Increases in abundance with decreasing MgO are observed for: Zr 100-250 ppm (2.5x), Nb 5-15 ppm (3x), Y 25-45 ppm (1.8x), La 5-20 ppm (4x) and Ba 100-350 ppm (3.5x). Ostensibly therefore the cycle-controlled RTF model can account for these enrichments if the bulk partition coefficients for these elements are less than the values indicated for the required enrichments in the tabulation above. The question remains: can a fractionating assemblage be derived which buffers its major element content sufficiently to generate the observed enrichment in incompatible elements? For the variety of permutations tested, the mineral assemblage and proportions in Table 8.2a calculated using the least-squares mixing model of Le Maitre (1976) for NPRIM satisfy these conditions. The clinopyroxene and olivine compositions used are both analyses from a N-group sample. The magnetite composition used is from a HFE-group sample, which is acceptable as there are no obvious differences between the magnetites analysed for the N and HFE groups (Chapter 4.5). However, it was only by using a relatively sodic plagioclase (An_{42}) that a 'mix' with a sum-of-squares <5 was obtained. There are two inconsistencies in this selected assemblage:
(1) The plagioclase composition is more sodic than all but two of the compositions actually observed for fresh samples of the N group (Fig. 4.8).
(2) Ti-magnetite is necessary as a fractionating phase in the indicated proportions to ensure a low sum-of-squares, but the magnitude of the increase of Ti with decreasing MgO (Fig. 6.3) requires that there is no Ti-bearing opaque phase in the fractionating assemblage (Chapter 6).

Excluding Ti-magnetite from the assemblage and using a plagioclase composition more compatible with observed variations, the mixing model of Le Maitre (1976) is given in Table 8.2b. The proportions suggested by this model are similar to those calculated by least-squares mixing between NPRIM and two N-group samples (RSS169, RSS40), representing the range in "evolved" compositions (Table 8.3). In fact the assemblages in Table 8.3 have a lower proportion of mafic minerals and would therefore not deplete the residual melt in MgO as much as the assemblage in Table 8.2b, i.e. the assemblages in Table 8.3 would buffer MgO more effectively than that in Table 8.2b.

Table 8.2. Calculated mineral mode for a N-group "primitive" composition (NPRIM) using least squares mixing (Le Maitre, 1976).

(a) the "best-fit" solution (using **uncharacteristic** mineral compositions).

Whole Rock composition
NPRIM

	Actual	Estimated	Difference	Mineral	Proportions
SiO_2	51.03	50.88	-.15	ol4E-RSC22	: 4.31%
TiO_2	1.50	1.87	.37	cpx20-RSC22	: 39.28%
Al_2O_3	14.70	14.62	-.08	plag-ideal	: 50.69%
FeOt	11.08	10.85	-.23	mt13A-RSS160	: 4.31%
MgO	7.09	7.20	.11		
CaO	11.00	11.13	.13		
Na_2O	2.90	3.36	.46		
K_2O	.35	.09	-.26		
P_2O_5	.17	0.00	-.17		
Total	99.82	100.00			

Residual sum of squares = .56

(b) the "best-fit" solution (using **characteristic** mineral compositions).

Whole Rock composition
NPRIM

	Actual	Estimated	Difference	Mineral	Proportions
SiO_2	51.03	50.35	-.68	ol4E-RSC22	: 9.01%
TiO_2	1.50	.39	-1.11	cpx20-RSC22	: 42.92%
Al_2O_3	14.70	15.26	.56	plag-ideal	: 48.07%
FeOt	11.08	8.71	-2.37		
MgO	7.09	9.60	2.51		
CaO	11.00	13.70	2.70		
Na_2O	2.90	1.91	-.99		
K_2O	.35	.07	-.28		
P_2O_5	.17	0.00	-.17		
Total	99.82	100.00			

Residual sum of squares = 22.3

Table 8.3. N-group least-squares mixing model initiated from a "primitive" N-group (NPRIM) for different target compositions:

(a) RSS169 (a relatively fresh sample)

	Target Composition RSS169			Starting Composition NPRIM
	Actual	Estimated	Difference	Fractionating Phases
SiO_2	50.63	51.70	1.07	ol4E-RSC22 : 9.53%
TiO_2	2.62	2.71	.09	cpx20-RSC22 : 35.11%
Al_2O_3	12.72	12.04	-.68	plag10-RSC22: 55.37%
FeOt	15.81	14.52	-1.29	
MgO	4.91	5.44	.53	
CaO	9.40	8.61	-.79	
Na_2O	2.54	3.65	1.11	
K_2O	.75	.62	-.13	
P_2O_5	.38	.34	-.04	
Total	99.76	100.00		F-value = .594

Residual sum of squares = 5.43

(b) RSS40 (a relatively altered sample)

	Target Composition RSS40			Starting Composition NPRIM
	Actual	Estimated	Difference	Fractionating Phases
SiO_2	52.59	51.58	-1.01	ol4E-RSC22 : 8.06%
TiO_2	2.16	2.64	.48	cpx20-RSC22 : 42.21%
Al_2O_3	13.49	13.62	.13	plag10-RSC22: 49.73%
FeOt	13.53	13.86	.33	
MgO	5.31	4.98	-.33	
CaO	7.64	8.12	.48	
Na_2O	3.84	3.85	.01	
K_2O	1.03	.63	-.40	
P_2O_5	.24	.34	-.10	
Total	99.83	100.00		F-value = .593

Residual sum of squares = 1.90

Table 8.4. Maximum enrichment test for incompatibles in the N group using an RTF model for various parameters (columns 1 to 4). A closed-system fractional crystallization model is given for comparative purposes (column 5). C_0 for trace elements is set = 1. RSS169 is an evolved N-group dolerite.

	1	2	3	4	5	RSS169
parameters (z=x+y)						
x	.100	.020	.010	.005	.590	
y	.001	.001	.001	.001		
n	13	74	153	340		
%						
SiO2	51.68	51.70	51.69	51.70	51.70	50.63
TiO2	3.10	3.16	3.14	3.16	3.16	2.62
Al2O3	11.58	11.46	11.50	11.46	11.47	12.72
FeOt	15.68	15.86	15.80	15.86	15.84	15.81
MgO	5.09	5.01	5.03	5.01	5.02	4.91
CaO	7.33	7.19	7.24	7.19	7.21	9.40
Na2O	3.98	4.02	4.01	4.02	4.02	2.54
K2O	.72	.74	.73	.74	.74	.75
P2O5	.41	.42	.41	.42	.41	.38
trace element enrichment factors						
A (D=.001)	2.54	2.47	2.44	2.45	2.44	
B (D=.005)	2.53	2.46	2.43	2.44	2.43	
C (D=.01)	2.52	2.45	2.42	2.43	2.42	
D (D=.05)	2.41	2.35	2.32	2.32	2.33	
E (D=.1)	2.29	2.23	2.20	2.21	2.23	
F (D=.5)	1.55	1.52	1.51	1.50	1.56	
G (D=1)	1.00	1.00	1.00	1.00	1.00	
H (D=2)	.50	.53	.54	.55	.41	
I (D=5)	.16	.20	.21	.23	.03	
J (D=10)	.06	.10	.10	.12	.00	

The model is initiated from NPRIM using a fractionating assemblage which is a compromise between the two assemblages predicted in Table 8.3: olivine (ol4E RSC22) 8%, clinopyroxene (cpx20 RSC22) 38%, plagioclase (plag10 RSC22) 54%. This assemblage and the n values selected, ensured that the major element composition of the derivative melt remains within the bounds of a typical basaltic rock for the range 7-5% MgO. The values of x and y are varied as on O'Hara's (1977) fig. 3 (Fig. 8.1 here) for comparative purposes, while z is set at a value equal to x+y (M_{rel}-1). Initial trace element concentrations (C_0) are set at 1. Thus all the hypothetical incompatible trace element (A to F) concentrations represent the degree of enrichment which takes place for elements with various bulk distribution coefficients (Table 8.4). The results are clearly very different from O'Hara's (1977) predictions in Fig. 8.1, i.e. varying the number of cycles (n-set) to produce a similar range in major element content in each model, the incompatible trace element enrichments predicted by each x-y combination for the same D are almost identical (Table 8.4). Varying the mineral proportions in the fractionating assemblage in an attempt to limit the change in major element content does not improve the situation. For example, if the assemblage is set such that MgO is maintained at a constant value (e.g. increase the proportion of plagioclase at the expense of olivine in the fractionating assemblage) then CaO and Al_2O_3 decrease to unrealistic values for no greater enrichment in incompatibles. Also shown in Table 8.4 is the amount of closed-system fractional crystallization necessary (59%) to produce the indicated levels of enrichment which are not much different from the RTF predictions. The maximum possible predicted levels of enrichment in incompatibles with decreasing MgO content is therefore *ca* 2.5xC_0. It is impossible to generate some of the HFSE ranges observed for this group (i.e. Nb, La, Ce, and Nd), and only for Zr when the bulk D_{Zr} is <.05.

A model which proceeds incrementally with fractionating phases consistent with observed variations is also calculated (Table 8.5). The discussion of the selection of the fractionating assemblage for this group in Chapter 6 is equally applicable here. A value of 10 is set for the number of cycles (n) in each increment (7 increments) proposed in Table 8.5 to account for the range in major element content in the N group (e.g. 7.1-4.8% MgO). An average flow thickness of 7.1 m is therefore required to account for the stratigraphic thickness of the N group in the Sabie River section. This is not too different from the measured average of 4.9 m for basaltic flows in

Table 8.5. RTF model for the N group. RTF parameters are set at: x=.01, y=.01, z=.0208, n=10 for each increment.

incr.	%MgO	minerals and proportions (%)	
NPRIM - 1	7.07	ol-KS3	10
		cpx3-RSS35	40
		plag8-RSC22	50
1 - 2	6.71	ol4A-RSC22	10
		cpx3-RSS35	40
		plag8-RSC22	50
2 - 3	6.31	ol4A-RSC22	10
		cpx3-RSS35	35
		plag10-RSC22	55
3 - 4	5.94	ol4E-RSC22	10
		cpx20-RSC22	35
		plag10-RSC22	55
4 - 5	5.63	ol4E-RSC22	10
		cpx20-RSC22	35
		plag4-RSV16	55
5 - 6	5.30	ol4E-RSC22	5
		cpx20-RSC20	40
		plag3-RSC22	55
6 - 7	5.06	ol4E-RSC22	5
		cpx20-RSC22	40
		plag3-RSC22	55
7 - 8	4.79		

Table 8.6. RTF model for the HFE group. RTF parameters are set at x=.02, y=.01, n=10 for each increment.

incr.	%MgO	z	minerals and proportions (%)	
HEPRIM - 1	5.00	.0308	ol4E-RSC22	3
			cpx10-RSS150	36
			plag3-RSS150	47
			mtl3A-RSS160	12
			il11B-RSS160	2
1 - 2	4.64	.0308	ol4E-RSC22	3
			cpx10-RSS150	36
			plag3-RSS150	47
			mtl3A-RSS160	12
			il11B-RSS160	2
2 - 3	4.20	.0308	ol4E-RSC22	3
			cpx13-RSS160	36
			plag5-RSS150	49
			mtl3A-RSS160	10
			il11B-RSS160	2
3 - 4	3.74	.0300	ol4E-RSC22	3
			cpx13-RSS160	35
			plag8-RSS150	49
			mtl3A-RSS160	10
			il11B-RSS160	3
4 - 5	3.21	.0290	ol4E-RSC22	3
			cpx13-RSS160	35
			plag8-RSS150	49
			mtl3A-RSS160	10
			il11B-RSS160	3
5 - 6	2.56			

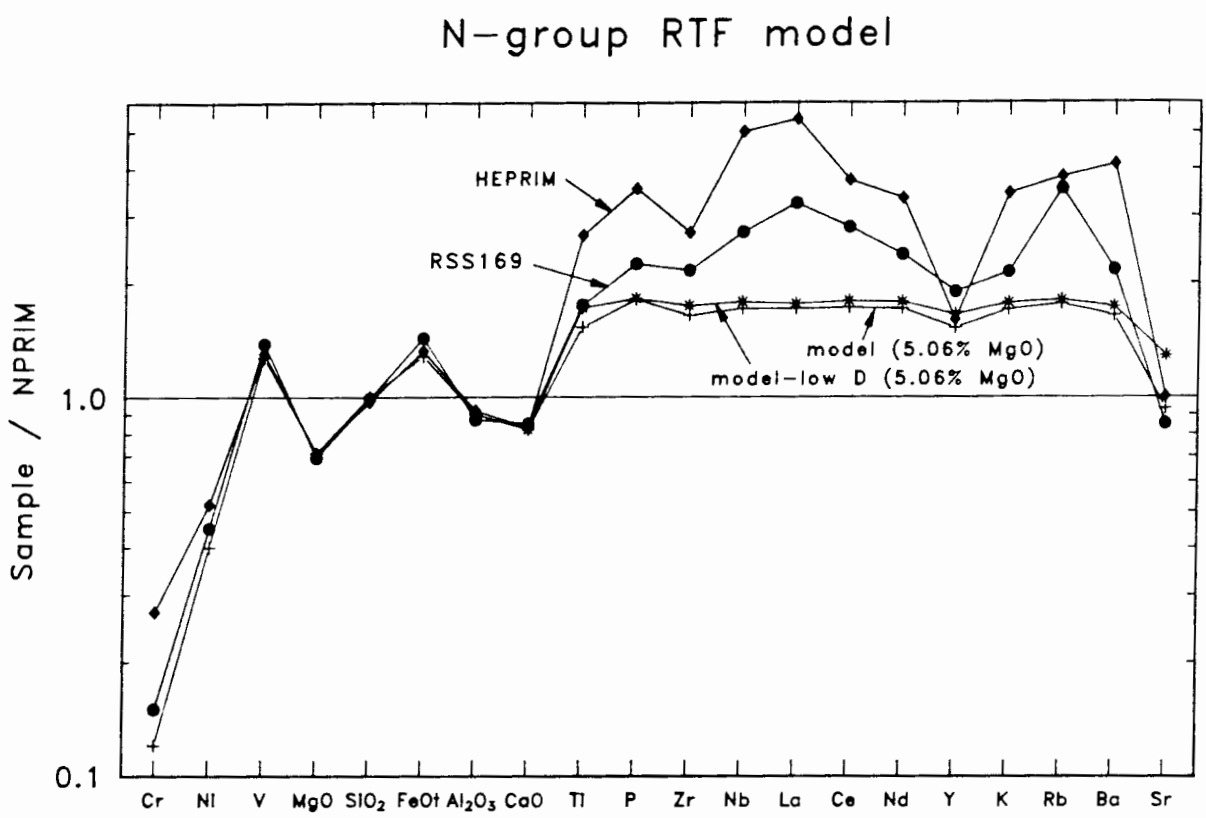

Figure 8.10. Spidergram for N-group RTF models, with calculated derivative liquids and a relatively unaltered and evolved N-group sample (RSS169) normalized to the model starting composition. Model parameters are given in Table 8.5. The model demonstrates the inability of RTF processes to account for the increase in incompatibles in the N group and the even greater increase necessary to reach HFE-group compositions (HEPRIM, a hypothetical unevolved HFE-group composition).

the central Lebombo (Chapter 2). The values of x and y selected ensures that the model major element variation corresponds to the observed variation for the number of cycles used (n-set). The value of z was set to ensure continued growth of the magma chamber, i.e. M_{rel} just >1. The constant values of x, y, z for this model ensure a constant M_{rel} (1.008) and therefore constant M_y (.01). Magma density is extrapolated for MgO = 6% from the two determinations reported in the previous section. Thus a magma chamber of size 4 x 10 x 10 km filled with a magma of density 2.5 g/cm^3 gives rise to a flow of dimensions 7.1 m x 25 km x 23 km which is reasonable.

A RTF model composition and the composition of an evolved Fe-rich N-group sample (RSS169) are plotted normalized to the model starting composition (NPRIM) in Fig. 8.10. Also plotted normalized to NPRIM is the HFE-group model starting composition (HEPRIM) which may represent an evolved N-group composition if the N and HFE groups are related.

The RTF model is consistent with the major element variations in this group (Fig.8.10). The highly variable nature of FeO in this group has been discussed in Chapter 7. It is important to stress that the RTF model in Table 8.5 maximizes the levels of incompatible element enrichment for the major element constraints and the estimates of erupted volumes. The total enrichment observed in some N-group samples with decreasing MgO for P, Zr, La, Ce, Nd, Nb and Y is still unexplained (Fig. 8.10) by any petrogenetic model examined thusfar. This situation is not improved by the selection of lowest possible partition coefficients (given in Table 6.2b).

Although the RTF model is only marginally more efficient in explaining the total range in incompatible elements than closed-system crystallization processes, it is a useful mechanism to explain the absence of any element correlations with stratigraphic height (Cox, 1988). This is a particular problem in the N group (Chapter 5, Fig. 5.3). Cox (1988) investigates what effect random values for x, y and z (within preset ranges) would have on element distribution. A similar model is applied to explain the observed variations in N-group samples occuring in a stratigraphic interval in the Sabie section for which data is most abundantly available (1000-1900 m, Fig. 8.11). However, Cox (1988) uses large values of x and y (.3 and .2 respectively), and an unrealistically high z value (1.0) which gives a two-fold increase in chamber size with 16 cycles and neglects to model major elements. Here the RTF parameters x and z are randomly varied with maximum

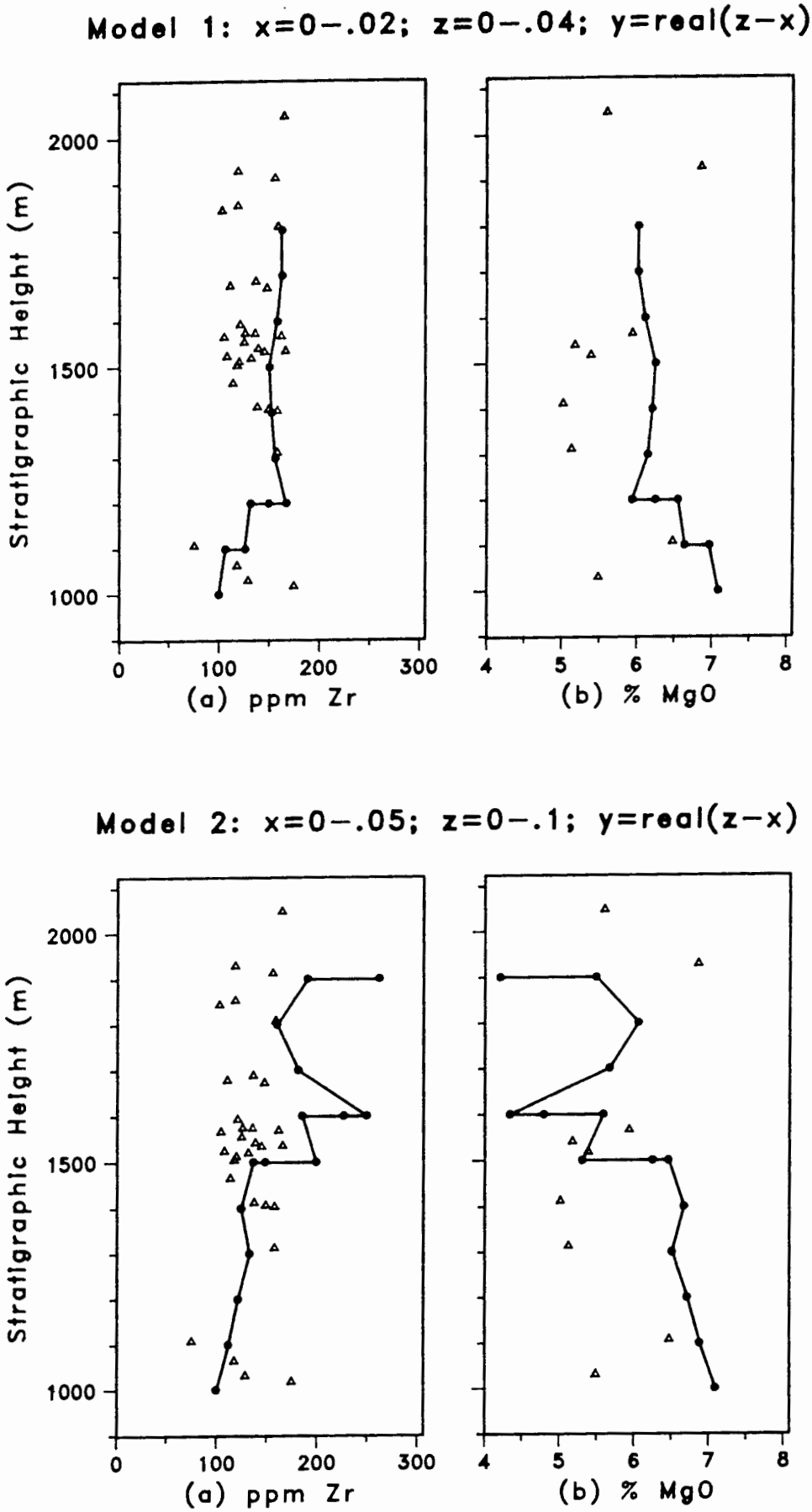

Figure 8.11. Effect of randomly varying x and z values between preset limits, on element abundances in the N group for a specific stratigraphic interval in the Sabie River section (Fig. 5.3). The value of y = z - x when z>x and y = 0 when z<x, to ensure the dynamic stability of the chamber. Each increment represents 10 cycles and where height does not change then y = 0, i.e. 10 cycles corresponds to 100 m of section when y is non zero. Quantitative and semi-quantitative (slab data, when quantitative data is unavailable) are plotted for Zr, and quantitative data only for MgO.

values set considerably smaller than those used by Cox (1988) to be consistent with values used in the model given in Table 8.5, e.g. x is varied in the range 0-.05 (Cox ,1988, used .2-.4). It is reasoned that the value of y will not be random but governed by chamber dynamics (i.e. volume considerations) and y is therefore set equal to z-x for z>x and 0 when z is less than or equal to x (i.e. the real portion of z-x). The "plateaus" on Fig. 8.11 are cases where y=0. The concentration in the replenishing magma is set as NPRIM (Table 6.3) throughout while the composition and proportions of the mineral phases used are as those used to construct the model in Table 8.5. Fig. 8.11 shows that considerable changes in Zr abundance are possible for each increment of 10 cycles and coupled with the other petrogenetic processes affecting the N group is a more than adequate explanation for observed fluctuations with stratigraphic height.

8.6.2 HFE Group

The HFE-group model is initiated from the hypothetical, relatively unevolved composition HEPRIM (Table 6.3). Table 8.6 gives the phase assemblage and proportions in the fractionating assemblage. As with the N-group model, selection is governed by major element constraints and petrographic data (Chapter 6). Mineral compositions and mineral-melt partition coefficients are listed in Tables 6.1 and 6.2 respectively.

The stratigraphic thickness of the HFE group in the central Lebombo is estimated to be 300 m (Chapter 8.1.2). Thus for n=10 for each of the 5 increments in Table 8.6, this represents a total of 50 flows which should average 6 m each to account for the stratigraphic thickness of the HFE group. Again this is similar to the 4.9 m average measured for the central Lebombo and if the flow thicknesses predicted by the model for each group are averaged, a value of 5.3 m is obtained. The values of x and y were set to account for both reasonable estimates of lava volumes and to accommodate the major element variation in the specified number of cycles. The value of z was set to sustain eruption (M_{rel} just >1) until the more evolved compositions in the series (MgO = 3.21%, Table 8.6) were reached when eruption is in the process of ceasing (M_{rel} <1). The constant values of x and y and using an average z-value of .3 gave a M_{rel} value of 1 and therefore M_y = .01. Magma density is extrapolated for MgO = 4% from the

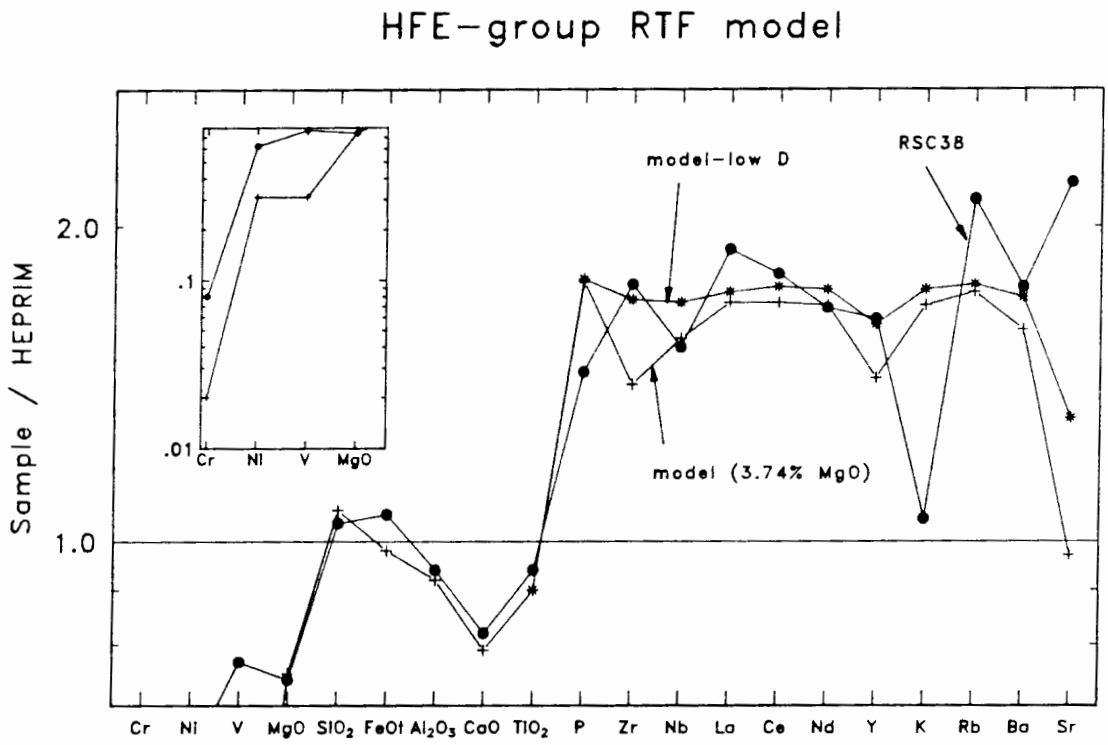

Figure 8.12. Spidergram for the HFE-group RTF model, with calculated derivative liquids and an evolved HFE-group sample (RSC38) normalized to the model starting composition. Model parameters are given in Table 8.6. There is consistency of the model compositions for bulk mineral/liquid partition coefficients between the values given in Table 6.2a and b, with the abundances observed in RSC38, with the exception of K, Rb and Sr.

two determinations reported in the previous section. Thus a magma chamber of size 4 x 10 x 10 km filled with a magma of density 2.46 g/cm^3 gives rise to a flow of dimensions 6 m x 26 km x 26 km, again reasonable in size.

The model composition of 3.74% MgO and an evolved HFE-group sample (RSC38, MgO = 3.71%) normalized to the model starting composition (HEPRIM) are plotted in Fig. 8.12. The presence of fractionating phases which contain TiO_2 as a stoichiometric (essential structural constituent) component (Ti-magnetite, ilmenite) requires Ti to be modelled by a mass-balance and not a Rayleigh fractionation process. For the change in major element content the RTF model can reasonably produce the variation in **all** trace elements with the sole exception of the more random spread in K, Rb, Ba and Sr contents (Fig. 3.3).

8.6.3 N/HFE-group Comparison

A possible relationship **between** the N and HFE groups remains to be considered. It is tempting to suggest such a relationship because of the continuum of compositions observed from one group to the other and the apparent absence of a "less-evolved" suite parental to the HFE group. The existence of a "bimodality" in the N group was suggested in Chapter 7 where it was proposed that some of the N-group samples (i.e. those low in SiO_2 and high in FeO) may be parental to the HFE group while others may interact with a granitic continental crust. At higher MgO compositions (6.5%- 7%) it is impossible to distinguish between these two alternatives, as granitic contamination in an AFC process proceeds with fractional crystallization (Chapter 7) and is therefore less significant in more primitive compositions.

RTF is unable to explain most of the enrichments in incompatibles (except Ti and P) **within** the N group. If some process is invoked to explain the range of incompatible elements within the N group then conceivably the same process could account for the differences between the two groups. The "gap" in TiO_2 content between the two groups (*ca* 1.4%, Fig. 6.3), however, is still unexplained. Thus, RTF models cannot produce the levels of incompatible element enrichment observed with decreasing MgO between the N and HFE groups.

8.7 SUMMARY AND CONCLUSIONS

RTF is able to duplicate the results of closed-system fractional crystallization for the northern Lebombo picrites and the LFE group, account for field observations (e.g. flow thickness) and maintain reasonable magma chamber and flow volumes. The dynamic nature of RTF models suggests they may approximate reality more closely and are therefore preferred to closed-system fractional crytallization.

RTF models are unable in most part to produce the levels of incompatible element enrichment observed in the N group and O'Hara's (1977) and O'Hara and Mathews' (1981) predictions (Figs. 8.1 and 8.2) are not entirely justified in this instance. It is only when the major element composition of the fractionating assemblage matches the composition of the resident magma in a chamber that these predictions may be realised, and this does not appear to be the case. Thus, although the differences in incompatible element content between an unevolved N-group (NPRIM) and the HFE-group (HEPRIM) compositions cannot be produced by RTF models, the increases **within** the HFE group hitherto unaccounted for by simple closed-system fractional crystallization, are explained.

The advantages of the RTF model of O'Hara (1977) and O'Hara and Mathews (1981) as modified here, is that vast magma chambers are not required to generate considerable volumes of basalt as these volumes may be cycled through a chamber of more reasonable dimensions for the same geochemical effect and such a model provides a convenient explanation for the absence of element correlations with stratigraphic height. Thus RTF models produce more flexibility in resultant magma composition than does simple CSF. Conversely the observed geochemical variation and field evidence may be used to constrain the RTF parameters and examine possible magma chamber dynamics.

9. PARTIAL MELTING

9.1 INTRODUCTION

Models of mantle partial melting are now examined in an attempt to explain two aspects of the basaltic rock chemistry of the central Lebombo hitherto unexplained by any other petrogenetic process.

(1) Can the differences between the LFE and N groups be attributed to different degrees of partial melting of a similar source composition? Alternatively, do the two rock types originate from chemically distinct regions in the earth's mantle?

(2) Previous discussions have indicated that the HFE group may be related to a N-type "parent" composition and those N-group samples which appear to be unaffected by contamination with a granitic crust. The HFSE (with the notable exception of Ti) appear to constitute a continuum of values increasing with decreasing MgO from the N to the HFE groups. As shown in the previous chapter, correlations within the HFE-group can be attributed to fractional crystallization in a replenished and tapped (RTF) magma chamber. This is not so for the N group, however, and thus the increase in incompatibles from an unevolved to an evolved N-group composition (or unevolved HFE-group composition, HEPRIM) cannot be generated by fractional crystallization. Partial melting is investigated as a mechanism to account for this difference.

The geochemical and physical characteristics of potential mantle source areas suggested by kimberlite-bourne mantle xenolith data and MORB are reviewed. Radiogenic isotope ratios, because they are insensitive to many petrogenetic effects (see Chapters 6 to 8), are extremely useful in determining likely mantle regimes for central Lebombo basaltic volcanic sources. Theoretical partial melting models in the literature are then reviewed and utilized in order to model the variations observed between the N and LFE groups and within the N group (the two problems outlined above). This enables suggestions to be made regarding the nature of the partial melting process and the source(s) from which the volcanics were derived.

9.2 POTENTIAL MANTLE SOURCE AREAS

Evidence from previous studies on mantle-derived rocks is examined below to determine the nature of mantle sources from which the central Lebombo basaltic rocks may have been derived.

9.2.1 The Structure of the Earth's Mantle

It is not appropriate to give a detailed historical review of the very complex and diverse nature of the Earth's mantle; rather the subject is discussed more briefly with reference to mostly recent reviews. The development of the standard model for the structure of the Earths's mantle has been reviewed by Hofmann (1984): a depleted (with respect to basaltic constituents and incompatible elements) upper mantle (asthenosphere), supposed as the source for MORB, and a primitive (undepleted) lower mantle separated by a pronounced seismic discontinuity at *ca* 650 km. Allegre and Turcotte (1985) suggest that the boundary layer between the upper and lower mantle (650 km discontinuity) is potentially a site for mixing of continental crust, continental lithosphere, depleted mantle (upper) and pristine mantle (lower), and as such may be a major source for observed upper mantle heterogeneities (e.g. ocean island basalts). O'Nions (1987) reviews evidence in favour of chemical layering in the Earth's mantle (implying different convective regimes), and summarizes evidence for the existence of such layering for much of the Earth's history. Recently, Ringwood and Irifune (1988) focussed on the supposed chemical inviolatibility of the 650 km discontinuity and suggested that it may be penetrated by **thick** subducted oceanic crustal plates (a variation on the "megalith model" of Ringwood, 1982; 1985), which eventually become entrained in the lower mantle. The main implication of this model is that mass-balance considerations require an equivalent volume of the of lower mantle material to rise diapirically into the depleted upper mantle (Ringwood and Irifune, 1988). Aside from the entrainment of oceanic crust directly into the upper mantle from a subducting oceanic slab, this provides a mechanism for renewing the upper mantle in basaltic constituents and incompatible elements.

The incompatible element depleted nature of the upper mantle is thought to be complementary to the relatively enriched nature of the continental crust (Gast, 1960). Assuming the Earth accreted with cosmic abundances of at

least the non-volatile elements (the modified 'Chondritic Earth Model' of Gast, 1960), mass balance calculations show that 30-80% of the mantle must be depleted to account for the corresponding enrichment in the continental crust (Norry and Fitton, 1983; Hofmann, 1984). The voluminous nature of MORB in oceanic basalt environments is convincing evidence for the overall depleted nature of the asthenosphere, though detailed studies (Gast *et al.*, 1964; Richardson *et al.*, 1984a; le Roex *et al.*, 1987; le Roex, 1987; Hawkesworth *et al.*, 1987) have established its heterogeneity particularly beneath the Southern and south Atlantic Oceans. Hofmann (1984) divides the models attempting to explain this heterogeneity into those involving oceanic or continental lithosphere re-cycling and those involving internal magmatic or metasomatic differentiation of the mantle. It is likely that both types of process have acted and continue to act to cause the observed chemical diversity.

The above discussion has dealt only with the portion of the upper mantle which is characterized dynamically by convection (the asthenosphere). Recent studies have shown that portions of the upper mantle beneath the continental crust have been isolated from this asthenospheric convection and this has been particularly well documented beneath southern Africa (e.g. Jordan, 1978; Gurney and Harte, 1980; Hawkesworth *et al.*, 1983; Richardson *et al.*, 1984b; Richardson *et al.*, 1985; Boyd *et al.*, 1985; Haggerty, 1986). Geophysical evidence suggests that this sub-continental mantle lithosphere is 100-250 km thick (Jordan, 1978). Evidence from mantle xenoliths, discussed below, has been particularly helpful in documenting the nature of the southern African sub-continental lithosphere below and adjacent to old stable cratonic regions.

9.2.2 The nature of the Upper Mantle beneath southern Africa - evidence from mantle xenoliths.

South Atlantic and south Indian Ocean MORB are obviously important probes into the asthenosphere, while mantle xenoliths carried to the surface by kimberlites may be derived from the sub-continental lithosphere or the asthenosphere. The Karoo basaltic rocks of the central Lebombo may have their origin in one or both of these potential source regions. The classification, occurrence and suggested source for mantle xenoliths is

summarized below along with any implications this may have for the age and structure of the sub-continental lithosphere. A most extensive classification scheme for mantle-derived xenoliths is given in Gurney and Harte (1980, table 1). These xenoliths may, in the first instance, be divided on the basis of their postulated source regions (i.e. P, T conditions based on mineral studies) into two categories:
(1) "cold" peridotites are xenoliths whose mineral chemistry implies relatively low P, T conditions of equilibration. This category includes common coarse peridotites, deformed peridotites with calcic clinopyroxene, modally-metasomatized xenoliths and "cold" megacrysts;
(2) "hot" peridotites reflect higher P,T conditions of formation. This suite includes deformed peridotites with sub-calcic clinopyroxene and "hot" megacrysts.

The more rare and exotic xenolith suites (e.g. MARID rocks and eclogites) have not been included above. The "cold" peridotites encompass a range in modal metasomatism resulting in a spectrum of mineralogies. The classification scheme of Erlank *et al.* (1987) is used to describe these xenoliths:

GP - garnet peridotites; includes those peridotites lacking garnet;

GPP - garnet phlogopite peridotite; primary phlogopite must be present and occasionally small amounts of primary edenitic-pargasitic amphibole are present;

PP - phlogopite peridotite; no garnet but contains primary phlogopite;

PKP - phlogopite K-richterite peridotite; no garnet but contains both phlogopite and the amphibole potassic richterite. Exotic titanates (LIMA) are important accessory minerals in these peridotites (Haggerty *et al.*, 1983).

Erlank *et al.* (1987) estimate the relative abundance of these xenoliths to be: GP=10%, GPP=50%, PP=30% and PKP=10%. The metasomatism which affects this suite of xenoliths involves the introduction of K, Ti, Fe, LREE, Nb, Zr, Hf, Ba, Rb, Sr, Na and H_2O with minor and sporadic enrichment of Ca, Cu and S

(Erlank *et al.*, 1987). Nixon *et al.* (1981) supposed that "hot" xenoliths are more fertile with respect to basaltic constituents (e.g. Al, Ca, Na, Fe and Ti) than the "cold" xenoliths. While this may be true for individual samples (e.g. PHN1611, Nixon and Boyd, 1973) this is not entirely consistent with data incorporated in the set here (Table 9.1, mostly from Jagersfontein and Premier). A comparison of averages in Table 9.1 shows little difference in Al_2O_3 or CaO contents. However, maximum values for basaltic constituents are higher for the "hot" xenoliths than the "cold" xenoliths indicating considerable fertility in basaltic constituents for some individual samples (Table 9.1). Generally, the "hot" xenoliths are consistently more depleted with respect to their incompatible element content (with the exception of Ba in this instance, Table 9.1) relative to "cold" xenoliths. Hereafter the terms "enriched" and "depleted" are used to refer to incompatible element abundances and/or the radiogenic component of isotope ratios only. Only averages for the garnet-bearing "cold" xenoliths are given in Table 9.1 as partial melting models attempting to explain REE variations in the volcanics require garnet in the source (detailed later in this chapter).

The "hot" xenoliths may have been derived from either the asthenosphere, the base of the lithosphere (Boyd and Nixon, 1973), or from zones of deformation around rising diapirs of proto-kimberlitic magma (Gurney and Harte, 1980). The question as to whether they are lithospheric or asthenospheric in origin, however, seems most effectively answered by their Sr- and Nd-isotopic compositions. The relatively low $^{87}Sr/^{86}Sr$ ($\varepsilon_{Sr} < -19.5$) and high $^{143}Nd/^{144}Nd$ ratios ($\varepsilon_{Nd} > +5.4$) in separated minerals belonging to this suite (Shimizu, 1975; Allegre *et al.*, 1982; Richardson *et al.*, 1985; Hops, pers. comm., 1987) indicates a source more akin to that for isotopically depleted MORB, i.e. asthenospheric. The relatively depleted incompatible element character of these xenoliths is also consistent with the generally incompatible element-poor character of MORB (Table 9.1). It is therefore likely that only "cold" xenoliths provide constraints on the age and structure of the sub-cratonic lithospheric mantle. Such evidence is summarized below.

In southern Africa only kimberlites which erupted within the boundaries of the Archaean cratons are diamondiferous (Gurney and Harte, 1980; Fig. 9.1). This implies that the preservation of diamonds in the southern

Table 9.1. Averages of "cold" garnet-bearing and "hot" xenoliths with minimum and maximum values. (all compositions are normalized 100% with total Fe as FeO).

	"cold" xenoliths				"hot" xenoliths			
	min	max	av.	n	min	max	av.	n
SiO_2	38.48	51.00	45.46	48	40.72	48.24	44.57	72
TiO_2	.01	.25	.06	48	.01	.56	.18	72
Al_2O_3	.23	2.47	1.37	48	.21	4.62	1.76	72
FeOt	4.42	8.22	6.77	48	5.51	11.57	8.05	72
MgO	34.41	44.67	43.90	48	37.09	48.50	43.56	72
CaO	.22	5.97	1.35	48	.11	3.72	1.26	72
Na_2O	.01	.46	.16	48	.00	.33	.07	72
K_2O	.00	.96	.16	48	.01	.58	.08	72
P_2O_5	-	.12	.05	48	-	.30	.03	28
CR_2O_3	.23	1.04	.42	48	.13	.57	.29	44
NiO	.20	.34	.30	48	.10	.33	.27	44
Ba	8.6	480	67	48	3.12	486	87.6	15
Sr	6.5	166	56	48	5.44	97.5	31.0	29
Rb	<1.7	38	7	48	2.08	25.5	5.63	20
Zr	2.3	34	13.7	48	2.09	20.7	8.56	28
Nb	<1.5	16	4.5	48	1.04	11.1	3.90	20
Y	<2.0	3.5	2.4	48	1.06	5.19	3.21	9
La	2.62	12.1	5.94	5	.88	3.14	1.60	5
Ce	4.84	19.7	10.8	5	2.10	7.54	3.52	7
Nd	2.37	9.87	5.07	5	.41	1.76	1.25	6
Sm	.394	1.34	.756	5	.23	.74	.44	5
Eu	.109	.355	.244	4	.09	.25	.17	7
Gd	.280	.842	.663	3			.78	1
Dy	.217	.521	.499	2	.27	.95	.61	5
Yb	.12	.216	.171	3	.16	.59	.37	7

Data sources:

"cold" xenoliths: GP + GPP xenolith data with averages weighted in terms of their relative abundances (10:50), from Erlank *et al.* (1987).

"hot" xenoliths: data mainly from Jagersfontein (n=22) and Premier (n=46) xenoliths, from Gurney, pers. comm. (1987); Danchin (1979); Nixon *et al.* (1983); Boyd and Mertzman (1987) and Jagoutz, per. comm. (1987).

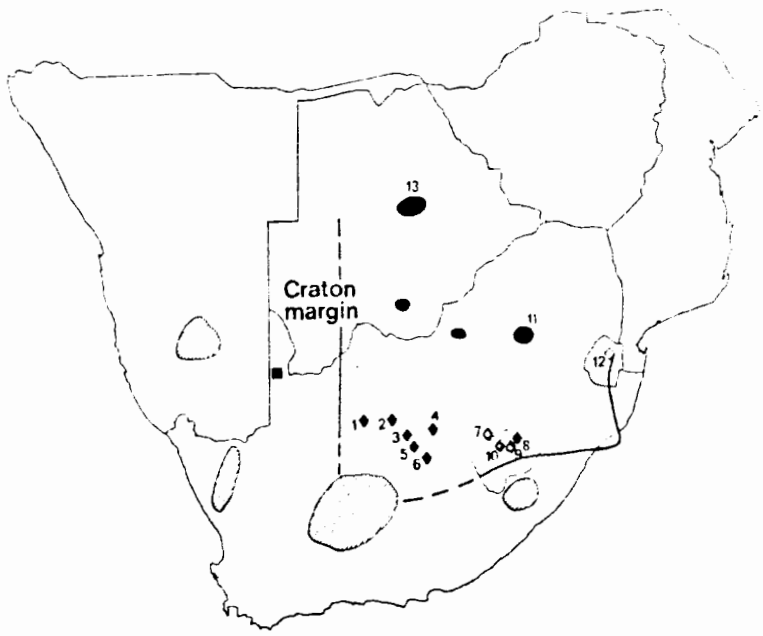

Figure 9.1. Distribution of some kimberlites in southern Africa. The heavy line indicates the southern margin of the Kaapvaal Craton (other lines are boundaries to countries). Shaded areas, with clusters of non-diamondiferous kimberlites; black areas, with clusters of diamondiferous kimberlites; black diamonds, diamond mines; white diamonds, diamondiferous kimberlites; black square, non-diamondiferous kimberlite. Numbered localities are: 1 Finsch; 2 Bellsbank; 3 Kimberley; 4 Roberts Victor; 5 Koffiefontein; 6 Jagersfontein; 7 Monastary; 8 Letseng la Terae; 9 Matsoku; 10 Thaba Putsoa; 11 Premier group; 12 Dokolwayo; 13 Orapa group. There is uncertainty in the south central region both with respect to the position of the craton margin and as to whether the large shaded kimberlite area is wholly non-diamondiferous. From Gurney and Harte (1980).

African mantle is only possible when they are encapsulated in a sub-continental mantle lithosphere inextricably linked to the continental cratons and that this 'linked' mantle must extend at least to the depths of the diamond stability field: >150 km (Haggerty, 1986). In an important study by Richardson *et al.* (1984b) sub-calcic garnet (peridotitic) inclusions in diamonds from 90 Ma old Kimberley and Finsch pipes yielded 3.22-3.3 Ga Sm-Nd and Rb-Sr model ages. This is good evidence for an old (3.2-3.3 Ga), thick (>150 km), stable sub-cratonic lithospheric mantle. The isotope systematics also indicate that diamond formation followed enrichment of sub-cratonic lithospheric mantle and indicated that such mantle has been subjected to enrichment events as far back as the Archaean (Richardson *et al.*, 1984b). Studies by Menzies and Murthy (1980) and Richardson *et al.* (1985) of minerals from common low temperature ("cold") coarse and deformed garnet lherzolite xenoliths from beneath the Kimberley area (within-craton, Fig. 9.1) also revealed trace element and isotopic signatures indicative of a variously enriched (low Sm/Nd, high Rb/Sr) mantle stabilized beneath the craton for up to 3 Ga. The geobarometry and geothermometry of olivine-garnet pairs in diamonds from Finsch (Fig. 9.1) provided further evidence for a thick (150-200 km) "cold" lithosphere (Boyd *et al.*, 1985).

In a complementary study of eclogitic diamond inclusions from Premier kimberlite (Fig. 9.1) and Argyle lamproite (Australia) pipes (both 1.1-1.2 Ga), however, Richardson (1986) obtained Sm-Nd isochron ages of 1.15 and 1.58 Ga respectively. Richardson (1986) concluded that eclogitic diamonds represent a distinctively different genetic origin (to peridotitic diamonds) apparently related in time and space to kimberlite or lamproite magmatism. Thus the eclogite suite is not discussed further.

The thickness of the sub-cratonic root is further established by measurement of the lower heat flow in the interior of southern African Archaean cratons relative to surrounding Proterozoic and younger terraines (Ballard and Pollack, 1987). This enabled estimates of 200-400 km thickness for the cratonic root to be made. Unfortunately Ballard and Pollack (1987) give no estimate for the thickness of the much thinner (non-diamondiferous) surrounding mobile belt lithosphere.

Thus, it appears that the mantle lithosphere sampled by "cold" xenoliths is old, thick and is confined to stable sub-cratonic regions.

9.2.3 Isotopic Characterization of Asthenospheric and Sub-cratonic Lithospheric Mantle

The insensitivity of radiogenic isotope ratios (Pb, Nd and Sr) to geological fractionation (excluding any mixing processes), makes them a powerful tool with which to characterize potential basalt source areas. Such isotope ratios, however, also reflect any changes indicative of open-system conditions. For instance the evidence for granitic contamination in some samples of the N group is convincing and such a process is able to explain much of the range in initial $^{87}Sr/^{86}Sr$ ratios in samples of this group in the central Lebombo (Chapter 7, Fig. 7.8). However, only if a granitic contaminant contains anomalously high Nd contents (*ca* 70 ppm), can the range in initial $^{143}Nd/^{144}Nd$ ratios in the N group be produced. Furthermore, if N-type samples from the southern Lebombo are included it is difficult to explain even the range in $^{87}Sr/^{86}Sr$ initial ratios by contamination with the granitic composition used (i.e. when $^{87}Sr/^{86}Sr_{190\ Ma} = .730$; Fig. 7.8) without assuming a range in "primary" compositions for the N-group: $\epsilon_{Nd} = +5$ to -5; $\epsilon_{Sr} = -8$ to $+20$ (Fig. 9.2b). The "primary" range for the N group on Fig. 9.2b is an estimate of the range in isotope ratios which must exist in their mantle source and may be reflecting the interaction of high-ϵ_{Sr} - low-ϵ_{Nd} and low-ϵ_{Sr} - high-ϵ_{Nd} end-members in these source regions. In the case of the LFE group (and N. Lebombo-Nuanetsi picrites), however, Sr- and Nd-isotope ratios are probably unaffected by contamination with granitic continental crust (Chapter 7) and it is suggested that the data on Fig. 9.2b is directly representative of variations in the mantle source regions of this group.

MORB on Fig 9.2a is represented by data from the South-East Indian Ridge (SEIR, Michard *et al.*, 1986) and South West Indian Ridge (SWIR, le Roex *et al.*, 1983) and is mostly isotopically depleted. Data from the Walvis Ridge have been included as representative of an enriched mantle component in the asthenosphere (Richardson *et al.*, 1984a). Isotopic data from garnet-bearing "cold" (sub-continental lithospheric) xenoliths have also been plotted (data from Erlank *et al.*, 1987.; Menzies *et al.*, 1987). No data for "hot" mantle xenoliths are plotted as only mineral separates are available and these have depleted ($\epsilon_{Nd} > +5.4$; $\epsilon_{Sr} < -19.5$) signatures (referred to earlier). Although the 190 Ma age correction for data plotted in Fig. 9.2a may be misleading because of the Cretaceous/Tertiary age of

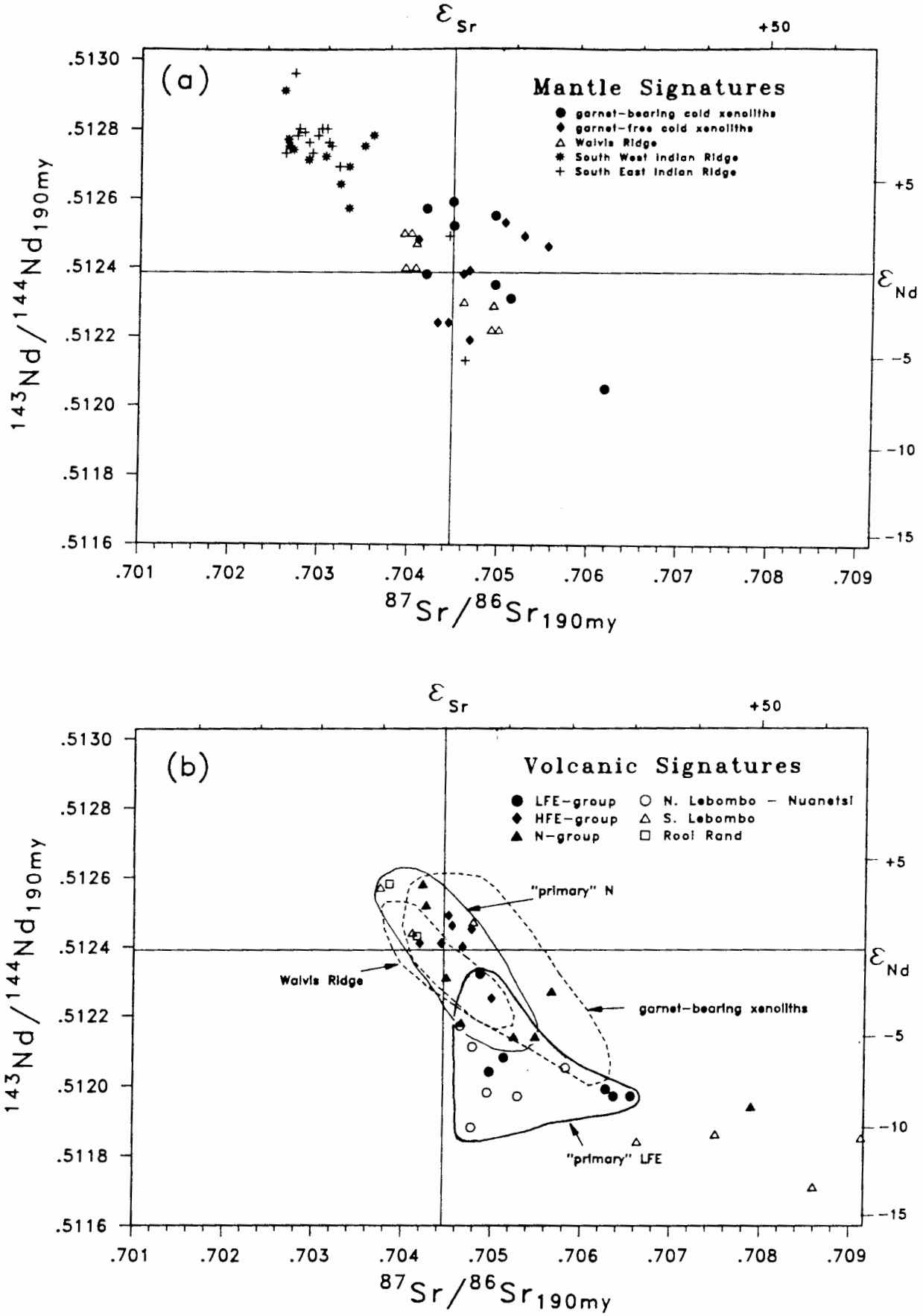

Figure 9.2. (a) Mantle ε_{Sr} and ε_{Nd} signatures determined from garnet-bearing and garnet-free "cold" xenoliths (from Erlank *et al.*, 1987 and Menzies *et al.*, 1987); Walvis Ridge basalts (Richardson *et al.* 1984a); SWIR (le Roex *et al.*, 1983) and SEIR (Michard *et al.*, 1986). (b) Lebombo ε_{Sr} and ε_{Nd} data (from this study; Hawkesworth *et al.*, 1984; and Hawkesworth, pers. comm., 1987).

these rocks, this procedure has been followed in order to estimate mantle values at the age of extrusion of the Lebombo lavas. This substantiates suggestions made earlier the "hot" xenoliths correlate isotopically with MORB (SWIR and SEIR here), thereby implying an asthenospheric source.

The estimates of the Nd- and Sr-isotope ratios of the N group (and HFE group?) source coincide with variations in an enriched asthenosphere (Walvis Ridge transect) and the range encompassed by sub-cratonic lithospheric xenoliths (Fig. 9.2b). The LFE group, however, has an isotopic composition which ranges from within both the Walvis Ridge and sub-cratonic lithospheric xenolith fields to compositions more enriched than the garnet-bearing "cold" xenolith whole-rock analyses (Fig. 9.2b). The only mantle-derived material which has an isotope composition sufficiently enriched in ^{144}Nd to account for the range described by the LFE-group compositions, have been some mantle-derived minerals, e.g. clinopyroxenes with enriched values up to $\epsilon_{Sr} = +40$ and $\epsilon_{Nd} = -15$ (Hawkesworth *et al.*, 1983; Erlank *et al.*, 1987). Thus, either the LFE group contains at least a component from this "enriched" sub-continental lithosphere or represents a region of the asthenospheric mantle hitherto unsampled.

Pb-isotope data for southern African mantle xenoliths are unfortunately almost non-existent. A comparison of Lebombo basic rock Pb-isotopes with those of MORB, Walvis Ridge, Bouvet and the Mesozoic high and low P-Ti tholeiites of the Parana Basin indicate that the central Lebombo rocks do not clearly identify with any of these groups (Fig. 9.3). The complications which may be induced by crustal contamination and mantle source heterogeneity (discussed in Chapter 7) may be responsible and Pb-isotopes and are not considered further.

Thus, on isotopic grounds the N group may correlate with an enriched asthenospheric source or a sub-cratonic lithospheric mantle source as typified by garnet-bearing "cold" xenoliths. The LFE group, however, appears to be most consistent with derivation from a sub-cratonic lithospheric mantle source, or at least contains a significant isotopic component from such a source. Partial melting models using incompatible element variations (specifically the HFSE) are now examined in an attempt to further constrain potential sources.

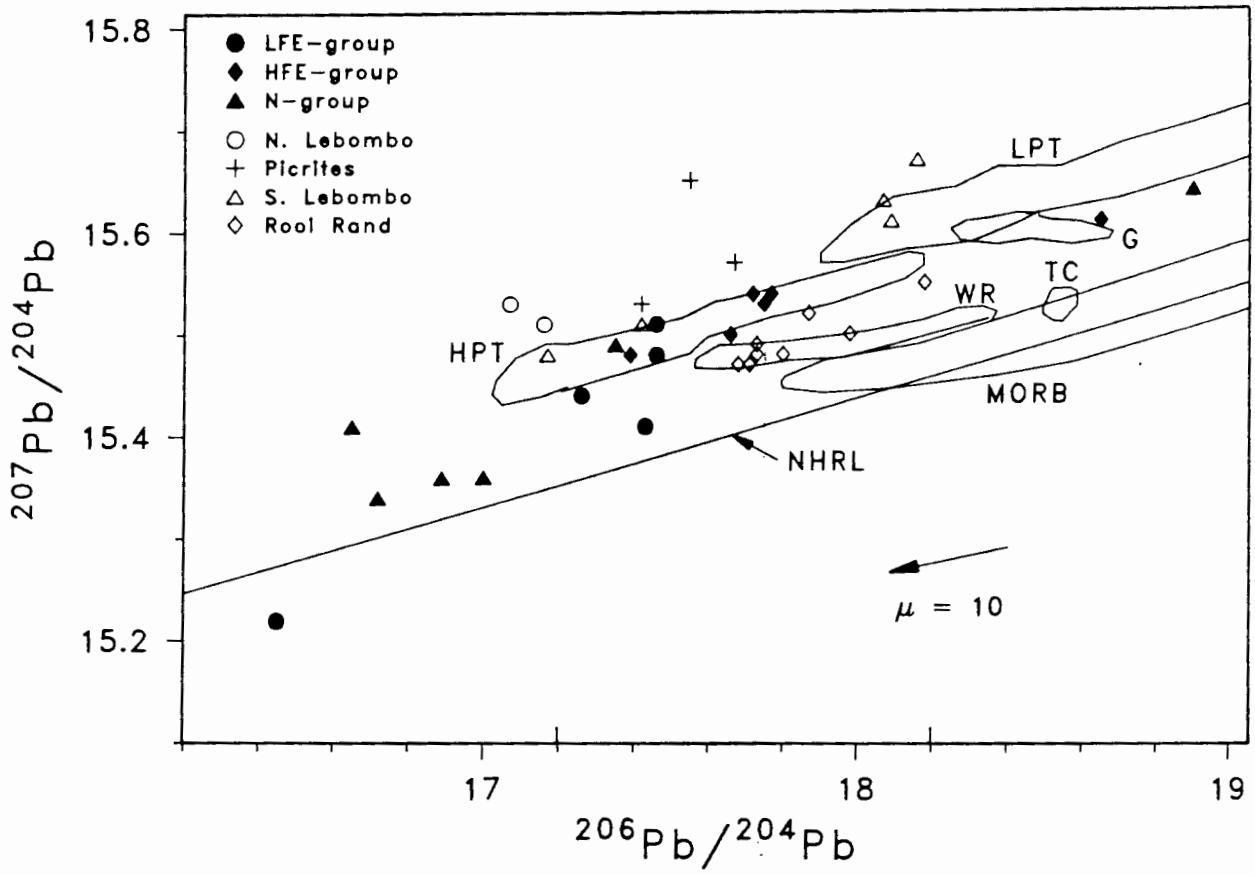

Figure 9.3. Pb-isotope data (present day) for Lebombo basaltic basaltic volcanics (from this study and Betton *et al.*, 1984). Also plotted are fields described by MORB, the Walvis Ridge (WR), Gough (G), Tristan da Cunha (TC) and the high- (HPT) and low- (LPT) phosphorous titanium Mesozoic basalts of the Parana basin (from Hawkesworth *et al.*, 1987). The northern hemisphere reference line (NHRL) is from Hart (1984).

9.3 PARTIAL MELTING MODELS

Emphasis is placed on examining processes controlling the geochemical properties of melt extracted from the mantle rather than the physical mechanisms (e.g. stress relief, Yoder, 1976) of melting.

A general problem with partial melting models is their poorly constrained nature, particularly with respect to source compositions and mineralogy and the dynamic behaviour of the melts in a mantle melting regime. A number of approaches to the problem have been explored. Gast (1968) first showed the potential of using mineral-melt partition coefficients for evaluating trace element behaviour in melt systems. The first mathematical model used by Gast (1968) was that of **equilibrium** or batch melting (modified by Shaw, 1970), where after a certain fraction of melting (F) the melt is removed from the solid and no further melting takes place. For non-modal melting the concentration of a trace element in the melt (C_L) relative to a starting composition (C_0) is given by:

$$C_L/C_0 = 1/[D_0 + F(1-P)] \qquad - (9.1)$$

where: $D_0 = \sum D^i.X^i$, D^i and X^i are the individual mineral-melt distribution coefficients and weight fraction of phases i in the source respectively.

$P = \sum D^i.P^i$, P^i is the weight fraction of phases i in the melting assemblage.

Conversely **fractional** (Rayleigh) melting involves the continuous and complete removal of melt from solid phases. For non-modal melting the equation given in Shaw (1970) is :

$$C_L/C_0 = 1/D_0(1 - PF/D_0)^{(1/P - 1)} \qquad - (9.2)$$

Many variants of these two 'end-member' models have been proposed. **Incremental batch** melting involves the repeated extraction of melts from the same source, each melt increment formed by an equilibrium/batch melting process (Wood, *et al.*, 1979). **Collection** melting on the other hand is a variant of Rayleigh melting where the fractional melts leave the source but gather somewhere in a chamber and mix thoroughly. A model which is more likely to occur in practice is the **continuous** partial melting model of Langmuir

et al. (1977) in which fractions of melt are continuously but incompletely removed from the solid phase as melting proceeds. A liquid is produced by a batch process (i.e. using the equilibrium partial melting equation above) with the source of the next increment being the sum of the residue and the trapped fraction of melt. For the case of non-modal melting equation (9) of Hertogen and Gijbels (1976) is used to model an increment of melting when a phase disappears.

Theoretical studies have placed constraints on partial melting processes. McKenzie (1984) states that melt volumes greater than 3% are unlikely to be retained in any mantle environment. This is supported by Ribe (1985) who maintains that the melt fraction retained is unlikely to exceed a few volume %. Richter (1986), however, in the case of rapid melting (e.g. melting associated with a rising plume) estimates the volume of melt present in the absence of segregation to be of the order of 10%. The voluminous nature of basaltic rocks in the Lebombo generally, however, suggests that this is likely to be associated with a more lengthy and sustained mantle melting event than is the case in plume environments. The melt retention limit (3%) of McKenzie (1984) is thus likely to pertain to the Karoo.

Richter (1986) examines in terms of theoretical melt dynamics, how well the equations for equilibrium partial melting and perfect fractional partial melting predict the degree of melting and original source composition given the different physical situations assumed in their derivation. He concludes that both equations when applied to the chemical properties of the accumulated melt recover the source composition to within a factor of 2, and that the best estimate of F (degree of melting) is obtained using the most incompatible element. Richter (1986), however, assumes that local chemical equilibrium exists, permitting the concentrations in a melt and matrix to be related by a distribution coefficient (D). This is a common assumption of virtually all petrogenetic models and in the absence of experimental data has been assumed throughout this thesis. Richter (1986) also assumes modal melting which, as he points out, is unrealistic but does not alter the conclusion that the concentration in any segregating melt depends upon the relative rates of melting *vs* segregation: if melting is fast relative to segregation, incompatible element concentrations increase with time, whereas if melting matches segregation then concentrations decrease with time.

Richter (1986) warns against interpreting such effects as the influence of a variably metasomatized mantle.

Ribe (1985) states that since melt may interact continuously with the matrix during ascent, melting occurs by equilibrium rather than fractional fusion, but this is not the same as batch melting as the elements partitioned into the melt are quickly dispersed by the migration of melt relative to the matrix. This issue is complicated further by the potential for interaction between this melt and a potentially variable matrix through which it rises (zone refining, Harris, 1957).

The "shape" of mantle-melting regimes has been introduced by O'Hara (1985) as another complicating factor. O'Hara (1985) states that mantle melting regimes are likely to contain areas of low (e.g. margins) and high (e.g. centre) degrees of melting. Assuming a regular mathematical distribution for such variation (e.g. linear, exponential) the relative contribution to the melt from the areas of high and low melting proportions would vary depending on shape: a circular (conical) melting regime would contain a greater component of melt for the peripheral (low degrees) regions of melting than a linear melting zone. O'Hara (1985) cautions against invoking heterogeneous mantle sources to explain the composition of erupted suites before the possible influences of shape of the mantle melting regime have been examined.

The discussion above illustrates the potential complexity of partial melting, models particularly when superimposed on the extra degrees of freedom introduced by a variable major component source composition. Unfortunately there are few direct probes into mantle compositions and evidence is usually interpolated from the compositions of mantle melts and experimental petrology - primarily in the form of phase equilibria studies. Major component mantle phase equilibria are not reviewed here, because of the scope and complexity involved and the scarcity of experimental data. Suffice it to say that the stable mantle assemblage below 18 kb (*ca* 60 km) is garnet peridotite which is generally regarded as the preferred source for basaltic magmas (Yoder, 1976).

The approach used here involves primarily the use of trace element arguments with only a commentary on the viability of the major component of any hypothetical source or melt. Although the numerical integration method

of O'Hara (1985) might better approximate reality, the continuous partial melting model of Langmuir (1977) outlined earlier, is adopted as an acceptable process for modelling trace element behaviour during melting. Given the uncertainty in the modelling, the uncertainty introduced by possible differences in equation, however, is considered to be irrelevant.

9.4 THE N AND LFE GROUPS - PARTIAL MELTING OR MANTLE HETEROGENEITY

Isotopic data indicated that the LFE group is most likely derived from the sub-cratonic lithospheric mantle while the N group may be derived from this mantle or from an enriched asthenospheric source. Another alternative for a N-group source is lithospheric mantle underlying more recent continental terraines. Unfortunately mantle xenolith data from such a region is scant, primarily because of the non-diamondiferous nature of kimberlites sampling these regions, implying thicknesses <150 km. In this section models are examined to test whether N- and LFE-group "primary" compositions may be generated from a similar compositional source by different degrees of partial melting or whether different sources are required. The geochemical and geodynamic validity of these models are discussed. Finally, sources which may produce these two "primary" melt compositions are then compared with data observed for mantle compositions ("cold" and "hot" xenoliths) and models deriving the two groups from these observed compositions are examined.

9.4.1 The Model

The objective initially is to test whether different degrees of continuous partial melting can produce the differences in incompatible elements observed between the LFE and N groups.

The geochemically defined basaltic groups in the central Lebombo have undergone considerable fractionation (Chapters 6, 8) and in some instances significant interaction with continental crust (Chapter 7). The estimation of primary melt compositions made in Chapter 6 (Table 6.9) are used for primary LFE- (LFEPR2) and N-group (NPRIY) melts. It is emphasized that while

the "back-fractionation" of the LFE group to a primary composition is constrained to some degree by observed variations in the N. Lebombo picrites to which they are allegedly related (Chapter 6), no such constraint exists for the N-group primary composition. However, fractionation of picritic magmas at different pressures only has a significant effect on the relative proportions of olivine and orthopyroxene in the fractionating assemblage and the partition coefficients for most trace elements in these two phases are similar (Chapter 6). Thus compositions of a LFE-group "primary" melt calculated using very different proportions of olivine and orthopyroxene in the fractionating assemblage are quite similar (Table 6.9), and the same may be reasonably expected for the N group.

Several REE are used in these partial melting models because of their ability to constrain any source and melting assemblage. The REE contents in the LFE- and N-group "primary" melts in Table 6.9, however, are limited to REE obtained by XRF analyses (La, Ce and Nd). The spectrum of REE data for the "primary " LFE- and N-group compositions was therefore obtained by addition of suggested liquidus assemblages to unevolved LFE- (RSV31) and N-group (RSC32) samples for which SSMS data are available. This data, back-calculated values and basaltic mineral-melt distribution coefficients used are given in Table 9.2. Fractionating assemblages are those used for the closed-system case in Chapter 6. Unfortunately, no judgement on the effectiveness of this calculation for estimating actual N-group "primary" REE compositions can be made because of the absence of a high-MgO equivalent. In the case of the LFE group, however, the coincidence of the REE profiles of the calculated composition and an observed picrite composition (N149, a Nuanetsi picrite basalt from Duncan *et al.*, 1984a) of a similar MgO content (15.3%) is remarkable (Fig. 9.4).

Mineral/melt partition coefficients used for mantle phases are given in Table 9.3. In order to get an indication of the relative degrees of partial melting involved, an expression relating the concentration of an element in the LFE-group (C_L^E) and N-group (C_L^N) "primary" melts may be derived from eqn. (9.1):

$$\frac{C_L^E}{C_L^N} = \frac{C_0^E(D_0 + F_N(1 - P_N)}{C_0^N(D_0 + F_E(1 - P_E)} \qquad - (9.3)$$

Table 9.2. REE element concentrations of hypothetical LFE- and N-primary melts back-calculated from the SSMS data obtained on two 'primitive' basalts of these suites (RSV31 and RSC32). Basaltic mineral-melt distribution coefficients (given below) are taken from Arth (1976) and Hanson (1980). The back-fractionation models described in Tables 6.9 and 6.10 are used.

Distribution Coefficients

	olivine	opx	cpx	plag
La	.0010	.0005	.0400	.1500
Ce	.0010	.0009	.0800	.1200
Nd	.0010	.0019	.1600	.0800
Sm	.0020	.0040	.3000	.0700
Eu	.0040	.0080	.3500	.3400
Gd	.0060	.0160	.4000	.0600
Dy	.0080	.0320	.4000	.0600
Er	.0100	.0640	.4000	.0600
Yb	.0120	.1200	.4000	.0600

Compositions*

	RSV31	LFEPR2	RSC32	NPRIY
Mg#		74.1		72.8
La	53.9	38.1	10.1	6.63
Ce	121	85.6	24.7	16.3
Nd	61.8	43.8	15.0	9.88
Sm	13.4	9.6	4.09	2.72
Eu	3.77	2.71	1.44	.989
Gd	10.2	7.35	4.38	2.94
Dy	8.01	5.78	4.54	3.05
Yb	2.20	1.61	1.87	1.26

*Normalized volatile-free compositions, Fe as FeO. LFEPR2 and NPRIY are 'primary' back calculated compositions for the LFE and N suites repectively (as in Table 6.11).

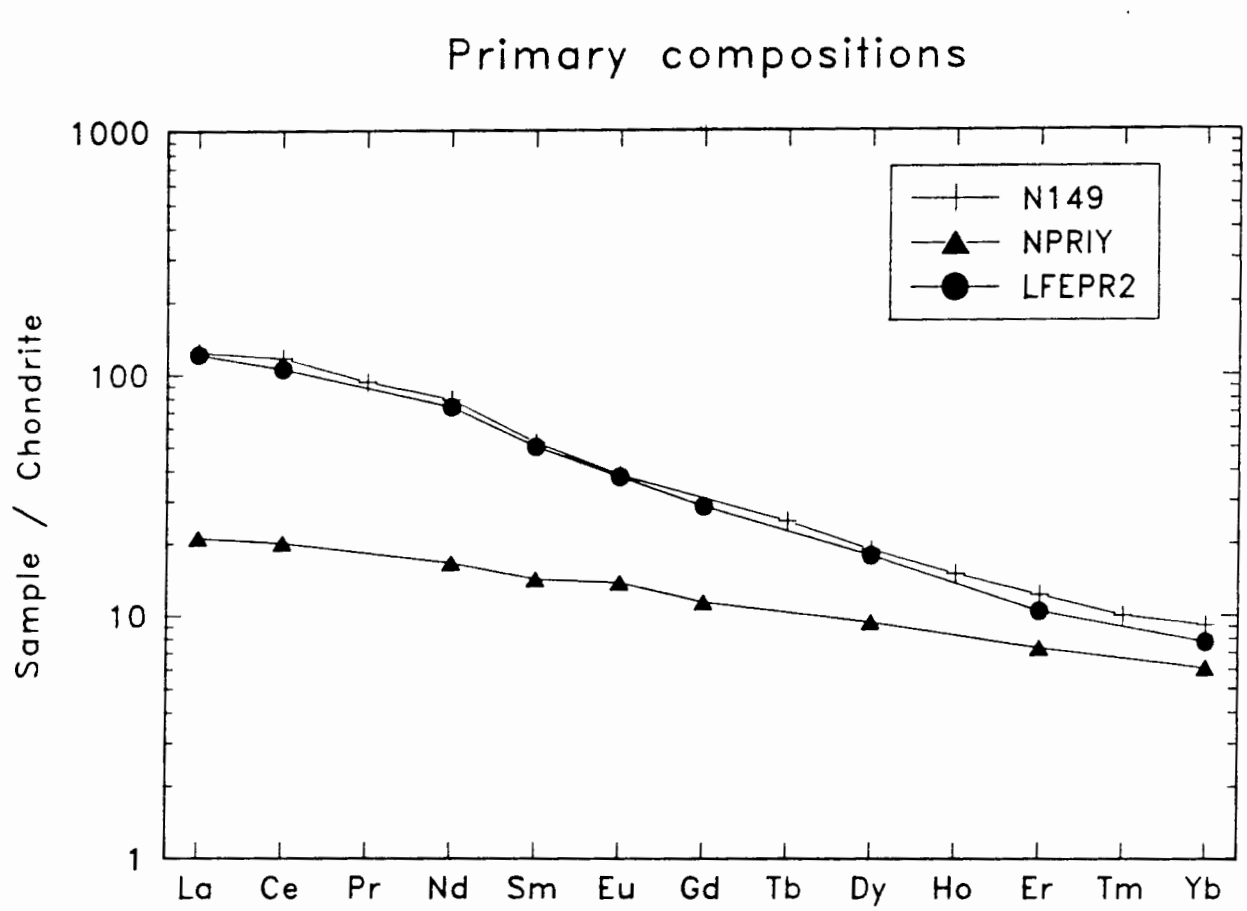

Figure 9.4. REE abundances in calculated "primary" N- and LFE-group compositions (with 15.35% and 15.57% MgO respectively) compared with a Nuanetsi picrite (N149, MgO = 15.3%; from Duncan *et al.*, 1984a).

Table 9.3. Mantle mineral distribution coefficients: with the exception of K, P, Cr (taken from the compilation in Appendix D) and Dy and Er (from Hanson, 1980), values are those used by Cox *et al.* (1984).

	olivine	opx	cpx	garnet	ilmenite	phlogopite
Ti	.0100	.1000	.3000	.3000	(50.0)	.9000
P	.0010	.0010	.0100	.0100	.0500	.0100
Zr	.0010	.0300	.1000	.3000	.3000	.6000
Nb	.0010	.1500	.1000	.1000	.8000	1.0000
Y	.0010	.0400	.3000	2.0000	.0100	.0300
La	.0002	.0010	.0690	.0100	.0100	.0300
Ce	.0005	.0030	.0980	.0210	.0100	.0300
Nd	.0010	.0065	.1800	.0800	.0100	.0300
Sm	.0013	.0100	.2600	.2170	.0100	.0300
Eu	.0015	.0130	.3100	.3200	.0100	.0300
Gd	.0015	.0160	.3000	.4980	.0100	.0300
Dy	.0015	.0220	.3000	1.0600	.0100	.0300
Er	.0015	.0300	.3000	2.0000	.0100	.0300
Yb	.0015	.0490	.2800	4.0300	.0010	.0300
K	.0010	.0010	.0500	.0100	.0100	(40.0)
Rb	.0010	.0010	.0500	.0100	.0100	3.0000
Ba	.0010	.0010	.0500	.0100	.0100	6.0000
Sr	.0010	.0100	.2000	.0100	.0100	.1000
Ni	4.4800	1.1200	.7800	1.1200	.0100	.1000
Cr	.6000	5.0000	12.0000	3.4000	6.0000	2.0000

Table 9.4. Mantle mineral compositions used in the petrological melt models (normalized to 100%, Fe as FeO).

	olivine (1)	opx (1)	cpx (2)	garnet (1)	ilmenite (3)	phlogopite (2)
SiO_2	41.20	57.78	55.92	43.61	.07	43.96
TiO_2	.00	.03	.15	.10	49.62	.60
Al_2O_3	.00	.72	2.76	21.85	.63	14.81
FeOt	8.35	5.14	2.58	7.80	41.16	3.31
MgO	50.34	35.76	16.22	21.15	8.28	26.73
CaO	.02	.35	19.67	5.08	-	.00
Na_2O	-	.12	2.62	.01	-	.05
K_2O	-	.00	.00	-	-	10.08
Mg/(Mg+Fe)	91.5	92.5		82.9		

(1) Erlank (pers. comm., 1987) GPP mineral averages normalized Ni and Cr free: olivine n=32, orthopyroxene n=33, garnet n=37.
(2) Erlank *et al.* (1987) GPP mineral averages normalized Ni and Cr free: clinopyroxene n=33, phlogopite n=44.
(3) Ilmenite from sample 2050A from Kao Pipe, Boyd and Nixon (1973).

(symbols as for eqn. 9.1).

Choosing an element for which the mineral/melt partition coefficients are well known and low for all possible mantle phases (e.g. La) will result in P and D_0 approximating 0. Assuming both types are derived from the same source ($C_0^N = C_0^E$) then eqn. (9.3) reduces to:

$$\frac{C_L^E}{C_L^N} = \frac{F_N}{F_E}$$

Thus for La: $F_N/F_E = 5.7$; i.e. if N is derived by 26% melting, E should approximate 4.6% melting. The relative differences involved should be bourne in mind in the ensuing discussion.

The approach adopted for a fuller set of elements, is to fix the source composition (C_0) to produce the N-group "primary" melt **exactly** at a high degree of melting (two cases, namely 15% and 26% melting are investigated here) and then melt this source at lower degrees to see whether the LFE-group "primary" composition (LFE primary 2) may be produced at reasonable degrees of melting. These models are presented in Tables 9.5 and 9.6. Although the composition of the N-group "primary" melt is less well known than in the case of the LFE-group "primary" melt, the model is conducted in this manner because the variations in LILE and Sr in the N group are more coherent than the LFE group (and N. Lebombo picrites). The N group thus places a more effective constraint on the source LILE and Sr composition than the LFE group.

The source mineral phases and modes used in the model calculations are reasonably typical of those observed for garnet-bearing "cold" xenoliths. Mathias *et al.* (1970) and Maaløe and Aoki (1977) suggested average modes of 62-64% olivine, 27-30% orthopyroxene, 5-6% garnet and 2-3% clinopyroxene for "cold" garnet lherzolites sampled by southern African kimberlites. Ilmenite and phlogopite are included as repositories for Ti, Nb, Zr and K respectively. The inclusion of phlogopite assumes a mantle source shallower than *ca* 170 km (the high pressure stability limit of phlogopite, Eggler and Wendlandt, 1979). Below these depths, K either exists in a fluid phase on grain boundaries (Erlank, 1970; Erlank, 1973) in which case it will partition almost totally into a melt, or resides in high-K clinopyroxene (Erlank, 1973; Rickard *et al.*, 1986). Mineral melting modes are subject to the major component constraints of the observed melt and the initial (source) mode is

Table 9.5. Continuous melting model (Langmuir *et al.*, 1977) for low degrees of melting: 2.5% and 15%. Boths models are initiated from C_0.

Mineralogy

Mineral	Initial wt. fraction	Weight fractions entering liquid (1)	(2)	(3)	(4)
olivine	.6000	.0100	.0100	.0200	.0200
orthoproxene	.3032	.2640	.2000	.1700	.4000
clinopyroxene	.0600	.3000	.2800	.2600	.5800
garnet	.0350	.2300	.4100	.5500	
ilmenite	.0035	.0460	.1000		
phlogopite	.0043	.1500			

Phase exhaustions at: 2.87% melting for phlogopite,
5.11% melting for ilmenite and
8.84% melting for garnet.

Melting Parameters

	low degrees	high degrees
Initial degree of melting:	.5%	1%
Final degree of melting:	2.5%	15%
Melting increment:	.5%	2%
Amount of melt held in the residue:	.5%	1%

Amount of Minerals in the melt for:

	2.5% melting	15% melting
olivine	.0100	.0166
orthopyroxene	.2640	.2869
clinopyroxene	.3000	.4021
garnet	.2300	.2420
ilmenite	.0460	.0238
phlogopite	.1500	.0287

Model Compositions

	NPRIY	N model	C_0-set	LFEPR2	LFE model
SiO_2	48.80	51.56	47.31	51.44	49.07
TiO_2	1.25	1.29	.198	2.39	2.44
Al_2O_3	11.54	7.04	1.21	8.73	8.29
FeO+MgO	26.97	29.31	50.06	26.61	30.46
CaO	8.83	9.24	1.48	8.10	7.16
Na_2O	2.28	1.09	.19	1.52	.82
K_2O	.29	.289	.0433	.784	1.51
(Ti)	7488	7583	1187†	14300	(5532)
P	621	621	85.2	1540	3780
Zr	83	83	11.6	279	260
Nb	4.1	4.1	.632	16.1	8.4
Y	21	21	2.98	28	27.5
La	6.63	6.63	.925	38.1	37.7
Ce	16.3	16.3	2.27	85.6	84.7
Nd	9.88	9.88	1.37	43.8	40.7
Sm	2.72	2.72	.378	9.60	8.75
Eu	.989	.989	.137	2.71	2.74
Gd	2.94	2.94	.410	7.35	7.36
Dy	3.05	3.05	.428	5.78	5.73
Er	1.56	1.56	.223	2.22	2.10
Yb	1.26	1.26	.182	1.61	1.05
(K)	2433	2571	359†	6508	(4966)
Rb	4.1	4.1	.573	14.2	20.5
Ba	82	82	11.5	385	363
Sr	198	198	27.5	479	814
Ni	1048	738	2300*	742	738
Cr	310	993	2200*	730	830

† set according to content in source mineralogy
* set to give credible values for the LFE primary model melt

Table 9.6. Continuous melting model (Langmuir *et al.*, 1977) for high degrees of melting: 5% and 26%. Both models are initiated from C_0.

Mineralogy

Mineral	Initial wt. fraction	Weight fractions entering liquid (1)	(2)	(3)	(4)
olivine	.6000	.0100	.0100	.0200	.0200
orthoproxene	.2250	.2640	.2000	.1700	.4300
clinopyroxene	.0913	.3000	.2800	.2600	.5500
garnet	.0600	.2300	.4100	.5500	
ilmenite	.0062	.0460	.1000		
phlogopite	.0075	.1500			

Phase exhaustions at: 5.00% melting for phlogopite,
9.11% melting for ilmenite and
15.59% melting for garnet.

Melting Parameters

	low degrees	high degrees
Initial degree of melting:	1%	1%
Final degree of melting:	5%	26%
Melting increment:	.5%	3%
Amount of melt held in the residue:	1%	1%

Amount of Minerals in the melt for:

	5% melting	26% melting
olivine	.0100	.0165
orthopyroxene	.2640	.2969
clinopyroxene	.3000	.3869
garnet	.2300	.2462
ilmenite	.0460	.0246
phlogopite	.1500	.0288

Model Compositions

	NPRIY	N model	C_0-set	LFEPR2	LFE model
SiO_2	48.80	51.47	45.77	51.44	49.07
TiO_2	1.25	1.33	.339	2.39	2.44
Al_2O_3	11.54	7.10	1.84	8.73	8.29
FeO+MgO	26.97	29.59	48.40	26.61	30.46
CaO	8.83	8.96	2.19	8.10	7.16
Na_2O	2.28	1.05	.27	1.52	.82
K_2O	.29	.290	.0756	.784	1.51
(Ti)	7488	8529	2038*	14300	(6078)
P	621	621	155	1540	3620
Zr	83	83	20.2	279	293
Nb	4.1	4.1	1.00	16.1	11.5
Y	21	21	4.96	28	28.9
La	6.63	6.63	1.65	38.1	36.3
Ce	16.3	16.3	4.04	85.6	84.1
Nd	9.88	9.88	2.41	43.8	42.3
Sm	2.72	2.72	.661	9.60	9.37
Eu	.989	.989	.239	2.71	2.97
Gd	2.94	2.94	.708	7.35	7.94
Dy	3.05	3.05	.727	5.78	6.09
Er	1.56	1.56	.368	2.22	2.17
Yb	1.26	1.26	.298	1.61	1.07
(K)	2433	2570	628*	6508	(7299)
Rb	4.1	4.1	1.02	14.2	20.6
Ba	82	82	20.4	385	378
Sr	198	198	48.5	479	864
Ni	1048	745	2300*	742	746
Cr	310	1134	2200*	730	826

* set according to content in source mineralogy
* set to give credible values for the LFE primary model melt

constrained by the melting mode, e.g. there must be sufficient garnet and clinopyroxene to produce a picritic melt after 15% and 26% melting. The amount of ilmenite and phlogopite in the melt is constrained by the TiO_2 and K_2O contents of NPRIY respectively, as these phases contain most if not all of these elements. Assuming that all phlogopite and ilmenite in a source are consumed at high degrees of melting (15% and 26% in this instance), the concentration of these elements in the melt (NPRIY) may be used to constrain source compositions:

For example, in the case of the model described in Table 9.6:

	N-primary (NPRIY)	wt. fractions ilmenite and phlogopite		source concentration
		melt mode	source mode 26% melting	ppm (oxide %)
	ppm (oxide %)			
Ti	7488 (1.25)	.0252	.0065	1948 (.325)
K	2433 (.29)	.0288	.0075	628 (.075)

The trace element content of NPRIY has been used above and mantle mineral modes are calculated using the averages from GPP nodules of Erlank *et al.* (1987, Table 9.4). The lower ilmenite component in the melt and source modes in Table 9.6, when compared to the prediction above, is necessary as clinopyroxene makes a contribution to Ti abundance (Table 9.4). The amount of phlogopite in melt and source modes, however, is quite accurately constrained by the K content of the melt (NPRIY) as K is not significant in any other mantle phase used (Table 9.4). Therefore, the concentrations of Ti and K in the source are set at 2038 ppm (1948 ppm + contributions by other minerals) and 628 ppm respectively.

There is some uncertainty attached to the back-calculated Ni and Cr contents in NPRIY as both these elements are critically dependent upon the relative amounts of olivine and orthopyroxene fractionation as well as the partition coefficients used (Chapter 6, Table 6.2). Cr and Ni are two of the few elements to show some consistency in the N. Lebombo picrites (suggested as LFE-group parent rocks). Thus C_0 values are set to produce the concentrations observed in a LFE-group "primary" melt at lower degrees of partial melting , i.e. at 15% MgO: Cr 700-900 ppm and Ni 700-850 ppm (Fig 6.9).

As is the case for the N-group "primary" melt, the melting mode at lower degrees of melting producing a LFE-group "primary" composition is constrained by the need to produce a picritic melt. Furthermore, it is not possible to produce a melt at these lower degrees of melting containing 14300 ppm Ti (2.39% TiO_2, LFEPR2, Table 6.9) without retaining some ilmenite in the residue. Thus, at low degrees (2.5% and 5% here) of melting 2.39% TiO_2 in a melt corresponds approximately to 4.6% ilmenite in the original source (allowing for some contribution to TiO_2 content by other phases). Therefore, in these models ilmenite only disappears in the residue after 5.11% and 9.11% melting (Tables 9.5, 9.6). Whether this is petrogically realistic cannot be stated. It is unrealistic to use the K_2O content in the LFE-group "primary" composition to constrain the amount of phlogopite in the melt, as K (and Rb and Ba) has a random distribution with MgO in the LFE-group and N. Lebombo picrites (Fig. 6.9). A reasonable explanation of this variation could be a variable phlogopite component in the melt at these low degrees of melting. For this reason the amount of phlogopite in the melt at low degrees of melting is set to ensure its disappearance as a residual phase at roughly the same degree of melting which produces the LFE-group "primary" melt (Tables 9.5, 9.6).

9.4.2 Validity of the Model

Where elements are present as essential structural constituents in mantle minerals present in the residue their distribution between minerals and melt will not obey Henry's law and a mass balance approach must be used, i.e. the proportion of a mineral in the melt is multiplied by the abundance of the oxide of interest in that mineral. This is true for K and Ti at low degrees of melting (where phlogopite and ilmenite are present as residual phases). The case at higher degrees of partial melting is more ambiguous, but it is contended that the major influence on melt composition will be the fractions of these elements contributed to the melt by the minerals in which they are structural constituents. Thus, K and Ti are modelled using a mass balance approach throughout. It is found that degrees of melting of 2.5% and 5% (when NPRIY is derived by 15% and 26% melting of the same source) produced compositions close to that observed for LFE primary 2 (LFEPR2) given in Tables 9.5 and 9.6. In all instances the partial melt increment is set at values <3% to be consistent with McKenzies' (1984) findings (see earlier).

In the light of a further study by McKenzie (1985) which postulated the extraction of a 1% picritic melt from the mantle, no problems are anticipated in extracting the lower melt proportions in these models.

The major element composition of the melt is calculated using the proportions of each mineral in the accumulated melt and the average GPP mineral compositions in Table 9.4. These compared favourably to the observed concentrations in LFE-primary 2 (LFEPR2) and N-primary (NPRIY, Tables 9.5, 9.6), notwithstanding the fact that the actual mineral compositions may be slightly different from the averages used in Table 9.4. Ni and Cr have been set to give realistic values for a LFE-group "primary" melt (see above) and the consistent variation of Al_2O_3 with these elements in the picrites may be used to gain an idea of the effectiveness of the major element model (Fig. 9.5). In both models (2.5% and 5% melting) the melt Cr (*ca* 840 ppm) and Ni (*ca* 725 ppm) concentrations are compatible with values in LFEPR2 (Tables 9.4, 9.5) and imply Al_2O_3 contents of 8-9% in the melt (from Fig. 9.5), which agrees with the abundance calculated (8.29%). Furthermore, an Al_2O_3 content of 8-9% in the melt would correspond to a Y content of 27-30 ppm in the "primary" LFE-group melt (Fig. 9.5).

Allowance for the partitioning of Fe and Mg between melt and the residue by ferromagnesium minerals such as olivine and pyroxene must be made in any melting model. The approach used by Cox *et al.* (1984) is used here; the Fe and Mg (as oxides) contents are simply added together. As is pointed out by Cox *et al.* (1984), the simplifying assumption is that Fe and Mg are the only major elements differentially partitioned in this manner.

The REE provide an effective constraint on mineral melting modes (particularly garnet). The REE content of the sources plotted in Fig. 9.6 are the compositions which give a melt of N-primary (NPRIY) composition exactly upon 15% and 26% melting. Also plotted on Fig. 9.6 are the LFE-group "primary" composition (LFEPR2) and model compositions calculated by the 2.5% and 5% melting of the sources defined to yield NPRIY at 15% and 26% melting respectively. The coincident nature of the 2.5% and 5% melts with LFEPR2 is encouraging insofar as the mineral modes chosen for the models (Tables 9.5, 9.6) are consistent with observed REE variations. The REE modelling is obviously consistent with the derivation of both basalt types by different degrees of partial melting of the same compositional source.

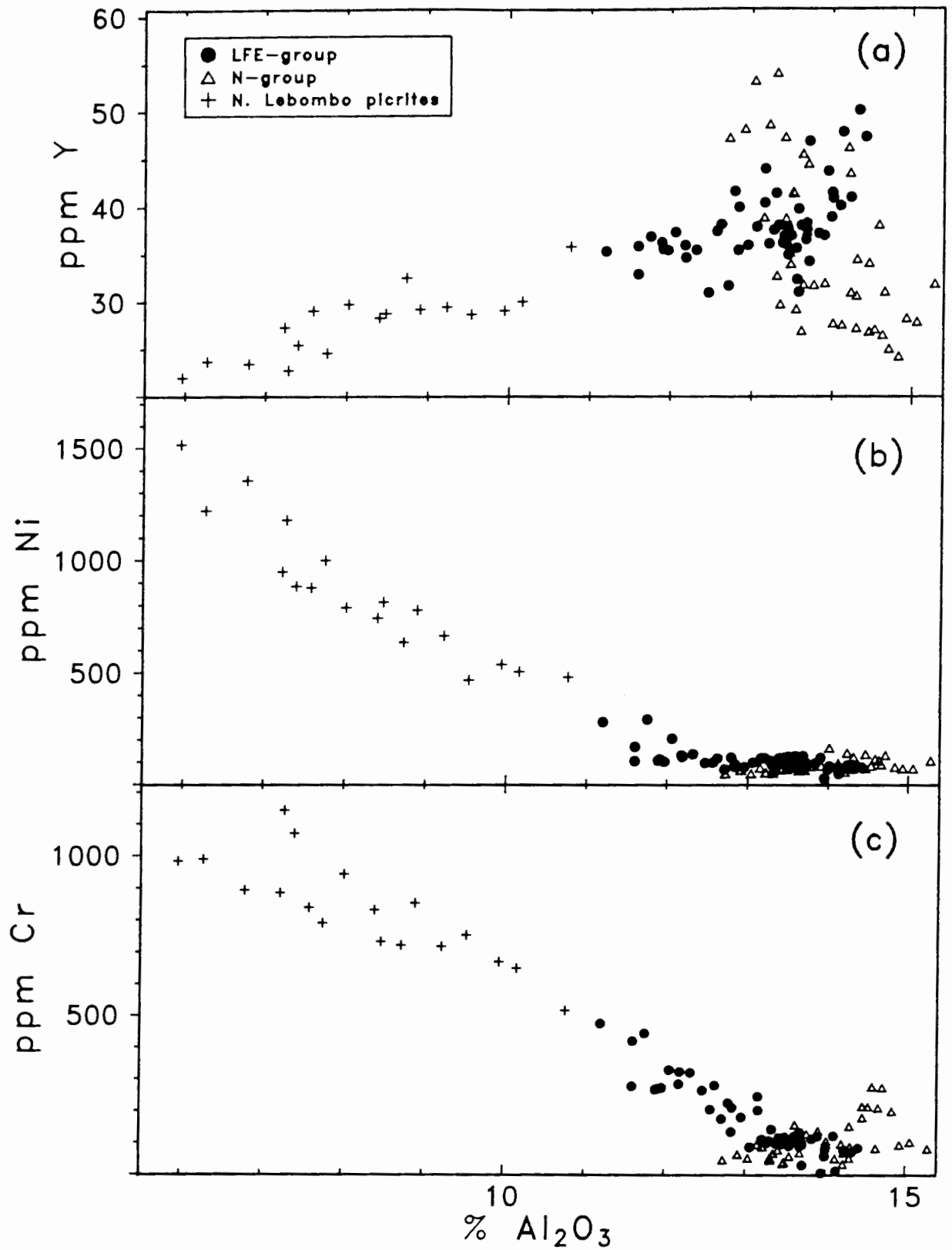

Figure 9.5. Al_2O_3 *vs* Cr, Ni and Y for N and LFE groups and N. Lebombo picrites (picrite data from Duncan *et al.*, 1984a) (all Fe as FeO, data normalized to 100% volatile-free).

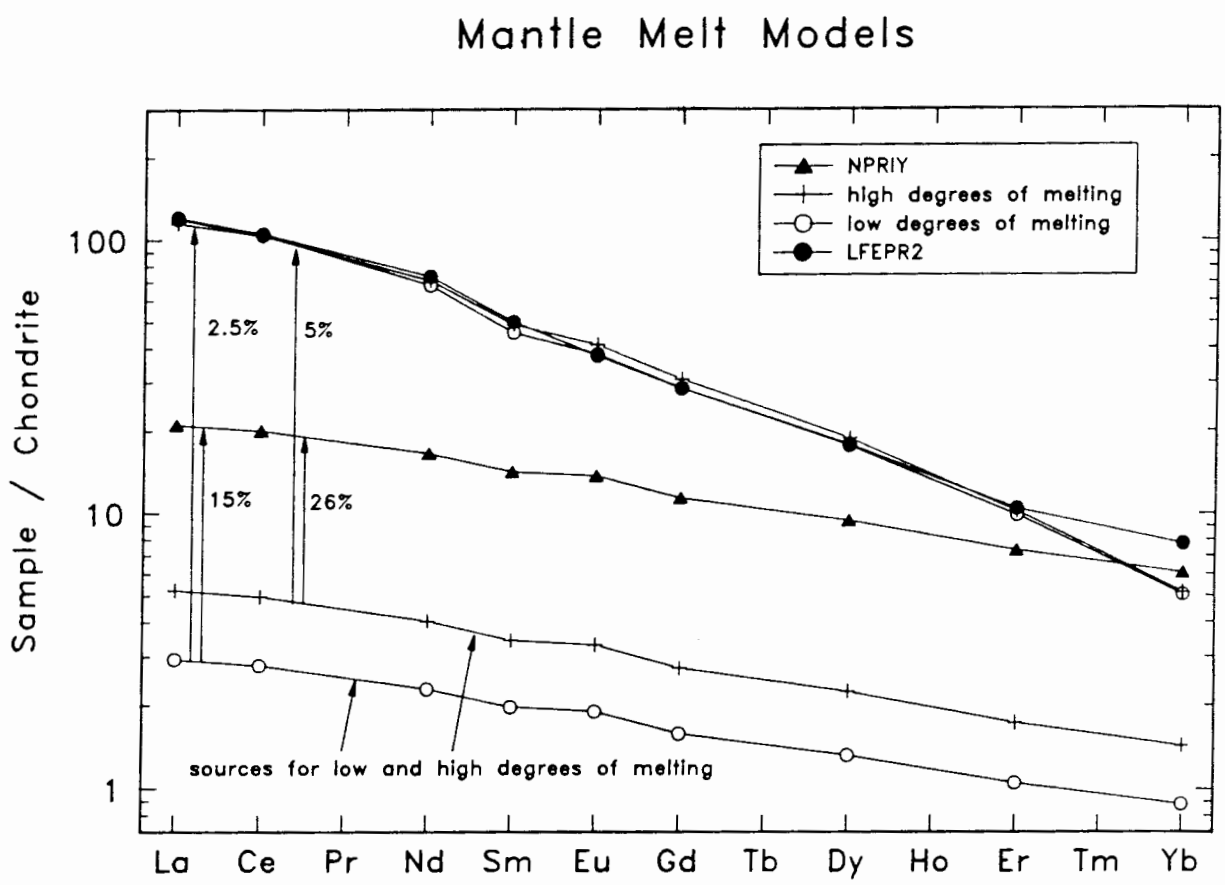

Figure 9.6. REE melt-model spidergram: sources are fixed assuming NPRIY is derived by high degrees of melting (15% and 26%) and this source is then melted at lower degrees to see whether LFEPR2 may be produced.

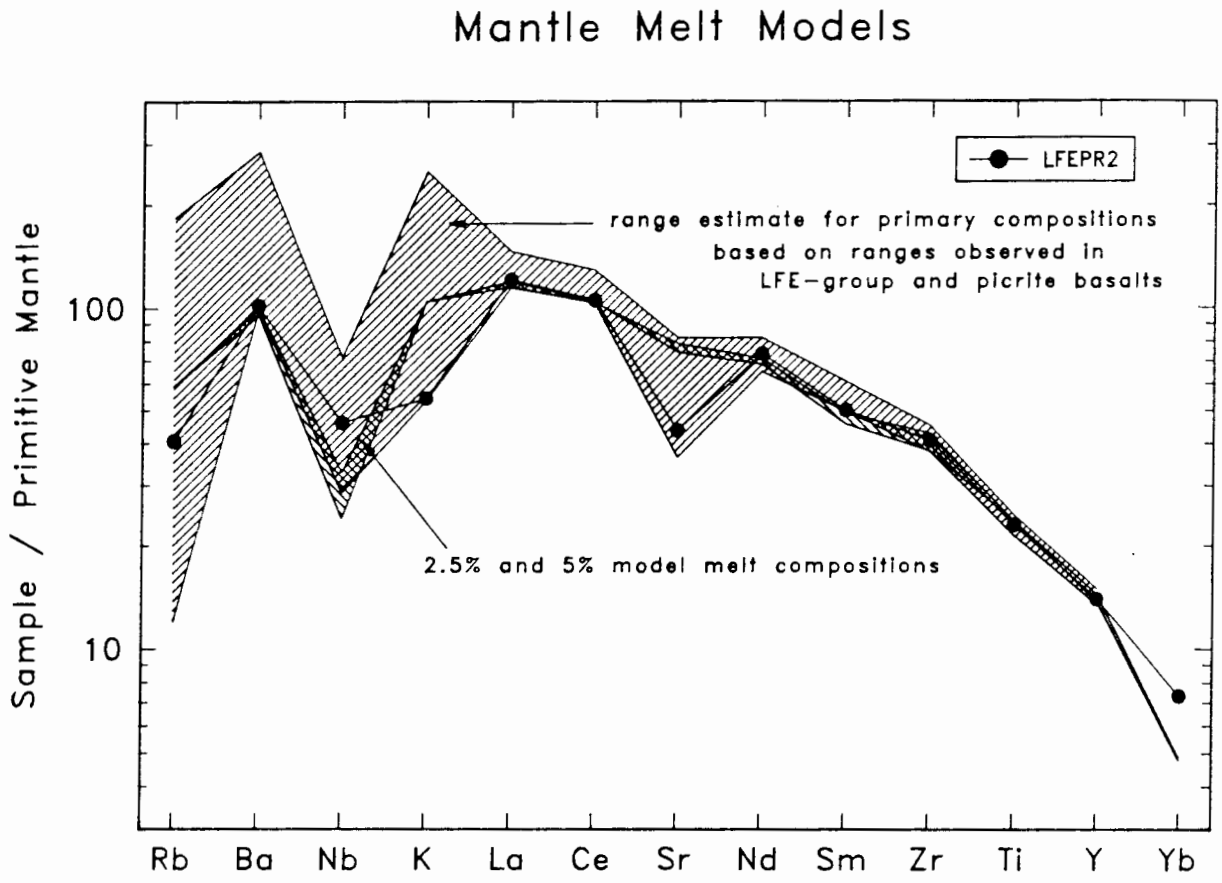

Figure 9.7. Incompatible element melt-model: sources are fixed assuming NPRIY is derived by high degrees of melting (15% and 26%) and this source is then melted at lower degrees to see whether LFEPR2 may be produced. The melt produced as these low degrees of melting is compared to the calculated LFE "primary" composition (LFEPR2) and a subjective estimate of the likely range of incompatible element contents in "primary" LFE-group melts based on ranges observed in the LFE group and the N. Lebombo picrites for a small MgO interval.

The ability of the melting models to produce the two basalt types from the same source is summarized for a spectrum of incompatible elements by Fig. 9.7. Again, the effectiveness of the model is measured by the displacement of the 2.5% and 5% model melts from the observed composition (LFEPR2). Whether large (26%) or small (15%) degrees of melting are chosen for NPRIY melt to define a source composition the result is essentially the same (i.e. 2.5% and 5% melt compositions are virtually identical). The estimate of the range of LFE-group "primary" compositions is a largely subjective estimate based on the element ranges in both the central Lebombo LFE group and the allegedly parental N. Lebombo picrites. The range in LILE and Sr are considerable and of a random nature when plotted *vs* MgO. Alteration, fractional cystallization and crustal contamination have been excluded as processes significantly influencing the distribution of Ba and Sr, (and to some extent K and Rb) in the LFE group (Chapters 3, 6, 7, 8) and it is quite likely that their distribution is a function of source composition. The distribution of phlogopite in any source area and the contribution made to any melt will profoundly affect the concentrations of the LILE but not Sr (see partition coefficients in Table 9.3). It is likely that at the lower degrees of melting that may produce LFE-group "primary" magmas magmas (2.5% and 5% melting) the proportion of phlogopite in the melting mode may be very variable, and hence result in the spread of K and Rb data observed in the LFE group and N. Lebombo picrites. Conversely when the higher degrees of melting producing N-group "primary" melts are reached, most phlogopite is likely to be consumed producing much more consistent variations in the LILE. Any partial melting model must be able to account for the consistent differences in incompatible element ratios observed between the N and LFE (including N. Lebombo picrites) groups. Ratios showing consistent differences between the two groups are plotted in Fig. 9.8 along with the model melt compositions from Tables 9.5 and 9.6 and show that the partial melting models proposed can account for these differences.

Thus the 2.5% and 5% models produce melts within the ranges of incompatible element abundances for LFE-group "primary" melts suggested by variations in N. Lebombo picrites and the LFE-group (Fig. 9.7) and the model is consistent with major element variations (Tables 9.5, 9.6). Thus, there is no reason on trace element grounds to believe that the LFE and N groups may not be derived from a compositionally homogeneous mantle by different degrees of partial melting, providing the degrees of melting used in the

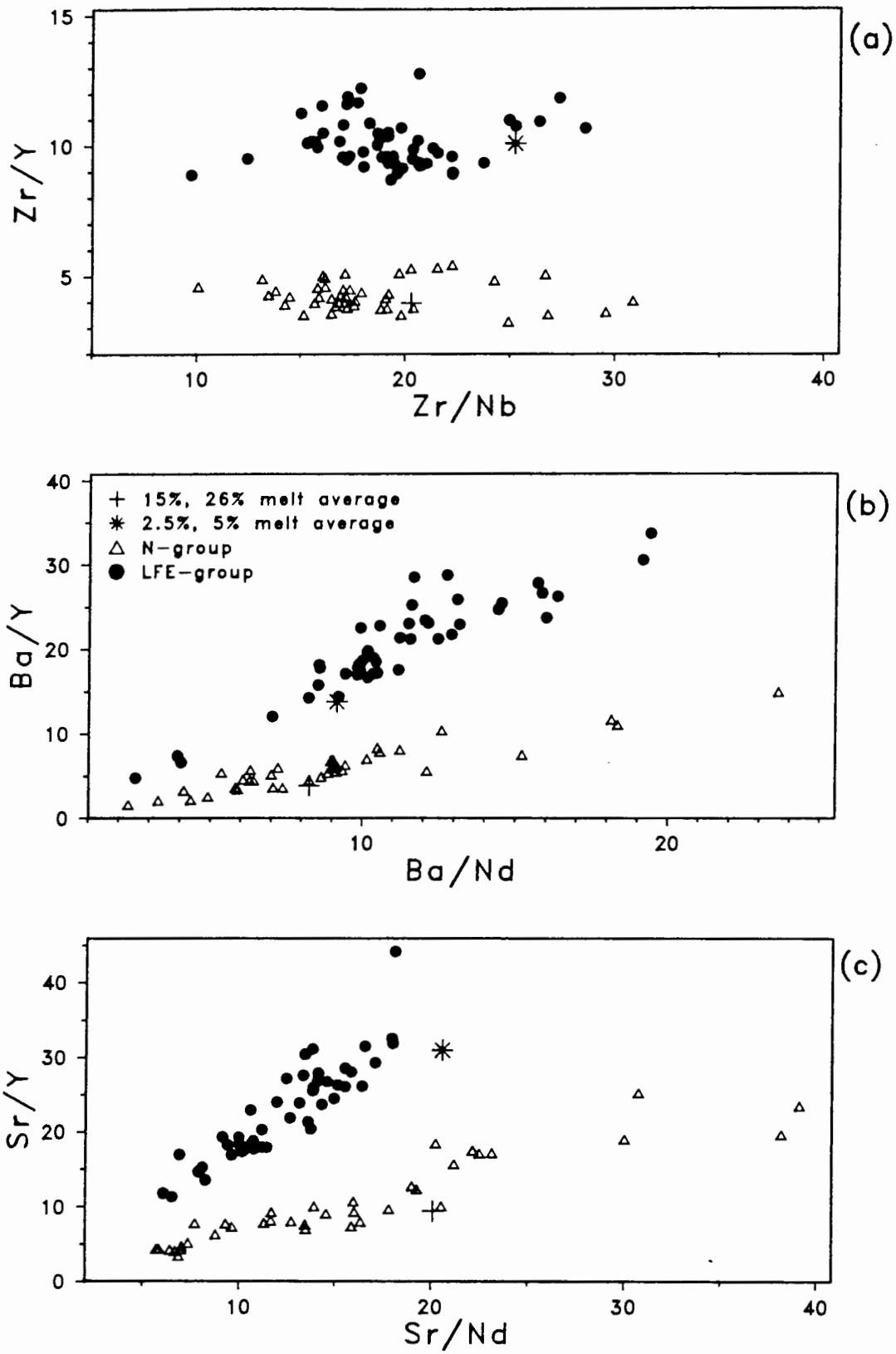

Figure 9.8. Diagnostic incompatible element ratios observed for N and LFE groups and ratios predicted (larger symbols) by the models in Tables 9.5 and 9.6.

modelling are acceptable and realistic. This is examined below.

9.4.3 Implications for Mantle Dynamics

It is useful to examine whether the volumes of mantle which must be tapped to produce the volumes of basalt observed in the central Lebombo, are realistic. Considering the N and HFE groups as one magma series, estimated basalt volumes are:

LFE: 1200 m (thickness) x 50 km (E-W extent) x 100 km (N-S extent)
= 6000 km^3

N/HFE: 800 m (thickness) x 50 km (E-W extent) x 100 km (N-S extent)
= 4000 km^3.

Assuming that each suite has undergone an average of 40% fractional crystallization, then these volumes represent primary melt volumes of 10000 km^3 and 6670 km^3 for the LFE and N/HFE groups respectively. Equating the mass % with volume % partial melting for simplicity, then 5% melting of the mantle to produce LFE-group primary melts requires the tapping of 200000 km^3 mantle which corresponds to dimensions of 50 km (width?) x 100 km^3 (length?) x 50 km (depth?). Obviously 2.5% melting would require twice this volume to be tapped, i.e. 100 km depth assuming the same lateral dimensions. The higher degrees of melting required to produce N/HFE group primary melts, would require a depth of 5.1 km and 8.9 km to be tapped for 26% and 15% melting respectively for the same lateral dimensions above. Conceivably the E-W estimate of the extent of melting in the mantle (50 km) could be larger if the Lebombo volcanics were erupted in the N-S linear fashion and thus approximately confined to the area preserved by their present outcrop. In any event, however, the longest "line of melt extraction" in the case of small degrees of melting is >50 km which implies an extremely efficient extraction mechanism.

McKenzie (1984) has suggested that typical melt separation velocities are of the order of 10-30 mm/yr. For the low degrees of melting needed to produce the LFE group (2.5-5%) from a source capable of producing the N group a "line of melting" in the range 20 km to 100 km would take 1-5 Ma to extract using a melt separation velocity of 20 mm/yr. This is well within the $\pm$ 20 Ma (200-180 Ma) during which time these basalts must have erupted (Fitch and Miller, 1984). Furthermore, McKenzie (1984) maintains that it is physically

possible to extract picritic melts occupying volumes as low as 1% of mantle sources. Thus, it appears that the low degrees of melting proposed for the models are dynamically realistic.

9.4.4 Implications for Mantle Source Composition

The earlier consideration of Sr- and Nd- isotopic variations (section 9.2.3) implied either an enriched asthenosphere source (e.g. similar to the Walvis Ridge source) or a sub-continental lithospheric source (e.g. garnet-bearing "cold" xenoliths) for the N group, with the LFE group consistent with derivation from the sub-cratonic lithospheric mantle (Fig. 9.2b). The trace element abundances in the source compositions calculated in the above models may be compared to the different potential sources available in an effort to resolve this problem (Fig. 9.9).

Three source options are represented in Fig. 9.9: "cold" sub-continental lithospheric garnet-bearing xenoliths, "hot" (asthenospheric?) xenoliths and a hypothetical primitive mantle composition (Rogers, 1979) which is used as a "normalization composition". Assuming that the xenolith compositions are representative of the upper mantle beneath southern Africa 200 Ma ago, the incompatible element profiles are more consistent with a source akin to the "hot" xenoliths (asthenospheric?) than a sub-continental lithospheric source ("cold" xenoliths). A source represented by these "hot" xenoliths, however, is enriched in the more incompatible elements (Rb, Ba, Nb, K, La and Ce) relative to the hypothetical source calculated for lower degrees (2.5% and 15%) of melting (Fig. 9.9b). Furthermore, the Sr- and Nd- isotopic signature of these "hot" xenoliths is similar to MORB - considerably more depleted than is observed in the basaltic rocks of the central Lebombo. The near-parallel nature of the hypothetical melt sources with Rogers' (1979) primitive mantle is remarkable (Fig. 9.9), and is very similar to primitive mantle estimates of Wood *et al.* (1979) and Jagoutz *et al.* (1979) (Fig. 9.10). Thus for this "common source" model, the most likely incompatible element source composition is similar to estimates of primitive mantle (Figs. 9.9; 9.10). This source would have to contain material having a range of Sr- and Nd-isotopic signatures to encompass variations observed in the LFE and N groups, and the mechanism of melting would have to be such that the isotopically enriched end-member would dominate a melt derived by small

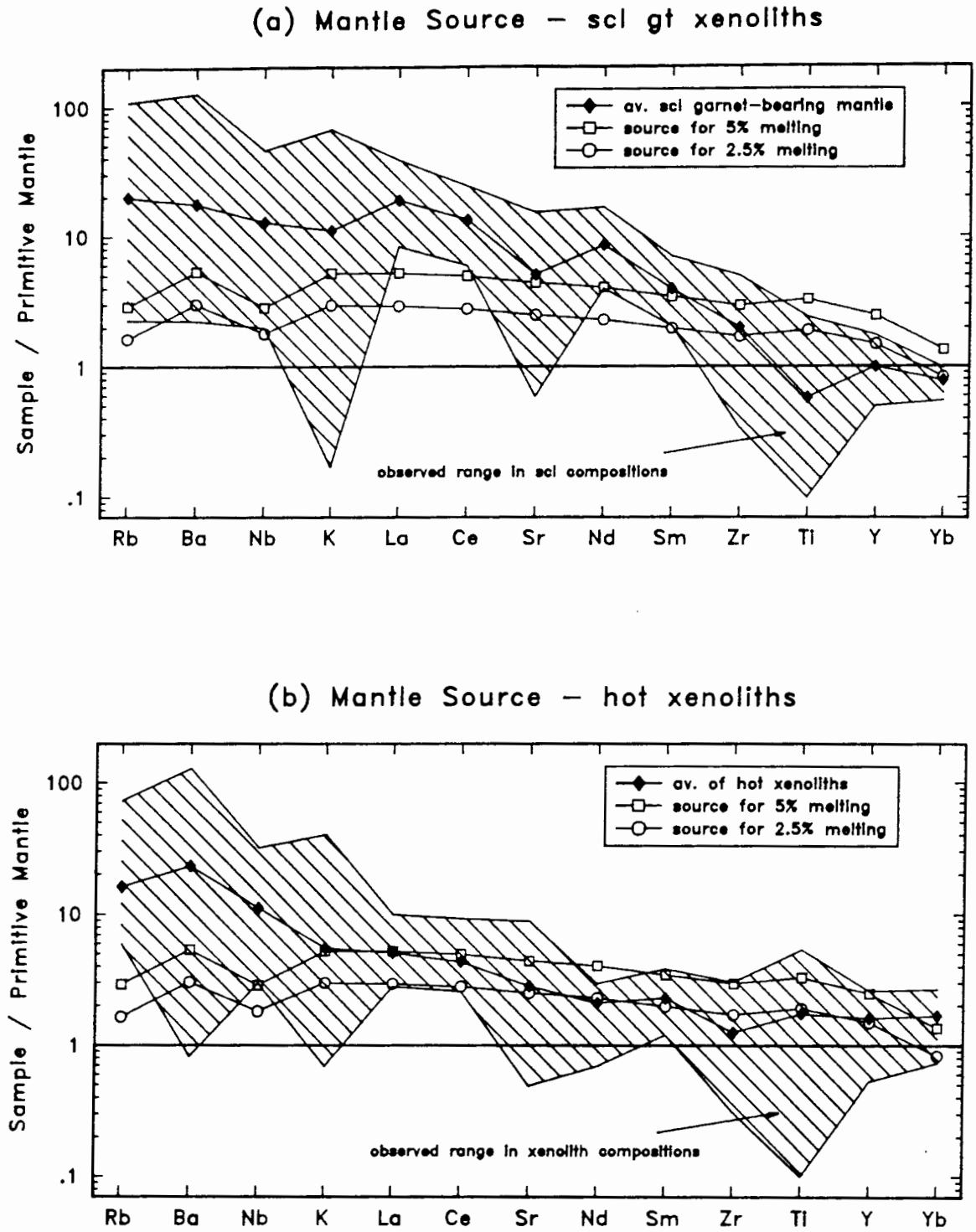

Figure 9.9. Model source compostions (from Tables 9.5 and 9.6) normalized to Rogers' (1979) primitive mantle estimate. Also given are the average and ranges for "cold" (a) sub-cratonic lithospheric (scl) garnet-bearing xenoliths and "hot" xenoliths (b) from Table 9.1.

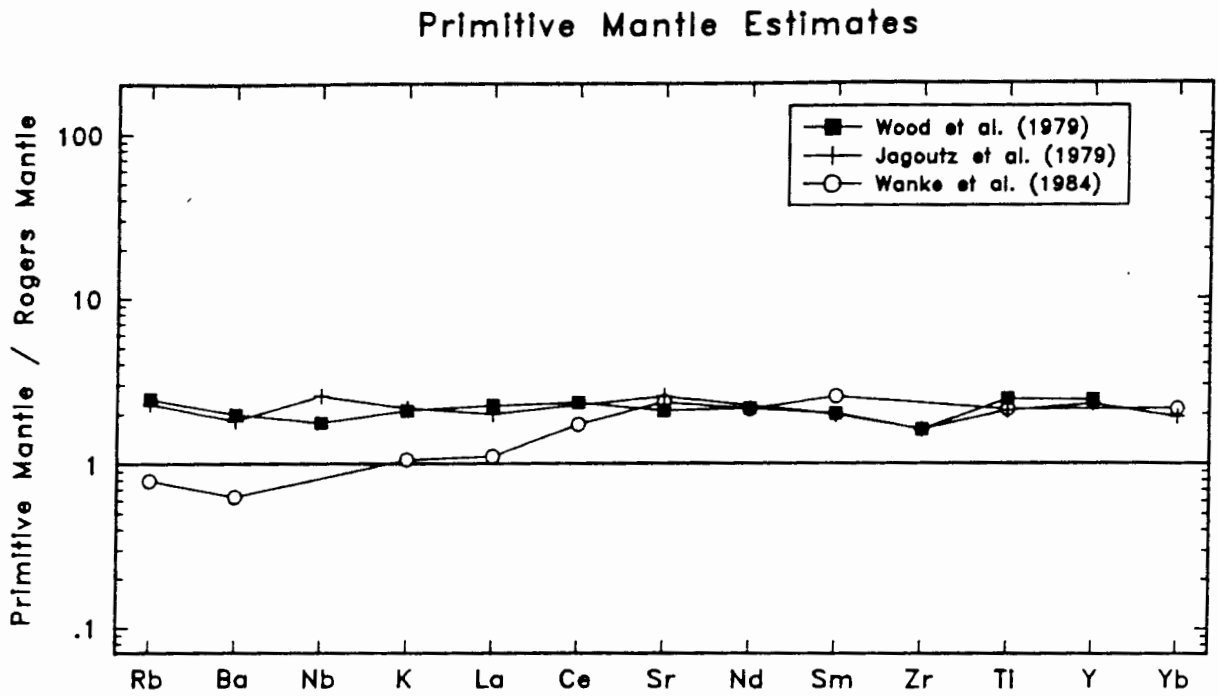

Figure 9.10. A comparison of primitive mantle estimates from Wood *et al.* (1979); Jagoutz *et al.* (1979) and Wanke *et al.* (1984) normalized to Rogers' (1979) values.

degrees of melting (LFE group) with the progressive involvement of a more depleted end-member at higher degrees of melting (N group). This mechanism implies an isotopic as well as an incompatible element continuum in any melts produced. An isotopic continuum in the LFE- and N-group "primary" melts is observed to some degree (Fig. 9.2b), but no incompatible element (specifically the the HFSE) continuum exists, rendering such a mechanism unlikely.

The source region suggested by the melting models, therefore, has an incompatible element signature similar to a primitive mantle, yet an isotopic signature similar to sub-cratonic lithospheric mantle. The existence of asthenosphere of yet undiscovered isotopic content or the selective modification of isotopes, but not of incompatible element concentrations, by the passage of an asthenospheric melt through a sub-continental lithosphere are both unlikely alternatives.

Another alternative is to postulate the existence 200 Ma ago of a sub-continental lithospheric mantle containing a similar incompatible element signature to primitive mantle (Fig. 9.10). Following extraction of the Karoo basaltic rocks, subsequent modification of the residual mantle (metasomatism?) produced the trace element signature observed today (Fig. 9.9a). The composition which could produce both the N and LFE groups, however, bears little resemblance to the composition of the old "cold" sub-cratonic lithospheric mantle (Fig. 9.9a) and it is important to consider whether this mantle source may produce one or both of the basalt groups (as implied by Sr- and Nd-isotopes for the LFE-group, see earlier).

9.4.5 Different Mantle Sources

An alternative to postulating complex hypotheses to explain the difference between calculated source compositions and observed mantle compositions, is to suppose that the two basalt types originate from compositionally distinct mantle source areas. Each source would then be represented by the "primary" fields defined for the two basalt types in terms of their Sr- and Nd-isotope content (Fig. 9.2b).

The continuous partial melting models in Table 9.7 give the sources which would produce LFE- and N-group "primary" melts at 10% melting. The

Table 9.7. Continuous melting model (Langmuir *et al.*, 1977) for the calculation of a NPRIY and LFEPR2 sources at 10% melting. Weight fractions of minerals in the melt are 'fixed' by the melt major component composition.

Mineralogy

Mineral	Initial wt. fractions		Weight fractions entering liquid			
	N source	LFE source	(1)	(2)	(3)	(4)
olivine	.6000	.6000	.0100	.0100	.0200	.0200
orthoproxene	.3129	.3175	.0600	.2000	.1700	.4000
clinopyroxene	.0370	.0390	.2000	.2900	.3300	.5800
garnet	.0450	.0240	.2800	.4000	.4800	
ilmenite	.0022	.0045	.0500	.1000		
phlogopite	.0029	.0150	.4000			

Phase exhaustions:	N model	LFE model
phlogopite:	.73%	3.75% melting
ilmenite:	2.58%	6.48% melting
garnet:	10.28%	7.14% melting

Melting Parameters

Initial degree of melting:	1%
Final degree of melting:	10%
Melting increment:	3%
Amount of melt held in the residue:	1%

Amount of Minerals in the:

	N melt	N residue	LFE melt	LFE residue
olivine	.0174	.6632	.0135	.6627
orthopyroxene	.1676	.3287	.2026	.3302
clinopyroxene	.3132	.0070	.3417	.0071
garnet	.4507	.0010	.2461	-
ilmenite	.0221	-	.0460	-
phlogopite	.0290	-	.1500	-

Model Compositions

	NPRIY	N model	C_0-set N source	LFEPR2	LFE model	C_0-set LFE source
SiO_2	48.80	48.35	46.96	51.44	48.70	46.95
TiO_2	1.25	1.22	.130	2.39	2.45	.248
Al_2O_3	11.54	11.18	1.36	8.73	8.72	1.09
FeO+MgO	26.97	28.49	50.21	26.61	29.41	45.50
CaO	8.83	8.44	1.08	8.10	8.04	1.01
Na_2O	2.28	.83	.13	1.52	.92	.14
K_2O	.29	.292	.0292	.784	1.51	.151
(Ti)	7493	7314	779*	14300	14690	1487*
P	621	621	56.5	1540	1540	140
Zr	83	83	8.1	279	279	26.7
Nb	4.1	4.1	.508	16.1	16.1	2.00
Y	21	21	2.42	28	28	2.91
La	6.63	6.63	.605	38.1	38.1	3.47
Ce	16.3	16.3	1.49	85.6	85.6	7.83
Nd	9.88	9.88	.917	43.8	43.8	4.05
Sm	2.72	2.72	.258	9.6	9.6	.902
Eu	.989	.989	.096	2.71	2.71	.258
Gd	2.94	2.94	.289	7.35	7.35	.705
Dy	3.05	3.05	.317	5.78	5.78	.567
Er	1.56	1.56	.176	2.22	2.22	.225
Yb	1.26	1.26	.166	1.61	1.61	.177
(K)	2433	2651	242*	6508	13750	1254*
Rb	4.1	4.1	.374	14.2	14.2	1.30
Ba	82	82	7.5	385	385	35.0
Sr	198	198	18.4	479	479	44.6
Ni	1048	1048	3270	742	738	2300
Cr	310	310	677	730	837	1860

* set according to content in source mineralogy

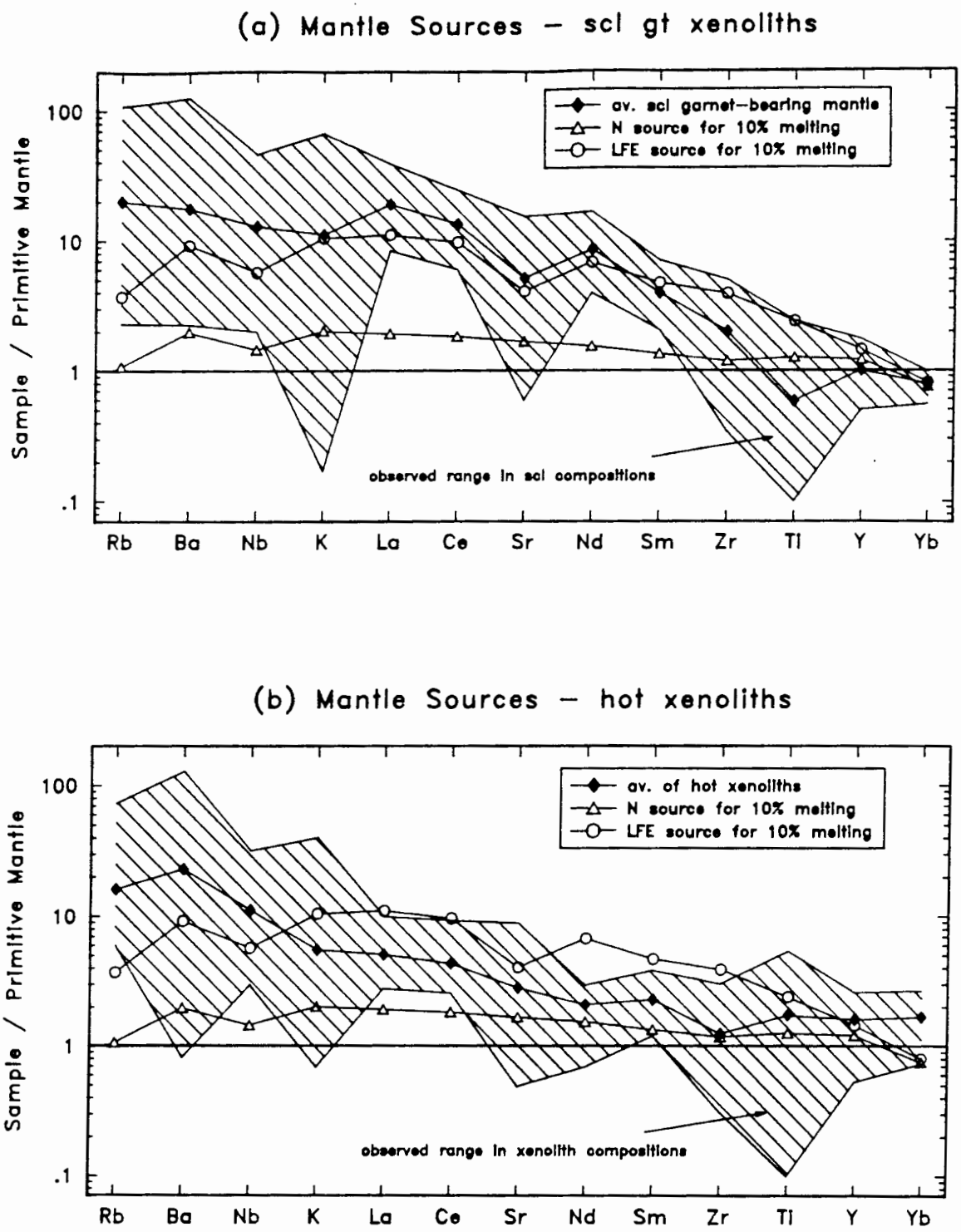

Figure 9.11. Model source compostions (from Table 9.7) assuming 10% melting for both N and LFE groups, normalized to Rogers' (1979) primitive mantle estimate. Also given are the average and ranges for "cold" (a) sub-cratonic lithospheric garnet-bearing xenoliths (scl) and "hot" xenoliths (b) from Table 9.1.

selection of 10% melting is arbitrary but does relax the need for an extremely efficient extraction mechanism neccesary at low (<5%) degrees of melting. Melting modes are kept constant for both models.

The model source composition producing the LFE-group "primary" melt (LFEPR2) at 10% melting shows a remarkable similarity to the average for sub-continental garnet-bearing lithospheric mantle and is within the range established (Erlank *et al.*, 1987) for these xenoliths (Fig. 9.11a). Elements which show significant discrepancies between the model and the observed average values are Ti and Zr (higher in model source) and Rb, Ba and Nb (lower in model source than observed in xenoliths). At the same degree of melting (10%) the N-group model source is substanitially depleted in incompatible elements, and is most akin to a primitive mantle composition in the spectrum represented by Rogers' (1979) and Wood *et al.*'s (1979) values (Fig. 9.11a). The N-group source is also similar to an average of N-MORB compositions (Fig. 9.11b) from Wood *et al.* (1979) except for greater Rb and Ba contents. However, this average of N-MORB represents compositions of basalts fractionated to varying degrees and their primary melts would be less enriched with mantle sources containing even lower incompatible element concentrations. Neither N- or LFE-group model sources appear to coincide with a source represented by the "hot" xenolith suite (Fig. 9.11b) and this is consistent with Sr- and Nd-isotopic data (see earlier).

9.4.6 Summary

If the LFE group is derived by the partial melting of garnet bearing sub-cratonic lithospheric mantle as represented by observed "cold" xenolith compositions, then the degree of melting must be of the order of 10%. Such a source for the LFE group would be consistent with Sr- and Nd-isotope variations. It is unlikely that such a source could produce the N group as the degrees of melting would have to be unrealistically large (>50%). Assuming more reasonable degrees of melting (10%) the N group may be derived from a source similar to estimates of primitive (or primordial) mantle - a mantle enriched in incompatible elements relative to that producing N-MORB. Isotopically such a source would be similar to that of the Walvis Ridge segment - i.e. an enriched portion of the asthenosphere.

Table 9.8. Incompatible trace element enrichments in the N group and a calculated major element content for a 6% partial melt of the model in Table 9.7.

	(1)	(2)	(3)	(4)
SiO_2				48.05
TiO_2				2.11
Al_2O_3				11.11
FeO+MgO				29.15
CaO				8.19
Na_2O				.81
K_2O				.49
ratios				
Ti	3.19	1.98	1.61	1.69
Zr	3.25	2.14	1.52	1.48
Nb	6.10	2.27	2.69	1.31
Y	1.90	1.95	.97	.98
La	4.07	2.44	1.67	1.73
Ce	4.11	2.44	1.68	1.71
Nd	5.06	2.83	1.79	1.64
K	4.09	2.20	1.87	1.66
Rb	4.63	2.37	1.95	1.74
Ba	5.00	2.17	2.30	1.74

(1) observed enrichment (HEPRIM/NPRIY) in the N group
(2) enrichment accountable by fractional crystallization the N group (Fig. 6.7)
(3) enrichment factor required by partial melting (col.(1)/col.(2))
(4) enrichment factor (trace elements) observed for a 6% partial melt for the model given in Table 9.7 (i.e. 6% melt/10% melt compositions).

9.5 INCOMPATIBLE ELEMENT VARIATIONS IN THE N GROUP

The generally consistent increase in incompatible element content within the N group from an unevolved composition (e.g. NPRIM, Table 6.3) to an unevolved HFE composition (e.g. HEPRIM, Table 6.3) is unaccounted for by the fractionation and crustal contamination models considered (Chapters 6, 7, 8). This is of critical importance for explaining the variation within the N group and for relating the N and HFE groups. Up to this point the only grounds for assuming a relationship between the two groups has been the continuum in chemical composition observed. However, if some process can account for the variation **within** the N group then most of the differences between the N and HFE groups may be explained.

The model for 10% continuous partial melting (Table 9.7) is examined in an effort to account for the observed incompatible element enrichments (column 1 in Table 9.8, given by HEPRIM/NPRIY) in the N group. Column 2 is the amount of enrichment which is accountable by fractional crystallization (RTF or closed-system, Chapters 6 or 8); column 3 is the enrichment factor required in a melt to account for the increase still unexplained (i.e. after subtraction of a "crystallization component"), and column 4 is the enrichment factor observed for 6% melting (6% melt composition/10% melt composition) of a source using the parameters given in Table 9.7.

The major element content of this melt is similar to that of the melt at 10% melting (Tables 9.7, 9.8), i.e. the major components are buffered to constant values while the minor and trace incompatible elements are enriched in the melt at lower degrees of melting. With the exception of Ba and Nb the enrichment factors necessary to account for the increase in concentration from NPRIY to HEPRIM are attainable in a magma chamber replenished with melt derived by a varying degree of partial melting (6-10%, Table 9.8). Obviously such a process necessitates different zones of the mantle to be tapped from those recently melted, e.g. the later melting of a source already subjected to 10% partial melting at lower degrees will not produce the desired result. The type of situation envisaged is illustrated schematically in Figure 9.11. Initially melts are extracted by larger degrees of melting (1) and, as the influence of the 'heat source' wanes, by progressively smaller degrees of melting (2).

Another mechanism of accounting for the increase in the incompatible element content with time (as measured by extent of fractional

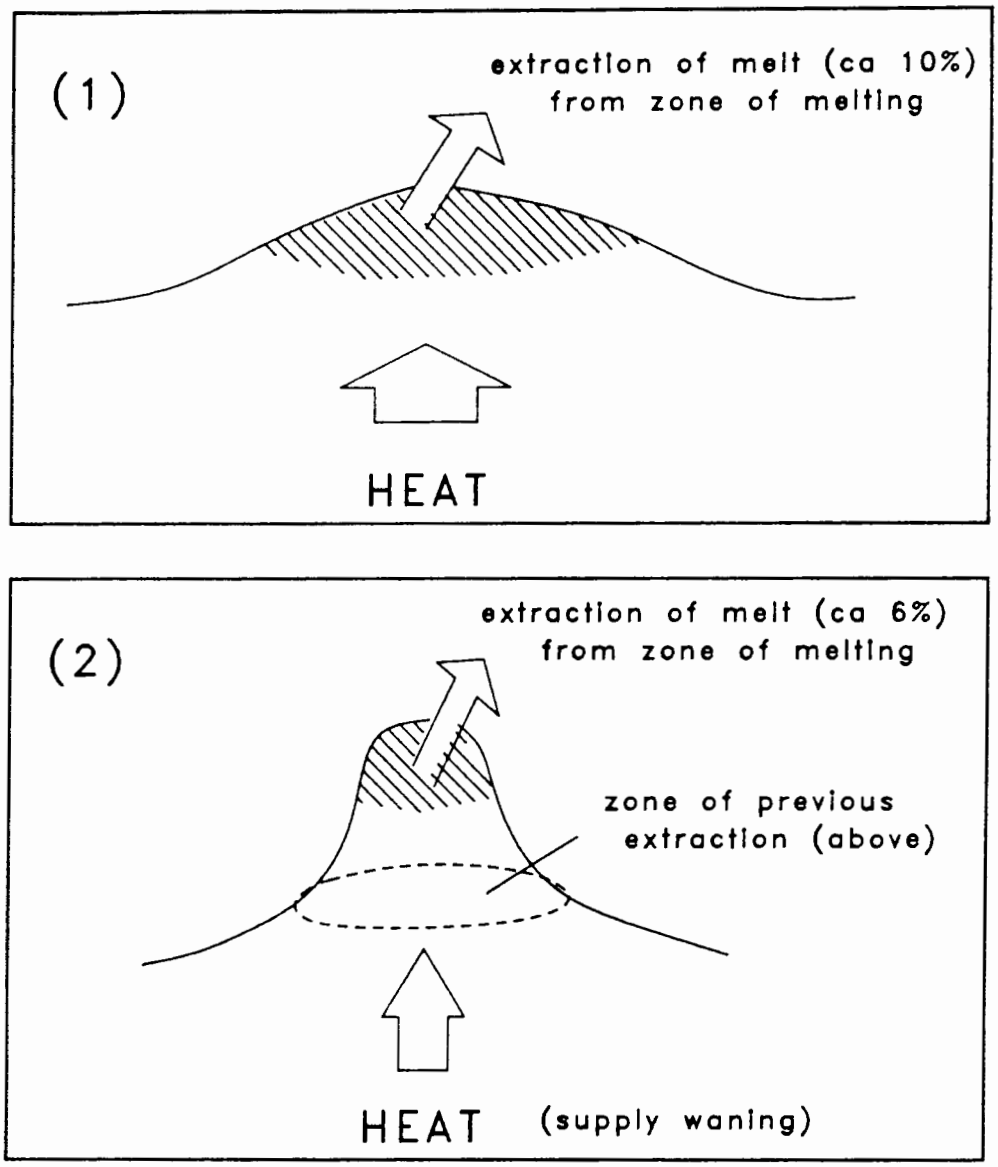

Figure 9.12. Schematic representation of a model which may produce different degrees of melting in the N-group mantle source, melting different mantle zones in each instance.

crystallization indicated by the MgO content of erupted melts), is the relative influence of melting and segregation: if melting is greater than segregation, the incompatible element content of the derivative melt may increase with time (Richter, 1986). A problem, however, is how such volumes of basalt could be produced if such rapid melting does occur, e.g. in a plume environment.

9.6 SUMMARY OF CONCLUSIONS

If the LFE and N groups are derived from mantle sources of similar composition then, unless a convoluted mantle source history is supposed (see above discussions), isotopic evidence indicates that this source must be in the sub-cratonic lithospheric mantle as sampled by garnet-bearing "cold" xenoliths. This is the only mantle region with sufficiently low $^{143}Nd/^{144}Nd$ ratios to account for the LFE-group and N. Lebombo-Nuanetsi basaltic rock data. The composition of this source is constrained by the difference in the relative degrees of partial melting required to produce LFE- and N-group "primary" compositions: the N group requires degrees of partial melting 4-6 times those of the LFE group (e.g. 2.5% *vs* 15% or 5% *vs* 26%). The source which may generate both magma types is represented on Fig. 9.9 (open symbols) and does not bear much resemblance to the range of incompatible element contents observed for garnet-bearing "cold" xenoliths suggested on isotopic grounds as the most suitable source for both. "Hot" xenoliths are discounted as a potential source for either the LFE or N groups on the basis of their too-depleted isotopic character. However, the LFE-group "primary" composition may be derived by *ca* 10% partial melting of a source quite similar to the average calculated for garnet-bearing "cold" xenoliths (Fig. 9.11). The N group could not could not be derived from such a source as unacceptably high (>50%) degrees of partial melting would be involved. A source akin to primordial mantle or "enriched" asthenosphere could conceivably produce the N group at more acceptable degrees of partial melting (e.g. 10%). Variations of the degree of partial melting (6 - 10%) and the degree of fractional crystallization could account for the increase in incompatible element content (excepting Ba and Nb) with decreasing MgO in some N group samples. This is an alternative model to that suggested in Chapter 7 which requires that any crustal contaminant derived by partial

melting of a granitic parent cannot have phases such as zircon or apatite in the residue.

In conclusion, it is preferable on combined trace element and isotopic evidence, to derive the LFE and N groups from different sources: the former within the sub-cratonic lithospheric mantle and the latter without. The N-group mantle source is isotopically (Sr and Nd) similar to the "enriched" asthenosphere from which the Walvis Ridge basalts were derived and may be more recently accreted (thinner) sub-continental lithospheric mantle. These possible mantle sources for the basalt types are examined in terms of regional variations in the following chapter.

10. MESOZOIC BASALTS OF SOUTH-WESTERN GONDWANALAND: A CASE FOR CRUST-MANTLE CORRELATIONS

10.1 INTRODUCTION

It was concluded in Chapter 9 that the LFE and N groups are most likely derived from compositionally different sources. It was suggested (Chapter 9) that the LFE group may be derived from old (i.e. Archaean) sub-cratonic mantle enriched from Archaean times in incompatible elements relative to a N-group mantle source. It was suggested that a possible N-group source may be thinner more recently accreted (i.e. <2.0 Ga) lithospheric mantle surrounding the cratons.

The central Lebombo, however, is only one remnant of Mesozoic basaltic rocks which crop out from south-east S. America across southern Africa to Antarctica, represented on a pre-drift Gondwanaland in Fig. 10.1. Available published data for selected diagnostic elements on the flood basalt province remnants now preserved in the Parana Basin of S. America (Bellieni *et al.*, 1984a, b), the Karoo Province of southern Africa (Erlank, 1984) and Dronning Maud Land, Antarctica (Furnes *et al.*, 1982) are given in Table 10.1. These averages are examined in terms of ranges of concentrations for the three groups in the central Lebombo to establish both the distribution of basaltic groups on a regional scale, and the implications this may have for their origins. A preferred model for the distribution of basalt types (crust-mantle correlations) is examined initially and the geographic distribution of basalt types is detailed in this context. This crust-mantle model is followed by a commentary on other alternatives. Finally the tectonic setting of the Lebombo volcanics is considered in some detail.

10.2 GEOCHEMICAL VARIATIONS IN MESOZOIC BASALTS OF GONDWANALAND

The distribution of Mesozoic basalts in southern Africa is given by Eales *et al.* (1984); in Malawi by Macdonald *et al.* (1983) and in Dronning Maud Land (Antarctica) by Harris *et al.* (1988) and Furnes *et al.* (1987). Data for basalts from these different areas are given in Table 10.1. For the

Figure 10.1. Simplified map of southern Gondwanaland (from Sweeney and Watkeys, 1988). Numbers correspond to the data given in Table 10.1 and plotted in Figs 10.2 and 10.3. Also show are the major Mesozoic dyke swarms in the Limpopo valley and eastern Botswana (not numbered) and the Rooi Rand (area 20). LFE- and N-group basalts (and their correlatives) are represented by a random stippling and v's respectively. Inset: Archaean (+), reworked Archaean (x) and post-Archaean crustal provinces. Gondwana reconstruction used is that of De Wit *et al.* (1988).

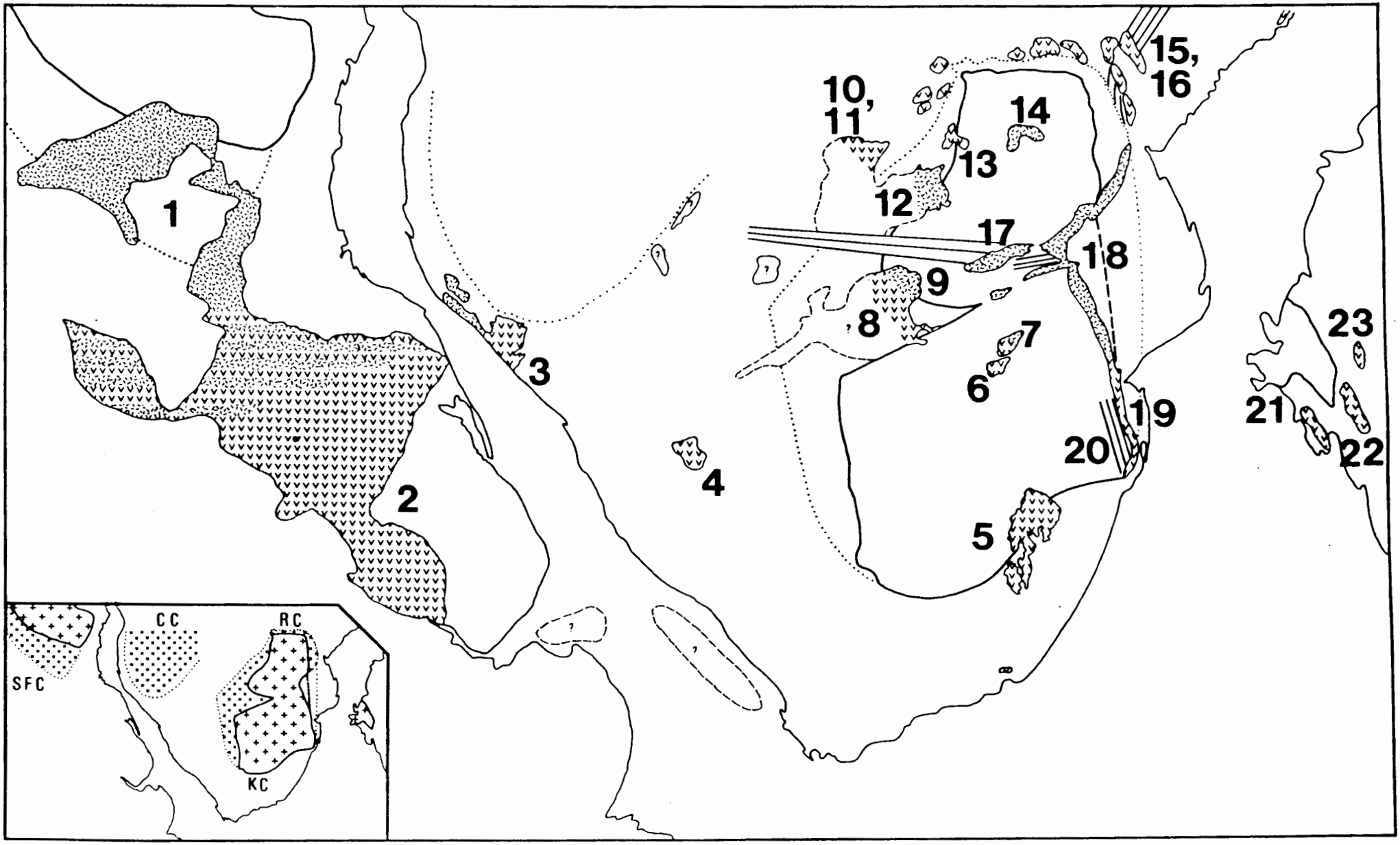
1
2
3
4
5
6
7
8
9
10,
11
12
13
14
15,
16
17
18
19
20
21
22
23
SFC
CC
RC
KC

Table 10.1. Enriched" and "normal" Mesozoic basalts: average analyses for selected elements from different areas in "southern" Gondwanaland. Data is normalized to 100% volatile-free with Fe as total Fe_2O_3.

	(1)	(2)	(3)	(4)	(5)	(6)	(7)	(8)	(9)
%									
MgO	3.82	5.22	5.25	7.71	7.01	7.58	3.93	7.64	3.71
Fe_2O_3t	14.30	12.95	12.61	10.08	10.96	11.01	11.86	11.07	14.64
TiO_2	3.33	1.36	1.38	.94	.95	.99	3.26	.89	3.12
P_2O_5	.56	.21	.19	.15	.16	.14	.66	.14	.83
ppm									
Zr	263	143	165	82	94	105	508	77	568
Y	34	34	31	23	24	26	45	22	55

	(10)	(11)	(12)	(13)	(14)	(15)	(16)	(17)	(18)
%									
MgO	5.08	7.24	5.22	6.59	7.66	3.98	6.50	4.61	5.61
Fe_2O_3t	13.53	13.36	13.89	12.08	11.92	13.15	11.85	13.99	12.17
TiO_2	3.14	2.46	3.19	1.93	2.81	1.84	.83	2.93	2.90
P_2O_5	.51	.17	.46	.22	.40	.37	.13	.47	.51
ppm									
Zr	-	169	387	-	358	220	85	321	340
Y	-	31	43	-	29	41	23	36	34

	(19)	(20)	(21)	(22)	(23)
%					
MgO	5.59	5.87	8.36	6.50	5.80
Fe_2O_3t	12.48	15.21	13.15	13.03	13.72
TiO_2	1.51	2.14	1.57	1.36	1.45
P_2O_5	.23	.22	.28	.19	.19
ppm					
Zr	135	144	97	113	108
Y	30	36	25	23	32

(1) Northern Parana (E) (n=178), Belleini *et al.* (1984a)
(2) Southern Parana (N) (n=118), Belleini *et al.* (1984a)
(3) Etendeka Formation (Tafelberg) (N) (n=39), Duncan *et al.* (1984b)
(4) Mariental, Namibia (N) (n=4), Duncan *et al.* (1984b)
(5) Central Area (N) (Lesotho Formation) (n=49), Duncan *et al.* (1984b)
(6) Springbok Flats aphyric (N) (n=39), Marsh (1984)
(7) Springbok Flats porphyritic (E) (n=6), Marsh (1984)
(8) Botswana (N) (n=4), Duncan *et al.* (1984b)
(9) Botswana (E) (n=3), Duncan *et al.* (1984b)
(10) Victoria Falls (E) (n=4), Maufe (1929)
(11) Victoria Falls (N) (n=4), Duncan *et al.* (1984b); Maufe (1929)
(12) Nyamandhlovu, Zimbabwe (E) (majors n=9, P n=8, traces n=4), Duncan *et al.* (1984b)
(13) Mafungabusi, Zimbabwe (N) (n=5), Sutton (1979)
(14) Featherstone (E) (majors n=6, traces n=3), Duncan *et al.* (1984b)
(15) Malawi porphyritic (N) (n=7), MacDonald *et al.* (1983)
(16) Malawi aphyric (N) (n=11), MacDonald *et al.* (1983)
(17) Tuli low MgO basalts (E) (majors n=20, Zr n=17, Y n=3), Duncan *et al.* (1984b)
(18) N. Lebombo and Nuanetsi low MgO basalts (E) (majors n=34, traces n=29), Duncan *et al.* (1984b)
(19) S. Lebombo (N) (majors n=48, traces n=41), Duncan *et al.* (1984b)
(20) Rooi Rand dolerites (N) (n=38), Duncan *et al.* (1984b)
(21) Vestfjella, Dronning Maudland (N) (n=34), Furnes *et al.* (1987)
(22) Heimefontfjella, Dronning Maudland (N) (n=9), Juckes (1972)
(23) Kirwanveggan, Dronning Maudland (N) (n=78), Harris *et al.* (1988)

purpose of initial discrimination, "enriched" basaltic rocks refers to the LFE group only and any basalts correlated with them, whilst the "normal" group refers the N group of the central Lebombo and any correlated suite.

The geochemistry and possible petrogenetic histories of these different basalt remnants will not be reviewed or discussed in detail here as these have been adequately documented elsewhere (Cox, 1983; Bellieni *et al.* 1984b; Erlank, 1984; Mantovani *et al.*, 1985 and Petrini *et al.*, 1987). With reference to these studies and models presented earlier for the central Lebombo, it is suggested that petrogenetic processes such as crustal contamination and fractional crystallization cannot produce the difference between the "enriched" and "normal" basalt suites, although they may well be responsible for some of the more subtle variations within each suite. Rather the data which account for the present distribution of "enriched" and "normal" basalts are discussed and this may be used to draw conclusions as to the nature of the mantle source regions.

Averages for the basaltic rocks in different areas are plotted on TiO_2 *vs* P_2O_5 and TiO_2 *vs* Zr variation diagrams (Fig. 10.2) which best discriminate between "enriched" and "normal" groups on the basis of experience in the central Lebombo. Of particular note is the classification of the Malawi "enriched" basalt-type (porphyritic, MacDonald *et al.*, 1983) with the central Lebombo N group. Thus only "normal" type basaltic rocks are present in Malawi. The greater Fe_2O_3t and lower MgO content of the Malawi "enriched"-type relative to the "normal" type (Table 10.1) and the greater proportion of phenocrysts in the "enriched" type suggest that these two basalt types may be related by continued fractional crystallization rather than being representative of different source areas.

MgO and Fe_2O_3t discriminate between samples of LFE or HFE group affinity and the Botswana, Tuli and Parana averages for these elements are intermediate between these two groups (Fig. 10.3a, Table 10.1). However, Zr and Y abundances are more definitive (Fig. 10.3b) and reveal that all "enriched" Mesozoic basaltic rocks in the area of interest more likely correlate with the central Lebombo LFE group than the HFE group and thus the latter group appears to be unique to the central Lebombo.

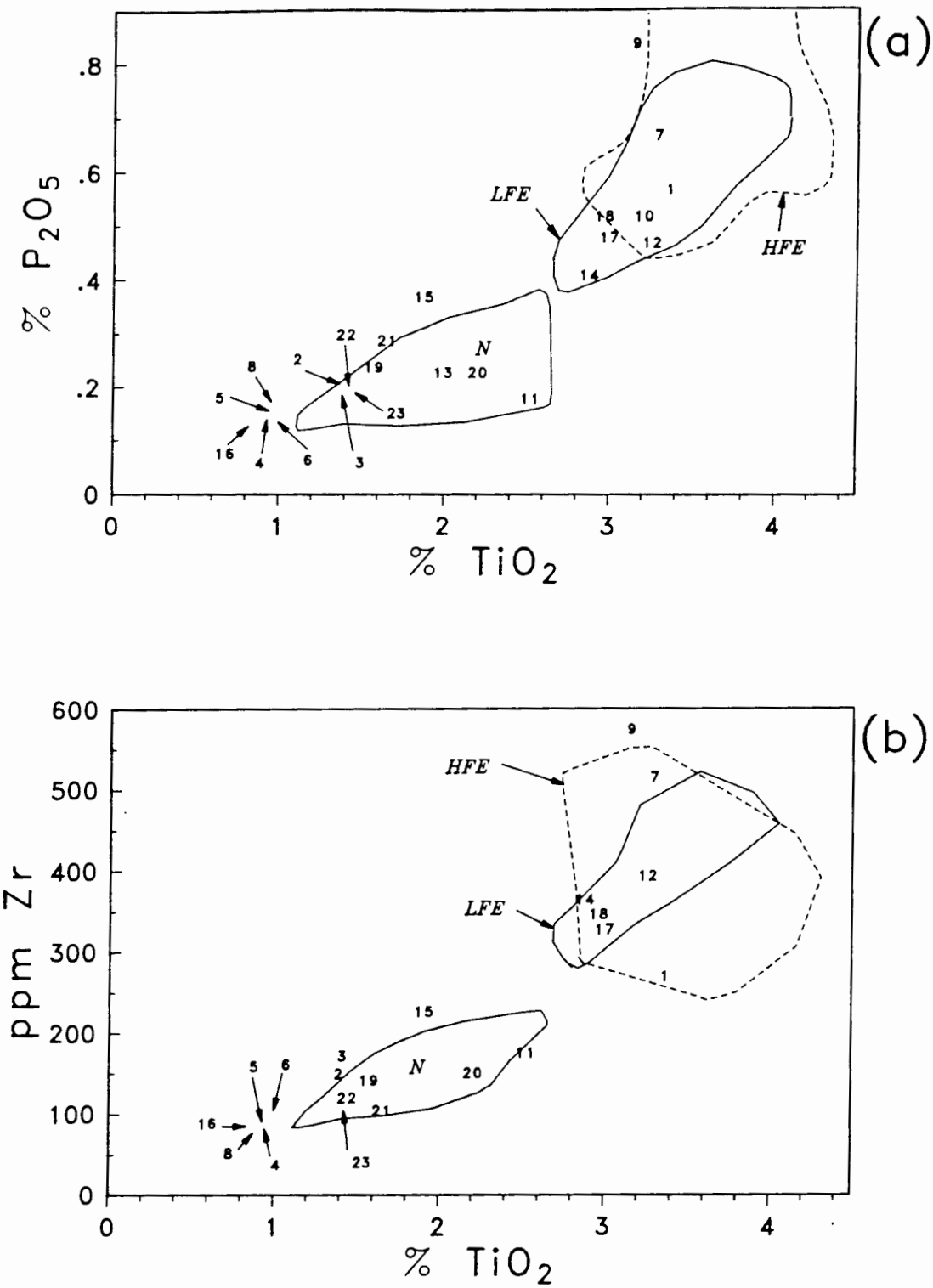

Figure 10.2. TiO_2 *vs* P_2O_5 and Zr diagram showing the fields established for the central Lebombo basaltic rocks and the averages for other areas. Numbers correspond to the areas on Fig. 10.1 and data in Table 10.1.

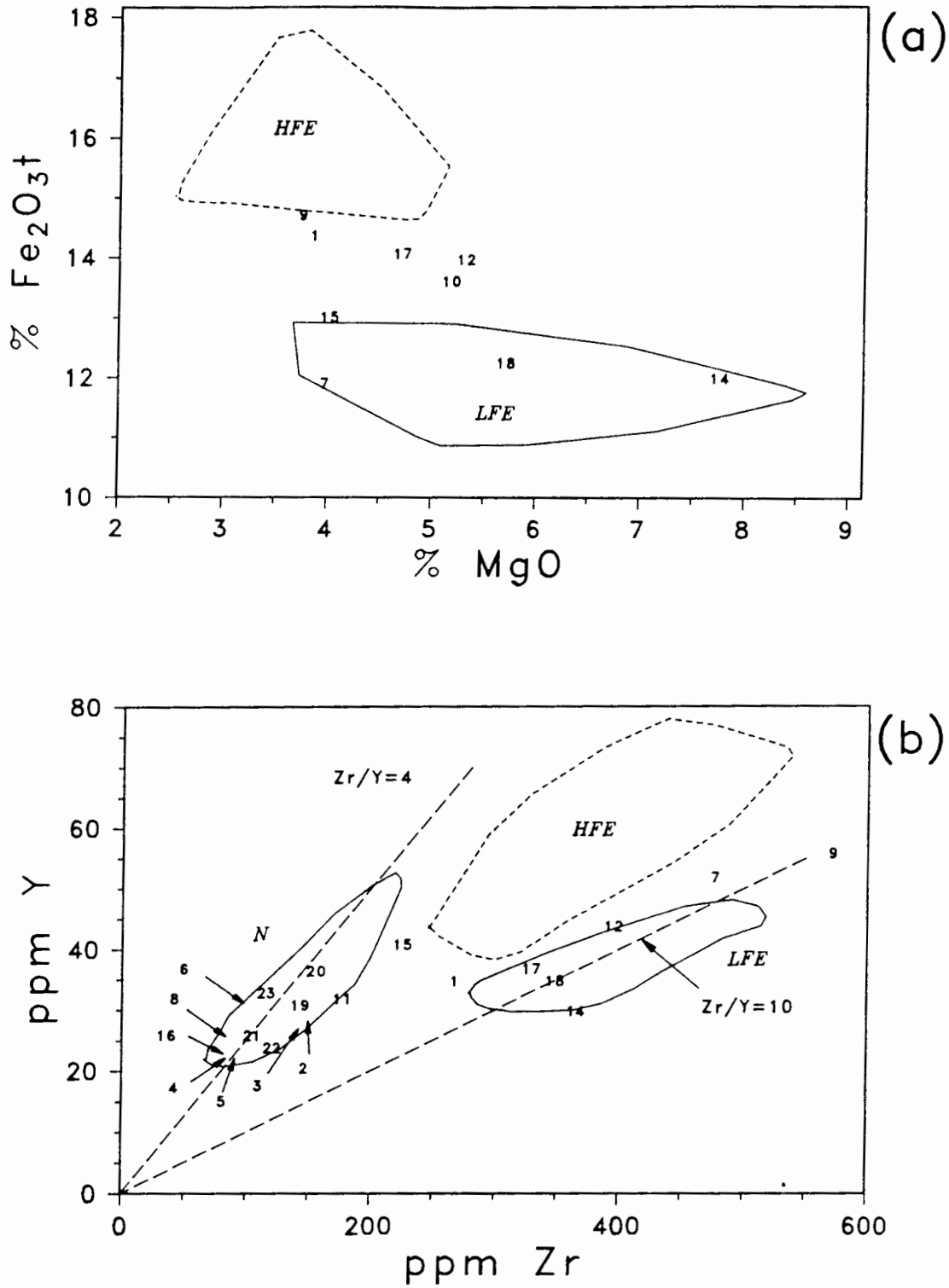

Figure 10.3. (a) Averages for MgO and Fe_2O_3t for the "enriched" Gondwana basalts only and the fields for the central Lebombo LFE and HFE groups. (b) Averages of Zr and Y data for Mesozoic basalts in Gondwanaland. Numbers correspond to the labelled areas in Fig. 10.1 and data compiled in Table 10.1.

10.3 CRUST-MANTLE RELATIONSHIPS

The division of Mesozoic basalts in south-western Gondwanaland into "enriched" and "normal" types has been regarded as reflecting two different mantle domains rather than different degrees of partial melting of compositionally similar sources (Erlank *et al.*, 1980; Cox, *et al.*, 1983; Duncan *et al.*, 1984b; Bellieni *et al.*, 1984b; Mantovani *et al.*, 1985). It is agreed here that the two basalt types most probably reflect different mantle domains and argued that crustal provinces exert a fundamental control on basalt compositions as they reflect the evolution of the lithospheric mantle (Sweeney and Watkeys, submitted). This crust-mantle model is examined on a geographical basis and then tested for geochemical consistency using the partial melting models presented in Chapter 9.

10.3.1 Crustal Framework

South-western Gondwanaland is dominated by a number of Archaean cratons which have played a central role in the development of the crust (Harris *et al.*, 1987; Hartnady *et al.*, 1985). Consequently the crustal framework will be considered in terms of:

(a) Archaean crust stable since *ca* 2.5 Ga,
(b) Archaean crust re-worked since *ca* 2.5 Ga, and
(c) post-Archaean crust formed since *ca* 2.5 Ga.

These divisions are consistent with work by Harris *et al.* (1987) who proposed that the growth of continental crust in southern Africa in the Archaean was by underplating, while lateral accretion dominated after *ca* 2.0 Ga. This is supported by palaeomagnetic data (Hale, 1987) which indicate an abrupt change in the rate and style of continental motion at about 2.5-2.6 Ga ago, when the apparent stability in the Archaean gave way to relative mobility in the Proterozoic.

There are a number of different ways of re-working any crustal fragment but the most important difference is between high T/low P metamorphism and low T/high P metamorphism. The former may involve magmas from lithospheric or asthenospheric mantle intruding the crust, thereby generating the high metamorphic temperatures (Wickham and Oxburgh, 1985) and disturbing the underlying sub-cratonic lithospheric mantle sufficiently to significantly disturb any characteristic geochemical (isotopic and incompatible element)

signature. In contrast, the latter may be major overthrust zones or merely manifestations of thin-skinned crustal processes which result in complicated PT paths (Chamberlain and Karabinos, 1987) often reflecting low T/high P metamorphism (Richardson and England, 1979) leaving the geochemical signatures of the lithospheric mantle and underlying regions comparatively unaffected.

Viewed in the above simplistic terms, south-western Gondwanaland may be considered as a number of Archaean nuclei enclosed by younger mobile belts with or without Archaean crust (Fig. 10.1). In S. America, the only Archaean crust exposed near the Parana Basin is the southern extremity of the Sao Fransisco Craton (SFC) with its reworked margin (the 2.7-2.6 Ga Gois belt, Bernasconi, 1983). In southern Africa, a western nucleus is formed by the southern-most extremities of the Congo Craton (CC) which contains Archaean inliers re-worked in a 2.2-1.9 Ga event and overprinted by younger episodes (Bassot *et al.*, 1981). An eastern nucleus consists of the Kaapvaal Craton (KC) and the Rhodesian Cratons (RC) with the intervening Limpopo Belt. This Archaean block has been re-worked in a variety of events along its western, northern and eastern margins (Tankard *et al.*, 1982; Hartnady *et al.*, 1985; Harris *et al.*, 1987). Thinned continental crust beneath the Mozambique plains (Eales *et al.*, 1984) has been interpreted as being Archaean (Harris *et al.*, 1987), whilst small remnants of Archaean crust are preserved in the dominantly Proterozoic basement of western Dronning Maud Land, Antarctica (Wolmarans and Kent, 1982; Barton *et al.*, 1987).

10.3.2 Geographic Correlations

10.3.2.1 "Normal" basalts

There is a general association of "normal" basalts with post-Archaean crust or Archaean crust re-worked in low P/high T events (Fig. 10.1). "Normal" basalts of southern Africa are found in the Central Area around Lesotho and along the southern Lebombo (Cox *et al.*, 1967; Duncan *et al.*, 1984b), both of which are regions peripheral to the Kaapvaal Craton (areas 5 and 19, Fig. 10.1). The Central Area basalts (Marsh and Eales, 1984) partially overlie craton but dominantly cover younger crust formed by the mid-Proterozoic Natal Belt (Tankard *et al.*, 1982). Further occurrences of "normal" basalts are on the Springbok Flats (Marsh, 1984; area 6, Fig. 10.1),

which are underlain by the Bushveld Complex intruding the Kaapvaal Craton, as well as in eastern Botswana (area 8, Fig. 10.1). In the latter region, the basement is thought to be represented by the western termination of the Archaean Limpopo Belt which was overprinted by early Proterozoic high T/low P re-working (Key *et al.*, 1983).

"Normal" basalts crop out north of Nuanetsi, at Mafungabusi on the western margin of the Rhodesian Craton (Sutton, 1979; area 13, Fig. 10.1), and at Victoria Falls (Maufe, 1929; Duncan *et al.*, 1984a) where they overlie "enriched" basalts (area 11, Fig. 10.1). Further north-west towards the Congo Craton, both types have been recognized from boreholes in Zambia (Ridgeway and Money, 1981). Only "normal" basalts occur in the Lupata region of Malawi and Mozambique (Macdonald *et al.*, 1983) where they overlie late Proterozoic crust (areas 15 and 16, Fig. 10.1).

Similarly only the "normal" basalt type is recognized in Antarctica (Juckes, 1972; Furnes *et al.*, 1982; Harris *et al.*, 1988; Furnes *et al.*, 1987; areas 21, 22 and 23, Fig. 10.1), preserved in rifts overlying Proterozoic crust (Wolmarans and Kent, 1982). Harris *et al.* (1988), however, have recorded the presence of Mesozoic dolerite dykes of "enriched" affinity in the Ahlmannryggen massif *ca* 150 km north-west of the Kirwanveggan as orientated in Fig. 10.1. The southern third of the Parana Basin in Brazil and the adjacent southern Etendeka region of Namibia consists of "normal" basalts (Bellieni *et al.*, 1984b; Duncan 1987; Petrini *et al.*, 1987; areas 2 and 3, Fig. 10.1), although in S. America there is a diffuse zone over 200 km wide where both "normal" and "enriched" types exist. The basement to this diffuse zone and regions to the south is Proterozoic or younger in age (Bernasconi, 1983).

There are, however, a number of areas where "normal" basalt occurs on Archaean crust that require explanation.

(a) Mafungabusi (area 13, Fig. 10.1) consists of "normal" basalts overlying the Rhodesian Craton. However, the absence of feeder dykes and the thickening of the basalt sequence to the north-west led Sutton (1979) to conclude that the source area for these basalts lay off-craton to the north-west.

(b) In eastern Botswana (area 8), "normal" basalts overlie the western end of the Limpopo Belt but this is an area affected by early high T/low P Proterozoic reworking (Key *et al.*, 1983).

(c) The Springbok Flats contain predominantly "normal" basalts with some "enriched" types in the north-east (Marsh, 1984; areas 6 and 7, Fig. 10.1). However, this is an anomalous cratonic area dominated by the *ca* 2.0 Ga Bushveld Complex, the intrusion of which may have disturbed the "enriched" signature of the sub-cratonic lithospheric mantle in this area, as well as providing potential conduits to an upper mantle (asthenosphere/lithosphere?) potentially exploited by the Karoo basalts which crop out in this area.
(d) The southern Lebombo is another region where "normal" basalts apparently overlie Archaean crust, although the actual basement immediately below the basalts is not exposed (area 19, Fig. 10.1). The presence of zircons of Proterozoic age in rhyolites overlying the Karoo basalts in the southern Lebombo (Van Niekerk, 1968; Armstrong, pers. comm., 1987) and assuming these zircons are crustal in origin, indicates that the crust (and therefore the associated lithospheric mantle) in this area has been affected by events since the Archaean. Further west, underneath the Central Area, Hawkesworth *et al.* (1983) consider the cratonic upper crust to be underlain by Proterozoic lower crust, implying underplating along the southern margin of the Kaapvaal Craton. Furthermore, an examination of thermobarometry data of mantle nodules in Lesotho kimberlites, suggests a lithospheric mantle thickness of 120-145 km in this region (Carswell and Gibb, 1987), suggesting either thinning of the *ca* 200 km thick "keel" (detailed in Chapter 9) near its margins or the presence of a thinner more recently accreted mantle lithosphere in this region.

10.3.2.2 "Enriched" basalts

Generally, "enriched" basalts overlie Archaean crust or Archaean crust re-worked in low T/high P events. The "enriched" basalts of southern Africa occur on the Rhodesian Craton at Featherstone (Duncan *et al.*, 1984b; area 14, Fig. 10.1), as well as at its western edge in eastern Botswana and western Zimbabwe (Duncan *et al.*, 1984b) across the Limpopo Belt (Cox *et al.*, 1967; Vail *et al.*, 1969), and in the Nuanetsi-N. Lebombo area (Cox and Bristow, 1984) (areas 9, 10, 12, 17 and 18; Fig. 10.1). All these regions are underlain by Archaean crust which has been stable since *ca* 2.5 Ga or undergone minimum low T/high P re-working.

In South America, the "enriched" basalts of the Parana Basin overlie or are adjacent to the Sao Fransisco Craton (area 1, Fig. 10.1). The nature of

the basement in the central Parana Basin, however, is poorly known and only assumed to have a similar age to the immediately adjacent exposed terrains. The northern portions of the Etendeka Plateau in Namibia, essentially an eastern extension of the Parana Basin, contains "enriched" basalts (Duncan, 1987) which overlie post-Archaean crust involved in the Damara orogeny (Guj, 1970) but which are close to the more ancient Congo Craton (Bassot *et al.*, 1981). Furthermore, the "enriched"/"normal" division in the Parana Basin is not geochemically or geographically as well defined as that in the Lebombo. This may be a result of differences in the age of the crust and the associated mantle underlying the central Parana Basin being spatially and therefore geochemically, in the case of the mantle, less well defined mantle underlying the central Parana Basin. In addition, off-axis volcanism in East Africa demonstrates that centres of major volcanism may be 100-150 km from rifts where most of the products are preserved (Bosworth, 1987) which may suggest the source for some of the "enriched" basalts may be some distance from present exposures.

10.3.2.3 Summary of basalt distribution

Examination of the regional geology of south-western Gondwana reveals that "enriched" basalts are found mainly on Archaean crust which has been stable since *ca* 2.5 Ga or undergone only low T/high P re-working. In contrast "normal" basalts tend to overlie or are adjacent to, crust younger than *ca* 2.5 Ga or Archaean crust which has undergone high T/low P re-working. This is illustrated in a schematic block diagram view of eastern southern Africa showing basalts preserved in the southern Lebombo to southern Malawi regions and their associated crustal provinces (Fig. 10.4).

As well as the central Lebombo, areas where both "enriched" and "normal" basalt types occur (Fig. 10.1) are the Springbok Flats (Marsh, 1984; Duncan, 1987); Botswana (Duncan *et al.*, 1984; Duncan, 1987); the Etendeka (Duncan, 1987) and in the central Parana Basin of south-east Brazil (Bellieni *et al.*, 1984a, 1985; Mantovani *et al.*, 1984; Petrini *et al.*, 1987). The South American Mesozoic volcanics have been correlated with the Karoo volcanics of north-west Namibia (Etendeka) in pre-Gondwana rift times by Erlank *et al.* (1984) and Bellieni *et al.* (1984b). These areas of simultaneous occurrence appear to overlie regions on or close to the Archaean/Proterozoic crustal boundary and, by implication, the lithospheric

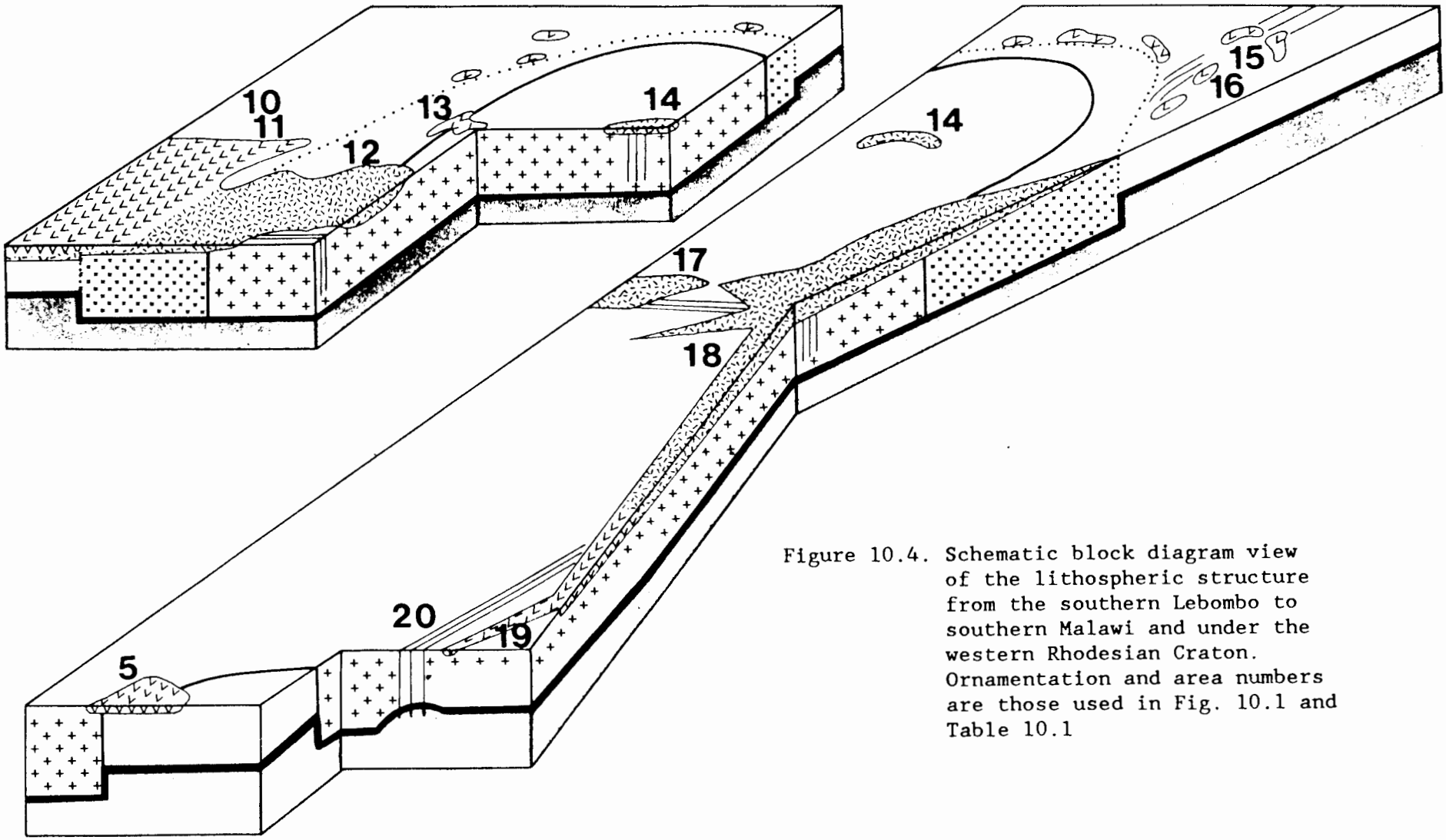

Figure 10.4. Schematic block diagram view of the lithospheric structure from the southern Lebombo to southern Malawi and under the western Rhodesian Craton. Ornamentation and area numbers are those used in Fig. 10.1 and Table 10.1

mantle associated with these crustal provinces.

10.3.2.4 Dykes and sills intruding Archaean and post-Archaean crust

One of the problems in relating basalts to underlying source areas is the distance lava may have flowed from vents. In the case of flood basalts, this may be hundreds of kilometres. An obvious solution is to examine the geochemistry of dykes and sills, even though both may have intruded some distance laterally and be areally misleading insofar as their volumetric significance is concerned.

Mesozoic dolerite dykes intrude the cratons but are heavily concentrated around craton margins and rifted areas such as the Limpopo. Sills are more common and widespread across the cratons where thick sequences of Karoo sediments (particularly the Beaufort Group) are preserved (Eales *et al.*, 1984). Unfortunately, with the exception of the Rooi Rand dyke swarm (Armstrong *et al.*, 1984), detailed geochemical data on dolerite dykes in the Karoo Igneous Province are absent. Existing data (Walker and Poldervaart, 1949; Duncan *et al.*, 1984a) with one exception (south of the Central Area, Walker and Poldervaart, 1949), indicates the presence of "normal" dolerites only, intruding Karoo sediments overlying the southern margin of the Kaapvaal Craton (south of a projection of the NE/SW trending Mozambique coastline, just east of the central Lebombo, Fig. 10.1). This may be due to the Proterozoic reworking of the crust along this southern margin suggested by Hawkesworth *et al.* (1983) from isotopic determinations on crustal xenoliths recovered from N. Lesotho kimberlite pipes.

Overall, the model presented here would seem to predict that dykes intruding Archaean crust should be "enriched" and those intruding more recent crust should be "normal". However, it is suggested that this may not necessarily be the case. It is likely that the melting of the relatively "cold" sub-cratonic lithospheric mantle (Gurney and Harte, 1980), which yields "enriched" basalts, is only possible in areas where heat flow is enhanced considerably. It is suggested that only in areas of major rifting will heat flow be enhanced sufficiently to melt the "cold" sub-cratonic lithospheric mantle. In the context of the crust-mantle model presented, this may explain the most voluminous occurrence of "enriched" basalts in the N. Lebombo-Tuli-Nuanetsi region which has been ascribed to a failed triple junction (Burke and Dewey, 1973). Generally, therefore, melting occurring

away from major rifts may be confined to mantle peripheral to the "cold" sub-cratonic lithospheric "keel" and if tapped, "normal" magmas may result. Thus the derivation of "normal" basalts from an upper mantle source, characterised by a higher heat flow (e.g. thinner lithospheric mantle underlying crust <2.5 Ga) or an asthenospheric mantle (isotopically enriched), is consistent with the greater abundance of this magma type relative to the "enriched" type. The difficulty of melting the "cold" sub-cratonic lithosphere is evidenced by its very nature, i.e. stability with time as established by many studies (*op cit.*, Chapter 9).

10.3.3 Geochemical Correlations

10.3.3.1 Incompatible elements

The partial melt modelling in Chapter 9 concludes that, with respect to the suite of incompatible elements considered, it is possible to derive the "enriched" group (LFE group) in the central Lebombo by *ca* 10% melting of old sub-cratonic lithospheric mantle as geochemically characterized by Erlank *et al.* (1987). If this is the case, the "normal" group would then need to be derived from a source more depleted in these incompatible elements, potentially located in more recently accreted and therefore thinner, lithospheric mantle beneath post-Archaean crust.

It is stressed that geochemical modelling alone does not refute a common source for the basalt types and the alternative explanation by different degrees of partial melting. Rather, it merely examines, with respect to some incompatible elements, whether it is feasible to extract the "enriched" group from the sub-cratonic lithospheric mantle as defined by a suite of mantle xenoliths. It is also important to stress that the incompatible element "enriched" nature of the sub-cratonic lithospheric mantle does not necessarily imply greater fertility with respect to basaltic constituents (e.g. Ca, Al, Fe) relative to asthenospheric mantle (Chapter 9).

10.3.3.2 Radiogenic Isotopes

Nd- and Sr-isotope data (this study, Hawkesworth *et al.*, 1983, 1984, 1986) show that the "enriched" basalts plot on or below an extension of the mantle array, while "normal" basalts plot on the array and to the right of it

(Fig. 10.5). Unfortunately it is difficult to resolve the difference between the contributions which crustal contamination and original mantle source heterogeneity may have made to the distributions of other Gondwana basalts elsewhere and therefore this discussion is confined to samples from the Lebombo.

It was concluded earlier in this thesis that Nd- and Sr-isotopic data for the HFE- and LFE-group basaltic rocks has not been significantly affected by crustal contamination and that these data represent "primary" values. In the case of the N group, however, granitic contamination is significant and is at least partially responsible for the higher $^{87}Sr/^{86}Sr$ initial ratios in some samples belonging to this group. However, granitic contamination cannot produce the range of $^{143}Nd/^{144}Nd$ initial ratios observed or the total spread in $^{87}Sr/^{86}Sr$ initial ratios for the N group in the Lebombo (Chapter 7). Thus some additional high-Sr and low-Nd initial ratio component is required to explain the full range in N-group isotopes. If this additional component is not crust (i.e. if $^{87}Sr/^{86}Sr$ ratio at 190 Ma >>.730, used in AFC models, Chapter 7), it appears that at least three mantle end-members are required to explain the variations in Sr- and Nd-isotopes: a low ϵ_{Sr}-high ϵ_{Nd} end-member; a low ϵ_{Sr}-low ϵ_{Nd} end-member and a high ϵ_{Sr}-low ϵ_{Nd} end-member (Fig. 10.6). These end-members may be similar to MORB mantle (DMM), and two enriched mantle components (EM1 and EM2) identified by Zindler and Hart (1986) for oceanic basalts. The HFE group would then contain a greater DMM component then the other basalt groups; the LFE group is dominated by an EM1 component and the N group significantly influenced by an EM2 mantle end-member. Obviously in the case of the N group, contamination with a granitic crust of variable $^{87}Sr/^{86}Sr$ content may be largely responsible for the spread to higher ϵ_{Sr} values, but not the spread to the low ϵ_{Nd} values observed (Chapter 7). However, even without the complicating effect of granitic contamination, there would still be overlap between the N and LFE groups, which may imply some isotopic homogenization of their sources.

Menzies (1988) has applied the isotopic end-members defined for sub-oceanic mantle by Zindler and Hart (1986) to sub-crustal lithospheric mantle xenoliths and volcanics in the western U.S.A. Menzies (1988) maintains that an EM1 component in that region is restricted to sub-Archaean terraines and that the EM2 component may exist beneath Proterozoic crust.

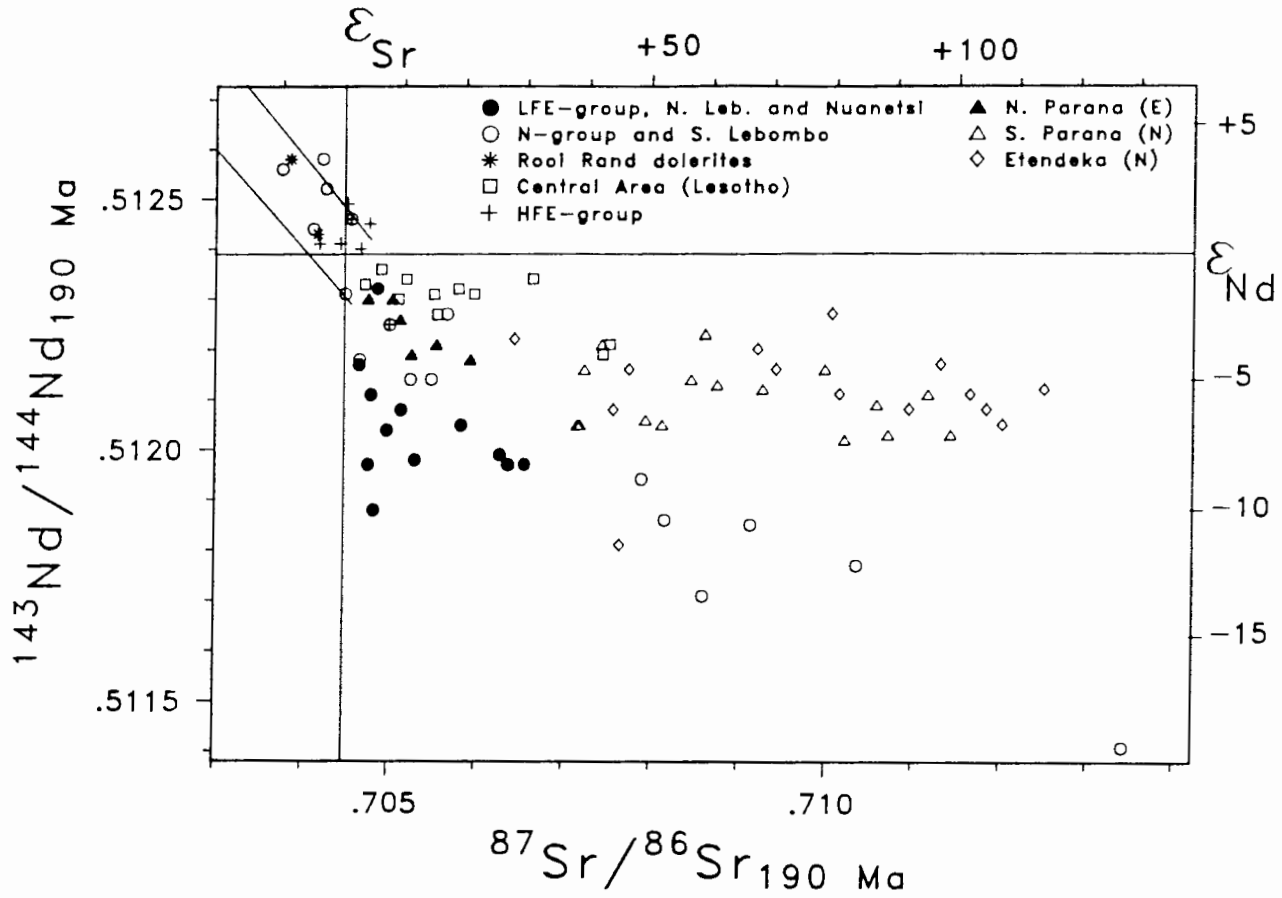

Figure 10.5. Nd- and Sr-isotope ratios for the "enriched" (solid symbols) and "normal" (open symbols) basalt types in the Gondwana remnants (data this study, Hawkesworth *et al.* 1984, 1986, calculated at 190 Ma).

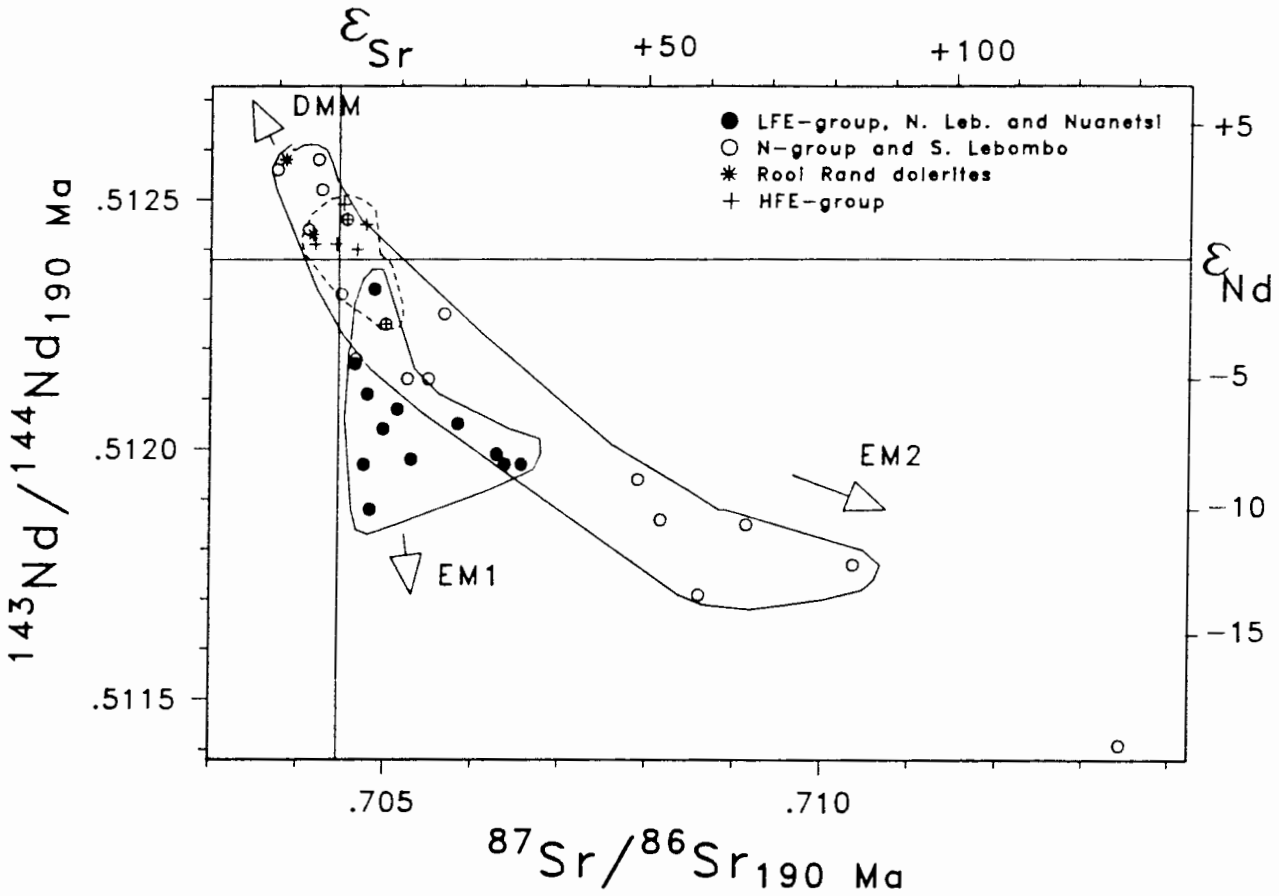

Figure 10.6. Nd- and Sr-istope ratios for the Lebombo only (ornamentation as Fig. 10.5, data calculated at 190 Ma) with suggested mantle 'end-member' components (from Zindler and Hart, 1986) which may be influencing the spread. DMM is depleted MORB, and EM1 and EM2 are two enriched mantle end-members.

Generally, Sr and Nd-isotopic evidence in south-western Gondwanaland basalts, coupled with geographic evidence would corroborate such a view for this region (Figs. 10.1, 10.6), although it would seem EM1 and EM2 sources may not be as isotopically discrete as the case suggested by Menzies (1988) for the western U.S.A.

10.4 ALTERNATIVE MODELS EXPLAINING BASALT GEOCHEMISTRY

I. Different degrees of partial melting of a homogeneous mantle.

This model may explain the incompatible trace element data for the central Lebombo rocks but is inconsistent with isotopic data (Chapter 9). Fodor (1987) has proposed such a model for the Parana basalts, in conjunction with the Tristan da Cunha hotspot. However, as pointed out by Erlank *et al.* (1988), his model has no garnet in the source required in the case of the central Lebombo (Chapter 9), and cannot account for lower $^{143}Nd/^{144}Nd$ initial ratios relative to typical asthenosphere (e.g. MORB) for Mesozoic basalts of southern Gondwanaland (Fig. 10.5). Furthermore, it is difficult to envisage plume activity giving rise to the present distribution of "enriched" and "normal" basalts as well as being responsible for such a sustained melting process implied by the volume of basaltic volcanics observed in southern Gondwanaland.

II. A linked subduction-convection model for the asthenosphere.

Cox (1978) and Froidevaux and Nataf (1981) point out that the distribution of the Parana, Karoo and Kirkpatrick (Antarctica) basalts forms a band which is near parallel to the Pacific margin of a reconstructed Gondwanaland, along which subduction has occurred since the Devonian. Froidevaux and Nataf (1981) have provided experimental evidence for large-scale convective rolls developing on the continental side of subduction zones which have an upwelling limb 3000-4000 km from the subduction zone. Erlank *et al.* (1988) note the similar orientation of the Pacific subduction zone with a boundary, *ca* 3000 km to the east, extrapolated between, and separating areas of, dominantly "enriched" basalts to the north from exclusively "normal" basalts to the south. Duncan (1987) suggested as one of

a number of alternatives, that the CAB signature of "normal" basalts, as determined from geochemical discrimination diagrams, may be induced by the upwelling limb of an asthenospheric convection cell linked to the Pacific subduction zone at its downgoing (southern) component. The other "half" (north) of such a convection cell may then be responsible for the chemistry of the "enriched" province (Duncan, pers. comm., 1988). A problem with such a model, however, is that it has difficulty in explaining the diffuse geographical nature of the "enriched"/"normal" division in the Parana area relative to the Lebombo and it is difficult to envisage the same convection cell producing such different results in the two areas, unless there is a significant lithospheric mantle control.

Erlank *et al.* (1988) suggest that, if the convective roll model is not responsible for the geochemical variations observed (no chemical mass transfer), it still may be the source of heat which initiated melting of the upper mantle and generation of the southern Gondwanaland basalt provinces.

Thus the melting of two pre-existing lithospheric mantle domains is the model preferred and it has been suggested that these domains are intimately linked to crustal evolution. A convective roll model, however, may be a useful heat supply mechanism causing generation of basalts in the Mesozoic. The tectonics and generation of the Lebombo volcanics is considered in more detail below.

10.5 TECTONICS OF THE LEBOMBO

10.5.1 Regional Setting

The age of the main Lebombo basaltic volcanism is 195-185 Ma (Duncan *et al.*, 1984) while the oldest magnetic anomaly off the south-east coast of Africa is M21 or M22 corresponding to an age of 145 Ma (Martin and Hartnady, 1986). Thus, ostensibly most of the basaltic volcanics in this area significantly predate Gondwana break-up.

The model proposed here is sketched in Fig. 10.7. It is proposed that continental movement was initiated *ca* 195 Ma ago and the crust responded by stretching and thinning which led to mantle upwelling and the eruption of the main sequence of volcanics in the Lebombo, Tuli and Nuanetsi areas (I).

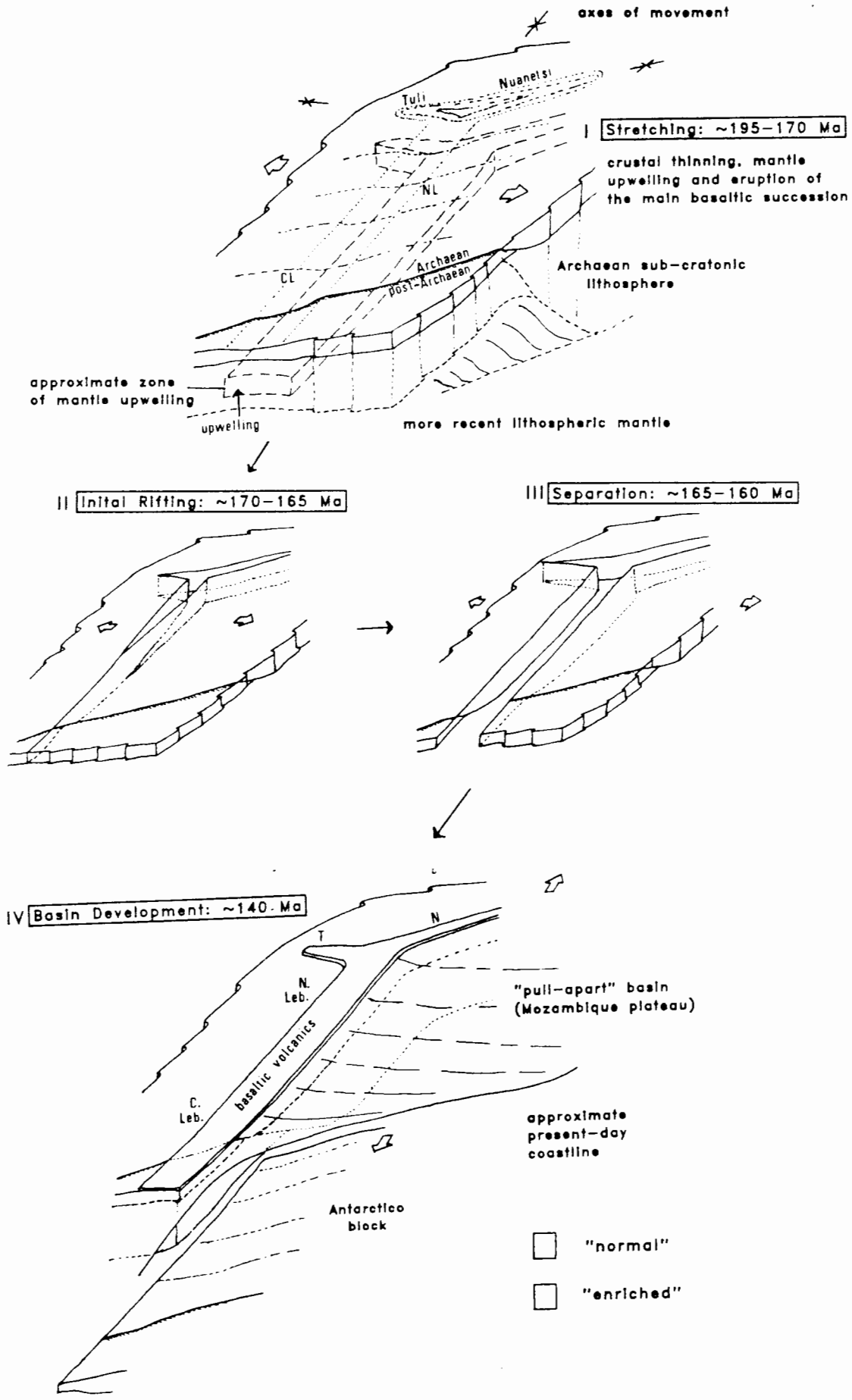

Figure 10.7. Suggested sequence of events for Gondwana associated rifting in the Lebombo-Nuanetsi regions

Alternatively some mechanism caused mantle-upwelling which initiated rifting and crustal thinning. The initiation of movement or cause of mantle upwelling may have been a build up of heat supplied by the Devonian Pacific subduction underneath the continental carapace of Gondwanaland (Cox, 1978; and above). Shown on Fig. 10.7 (I) is the suggested approximate position of the Archaean Kaapvaal craton/post-Archaean boundary along with their associated lithosphere. Also shown is the approximate location of a hypothetical zone of partial melting in the mantle from which the basaltic rocks are derived. The surface distribution of the basaltic rocks is given in IV (and Fig. 10.4). For stage I and until crust separation is complete (II and III), the relative movement of each plate was in an approximately E-W direction (Watkeys and Sweeney, 1988). The initiation of N-S strike-slip movement is accompanied by the development of a pull-apart basin which is presently the Mozambique Plateau (Watkeys and Sweeney, 1988) filled with Cretaceous and Tertiary sediments deposited by proto-Limpopo and Zambezi Rivers (Martin, 1984). It is interesting that Harris *et al.* (1986) report that the Mesozoic Kirwanveggan basalts of Dronning Maud Land (Antarctica) are compositionally closer to the southern Lebombo or N-group basalts than any other Karoo basalt type, which has obvious implications for Gondwana reconstructions (Figs. 10.1, 10.7).

10.5.2 Implications for Mantle Structure and Eruption Histories

The formation of the Mozambique Basin may be tested geodynamically using estimates of crust and lithospheric mantle thicknesses. Subsidence (S_c) caused by crustal thinning is given by McKenzie's (1978) equation:

$$S_c = \frac{C\,(P_m - P_c)[1-(aT_0/2)C/A]\,(1-1/B_c)}{P_m}$$

where: P_c = density of the crust (g/cm^3)

P_m = density of the mantle (g/cm^3)

a = the coefficient of thermal expansion (°C^{-1})

B_c = extension factor for crust (% thinning/extension in km)

T_0 = temperature at the base of the lithosphere (°C)

C = initial crustal thickness (km)

A - initial lithosphere thickness (km)

Values of P_c (=2.8 g/cm^3), P_m (=3.4 g/cm^3), a (3.4×10^{-5} °C^{-1}, T_0 (1350 °C) and C (40 km) are set similar to estimates made by Steckler (1985) for the Gulf of Suez area. Thus, for estimates of B_c and S_c, values for A may be calculated. Steckler (1985) reports values of B_c in the range 1.35-1.70 which for values of S_c of 2-3 km, estimated for the Mozambique Plateau cover thickness (Flores, 1973), corresponds to a lithosphere 150-200 km thick. This is in agreement with observed estimates (e.g. Haggerty, 1986; Boyd *et al.*, 1985) for the southern African sub-cratonic lithospheric mantle. Therefore a tectonic model accounting for the development of the Mozambique Basin adjacent to the N. Lebombo is consistent with the existence of thick (i.e. sub-cratonic) lithospheric mantle beneath the N. Lebombo in pre-drift times.

The initiation of rifting in the Tuli-Nuanetsi-Lebombo triple junction and propagation southwards (II and III, Fig. 10.7) would explain the relative timing (indicated by their relative stratigraphic positions) of the generally earlier eruption of "enriched" basalts in the N. Lebombo relative to the later "normal" volcanism further to the south. Each basalt type is derived from compositionally different mantle zones: one within the sub-cratonic lithospheric mantle and one most likely within more recently accreted sub-lithospheric mantle associated with more recently accreted crust. The surface expression of the basalt types does not coincide with the interpolated surface expression of the craton boundary (IV) as the margins of this boundary are assumed to slope away to the north-west. An east-west cross-section of the central Lebombo is suggested in Fig. 10.8 and shows the raising of the lithospheric mantle interface with the extensional tectonic regime proposed. The "enriched" (LFE group) melts then derive from sub-cratonic mantle, collect and fractionate at the mantle-crust boundary (the high-pressure crystallization of the N. Lebombo picrites) and feed higher level chambers (lower pressure crystallization) before eruption (Fig. 10.8). The "normal" (and the HFE group) "primary" melt may collect and fractionate at the crust-mantle boundary or feed higher level magma chambers before eruption. In the case of the "normal" samples affected by granitic contamination, these high-level chambers are sited in the continental crust. For the HFE group (not shown on Fig. 10.8) samples and any higher MgO correlatives in the N group (indistinguishable from N-group samples

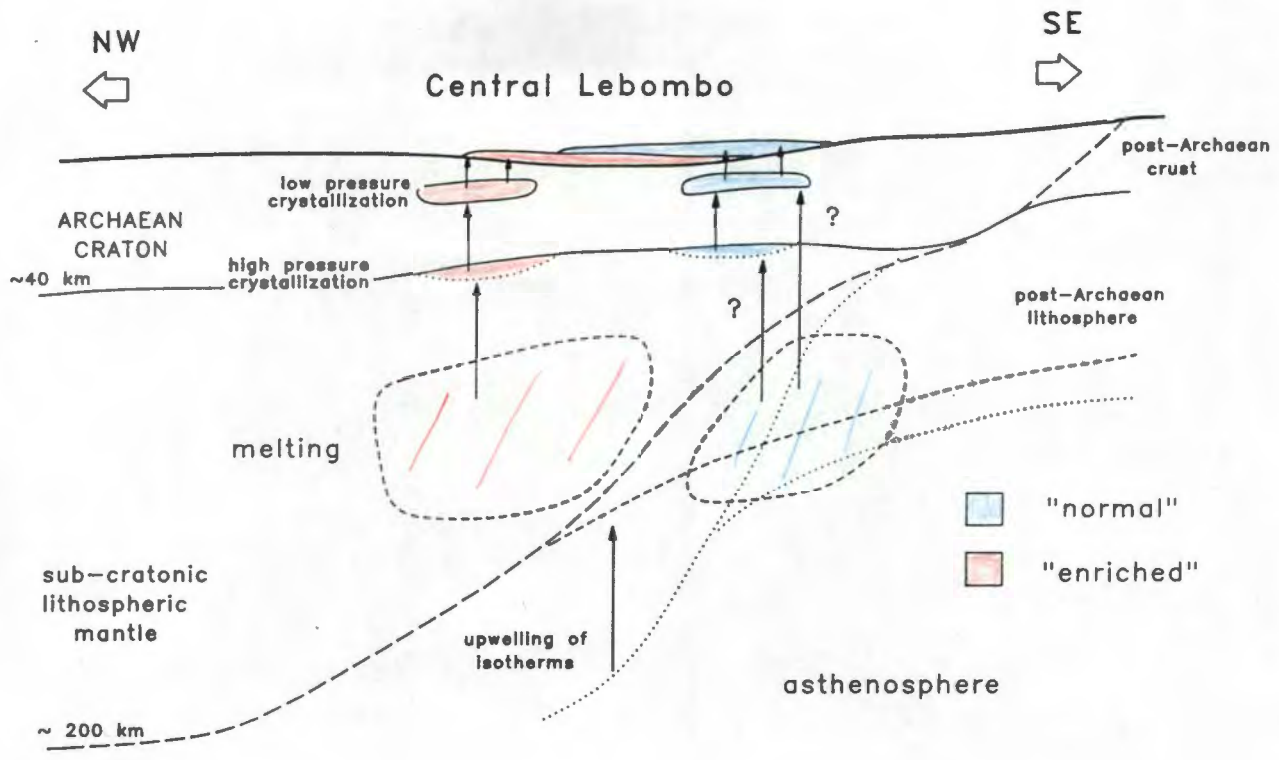

Figure 10.8. Cross section envisaged *ca* 195- 175 Ma ago for the central Lebombo showing the location of possible sources for the LFE- and N-groups.

uncontaminated with granitic crust), this fractionation may have taken place outside continental crust, e.g. in newly formed oceanic crust or at a crust-mantle boundary which has been brought to much shallower levels by attenuation of the continental crust.

It is significant that, while the two sources for "enriched" (LFE group) and "normal" (N group) basalts are juxtaposed in this model, there is no geochemical evidence in this study for any magma mixing of the two basalt types subsequent to their derivation from mantle source regions. Coupled with their interbedded nature, this necessitates discrete and well separated mantle source areas and eruption through spatially separated conduits. This is supported by the absence of LFE-group dolerites in the Crocodile/Komati River area although all dolerite types are present in the Sabie River area.

10.6 CONCLUSIONS

1. Regional geology shows that the "enriched" (LFE-group) basalts are associated with Archaean cratons whilst the "normal" basalts are found overlying post-Archaean crust.

2. Geochemical modelling and isotopic studies (Chapter 9) demonstrates that, if the sub-cratonic lithospheric mantle is represented by "cold" garnet-bearing xenoliths in kimberlites, the LFE-group "primary" composition may be extracted from this mantle by *ca* 10% melting. However, the N-group basalts in the central Lebombo then require an alternative source, and lithospheric mantle partially enriched in incompatible, elements, peripheral to the sub-cratonic mantle 'keel', is envisaged.

3. Tectonic modelling of the development of the Mozambique Basin is consistent with the existence of thick (150-200 km) lithospheric mantle beneath the N. Lebombo in pre-drift times. This implies that the N. Lebombo-Tuli-Nuanetsi area is representative of intracratonic rifting.

4. The petrogenesis of each basalt group in the central Lebombo is consistent with the lithospheric structure sketched in Fig. 10.8.

5. Previous studies of "on-craton" diamondiferous and "off-craton" non-diamondiferous kimberlites (*op cit.*) have revealed important

differences in the thickness of the lithospheric mantle under these two regions. This contrast is mirrored in the source regions for flood basalts and serves to re-emphasise the important difference between Archaean and post-Archaean lithosphere in south-western Gondwanaland.

6. The marked difference in thickness between sub-cratonic upper mantle and upper mantle underlying more recently accreted crust may be related to the mechanism of continental growth. It has been proposed by Harris *et al.* (1987) that the growth of continental crust in southern Africa in the Archaean was by underplating, while lateral accretion dominated after *ca* 2.0 Ga. This is supported by palaeomagnetic data (Hale, 1987) which indicate an abrupt change in the rate and style of continental motion at about 2.5-2.6 Ga ago, when the apparent stability in the Archaean gave way to relative mobility in the Proterozoic. Thus conditions may have been more favourable in the Archaean for the development of thick sub-continental lithosphere, and this provided a fundamental control on the composition of Karoo basalts during Gondwana rifting.

11. SUMMARY OF CONCLUSIONS

11.1 GEOCHEMICAL VARIATIONS

The division of Karoo basaltic rock types into the northern "enriched" and southern "depleted" ("normal") types of Cox *et al.* (1967) is substantiated in the central Lebombo. The set of elements which best shows the division are the high-field-strength elements (Ti, P, Zr, Nb, Y, La, Ce and Nd). The "enriched" group in the central Lebombo is subdivided on the basis of Fe_2O_3 (total Fe) and MgO into a low-Fe enriched group (typical northern "enriched") and a high-Fe enriched group, hitherto unreported in the Karoo Igneous Province. The different Zr/Y ratios of these suites is diagnostic. The N and HFE groups form a continuum in major element and most trace element (specifically the HFSE) abundances.

While each rock-type has a suite of petrographic characteristics, there is no definitive petrographic criterion by which the basaltic suites may be differentiated.

All three basalt types are interbedded in the Sabie River area and N- and HFE-group basalts are interbedded in the Crocodile/Komati River area. There is an increase in the amount of N-group basalt occupying the section southwards and a corresponding decrease in the amount of LFE-group basalt. Although the basalts are interbedded, most of the LFE-group was erupted first, followed by the N- and then the HFE-group basalts. This general time distribution and the interbedded nature of the basaltic rocks places constraints on any proposed petrogenetic and tectonic models.

11.2 PETROGENESIS

Detailed consideration and modelling of all available geochemical and isotopic data shows that the only petrogenetic process by which the N and LFE groups may be related is partial melting (Chapter 9). It is possible to explain the different incompatible element concentrations and similar major oxide concentrations in the two groups by different degrees of partial

melting of the same mantle source composition, e.g. 2.5% and 15% for the LFE- and N-group "primary" melts respectively. This hypothetical source which has a chemistry constrained by this model, bears no compositional resemblance to lithospheric mantle beneath cratonic regions as sampled by kimberlite xenoliths. Rather, it appears to have a composition similar to, or slightly more enriched in, incompatible elements than estimates of primordial or primitive mantle. However, differences in "primary" N and LFE group Nd- and Sr-isotopic compositions, although they overlap, cannot be explained by a common-source model. The preferred model is to suppose compositionally **different sources** and constrain the composition of each at 10% melting (arbitrary) using the estimates of "primary" melt compositions for each group. In the case of the LFE group such a source is compositionally akin to a sub-cratonic lithospheric mantle as defined by evidence from mantle xenoliths. The calculated N-group source would be similar to observed estimates for primordial/primitive mantle which isotopically (Sr and Nd), would be similar to a Walvis Ridge Basalt source (Fig. 9.2).

The LFE group may be related to the N. Lebombo picrites by continued fractional crystallization. These picrites do show evidence of high- and low-pressure crystallization (Chapter 6) and it is suggested that the crust/mantle interface (*ca* 40 km depth) may be a convenient collection point for any mantle-derived melt and the likely site for any high-pressure crystallization. Although a closed-system fractional crystallization model can account for observed geochemical correlations in this group, a model describing a magma chamber undergoing continuous fractionation with periodic tapping and replenishment (Chapter 8) is dynamically more reasonable. Contamination of the LFE-group with granitic continental crust may only affect K_2O and Rb distributions significantly and then the process must be highly selective.

A major motivation for considering RTF processes is the inability of closed-system fractional crystallization to account for incompatible element enrichments with decreasing MgO observed in some samples of the N group and most HFE-group samples. These enrichments can be explained by an RTF model for the HFE group, but not for the N group if it is assumed that the observed mineral chemistries are representative of those minerals in the fractionating assemblage. A model supposing a magma chamber replenished by melt derived by progressively lower degrees of partial melting (10% to 6%) of the

compositionally primitive mantle source suggested above would explain the geochemical correlations observed in the N group with the exception of Ba and Nb (Chapter 9).

Evidence for contamination with granitic material is only convincing in the case of the N group. Varying degrees of fractional crystallization and assimilation (AFC) may account for most N-group data, notably correlations observed between initial $^{87}Sr/^{86}Sr$ ratio with SiO_2, K and Rb. The HFE group shows no evidence for significant contamination with granitic continental crust and these samples may be related to uncontaminated N-group samples by a combination of continued fractional crystallization from an N-group parent and by varying degrees of partial melting of a N-type source.

Stratigraphic variations discussed in Chapter 5, show that there is no simple relationship between time (as measured by stratigraphic height) and abundance of elements for any of the groups (Fig. 5.3). A random variation of RTF parameters may account for the absence of such correlations (Chapter 8). It has been suggested (Chapter 7) that the K and Rb abundances in the LFE group may be influenced by selective contamination with granitic crust. This is not the case for Sr and Ba, however, whose heterogeneity in a magma chamber throughout the eruption of the LFE-group basalt sequence (Fig. 5.3) must reflect original heterogeneities in the material supplying such a chamber.

11.3 MANTLE PROVINCES AND TECTONIC SETTING

It is suggested (Chapter 10) that the eruption of the main Lebombo basaltic succession marked the onset of rifting *ca* 195 Ma ago. Detailed geochemical modelling shows that it is preferable to derive the LFE group from old enriched sub-cratonic lithospheric mantle, and the N and HFE groups from a zone of more recently accreted lithospheric mantle or anomalously enriched asthenospheric mantle, both peripheral to the old sub-cratonic "keel". The identification of these two mantle domains is extended by analogy to other occurrences of Mesozoic basalt in "southern" Gondwanaland (e.g. Etendeka, Parana, Kirwanveggan) It is suggested that melting of mantle underlying or attached to old cratonic regions will yield "enriched" (LFE-group) type melts while younger mantle underlying more recently accreted

crust will yield "normal" (N/HFE group) type melts. The chemistry of the low-MgO derivatives of these melts is then a complex function of fractional crystallization (open- or closed-system) and crustal contamination.

11.4 FURTHER WORK

Future studies should attempt to document the existence and distribution of "enriched" and "normal" magma types in detail as has been done here for the central Lebombo. Although such data are now becoming available for the Parana and Etendeka, detailed work is needed on basalts and dolerites from the Springbok Flats region, Botswana and other occurrences further north in Malawi and Zambia. Studies should also include detailed work on Mesozoic age dolerites cropping out in Archaean terraines to determine where they derive from and whether the explanation for the distribution of "enriched" and "normal" types suggested in this work may be substantiated, or whether other explanations must be sought. It is also important to accumulate data on the structure and geochemistry of the thinner lithospheric mantle underlying more recently (i.e. <2.0 Ga) accreted crustal terraines suggested as a source for "normal" volcanism. A source for such data may be mantle nodules in "off-craton" kimberlites intruding such areas which hitherto have been neglected largely because of their non-diamondiferous or marginallly diamondiferous nature. Only when such data are to hand can the full extent of these Mesozoic magma types and their relationship to Gondwana lithospheric architecture be more fully appreciated.

Acknowledgements

I am grateful for funding provided by Prof. A. J. Erlank from the CSIR (Foundation for Research and Development), from the CSIR directly and from the University of Cape Town.

I am most grateful to my two supervisors, Tony Erlank and Andy Duncan, for the time and effort they contributed both scientifically and, in some instances, personally, in aiding the birth of this thesis. Their efforts are most appreciated. Sincere appreciation is also extended to my "editorial board " and "army" of proof-readers, most of all Chris Harris and Mike Watkeys. The efforts of Anton le Roex, Rich Armstrong, Stuart Smith and James Willis in reading tracts of the thesis are also most appreciated. The efforts of my wife, Beverly, in typing considerable tracts and producing multiple copies of the thesis, is most appreciated.

I am indebted to James Willis for advancing my knowledge of XRF techniques from zero to somewhere approaching competence. Dave Hill, Andy Duncan, Dave Read, Stuart Smith and James Willis are thanked for their advice with regards to 'the system'. The modelling program 'Darts' largely written by Andy Duncan was extensively used and Andy is thanked for creating the "base" to which I could add the RTF subroutines and for assistance he provided me in their writing. Jock Harmer, Bruce Eglington, Alberto Tagliaro, Alan Butcher and Malherbe Auret of the NPRL (Pretoria) are thanked for assistance with accumulating the radiogenic isotope data and effectively helping me to become isotope-literate. Chris and Lillian Cousins kindly provided me with board, lodging and relaxation for the three months I spent at the NPRL in Pretoria. Stuart Smith and Chris Harris are thanked for the stable isotope data. Patrick Sieas is thanked for binding the thesis and assisting me in a quest for photostat quality.

I am grateful for the many interesting discussions with, and the advice and opinions of, Mike Watkeys, John Bristow, John Gurney, Chris Harris and colleagues in the Departments of Geology and Geochemistry at the University of Cape Town. Fellow research students at UCT provided much encouragement and support, particularly the '4^{th}-floor contingent' of Jenny Hops, Marshall Otter and Brian Hoal. John and Marilyn Bristow are thanked for their hospitality and assistance with my first field season despite my best efforts to incapacitate myself.

[Acknowledgements]

The National Parks Board are thanked for permitting me to work in the Kruger National Park and assistance in that regard. Freek and Rintsa Venter (Nature Conservation) are thanked for their support and Lynne Van Rooyen (Senior Ranger, Lower Sabie) for giving me the run of the land and extricating vehicles from streams. Louis Olivier (Ranger, Crocodile Bridge) is thanked for his buffalo steaks, impala wors, friendly support and his efforts in tracking down a consignment of samples which SAR and H had done their best to lose. I am most grateful to my game guide contingent, William Ngobene (chief of police, Lower Sabie), Benneth Mawalele and Samual Eoya for their time and vigilance - many are the experiences we have shared. To Benneth Mawalele I owe a debt than can never be repaid, he stood his ground to a buffalo charge which may have claimed one or both of our lives. His emergence from the attack with just a severe bruising must be regarded as almost miraculous.

The assistance an encouragement received from both my parents and parents-in-law is greatly appreciated. Finally, it is to my wife Beverly that I am most indebted, in addition to material assistance, she has been a constant source of encouragement and help throughout the last eight years.

RJS

24 April 1988

REFERENCES

Allègre, C. J. and Turcotte, D. L. (1985). Geodynamic mixing in the mesosphere boundary layer and the origin of ocean islands. Geophys. Res. Lett., 12(4), 207-210.

Allègre, C. J., Duprè, B., Richard, P., Rousseau, D. and Brooks, C. (1982). Subcontinental *vs* suboceanic mantle, II. Nd-Sr-Pb istopic comparison of continental tholeiites with mid-ocean ridge tholeiites and the structure of the continental lithosphere. Earth Planet. Sci. Lett., **57**, 25-34.

Allsopp, H. L. and Roddick, J. C. (1984). Rb-Sr and ^{40}Ar-^{39}Ar age determinations on phlogopite micas from the pre-Lebombo group Dokolwayo kimberlite pipe. Spec. Pub. geol. Soc. S. Afr., **13**, 267-272.

Allsopp, H. L., Bristow, J. W., Logan, C. T., Eales, H. V. and Erlank, A. J. (1984). Rb-Sr Geochronology of three Karoo-related intrusive complexes. Spec. Pub. geol. Soc. S. Afr., **13**, 281-287.

Anhausser, C. R. and Robb, L. J. (1983). Geological and geochemical characteristics of the Heerenveen and Mpuluzi Batholiths south of the Barberton Greenstone Belt and preliminary thoughts on their petrogenesis, Spec. Publ. geol. Soc. S. Afr., **9**, 131-152

Assunçao, C, F. T., Coelho, A. V. P. and Rocha, A. T. (1962). Petrologia das lavas dos Libombos (Mozambique). Estudos Ensais, e Documentos, Junta de Investigacoes do Ultramar., **99**, 1-74.

Armstrong, R. A., Bristow, J. W. and Cox, K. G. (1984). The Rooi Rand dyke swarm, southern Lebombo. Spec. Publ. geol. Soc. S. Afr., **13**, 77-86.

Arth, J. G. (1976). Behaviour of trace elements during magmatic processes - a summary of theoretical models and their applications. J. Res. U. S. Geol. Surv., **4**, 41-47.

Ballard, S. and Pollack, H. N. (1987). Diversion of heat by Archean cratons: a model for southern Africa. Earth Planet. Sci. Lett., **85**, 253-264.

Barton, J. M., Robb, L. J., Anhausser, C. R. and Van Nierop, D. A. (1983). Geochronologic and Sr-isotopic studies of certain units in the Barberton granite-greenstone terrane, South Africa, Spec. Publ. geol. Soc. S. Afr., **9**, 63-72.

[References]

Bassot, J. P., Pascal, M. and Vialette, Y. (1981). Données nouvelles sur la stratigraphie, la géochemie et la géochronologie des formation Précambriennes de la partie méridionale du Haut Plateau Angolais. Bull. Bur. Rech. Géol. Min. (2 série), sect. 4, no. 4. (1980-81), 285-309.

Bellieni, G., Brotzu, P., Comin-Chiaramonti, P., Ernesto, M., Melfi, A., Pacca, I. .G. and Piccirillo, E. M. (1984a). Flood basalts to rhyolite suites in the southern Parana Plateau (Brazil): paleaomagnetism, petrogenesis and geodynamic implications. J. Petrol., **25**(3), 579-618.

Bellieni, G., Comin-Chiaramonti, P., Marques, L. S., Melfi, A. J., Piccirillo, E. M., Nardy, A. J. R. and Roisenberg, A. (1984b). High- and low- TiO_2 flood basalts from the Parana plateau (Brazil): petrology and geochemical aspects bearing on their mantle origin. Neues Jhb. Miner. Abh., **150**(3), 273-306.

Bellieni, G., Comin-Chiaramonti, P., Marques, L. S., Melfi, A. J., Nardy, A. J. R., Papatrechas, C., Piccirillo, E. M., Roisenberg A. and Stolfa, D. (1986). Petrogenetic aspects of acid and basaltic lavas from the Parana plateau (Brazil): geological, mineralogical and petrochemical relationships. J. Petrol., **27**(4), 915-944.

Bence, A. E. and Albee, A. L. (1968). Empirical correction factors for the electron microanalysis of silicates and oxides. J. Geol., **76**, 382-403.

Bence, A. E. and Papike, J. J. (1972). Pyroxenes as recorders of lunar basalt petrogenesis: chemical trends due to crystal-liquid interaction. Proc. 3rd Lunar Sci. Conf., 431-469.

Bernasconi, A. (1983). The Archaean terranes of central eastern Brazil: a review. Precamb. Res., **23**, 107-131.

Betton, P. J. (1978). Geochemistry of Karoo volcanic rocks in Swaziland. Unpub. D. Phil. thesis, Univ. Oxford, 287 pp.

Betton, P. J., Armstrong, R. A. and Manton, W. I. (1984). Variations in the lead isotopic composition of Karoo magmas. Spec. Pub. geol. Soc. S. Afr., **13**, 331-339.

Boelrijk, N. A. I. M. (1968). A general formula for "double" isotope dilution analysis. Chem. Geol., **3**, 323-325.

Bottinga, Y. and Weill, D. F. (1972). The viscosity of magmatic silicate liquids: a model for calculation. Amer. J. Sci., **272**, 438-475.

Bosworth, W. (1987). Off-axis volcanism in the Gregory rift, east Africa: implications for models of continental rifting. Geology, **15**, 397-400.

Boyd, F. R. and Gurney, J. J. (1986). Diamonds and the African lithosphere. Science, **232**, 472-477.

Boyd, F. R. and Mertzman, S. A. (1987). Composition and structure of the Kaapvaal lithosphere, southern Africa. In B. O. Mysen (ed.), Magmatic Processes: Physiochemical Principles, Spec. Pub., 1, Geochemical Society.

Boyd, F. R. and Nixon, P. H. (1973). Origin of the ilmenite-silicate nodules in kimberlites from Lesotho and South Africa, 254-268. In: P. H. Nixon (ed.), Lesotho Kimberlites, Lesotho Nat. Dev. Corp., Maseru, 350 pp.

Boyd, F. R., Gurney, J. J. and Richardson, S. H. (1985). Evidence for a 150-200 km thick Archaean lithosphere from diamond inclusion thermobarometry. Nature, 315, 387-389.

Bristow, J. W. (1976). The geology and geochemistry of the southern Lebombo. Unpub. MSc thesis, Univ. of Natal, 331 pp.

Bristow, J. W. (1980). The geochronology and geochemistry of Karoo volcanics in the Lebombo and adjacent areas. Unpub. PhD thesis, Univ. of Cape Town, 256 pp.

Bristow J. W. (1982). Geology and structure of Karoo volcanic and sedimentary rocks of the northern and central Lebombo. Trans. geol. Soc. S. Afr., 85, 167-178.

Bristow, J. W. (1984a). Picritic rocks of the north Lebombo and south-east Zimbabwe. Spec. Pub. geol. Soc. S. Afr., 13, 105-124.

Bristow, J. W. (1984b). Nephelinites of the north Lebombo and south-east Zimbabwe. Spec. Pub. geol. Soc. S. Afr., 13, 87-104.

Bristow, J. W., Allsopp, H. L., Erlank, A. J., Marsh, J. S. and Armstrong, R. A. (1984). Strontium isotope characterization of Karoo volcanic rocks. Spec. Pub. geol. Soc. S. Afr., 13, 295-329.

Brooks, C., Hart, S. R. and Wendt, I. (1972). Realistic use of two-error regression treatment as applied to Rubidium-Strontium data. Rev. Geophys. and Space Phys., 10(2), 551-577.

Bryan, W. B., Finger, L. W. and Chayes, F. (1969). Estimating proportions in petrographic mixing equations by least-squares approximation. Science, 163, 926-927.

Buddington, A. F. and Lindsley, D. (1964). Iron-titanium oxide minerals and synthetic equivalents. J. Petrol., 5(2), 310-357.

Burke, K. and Dewey, J. F. (1973). Plume generated triple junctions. Key indicators in applying plate tectonics to old rocks. J. Geol., **81**, 403-433.

Carlson, R. W., Lugmair, G. W. and Macdougall, J. D. (1981). Columbia River volcanism: the question of mantle heterogeneity or crustal contamination. Geochim. Cos. Acta, **45**, 2483-2499.

Carlson, R. W., Hunter, D. R. and Barker, F. (1983). Sm-Nd age and isotopic systematics of the bimodal suite, Ancient Gneiss Complex, Swaziland. Nature, **305**, 701-704.

Carmichael, I. S. E., Turner, F. J. and Verhoogen, J. (1974). Igneous Petrology. McGraw-Hill, New York, 739 pp.

Carswell, D. A. (1975). Primary and secondary phlogopites and clinopyroxenes in garnet lherzolite xenoliths, 417-429. Physics and Chemistry of the Earth, **9**, Pergamon Press.

Carswell, D. A. and Gibb, F. G. F. (1987). Garnet lherzolite xenoliths in the kimberlites of northern Lesotho: revised conditions and upper mantle palaeogeothermometry. Contrib. Min. Petrol., **97**, 473-487.

Chamberlain, C. P. and Karabinos, P. (1987). Influence of deformation on pressure-temperature paths of metamorphism. Geology, **15**, 42-44.

Cleverly, R. W. (1977). The structural and magmatic evolution of Lebombo Monocline, southern Africa, with particular reference to Swaziland. Unpub. D. Phil. thesis, Univ. Oxford, 316 pp.

Cleverly, R. W. (1979). The volcanic geology of the Lebombo monocline in Swaziland. Trans. geol. Soc. S. Afr., **82**, 343-348.

Cleverly, R. W. and Bristow, J. W. (1979). Revised volcanic stratigraphy of the Lebombo monocline. Trans. geol. Soc. S. Afr., **82**, 343-348.

Cleverly, R. W., Betton, P. J. and Bristow, J. W. (1984). Geochemistry and petrogenesis of the Lebombo rhyolites. Spec. Pub. geol. Soc. S. Afr., **13**, 171-194.

Condie, K. C. and Hunter, D. R. (1976). Trace element geochemistry of Archaean granitic rocks from Barberton, South Africa. Earth Planet. Sci. Lett., **29**, 389-400.

Cox, K. G. (1970). Tectonics and vulcanism of the Karoo period and their bearing on th postulated fragmentation of Gondwanaland, 211-235. In: T. N. Clifford and I. G. Gass (eds.), African Magmatism and Tectonics. Oliver and Boyd, Edinburgh, 461 pp.

Cox, K. G. (1978). Flood basalts, subduction and the breakup of Gondwanaland. Nature, **274**, 47-49.

Cox, K. G. (1980). A model for flood basalt vulcanism. J. Petrol., **21**, 629-650.

Cox, K. G. (1983). The Karoo Province of southern Africa: origin of trace element enrichment patterns in the Karoo, 139-157. In: C. J. Hawkesworth and M. J. Norry (eds.), Continental Basalts and Mantle Xenoliths. Shiva Press, U. K., 272 pp.

Cox, K. G. (1987). Postulated restite fragments from Karoo picrite basalts: their bearing on magma segregation and mantle deformation. J. geol. Soc. Lond., **144**, 275-280.

Cox, K. G. (1988). Numerical modelling of a randomised RTF magma chamber: a comparison with continental flood basalt sequences. (submitted).

Cox, K. G. and Bell, J. D. (1972). A crystal fractionation model for basaltic rocks of the New Georgia Group, British Solomon Islands. Contrib. Min. Petrol., **37**, 1-13.

Cox, K. G. and Bristow, J. W. (1984). The Sabie River Basalt Formation of the Lebombo monocline and south-east Zimbabwe. Spec. Pub. geol. Soc. S. Afr., **13**, 125-148.

Cox, K. G. and Hawkesworth, C. J. (1985). Geochemical stratigraphy of the Deccan Traps at Mahabaleshwar, Western Ghats, India, with implications for open system magmatic processes. J. Petrol., **26**(2), 355-377.

Cox, K. G. and Jamieson, B. G. (1974). The olivine-rich lavas of Nuanetsi: a study of polybaric magmatic evolution. J. Petrol., **15**, 269-301.

Cox, K. G., Johnson, R. L., Monkman, L. J., Stillman, C. J., Vail, J. R. and Wood, D. N. (1965). The geology of the Nuanetsi igneous province. Phil. Trans. R. Soc. Lond., **A297**, 71-218.

Cox, K. G., Macdonald, R. and Hornung, G. (1967). Geochemical and petrogenetic provinces in the Karroo basalts of southern Africa. Amer. Mineral., **52**, 1451-1474.

Cox, K. G., Duncan, A. R., Bristow, J. W., Taylor, S. R. and Erlank, A. J. (1984). Petrogenesis of the basic rocks of the Lebombo. Spec. Pub. geol. Soc. S. Afr., **13**, 149-170.

Danchin, R. V. (1979). Mineral and bulk chemistry of garnet lherzolite and garnet-harzburgite xenoliths from the Premier mine, South Africa, 104-126. In: F. R. Boyd and H. O. A. Meyer (eds.), The MAntle Sample: Inclusions in kimberlites and other volcanics

Darracott, B. W. and Kleywegt, R. J. (1974). The structure of the southern portion of the Lebombo volcanic belt deduced from gravity data. Trans. geol. Soc. S. Afr., **77**, 301-308.

Deer, W. A., Howie, R. A. and Zussman, J. (1966). An Introduction to the Rock-forming Minerals, Longman, 528 pp.

De Paolo, D. J. (1981). Trace element and isotopic effects of combined wallrock assimilation and fractional crystallization. Earth Planet. Sci. Lett., **53**, 189-202.

De Wit, M. J., Jeffery, M., Bergh, H. and Nicolaysen, L. (1988). Geological map of sectors of Gondwana reconstructed to their disposition ~ 150 Ma. Amer. Assoc. Petrol. Geol., 1988.

Drake, M. J. (1976). Plagioclase-melt equilibria. Geochim. Cos. Acta, **40**(5), 457-466.

Drake, M. J. and Weill, D. F. (1972). The distribution of Sr, Ba, Eu^{2+}, Eu^{3+} and other REE between plagioclase feldpsar and magmatic liquid: and experimental study. Abs. Trans. Amer. Geophys. Union, **53**, 553.

Duncan, A. R. (1987). The Karoo Igneous Province - a problem area for inferring tectonic setting from basalt geochemistry. J. Volc. and Geotherm. Res., **32**, 13-34.

Duncan, A. R. , Erlank, A. J. and Betton, P. J. (1984a). Appendix 1: analytical techniques and database descriptions. Spec. Pub. geol. Soc. S. Afr., **13**, 389-395.

Duncan, A. R. , Erlank, A. J. and Marsh, J. S. (1984b). Regional geochemistry of the Karoo Igneous Province. Spec. Pub. geol. Soc. S. Afr., **13**, 355-388.

Dupuy, C. and Dostal, J. (1984). Trace element geochemistry of some continental tholeiites. Earth Planet. Sci. Lett., **67**, 61-69.

Du Toit, A. L. (1929). The volcanic belt of the Lebombo: a region of tension. Trans. R. Soc. S. Afr., **18**, 189-218.

Eales, H. V. , Marsh, J. S. and Cox, K. G. (1984). The Karoo Igneous province: an introduction. Spec. Pub. geol. Soc. S. Afr., **13**, 1-26.

Eby, G. N. (1975). Abundance and distribution of the rare earth elements and Yttrium in the rocks of the Oka Carbonatite Complex, Quebec. Geochim. Cos. Acta, **39**, 497-520.

Eggler, D. H. and Wendlandt, R. F. (1979). Experimental studies on the relationship between kimberlite magmas and partial melting of peridotites, 330-338. In: F. R. Boyd and H. O. A. Meyer (eds.), Kimberlites, Diatremes and Diamonds, A. G. U., Washington.

Erlank, A.J. (1970). Distribution of K in mafic and ultramafic nodules. Carnegie Instn. Wash. Yearb., **68**, 533-439.

Erlank, A.J. (1973). Kimberlite potassic richterite and the distribution of potassium in the upper mantle. Ext. Abs. First Int. Kimberlite Conf., Cape Town, 103-106.

Erlank, A. J. (1984). Ed.: Petrogenesis of the volcanic rocks of the Karoo Igneous Province. Spec. Pub. geol. Soc. S. Afr., 13, 395 pp.

Erlank, A. J., Allsopp, H. L., Duncan, A. R. and Bristow, J. W. (1980). Mantle heterogeneity beneath southern Africa: evidence from the volcanic record. Phil. Trans.Roy. Soc. Lond., **A297**, 295-307.

Erlank, A. J., Marsh., J. S., Duncan, A. R., McG. Miller, R., Hawkesworth, C. J., Betton, P. J. and Rex, D. C. (1984). Geochimistry and petrogenesis of the Etendeka volcanic rocks from SWA/Namibia. Spec. Pub. geol. Soc. S. Afr., 13, 195-245.

Erlank, A. J., Waters, F. G., Hawkesworth, C. J., Haggerty, S. E., Allsopp, H. L., Rickard, R. S. and Menzies, M. A. (1987). Evidence for mantle metasomatism in peridotite nodules from the Kimberley pipes, South Africa, 221-311. In: C. J. Hawkesworth and Menzies (eds.), Mantle Metasomatism, Academic Press, 472 pp.

Erlank, A. J., Duncan, A. R., Marsh, J. S., Sweeney, R. J., Hawkesworth, C. J., Milner, S. C., McG-Miller, R. and Rogers, N. W. (1988). A laterally extensive geochemical discontinuity in the sub-continental Gondwana lithosphere. Ext. Abs. Conf. Geoch. Evol. Crust, Brazil.

Fitch, F. J. and Miller, J. A. (1984). Dating Karoo igneous rocks by the conventional K-Ar and $^{40}Ar/^{39}Ar$ age spectrum methods. Spec. Pub. geol. Soc. S. Afr., 13, 247-266.

Flores, G. (1973). The Cretaceous and Tertiary sedimentary basins of Mozamibique and Zululand, 81-111. In: G. Blant (ed.), Sedimentary Basins of the African Coasts. Assoc. Afr. Geol. Surv., Paris.

Fodor, R. V. (1987). Low- and high-TiO_2 flood basalts of southern Brazil: origin from picritic parentage and a common mantle source. Earth Planet. Sci. Lett., **84**, 423-430.

Frey, F. A. , Haskin, M. A. , Poetz, J. A. and Haskin, L. A. (1968). Rare earth abundances in some basic rocks. J. Geophys. Res. , **73**, 6085-6098.

Froidevaux, C. and Nataf, H. C. (1981). Continental drift: what driving mechanism? Geol. Rundsch., **70**, 166-176.

Furnes, H., Neumann, E-R. and Sundvoll, B. (1982). Petrology and geochemistry of Jurassic basalt dykes from Vestfjella, Dronning Maud Land, Antarctica. Lithos, **15**, 295-304.

Furnes, H., Vad, E., Austreim, E., Mitchell, J. G. and Graham, L. B. (1987). Geochemistry of basalt lavas from Vestfjella and and adjacent areas, Dronning Maud Land, Antarctica. Lithos, **20**, 337-356.

Gast, P. W. (1960). Limitations on the composition of the upper mantle. J. Geophys. Res., **65**, 1287-1296.

Gast, P. W. (1968). Trace element fractionation and the origin of tholeiitic and alkaline magma types. Geochim. Cos. Acta, 32, 1057-1086.

Gast, P. W., Tilton, G. R. and Hedge, C. (1964). Isotopic composition of lead and strontium from Ascension and Gough Islands. Science, **145**, 1181-1185.

Graham, C. M. and Harmon, R. S. (1983). Stable isotope evidence on the nature of crust-mantle interactions, 20-45. In: C. J. Hawkesworth and M. J. Norry (eds.), Continental flood basalts and mantle xenoliths, Shiva, 272 pp.

Grover, J. E. and Lindsley, D. H. (1972). Ca-Mg-Fe pyroxenes: subsolidus phase relations in iron-rich portions of the pyroxene quadrilateral. Geol. Soc. Amer., Abstr. Programs, 4, 521-522.

Guj, P. (1970). The Damara mobile belt in the south-western Kaokoveld, South West Africa. Bull. Precamb. Res. Unit, Univ. Cape Town. 168 pp.

Gurney, J. J. and Harte, B. (1980). Chemical variations in upper mantle nodules from southern African kimberlites. Phil. Trans. R. Soc. Lond., **A297**, 273-293.

Haggerty, S. E. (1976). Oxidation of opaque mineral oxides in basalts, Hgl-Hg98. In: D. Rumble III (ed.), Reviews in Mineralogy, v3: Oxide Minerals, Miner. Soc. Amer.

Haggerty, S. E. (1986). Diamond genesis in a multiply-constrained model. Nature, **320**, 34-38.

Haggerty, S. E., Smyth, J. R., Erlank, A. J., Rickard, R. S. and Danchin, R. V. (1983). Lindsleyite (BA) and mathiasite (K): two new chrome titanates in the crichtonite series from the upper mantle. Amer. Mineral., **68**, 494-505.

Hale, C. J. (1987). Palaeomagnetic data suggest a link between the Archaean-Proterozoic boundary and inner core nucleation. Nature, 329, 233-234.

Hanson, G. N. (1978). The application of trace elements to the petrogenesis of igneous rocks of granitic composition. Earth Planet. Sci. Lett., **38**, 26-43.

Harmer, R. H. and Eglington, B. M. (1986). Technical manual for isotope Geochemistry and a compilation of useful formulae and constants. Geochronology Division, National Physical Research Laboratory, CSIR, Pretoria,

Harmer, R. H., Eglington, B. M., Farrow, D., Butcher, A. R., Auret, J. M., Stander, Y. Y. and Grosser, E. (1986). Manual of laboratory procedures for isotope analysis. Geochronology Division, National Physical Research Laboratory, CSIR, Pretoria.

Harris, C., Marsh, J. S., Erlank, A. J. and Duncan, A. R. (1986). Geology of the Jurassic basalts of the Kirwanveggan, Antarctica and their significance for Gondwana volcanism. Ext. abs. Geocongress '86, Geol. Soc. S. Afr., 731-734.

Harris, C., Erlank, A. J., Duncan, A. R. and Marsh, J. S. (1988). The Geochemistry of the Kirwanand other Jurrassic basalts of Dronning Maud Land and their petrogenetic significance for Gondwana reconstruction. Proc. 5th Antarctic Earth Sci. Conf., Cambridge. Cambridge Univ. Press (in press).

Harris, N. B. W., Hawkesworth, C. J., Van Calsteren, P. and McDermott, F. (1987). Evolution of continental crust in southern Africa. Earth Planet. Sci. Lett., **83**, 85-93.

Harris, P. G. (1957). Zone refining and the origin of potassic basalts. Geochim. Cos. Acta, **12**, 195-208.

Hart, S. R. (1984). A large-scale isotope anomaly in the southern hemisphere mantle. Nature **309**, 753-757.

Hart, S. R. and Davies, K. E. (1978). Nickel partitioning between olivine and silicate melt. Earth Planet. Sci. Lett. , **40**, 203-219.

Hartnady, C. J. H., Joubert, P. and Stowe, C. (1985). Proterozoic crustal evolution of southern Africa. Episodes, **8**, 236-244.

Haskin, L. A., Haskin,M. A. and Frey, F. A. (1968). Relative and absolute terrestrial abundance of the rare earths, 889-912. In: L. H. Ahrens (ed.), Origin and Distribution of the Elements, Oxford, Pergamon Press.

Hattori, K. and Muehlenbachs, K. (1982). Oxygen isotope ratios of the Icelandic crust (paper 1B1014). J. Geophys. Res., **87** (B8), 6559-6565.

Hawkesworth, C. J., Erlank, A. J., Marsh, J. S., Menzies, M. A. and Van Calsteren, P. (1983). Evolution of the continental lithosphere: evidence from volanics and xenoliths in southern Africa, 111-1368. In: C. J. Hawkesworth and M. J. Norry (eds.), Continental Basalts and Mantle Xenoliths, Shiva Press, 272 pp.

Hawkesworth, C. J., Marsh, J. S., Duncan, A. R., Erlank, A. J. and Norry, M. J. (1984). The role of continental lithosphere in the generation of the Karoo volcanic rocks: evidence from combined Nd- and Sr-isotope studies. Spec. Pub. geol. Soc. S. Afr., **13**, 341-354.

Hawkesworth, C. J., Mantovani, M. S. M., Taylor, P. N. and Palacz, Z. (1986). Evidence from the Parana of south Brazil for a continental contribution to Dupal basalts. Nature, **322**, 356-359.

Hawkesworth, C. J., Van Calsteren, P., Rogers, N. W. and Menzies, M. A. (1987). Isotope variations in recent volcanics: a trace element perspective (365-388). In: C. J. Hawkesworth and M. Menzies (eds.), Mantle Metasomatism, Academic Press, 472 pp.

Henoc, J., Heinrich, K. F. J. and Myklebust, R, L. (1973). A rigorous correction procedure for quantitative electron probe microanalysis (COR 2). U. S. Bureau of Standards, Technical Note 769. U. S. Govt. printing Office, Washington D. C.

Hensen, B. J. (1973). Pyroxenes and garnets as geothermometers and barometers. Carnegie Inst. Washington Year Book 72, 527-534.

Hertogen, J. and Gijbels, R. (1976). Calculation of trace element fractionation during partial melting. Geochim. Cos. Acta, **40**, 313.

Heubner,J. S. (1980). Pyroxene phase equilibria at low pressure, 213-288. In: C. T. Prewitt (ed.), Reviews in Mineralogy, v7: Pyroxenes, Miner. Soc. Amer.

Hofmann, A. W. (1984). Geochemical mantle models. Terra Cognita, **4**, 157-165.

Hulme, G. (1974). The interpretation of lava flow morphology. Geophys. J. R. astr. Soc., **39**, 361-383.

Hunter, D. R. , Barker, F. and Millard, H. T. (1984). geochemical investigation of Archaean Bimodal and Dwalile metamorphic suites, Ancient Gneiss Complex, Swaziland. Precamb. Res. , **24**, 131-155.

Huppert, H. E. and Sparks, R. S. J. (1981). The fluid dynamics of a basaltic magma chamber replenished by an influx of hot, dense, ultrabasic magma. Contrib. Min. Petrol., **75**, 279-289.

Huppert, H. E. and Sparks, R. S. J. (1985). Cooling and contamination of mafic and ultramafic magmas during ascent through continental crust. Earth Planet. Sci. Lett., **74**, 371-386.

Jackson, M. P. A. and Robertson, D. I. (1983). Regional implications of early-Precambrian strains in the Onverwacht Group adjacent to the Lochiel Granite, North-west Swaziland. Spec. Pub. geol. Soc. S. Afr., **9**,45-62.

Jagoutz, E., Palme, H., Baddenhaussen, H., Blum, K., Cendales, M., Driebus, G. Spettel, B., Lorrenz, V. and Wanke, H. (1979). The abundances of major, minor and trace element in the Earths mantle as derived from primitive ultramafic nodules. Proc. 10^{th} Lunar Plant. Sci.Conf., 2031-2050.

Jordan, T. H. (1978). Composition and development of the continental tectosphere. Nature, **274**, 544-548.

Juckes, L. M. (1972). The geology of north-eastern Heimfrontfjella, Dronning Maud Land. Brit. Ant. Surv. Sci. Report, **65**, 44 pp.

Kalamarides, R. I. (1984). Kiglapait geochemistry VI: Oxygen isotopes. Geochim. Cos. Acta, **48**, 1827-1836.

Key, R. M., Ermanovics, I. F. and Skinner, A. C. (1983). The evolution of the southern margin of the Limpopo mobile belt in Botswana. Spec. Pub. geol. Soc. S. Afr., **8**, 169-174.

Koringa, M. K. and Noble, D. C. (1971). Distribution of Sr between natural feldpar and igneous melt. Earth Planet. Sci. Lett., **11**, 147-151.

Kretz, R. (1963). Distribution of magnesium and iron between orthopyroxene and calcic pyroxene in natural mineral assemblages. J. Geol., **71**, 773-784.

Krishnamurthy, P. and Cox, K. G. (1977). Picrite basalts and related lavas from the Deccan Traps of Western India. Contrib. Min. Petrol., **62**, 53-75.

Kyser, T. K., O'Neill, J. R., and Carmichael, I. S. E. (1981). Oxygen isotope thermometry of basic lavas and mantle nodules. Contrib. Min. Petrol., **81**, 88-102.

Lagache, M. (1984). The exchange equilibrium distribution of alkali and alkaline-earth elements between feldspars and hydrothermal solutions, 247-279. In: W. L. Brown (ed.), Feldspars and Feldspathoids, D.Reidel Press, 541 pp.

Langmuir, C. H. , Bender, J. F. , Bence, A. E. and Hanson, G. N. (1977). Petrogenesis of basalt from the FAMOUS area: Mid-Atlantic Ridge. Earth Planet. Sci. Lett. , **36**, 133-156.

Le Maitre, R. W. (1976). GENMIX - a generalized petrological mixing model program. Computers and Geosciences, **7**, 229-247.

Le Roex, A. L. (1985). Geochemistry, mineralogy and magmatic evolution of the basaltic and trachytic lavas from Gough Island, South Atlantic. J. Petrol., **26**(1), 146-186.

Le Roex, A. L. (1987). Geochemical correlation between southern African kimberlites and South Atlantic hotspots. Nature, **324**, 243-245.

Le Roex, A. P., Erlank, A. J. and Needham, H. D. (1981). Geochemical and mineralogical evidence for the occurrence of at least three distinct magam types in the FAMOUS region. Contrib. Min. Petrol., **77**, 24-37.

Le Roex, A. L., Dick, H. J. B., Erlank, A. J., Reid, A. M., Frey, F. A. and Hart, S. R. (1983). Geochimistry, mineralogy and petrogenesis of lavas erupted along the south-west Indian Ridge between the Bouvet Triple Junction and 11° east. J. Petrol., **24**, 267-318.

Le Roex, A. L., Dick, H. J. B., Gulen, L., Reid, A. M. and Erlank, A. J. (1987). Local and regional heterogeneity in MORB from the Mid-Atlantic Ridge between 54.5°S and 51°S: evidence for geochemical enrichment. Geochim. Cos. Acta, **51**, 541-555.

Levine, I. N. (1978). Physical Chemistry. McGraw-Hill/Kogakusha. pp 847.

Logan, C. T. (1979). Aspects of Karoo volcanicity in the Komatipoort area, Lebombo. Unpub. PhD thesis, Univ. Natal (Durban), 328 pp.

Maaløe, S. and Johnston, A. D. (1986). Geochemical aspects of some accumulation models for primary magmas. Contrib. Min. Petrol., **93**, 449-458.

Maaløe, S. and Aoki, K. (1977). The major element composition of the upper mantle estimated from the composition of lherzolites. Contrib. Min. Petrol., **76**, 127-147.

Macdonald, G. A. (1967). Forms and structures of extrusive basalt rocks, 1-61. In: H. H. Hess and A. Poldervaart (eds.), The Poldervaart Treatise on Rocks of Basaltic Composition, **1**. New York, Interscience.

Macdonald, R. (1967). geochemical and petrographic provinces of Karoo basalts. Proc. geol. Soc. Lond., **1637**, 45.

Macdonald, R., Crossley, R. and Waterhouse, K. S. (1983). Karroo basalts of southern Malawi and their regional petrographic significance. Min. Mag., **47**, 281-289.

Mahoney, J., Macdougall, J. D., Lugmair, G. W., Murali, A. V., Sankar Das, M. and Goplan, K. (1982). Origin of the Deccan Trap flows at Mahabaleshwar inferred from Nd and Sr isotopic and chemical evidence. Earth Planet. Sci. Lett., **60**, 47-60.

Mantovani, M. S. M. , Marques, L. S. , De Sousa, M. A. , Civetta, L. , Atalla, L. and Innocenti, F. (1985). Trace element and strontium isotope constraints on the origin and evolution of Parana continental flood basalts of Santa Catarina State (southern Brazil). J. Petrol. , **26**(1), 187-209.

Marsh, J. S. (1984). Karoo basalts of the Springbok Flats, Transvaal: Geochimistry and correlation. Ext. Abs. , Geocongress '84, Geol. Soc. S. Afr.

Marsh, J. S. and Eales, H. V. (1984). The chemistry and petrogenesis of igneous rocks of ths Karoo Central Area, southern Africa. Spec. Pub. geol. Soc. S. Afr., **13**, 27-68.

Martin, A. K. (1984). Plate tectonic status and sedimentary basin in-fill of the Natal Valley (SW Indian Ocean). Marine geol. progress bull., Geol. Surv. S. A./UCT, **24**, 209 pp.

Mathias, M. , Siebert, J. G. and Ringwood, P. C. (1970). Some aspects of the mineralogy and petrology of ultramafic xenoliths in kimberlite. Contrib. Min. Petrol., **26**, 75-123.

Maufe, H. B. (1929). Int. Geol. Congress, XV session, South Africa, Guidebook C20, 58-60.

McKenzie, D. (1978). Some remarks on the development of sedimentary basins. Earth Planet. Sci. Lett., **40**, 25-32.

McKenzie, D. (1984). The generation and compaction of partially molten rock. J. Petrol., **25** (3), 713-765.

McKenzie, D. (1985). The extraction of magma from the crust and the mantle. Earth Planet. Sci. Lett., **74**, 81-91.

Menzies, M. A. (1988). Cratonic, circum-cratonic and oceanic mantle domains in the western U. S. A. submitted to "Magmatism associated with Lithospheric Extension", G. Fitton and W. P. Leeman (eds.), F. Geophys. Res. in press.

Menzies, M. A. and Murthy, R. (1980). Enriched mantle: Nd and Sr isotopes in diopsides from kimberlite nodules. Nature, **283**, 634-636.

Menzies, M. A., Rogers, N., Tindle, A. and Hawkesworth, C. J. (1987). Metasomatic and enrichment processes in lithospheric peridotites, an effect of asthenosphere-lithosphere interaction (313-364). In: C. J. Hawkesworth and M. A. Menzies (eds.), Mantle Metasomatism, Academic Press, pp 472.

Michard, A., Montigny, R. and Schlich, R. (1986). Geochemistry of the mantle beneath the Rodriguez Triple Junction and the south-east Indian Ridge. Earth Planet. Sci. Lett., **78**, 104-114.

Mitchell, R. H. (1984). Garnet lherzolites from the Hanaus-I and Louwnensia kimberlites of Namibia. Contrib. Min. Petrol., **86**, 178-188.

Mori,T. (1978). Experimental study of pyroxene equilibria in the system of CaO-MgO-FeO-SiO_2. J. Petrol., **19**, 45-65.

Nakamura, E. (1978). Determination of REE, Ba, Fe, Mg, Na and K in carbonaceous and ordinary chondrites. Geochim. Cos. Acta, **38**, 757-775.

Nathan, H. D. and Van Kirk, C. K. (1978). A model for magmatic crystallization. J. Petrol., **19**(1), 66-94.

Nesbitt, H.W. and Young, G. M. (1982). Early Proterozoic climates and plate motions inferred from major element chemistry of lutites. Nature, **299**, 715-717.

Nesbitt, R. W., Mastins, H., Stolz, G. W. and Bruce, D. R. (1976). Matrix corrections in trace element analysis by XRF: an extension of the Compton scattering effect to longer wavelengths. Chem. Geol., **18**, 203-213.

Newsom, H. E., White, W. M., Jochum, K. P. and Hofman, A. W. (1986). Siderophile and chalcophile element abundances in oceanic basalts, Pb isotope evolution and growth of the Earth's core. Earth Planet. Sci. Lett., **80**, 299-313.

Nielsen, R. L. (1985). EQUIL: a program for the modeling of low-pressure differentiation processes in natural mafic magma bodies. Comp. and Geosci., **11**(5), 531-546.

Nielsen, R. .L. and Drake, M. J. (1979). Pyroxene-melt equilibria. Geochim. Cos. Acta, **43**(8), 1259-1273.

Nielsen, R. .L. and Dungan, M. A. (1983). Low-pressure mineral-melt equilibria in natural anhydrous mafic systems. Contrib. Min. Petrol., **84**(2), 310-326.

Nixon, P. H. and Boyd, F. R. (1973). Petrogenesis of the granular and sheared ultrabasic nodule suite in kimberlites, 48-56. In: P. H. Nixon (ed.), Lesotho Kimberlites, Lesotho Nat. Development Corp., Maseru, 350 pp.

Nixon, P. H., Rogers, N. W., Gibson, I. L. and Grey, A. (1981) Depleted and fertile mantle xenoliths from southern African kimberlites. Ann. Rev. Earth Planet. Sci., **9**, 671-686.

Nixon, P. H., Boyd, F. R. and Boctor, N. Z. (1983). E. Griqualand kimberlites. Trans. geol. Soc. S. Afr., **86**, 221-236.

Norrish, K. and Hutton, J. T. (1969). An accurate X-ray spectrographic method for the analysis of a wide range of geological samples. Geochim. Cos. Acta, **33**, 431-453.

Norry, M. J. and Fitton, J. G. (1983). Compositional differences between oceanic and continental basic lavas and their significance, 5-19. In: C. J. Hawkesworth and M. J. Norry (eds.), Continental Basalts and Mantle Xenoliths, Shiva, 272 pp.

Norton, I. O. and Sclater, J. G. (1979). A model for the evolution of the Indian Ocean and the breakup of Gondwanaland. J. Geophys. Res., **84**, 6803-6830.

O'Hara, M. J. (1977). Geochemical evolution during fractional crystallization of a periodically refilled magma chamber. Nature, **266**, 503-507.

O'Hara, M. J. (1985). Importance of the 'shape' of the melting regime during partial melting of the mantle. Nature, **314**, 58-62.

O'Hara, M. J. and Mathews, R. E. (1981). Geochemical evolution in an advancing periodically replenished, periodically tapped, continuously fractionated magam chamber. J. Geol. Soc. Lond., **138**, 237-277.

O'Neill, J. R. (1986a). Theoretical and experimental aspects of isotopic fractionation, 1-40. In: J. W. Valley, H. P. Taylor and J. R. O'Neill (eds.), Stable Isotopes in High Temperature Geological Processes. Mineral. Soc. Amer., Rev. Mineral., **16**, 570 pp.

O'Neill, J. R. (1986b). Appendix: terminology and standards, 561-570. In: J. W. Valley, H. P. Taylor and J. R. O'Neill (eds.), Stable Isotopes in High Temperature Geological Processes. Mineral. Soc. Amer., Rev. Mineral., **16**, 570 pp.

Papike, J. J., Hodges, F. N., Bence, A. E., Cameron, M. and Rhodes, J. M. (1976). Mare basalts: crystal chemistry, mineralogy and petrology. Rev. Geophys.Space Phy., **14**, 475-540.

Parsons, I. and Brown, W. L. (1984). Feldspars and the thermal history of igneous rocks, 317-371. In: W. L. Brown (ed.), Feldspars and Feldspathoids. D. Reidel Pub., 541 pp.

Peterson, D. W. and Tilling, R. I. (1980). Transition of basaltic lava from pahoehoe to aa, Kilauea volcano, Hawaii: field observations and key factors. J. Volc. and Geotherm. Res., **7**, 271-293.

Petrini, R., Civetta, L., Piccirillo, E. M., Bellieni, G., Comin-Chiaramonti, P., Marques, L. S. and Melfi, A. J. (1987). Mantle heterogeneity and crustal contamination in the genesis of low-Ti continental flood basalts from the Parana Basin (Brazil): Sr-Nd isotope and geochemical evidence. J. Petrol., **28**, 701-726.

Philpotts, J. A. and Schnetzler, C. C. (1970). Phenocryst-matrix partition coefficients for K, Rb, Sr and Ba with applications to anorthite asnd basalt genesis. Geochim. Cos.Acta., **34**, 307-322.

Prestvik, T. and Goles, G. G. (1985). Comments on the petrogenesis and tectonic setting of Columbia River basalts. Earth and Planet. Sci. Lett., **72**, 65-73.

Reynolds, R. C. (1963). Matrix corrections in trace element analysis by X-ray fluorescence - estimation of mass absorption coefficient by Compton scattering. Amer. Mineral., **48**, 1133-1143.

Reynolds, R. C. (1967). Estimation of mass absorption coefficients by Compton Scattering: improvements and extensions of the method. Amer. Mineral., **52**, 1493-1502.

Ribe, N. M. (1985). The generation and compaction of partial melts in the Earths mantle. Earth Planet. Sci. Lett., **73**, 361-376.

Richardson, S. H. (1986). Latter-day origin of diamonds of eclogitic paragenesis. Nature, **322**, 623-626.

Richardson, S. H., Erlank, A. J., Reid, D. L. and Duncan, A. R. (1984a). 25. Major and trace elements and Nd and Sr isotope Geochimistry of basalts from the deep sea drilling project Leg 74, Walvis Ridge Transect, 739-754. In: T. C. Moore *et al.*, Initial Reports of the Deep Sea Drilling Project, **74**, U. S. G. printing office, Washington D. C.

Richardson, S. H., Gurney, J. J., Erlank, A. J. and Harris, J. W. (1984b). Origin of diamonds in old enriched mantle. Nature, **310**, 198-202.

Richardson, S. H., Erlank, A. J. and Hart, S. R. (1985). Kimberlite-bourne garnet peridotite xenoliths from old enriched subcontinental lithosphere. Earth Planet. Sci. Lett., **75**, 116-128.

Richardson, S. W. and England, P. C. (1979). Metamorphic consequences of crustal eclogite production in overthrust orogenic zones. Earth Planet. Sci. Lett., **42**, 183-190.

Richter, F. M. (1986). Simple models for trace element fractionation during melt segregation. Earth Planet. Sci. Lett., **77**, 323-344.

Rickard, R. S., Harris, J. W., Gurney, J. J. and Cardoso, P. (1986). Mineral inclusions in diamonds from Koffiefontein Mine. Ext. Abstr. 4th Int. Kimberlite Conf., Geol. Soc. Australia, **16**, 389.

Ridgway, J. and Money, N. J. (1981). Karroo basalts from western Zambia and geochemical provinces in central and southern Africa. Geol. Rundsch., **70**, 868-873.

Ringwood, A. E. (1975). Composition and petrology of the Earths mantle. McGraw-Hill, New York, 618 pp.

Ringwood, A. E. (1982). Phase transformations and differentiation in subducted lithosphere: implications for mantle dynamics, basalt petrogenesis and crustal evolution. J. Geol., **90**, 611-643.

Ringwood, A. E. (1985). Mantle dynamics and basalt petrogenesis. Tectonophys., **112**, 17-34.

Ringwood, A. E. and Irifune, T. (1988). Nature of the 650-km seismic discontinuity: implications for mantle dynamics and differentiation. Nature, **331**, 131-136.

Robb, L. J., BArton, J. M., Kable, E. J. D. and Wallace, R. C. (1986). geology, geochemistry and isotopic characteristics of the Archaean Kaap Valley Pluton, Barberton Mountainland, South Africa. Precamb. Res., **31**, 1-36.

Roeder, P. L. and Emslie, R. F. (1970). Olivine-liquid equilibrium. Contrib. Min. Petrol., **29**, 275-289.

Rogers, N. W. (1979). Trace element analysis of kimberlites and associated rocks and xenoliths. Unpub. PhD thesis, Univ. of London, 266 pp.

Ross, M., Huebner, J. S. and Dowty, E. (1973). Delineation of the one atmosphere augite-pigeonite miscibility gap for pyroxenes from lunar basalt 12021. Amer. Mineral., **58**, 619-635.

Saggerson, E. P. and Bristow, J. W. (1983). The geology and structural relationships of volcanic and intrusive rocks of the southern Lebombo. Bull. Volcanol., **46**(2), 161-181.

Saggerson, E. P. and Logan, C. T. (1970). Distribution controls of layered and differentiated mafic intrusions in the Lebombo volcanic sub-province. Spec. Publ. geol. Soc.S. Afr., **1**, 721-733.

Saggerson, E. P., Bristow, J. W. and Armstrong, R. A. (1983). The Rooi Rand dyke swarm. S. Afr. J. Sci., **79**, 365-369.

Scrutton, R. A. , Du Plessis, A. , Barnaby, A. M. and Simpson, E. S. W. (1979). Contrasting structures and origins of the western and south-eastern continental margins of southern Africa, 651-661. In: K. S. W. Campbell (ed.), Third International Gondwana Symposium. ANU Press, Canberra.

Shaw, D. M. (1970). Trace element fractionation during anatexis. Geochim. Cos. Acta, **34** (2), 237-243.

Shimizu, N. (1975). Geochemistry of ultramafic inclusions from Salt Lake Crater, Hawaii, and from southern African kimberlites. Phys. Chem. Earth, **9**, 655-669.

Siedner,G. and Mitchell, J. A. (1976). Episodic Mesozoic volcanism in Namibia and Brazil: A K-Ar isochron study bearing on the opening of the South Atlantic. Earth Planet. Sci. Lett., **30**, 292-302

Sinha, A. K. (1972). U-Th-Pb systematics and the age of the Onverwacht series, South Africa. Earth Planet. Sci. Lett., **16**, 219-227.

Smith, H. S. (1988). Silicification of basalts in the Barberton Greenstone Belt: major element, trace element and oxygen isotope evidence. Amer. Geophys. Union, (in press).

Snetsinger, K. G., Bunch, T. E. and Keil, K. (1968). Electron microprobe analysis of vanadium in the presence of titanium. Amer. Mineral., **53**, 1770-1773.

South African Committee for Stratigraphy (SACS) (1980). Stratigraphy of South Africa. Part I. Handbk. Geol. Surv. S. Afr., **8**, pp 690.

Spencer, K. J. and Lindsley, D. H. (1981). A solution model for co-existing iron-titanium oxides. Amer. Mineralog., **66**, 1189-1201.

Steckler, M. S. (1985). Uplift and extension at the Gulf of Suez: indications of induced mantle convection. Nature, **317**, 135-139.

Sun, C., Williams, R. J. and Sun, S. (1974). Distribution coefficients of Eu and Sr for plagioclase-liquid and clinopyroxene-liquid equilibria in oceanic ridge basalt: an experimental study. Geochim. Cos. Acta, **38**, 1415-1433.

Sutton, E. R. (1979). The geology of the Mafungabusi area. Rhod. geol. Surv. Bull., **81**, 318 pp.

Sutton, J. (1977). Some consequences of horizontal displacements in the Precambrian. Tectonophys., **40**, 161-181.

Sweeney, R. J. and Watkeys, M. K. (1988). Lithospheric architecture and Gondwana basalts. (submitted).

Tankard, A. J., Jackson, M. P. A., Eriksson, K. A., Hobday, D. K., Hunter, D. R. and Minter, W. E. L. (1982). Crustal evolution of southern Africa. Springer-Verlag, New York, 523 pp.

Taylor, H. P. (1968). The oxygen isotope geochemistry of igneous rocks. Contrib. Min. Petrol., **19**, 1-71.

Taylor, H. P. (1980). The effects of assimilation of country rocks by magmas on $^{18}O/^{16}O$ and $^{87}Sr/^{86}Sr$ systematics in igneous rocks. Earth Planet. Sci. Lett., **47**, 243.

Taylor, H. P. and Sheppard, S. M. F. (1986). Igneous rocks: I. Processes of isotopic fractionation and isotope systematics, 227-272. In: J. W. Valley, H. P. Taylor and J. R. O'Neill (eds.), Stable Isotopes in High Temperature Geological Processes. Mineral. Soc. Amer., Rev. Mineral., **16**, 570 pp.

Taylor, S. R. (1965). Geochemical analysis by spark-source mass spectrography. Geochim. Cos. Acta, **29**, 1243-1261.

Taylor, S. R. (1971). Geochemical application of spark-source mass spectrography-II. Photoplate data processing. Geochim. Cos. Acta, **35**, 1187-1196.

Taylor, S. R. and Gorton, M. P. (1977). Geochemical application of spark source mass spectrography-III. Element sensitivity, precision and accuracy. Geochim. Cos. Acta, **41**, 1375-1380.

Thompson, R. N. (1972). The 1-atmosphere melting patterns of some basaltic volcanic rock series. Amer. J. Sci., **272**, 901-932.

Thompson, R. N., Esson, J. and Dunham, A. C. (1972). Major element chemical variation in the Eocene lavas of the Isle of Skye, Scotland. J. Petrol., **13**, 219-253.

Vail, J. R. (1962). Late Karoo intrusion breccias from the Nuanetsi district of Southern Rhodesia, with special reference to the granite complex of Dembe-Divula. Trans. geol. Soc. S. Afr., **65**, 139-152.

Vail, J. R. (1966). Dembe-Divula, a late Karoo granite-gabbro ring complex in the Nuanetsi igneous province of Southern Rhodesia. Trans. geol. Soc. S. Afr., **69**, 71-85.

Vail, J. R., Hornung, G. and Cox, K. G. (1969). Karoo basalts of the Tuli Syncline, Rhodesia. Bull. Volcanol., **33**, 398-418.

Van Niekerk, C. B. (1968). The suitability of extrusive rocks for U-Pb radiometric dating. Unpub. PhD thesis, Univ. of Cape Town, 129 pp.

Wachendorf, H. (1971). Die rhyolithe und basalte der Lebombos in hinterland von Lorenco Marques (Mocambique). Geotekt. Forsch., **40**, 1-86

Wachendorf, H. (1973). The rhyolitic lava flows of the Lebombo (south-east Africa). Bull. volcan., **37**, 515-529.

Walker, F. and Poldervaart, A. (1949). Karoo dolerites of the Union of South Africa. Bull. geol. Soc. Amer., **60**, 591-706.

Wanke, H., Driebus, G. and Jagoutz, E. (1984). Mantle chemistry and accretion history of the Earth, 1-46. In: A. Kroner, G. N. Hanson and A. M. Goodwin (eds.), Archaean Geochemistry, Springer-Verlag.

Watkeys, M. K. and Sweeney, R. J. (1988). Karoo tectonics of the Tuli-Sabi-Lebombo region, southern Africa: implications for Gondwana rifting. Ext. Abs. Geocongr. '88, S. Afr. geol. Soc., in press.

Watson, E. B. (1979). Zircon saturation in felsic liquids: experimental results and applications to trace element Geochimistry. Con. Min. Petrol., **70**, 407-419.

Watson, E. B. (1982). Basalt contamination by continental crust: some experiments and models. Contrib. Min. Petrol., **80**, 73-87.

Watson, E. B. and Jurewicz, S. R. (1984). Behaviour of alkalies during diffusive interaction of granitic xenoliths with basaltic magma. J. Geol., **92** (2), 121-131.

Watson, E. B. (1985). Henrys Law behaviour in simple systems and in magmas: criteria for discerning concentration-dependent partition coefficients in nature. Geochim. Cos. Acta, **49**, 917-923.

Wernicke, B. and Burchfiel, E. C. (1982). Modes of extensional tectonics. J. Structural Geol., **4**(2), 105-115.

Wickham, S. M. and Oxburgh, E. R. (1985). Contnental rifts as a setting for regional metamorphism, Nature, **318**, 330-333.

Wilkinson, J. F. G. and Binns, R. A. (1981). Relatively iron rich lherzolite xenoliths of the Cr-diopside suite: a guide to the primary nature of anorogenic tholeiitic andesite magmas. Contrib. Min. Petrol. , **65**, 199-212.

Willis, J. P. W., Ahrens, L. H., Danchin, R. V. Erlank, A. J., Gurney, J. J., Hofmeyr, P.K., McCarthy, T. S. and Orren, M. J. (1971). Some interelement relationships between lunar rocks and fines and stony meteorites. Proc. 2nd Lunar Sci. Conf., Geochim. Cos. Acta, suppl. 2, **2**, 1123-1138.

Willis, J. P. , Erlank, A. J. , Gurney, J. J. , Theil, R. H. and Ahrens, L. H. (1972). Major and minor trace element data for some Apollo 11, 12, 14 and 15 samples, 1269-1273. In: L. D. Heymann (ed.), Proc. Third Lunar Conf. MIT Press, Boston, 2155 pp.

Wolmarans, L. G. and Kent, L. E. (1982). Geological investigations in western Dronning Maud Land, Antarctica - a synthesis. S, Afr. Antarct. Res. Suppl., **2**, 93 pp.

Wood, D. A., Joron, J. L., Treuil, M., Norry, M. and Tarney, J. (1979). Elemental and Sr isotope variations in basic lavas from Iceland and the surrounding ocean floor. Contrib. Min. Petrol., **70**, 319-339.

Yoder, H. S. (1976). Generation of basaltic magmas. National Academy of Sciences, Washington D. C., pp 265.

York, D. (1969). Least squares fitting of a straight line with correlated errors. Earth Planet. Sci. Lett., **5**, 320-324.

Zindler, A. and Hart, S. (1986). Helium: problematic primordial signals. Earth Planet. Sci. Lett., **79**, 1-8.

Zindler, A., Jagoutz, E. and Goldstein, S. (1982). Nd, Sr and Pb isotope systematics in a three component mantle: a new perspective. Nature, **58**, 519-523.